Dimensional Stability and Properties of Thermoplastics Reinforced with Particulate and Fiber Fillers

By

Wade S. DePolo

Dissertation Submitted to the Faculty of

Virginia Polytechnic Institute and State University

in partial fulfillment of the requirements for the degree of

DOCTOR OF PHILOSOPHY

in

Chemical Engineering

Dr. Donald G. Baird, Chairman

Dr. Richey M. Davis
Dr. Eva Marand
Dr. Jack Lesko

September, 2005

Blacksburg, VA

Keywords: Dimensional Stability, Warpage, Nanocomposites, and Structure-Property Relationships

Dimensional Stability and Properties of Thermoplastics Reinforced with Particulate and Fiber Fillers

Wade S. DePolo

(ABSRACT)

This work has been concerned with the dimensional stability and the structure-property relationships of thermoplastics reinforced with particulate and fiber fillers. The first part of this study was concerned with ascertaining the main causes of warpage observed for injection-molded thermoplastics reinforced with high aspect ratio fibers. Typically, warpage in injection-molded fiber reinforced thermoplastics is primarily attributed to residual thermal stresses associated with shrinkage and thermal contraction of the parts. Therefore, it is assumed that flow-induced stresses generated during mold filling do not play a significant role in the warpage. The warpage of PP composites reinforced with TLCP fibers was found to increase with an increase in fiber loading. The shrinkage and the thermal expansion of the TLCP/PP composites and, hence, the thermally induced stresses decreased with an increase in fiber loading while the flow-induced stresses increased. The increase in the flow-induced stresses was attributed to an inhibition of stress relaxation and greater generation of orientation of the polymer chains with an increase in fiber loading. Therefore, it was found that in order to accurately predict the warpage of fiber reinforced thermoplastics, the flow-induced residual stresses must be accounted for.

The second part of this work was concerned with minimizing the particle loading of reinforced PC/PBT composites while maintaining the stiffness, i.e. modulus, and the dimensional stability of injection molded flat panels. This was accomplished by using high aspect ratio (≈ 100-150) nano-clays as opposed to micron-size talc (≈ 5-10). It was found that by using nano-clays surface modified with a quaternary ammonium salt that contained two hydroxyl groups as opposed to fine talc particles, the level of particle reinforcement could be reduced from 6 to 1 wt% without sacrificing the modulus of the

reinforced PC/PBT composites. Further benefits included a 26% increase in flexural strength, 77% increase in the tensile toughness and 3% reduction in the density of the reinforced PC/PBT composites. An increase in the modulus and tensile toughness was observed even though there was evidence of loss in molecular weight of the PC/PBT matrix, which was supported by the rheological behavior of the composites.

Acknowledgements

The author wishes to express his appreciation to Professor Dr. Baird for his help in maintaining my focus on the objectives of this dissertation as well as his guidance that led to a better understanding of the topic and the eventual completion of this study. Furthermore, the author would like to thank those to my committee, Professor Davis, Mirand, Lesko, and Case for contributing helpful suggestions on the direction of this research.

The author would also like to express his appreciation to the following people:

- His parents, grandmother, brother, and sister for helping shape the author into the person he is today.
- Dr. Phillip Doerpinghaus and Dr. Eric Scribben for training the author on all the equipment and their helpful suggestions that were necessary for him to complete this study.
- Mr. Steve McCartney for photographing and developing the images obtained by means of transmission electron microscopy (TEM).
- Brandon Baird, Dave Litchfield, Chris Seay, and Brian St. George for performing many experiments that helped the author complete his study.
- All the graduate students and Post-Docs, in the past and present, that the author has had the pleasure of knowing and working alongside with at Virginia Tech: Philip, Eric, Jianhua, Matt, Quang, Aaron, Dave and Dave, Chris, Brent, Desmond, Myoungbae and Gregorio.
- Mr. Wendall Brown and Mike for all the machining jobs performed.
- Mr. Riley Chan for all the assistance provided when it came to dealing with electronics.
- All the secretaries for all their help over the years.
- Daimler-Chrysler for providing financial support during most of my stay at Virginia Tech.

- To Matt and his wife Heather for all the free food and beer they have provided me throughout the years, and especially for supporting the author during some of the rough times that the author has had during his stay at Virginia Tech. I do forgive Matt for not blowing up the lab with his high pressure pump; he'll have to try harder in the future.

- To the other Matt and his wife Michelle, for being such good friends during my stay at Tech, and making sure that I got plenty of exercise and enough time to goof-off so that the author kept his sanity while completing his doctorate.

- To Quang for kicking my butt in every game we play against one another, oh yeah, and also for being a good friend during my time at Virginia Tech.

- And finally to my mother, for teaching me how to swim at a very young age, so that I had no chance in drowning at the lake while visiting Dr. Baird's lake house for all these years.

Format of Dissertation

This dissertation is written in journal format. Chapters 3 to 6 are self-contained papers that separately describe the experiments, results and conclusions pertinent to each chapter. With the exception of the literature review (Chapter 2), the figures and tables are inserted after the reference section of each chapter.

Table of Contents

List of Figures

List of Tables

1.0 Introduction

1.1 Role of Fillers on the Dimensional Stability of Thermoplastics

The addition of fillers to thermoplastic polymers has received much commercial interest throughout the last 30-40 years, especially in the automotive industry. Fillers are added to polymer primarily to increase their stiffness or rigidity and/or reduce the cost of the polymer system. Composites generated with fillers can be divided into two broad categories: systems that have strong particle-particle interactions and systems where hydrodynamic interactions dominate, i.e. non-interacting particles. Fillers that exhibit strong particle-particle interactions are commonly called particulates, and they are characterized by their small particle sizes (< 10 μm) and aspect ratio (diameter/thickness). Talc, mica, calcium carbonate, and carbon black are just a few examples of fillers that fit into this category. The second class of fillers is commonly referred to as fibers, and they are characterized by their large particle sizes and aspect ratios (length/diameter). Fiber fillers of commercial interest include aramid, carbon, and short-glass fibers. One should note that nano-particles, with their small particle sizes and high aspect ratios, could fit in either one of the two major categories listed above. The particle-particle interactions of nano-particles are highly dependent upon the surface treatment used and polymer matrix that they are combined with [1].

During injection molding, a process commonly used to convert particulate and fiber filled composites from pellets into various useful shapes, the size and shape of the molded part does not typically conform to that of the mold. Instead, the part warps and shrinks relative to the mold. For both particulate and fiber filled composites, the addition of filler leads to a reduction in mold shrinkage, but it is observed that warpage (bending and twisting of a molded part) of thermoplastics reinforced with low aspect ratio fillers (particulates) is considerably less than that for systems reinforced with high aspect ratio fibers [2-5].

The most common belief is that warpage in injection molded thermoplastics is due to residual thermal stresses associated with shrinkage and non-uniform cooling of the

parts [3,6-11]. While non-uniform thermally induced stresses generated during the cooling and solidification process may be the primary cause for warpage in unfilled thermoplastic composites, the additional warpage observed for fiber-reinforced matrices cannot be accounted for by the mechanism of thermal stresses for various reasons. For example, if a part made from a thermoplastic matrix with and without glass is cooled under the same conditions, then the thermal stresses should be nearly the same and warpage should be similar. Furthermore, an amorphous polymer was reinforced with short-glass fibers at the same molding conditions with the exception of ejection from the mold [12]. The molded part that was left in the mold for 30 seconds warped significantly, whereas, the molded part that was left in the mold overnight did not warp. Therefore, it is our hypothesis that the addition of fiber to the thermoplastic significantly affects the viscoelastic flow behavior of the polymer melt during the filling process. In particular, high aspect ratio fibers promote both increased chain alignment, and, therefore, orientation relative to particulate filled and unfilled thermoplastic polymers. Thus, the long relaxation times are increased, thereby retarding the process of stress relaxation and orientation on cessation of the filling process. As the polymer melt cools inside the mold, "frozen-in" flow-induced stresses and, hence, orientation is generated. If any imbalance in the cooling process of the part occurs, then one can expect a non-uniform variation in relaxation of stresses and orientation and, therefore, an increase in warpage of fiber-reinforced thermoplastics.

Therefore, the first objective of this work is to evaluate the role of the residual flow-induced stresses relative to that of thermally induced stresses, as governed by fiber concentration and aspect ratio, on the dimensional stability of injection-molded composites. In particular**,** injection molded plaques of polypropylene (PP) reinforced with pregenerated thermotropic liquid crystalline polymer (TLCP) micro-fibrils will be generated as a function of TLCP concentration and fiber aspect ratio in order to investigate the role of the residual flow-induced stresses relative to that of the thermal stresses on the warpage. The flow-induced and thermally induced stresses will be estimated as a function of TLCP loading and aspect ratio using the governing equations for fluid flow and heat transfer in rectilinear end-gated mold by assuming that the flow behavior can be represented by parallel-plate pressure driven flow. The estimated flow

induced and thermally induced stresses will then be correlated to the observed warpage of the molded plaques and the rheological properties of the melts.

1.2 Optimizing the Dimensional Stability and Mechanical Properties of Particulate Filled PC/PBT Composites

The second and third objective of this work deals with particulate filled PC/PBT composites for the application to exterior car door panels. PC has a good balance of properties, which include high modulus and strength, heat deflection temperature, and toughness. However, it has poor solvent and hydrolysis resistance [13]. Therefore, PBT is blended with PC to improve the chemical resistance of the molded parts.

PC/PBT blends by themselves do not have high enough modulus for the application of car door panels so some type of reinforcement is required to improve upon these properties. Fiber reinforcements can be used to increase the modulus of the PC/PBT blends but this may lead to a significant degree of warpage as well as a reduction in paintability due to increased surface roughness. Therefore, particulate fillers are more suited for the purpose of increasing the modulus of molded parts for the use of exterior car door panels. They provide adequate stiffness for vertical panels ($\geq$ 2.75 GPa) but not horizontal panels ($\approx$ 7.0 GPa).

Addition of fillers may increase the stiffness of a polymeric blend, but it also increases the weight of molded parts relative to the unfilled blends. The increase in weight is due to density differences between fillers and thermoplastics. Densities for fillers range from 2.0 – 2.8 g/cm^3, whereas, the density of polymers typically range from 0.8-1.4 g/cm^3. Furthermore, the impact resistance and tensile toughness, generally, decrease with an increase in filler concentration. Added weight and a reduction in impact resistance are not desirable for automotive purposes.

1.2.1 Effect of Blend Sequencing on the Dimensional Stability and Mechanical Properties of Filled PC/PBT Blends

Based on work performed on talc filled PBT and talc filled PC composites generated at various filler loadings, it was determined that keeping the filler in the PBT

phase can be advantageous to both the coefficient of thermal expansion (CLTE) and in maintaining the tensile toughness of filled PC/PBT blends. The CLTE and the overall dimensional changes of talc filled PBT and talc filled PC were investigated as a function of temperature and talc loading. The CLTE of the PBT/talc composites have much greater influence on talc loading than the talc filled PC composites in the temperature range studied due to PBT's low glass transition temperature of 50-55 °C relative to that of PC, which is 150°C. At a talc loading of 8% by weight, the CLTE of the PBT/talc composite is reduced by 18% relative to the base resin while the CLTE of the PC/talc composite is only reduced by half as much as that of the PBT/talc composite (9%) relative to its base resin. Furthermore, the overall dimensional change of the PBT and PC talc filled composites at a talc loading of 8% by weight and a temperature of 100°C is reduced by 20% and 8%, respectively, relative to the values of the neat resin components. These results indicated that dimensional stability could be improved by maintaining the talc particles in the PBT phase. A further benefit of maintaining the talc particles in the PBT is that the PBT can maintain its toughness with an increase in filler loading to a much greater degree than PC. Therefore, tensile toughness may be improved by maintaining the talc in the PBT phase.

The location of filler particles can be affected by blending sequence and the intensity of mixing, which in turn affect the mechanical properties [13-19]. Improved impact resistance has been observed when filler particles are encapsulated within the dispersed phase while the modulus tends to increase when the filler particles are separately dispersed with the minor phase within the continuous phase. An increase in the intensity of mixing can lead to co-continuous morphological structures, which have been shown to greatly enhance the properties of binary blends. Thus, maintaining the tensile toughness and improving the CLTE of filled PC/PBT blends may be accomplished by controlling the location of the particles within the filled blend by modifying the blending sequence and reducing the intensity of mixing during the processing of filled thermoplastic blends. Therefore, the second objective of this work is to establish the influence of blending sequence on the blend morphology and mechanical properties of particulate filled PC/PBT blends, focusing on the role of mixing intensity and sequencing on particle placement of the particulate filled particles. The effects of such factors as

blending order, particle loading, and viscosity ratio on the morphology, mechanical properties, and dimensional stability will be determined.

1.2.2 Minimizing Filler Loading by use of Nano-Particles Opposed to Fine Particles

Minimizing particle loading without a significant reduction in stiffness may be accomplished by filling thermoplastics with nano-size particles (nanocomposites) as opposed to fine (micron-sized) particles, which are typically used in conventional thermoplastic composites. It has been shown that a major advantage of nanocomposites is that much lower reinforcement levels (< 5% by weight) are required to achieve the same level of reinforcement that is typically observed in conventional particulate filled thermoplastic composites (20%-30% by weight), due to the higher aspect ratio of the nanoparticles relative to that of micron-size particles [20-23]. Thus, the stiffness level normalized by the density, i.e. specific modulus, of nanocomposites is potentially much higher than that of conventional thermoplastic composites. This offers a distinct advantage in that the weight of the part is reduced without a loss in stiffness. Thus, for automotive applications, such as exterior car door panels, the automobile will be more fuel efficient due to the reduction in weight. Hence, the third objective of this work is to determine if the use of nano-particles relative to fine particles can allow lower loadings of reinforcement for filled PC/PBT blends while maintaining the desired mechanical properties, such as stiffness, impact strength, and tensile toughness. This can be accomplished by generating filled PC/PBT blends consisting of fine particles or nano-particles at various loading levels. The effects of factors such as filler loading, surface treatments, and viscosity ratios on the morphology and mechanical properties of the filled blends will be determined. In particular, flexural, tensile, and impact properties will be determined and correlated with morphological structure determined by means of transmission electron microscopy to ascertain if the addition of nano-particles opposed to fine particles presents any advantages in reducing the loading levels required to maintain an adequate stiffness for the use of vertical car door panels.

1.3 Research Objectives

1.3.1 Research Objective #1

Fillers are added to polymer melts primarily to increase the stiffness or rigidity and/or reduce the cost of the blend. However, the addition of fillers also leads to warpage of injection-molded parts. Warpage (bending and twisting of a molded part) tends to be much greater in fiber-reinforced composites relative to particulate reinforced composites at an equivalent level of reinforcement (on a volume basis) and polymer matrix. Therefore, variables such as particle loading and particle shape (aspect ratio) play a large role on the dimensional stability of composites. A fundamental understanding on how the flow-induced stresses relate to the dimensional stability of filled composites is of paramount importance to accurately predicting the degree of warpage in injection-molded parts. With this in mind, the first research objective is:

Evaluate the role of the residual flow-induced stresses relative to that of thermally induced stresses, as governed by fiber concentration and aspect ratio, on the dimensional stability of injection-molded composites.

1.3.2 Research Objective #2

Although, the stiffness of a polymer is increased with an increase in particle loading, the impact resistance and tensile toughness generally decrease. It was observed that the dimensional stability and tensile toughness of talc filled PC/PBT blends might improve if the talc particles are located solely in the PBT phase. Factors such as the blending order, intensity of mixing, and viscosity ratio has a significant impact on the morphology, and therefore, the placement of filler particles for ternary blends consisting of particles and two thermoplastic polymers. Therefore, the second objective of this research is to:

Establish the influence of blending sequence on the blend morphology and mechanical properties of particulate filled PC/PBT blends, focusing on the role of mixing intensity and sequencing on particle placement of the filled blends.

1.3.3 Research Objective #3

Addition of fillers increases the weight of molded parts relative to the unfilled blends. The increase in weight is due to density differences between fillers and thermoplastics. Densities for fillers range from 2.0 – 2.8 g/cm^3, whereas, the density of polymers typically range from 0.8-1.4 g/cm^3. Added weight is undesirable for the application of vertical car door panels due to a reduction in fuel efficiency. Therefore, minimizing the particle loading without sacrificing the stiffness of the molded part is beneficial for automotive applications. A possible method for reducing the loading level is by using nano-particles opposed to fine particles due to their small particle size and much higher aspect ratios. In light of this, the third objective of this work is to:

Determine if the use of nano-particles opposed to fine particles can allow lower loadings of reinforcement for filled PC/PBT blends while maintaining desired mechanical properties, such as stiffness, impact strength, and tensile toughness.

1.4 References

1. Lee, K. M., and Han, C. D., "Rheology of Organoclay Nanocomposites: Effects of Polymer Matrix/Organoclay Compatibility and the Gallery Distance of Organoclay", *Macromolecules*, **36**, 7165 (2003).

2. Kikuchi, Hiroyuki, and Koyama, Kiyohito, "Material Anisotropy and Warpage of Nylon 66 Composites", *Polym. Sci. Eng.*, **34** (18), 1411 (1994).

3. Kikuchi, Hiroyuki, and Koyama, Kiyohito, "The Relation Between Thickness and Warpage in a Disk Injection Molded From Fiber Reinforced PA66", *Polym. Sci. Eng.*, **36** (10), 1317 (1996).

4. Kikuchi, Hiroyuki, and Koyama, Kiyohito, "Warpage, Anisotropy, and Part Thickness", *Polym. Sci. Eng.*, **36** (10), 1326 (1996).

5. Kikuchi, Hiroyuki, and Koyama, Kiyohito, "Generalized Warpage Parameter", *Polym. Sci. Eng.*, **36** (10), 1309 (1996).

6. Choi, D-S and Im, Y-T, "Prediction of Shrinkage and Warpage in Consideration of Residual Stress in Integrated Simulation of Injection Molding", *Composite Structures*, **47**, 655 (1999).

7. Zheng, R., Kennedy, P., Phan-Tien, N., and Fan, X. J., "Thermoviscoelastic Simulation of Thermally and Pressure-Induced Stresses in Injection Moulding for the Prediction of Shrinkage and Warpage for Fibre-Reinforced Thermoplastics", *J. Non-Newtonian Fluid Mech.*, **84**, 159 (1999).

8. Kamal, M. R., Lai-Fook, R. A., and Hernandez-Aguilar, "Residual Thermal Stresses in Injection Moldings of Thermoplastic: A Theoretical and Experimental Study", *Polym. Eng. Sci.*, **42** (5), 1098 (2002).

9. Zoetelief, W. F., Douven, L. F. A., and Ingen Housz, A. J., "Residual Thermal Stresses in Injection Molded Products", *Polym. Eng. Sci.*, **36** (14), 1886 (1996).

10. Shen, Chang-Yu, and Li, Hai-Mei, "Numerical Simulation for Effects of Injection Mold Cooling on Warpage and residual Stresses", *Polym-Plast. Technol. Eng.*, **42** (5), 971 (2003).

11. Kwon, T. H., and Lee, Y. B., "Modeling and Numerical Simulation of Residual Stresses and Birefringence in Injection Molded Center-gated Disks", *Journal of Materials Processing Technology*, **111**, 214 (2001).

12. Panasiewicz, Jeremy, Daimler-Chrysler, *Private Communications*.

13. Cheng, T. W., Keskkula, H., and Paul, D. R., "Property and Morphology Relationships for Ternary Blends of Polycarbonate, Brittle Polymers, and an Impact Modifier", *Polymer*, **33** (8), 1606 (1992).

14. Kim, B. K., and Lee, Y. M., "Physical Properties of ABS/SMA/Nylon-6 Ternary Blends: Effect of Blending Sequence", *Polymer*, **34** (10), 2075 (1993).

15. Sahnoune, P., Lopez Cuesta, J. M., and Crespy, A., "Improvement of the Mechanical Properties of an HDPE/PS Blend by Compatibilization and Incorporation of $CaCO_3$", *Polym. Eng. Sci.*, **43** (3), 647 (2003).

16. Zheng, Mingjia, and Li, Huilin, "Study on Isotactic Polypropylene/Zinc-Neutralized Sulfonated Ethylene Propylene Diene Monomer Rubber/$CaCO_3$ Ternary Blends", *J. Appl. Polym. Sci.*, **91**, 1635 (2004).

17. Steinmann, Sandra, Gronski, Wolfram, and Friedrich, Christian, "Influence of Selective Filling on Rheological Properties and Phase Inversion of Two-phase Polymer Blends", *Polymer*, **43**, 4467 (2002).

18. MacKenzie, B. T., "Filler Effects and Treeing Phenomena in Laboratory Models and Cable Sections", *Ann. Rep. Conf. Elec. Insul. Dielec. Phenomena*, 232 (1972).

19. Kylma, Janne, and Seppala, Jukka, "Ternary-Phase Poly(ester-urethane)/Elastomer/Filler Composites", *J. Appl. Polym. Sci.*, **79**, 1531 (2001).

20. Maiti, S. N., and Sharma, K. K., "Studies on Polypropylene Composites Filled with Talc Particles", *J. Mater. Sci.*, **27**, 4605 (1992).

21. Li, Zhigang, and Narh, K. A., "Experimental Determination and Numerical Prediction of Mechanical Properties of Injection Molded Self-reinforcing polymer Composites", *Composites: Part B*, **32**, 103 (2003).

22. Brune, Douglas A., and Bicerano, Jozef, "Micromechanics of Nanocomposites: Comparison of Tensile and Compressive Elastic Moduli, and Prediction of Effects of Incomplete Exfoliation and Imperfect Alignment on Modulus", *Polymer*, **43**, 369 (2002).

23. Maine, F. W., and Shepard, P. D., "Mica reinforced plastics. Review", *Composites*, **5** (5), 193 (1974).

2.0 Literature Review

2.1 Dimensional Stability of Polymer Melts and Filled Polymer Systems in Injection Molding

Injection molding is a widely used process to convert solid polymers or polymer composites in the form of pellets into various useful shapes. However, the size and shape of the molded part, typically, does not conform to that of the mold. Instead, the part warps and shrinks relative to the mold. Warpage is due to an imbalance of frozen-in residual stresses that are generated during mold filling and solidification of the part while shrinkage is attributed to thermal contraction (coefficient of linear thermal expansion, CLTE), an increase in density due to crystallization, and elastic recovery. This section is concerned with the origins of the residual stresses that lead to warpage, the factors that affect the dimensional variations (warpage and shrinkage) of molded parts, and the observed experimental and theoretical predictions of the frozen-in residual stresses. In section 2.1.1, the processing and flow behavior of polymer melts and filled polymer systems during injection molding and how it relates to the development of imbalanced frozen-in residual stresses will be discussed. This will be followed by how injection molding variables, such as melt temperature, mold temperature, packing pressure, and flow rate affect the dimensional stability of molded parts in section 2.1.2. Finally, theoretical predictions of warpage attributed to frozen-in residual stresses will be discussed in 2.1.3.

2.1.1 Development of Residual Stresses Due to the Processing and Flow Behavior of Injection Molded Parts

Warpage (bending and twisting of a molded part) is caused by residual stresses that remain in an injection molded part after it has been ejected from the mold and cooled down to ambient temperatures. These residual stresses originate from two main sources: frozen-in flow-induced stresses as well as thermally and pressure induced stresses [1-5]. During the filling and packing stages, the viscoelastic flow of the melt promotes orientation (alignment in the direction of flow) of polymer chains due to the high shear and elongational deformation rates that are developed during flow. The oriented

macromolecules relax once flow is stopped, but they are not able to completely relax into their initial coiled state due to rapid solidification of the molded part. Therefore, flow-induced orientation becomes locked into the molded part. In the case of polymer composites, the reinforcing filler will also align or orient in the flow direction. The alignment of the reinforcing filler may in turn directly influence the orientation of the polymer chains. Bessel et al. [6,7] showed that in the case of a semi-crystalline polymer, Nylon 6, filled with 15% by volume of glass fibers, the crystalline regions around adjacent fibers tend to impinge on each other, thus, modifying the matrix material overall. They showed that this generated a high degree of chain alignment parallel to the fiber axis by stressing the composite to fracture along the fiber axis. This resulted in fiber pullout that had a sheath of matrix material adhering to it [8]. Typically, the degree of frozen-in orientation within the molded parts varies considerably across its cross-section from the surface to core and, therefore, it is non-uniform throughout the molded part. This leads to anisotropic thermal properties (CLTE and shrinkage) as well as mechanical properties. Furthermore, these anisotropic properties will contribute to the warpage.

The non-uniform distribution of frozen-in orientation between the surface of an injection molded part and its core can be accounted for by the fountain flow mechanism that was proposed by Tadmor [9]. Fountain flow occurs in the filling stage. Tadmor describes it from the frame of reference moving with the advancing front where the particles appear to decelerate as they approach the advancing front and then the particles stretch in an orthogonal direction towards the wall of the mold. The stretching generates considerable orientation, and, thus, as the particles are laid up on the wall, they are rapidly solidified into a highly oriented state. Hence, the extensional flow at the melt front leads to a higher state of orientation at the surface of the molded part than in the core. In the case of filled polymer systems, such as a glass fiber filled composite, the fountain flow effect is extremely important because it leads to highly oriented fibers at the surface of the molded part. Behind the advancing front, the polymer flow is essentially fully developed non-isothermal shear flow. These flows with a frozen-in skin layer are illustrated in Figure 2.1. In the core of the part, some degree of orientation can be generated due to shearing and velocity gradients, but it gradually diminishes as the centerline is approached. Due to the fountain flow effect and poor thermal conductivity

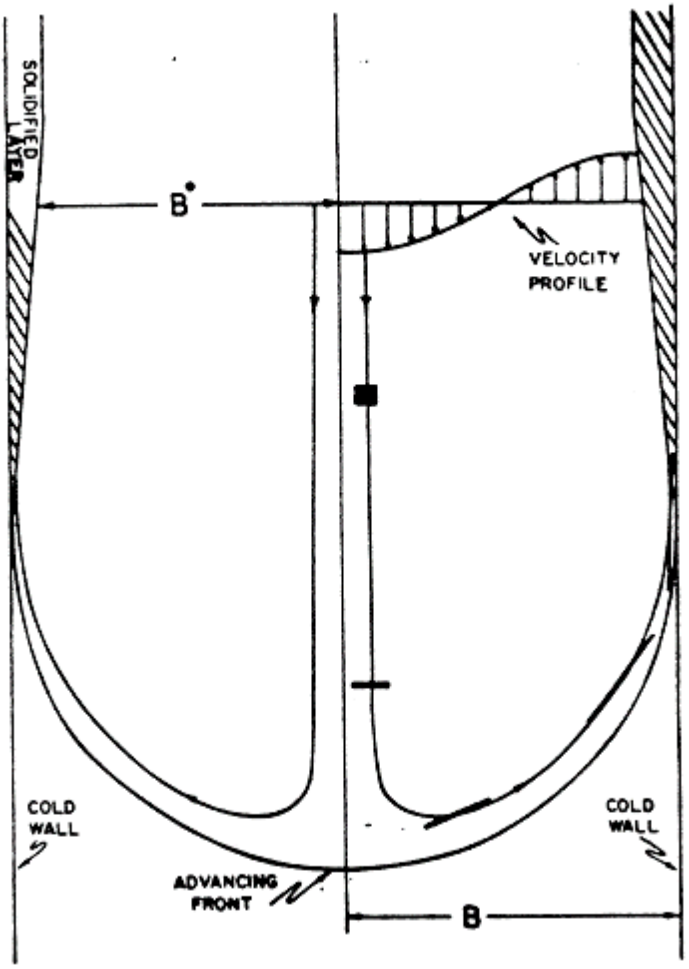

Figure 2.1 Fountain flow, fully developed flow, and solidified layer shown in a frame of reference that moves with the front [9].

of polymer melts, the surface of injection molded parts solidify at a much faster rate and a much higher state of orientation than the core. This leads to a non-uniform distribution of frozen-in orientation throughout the part as it cools in the mold.

Besides frozen-in flow-induced stresses, thermally and pressure induced stresses also contribute to the development of residual stresses in injection molded parts, and hence, warpage. When the polymer melt is solidified under pressure during the packing, filling, and cooling stages, thermal contraction (shrinkage) is constrained by the mold and thus thermally and pressure induced stresses are generated [1]. In particular, the thermal stresses arise as a consequence of thermal gradients that are present during solidification of the molded part. They are due to non-equilibrium density change or shrinkage of the polymeric material during the inhomogeneous rapid cooling of the molded part both inside and outside the mold [2]. The highly non-uniform temperature distribution that exists through the thickness of an injection molded part causes the material to solidify at the surface sooner than at the core. This causes differential shrinkage throughout the thickness of the part and leads to thermally induced residual stresses. During the packing stage, an applied pressure (packing or holding pressure) acts on the melt resulting in a compressive stress. At this stage, the injection molded part has already begun to solidify due to cooling. Solidification of the polymer melt, while the holding pressure is still acting on it, results in frozen-in compressive stresses. These frozen-in compressive stresses are referred to as pressure induced stresses. Typically, the frozen-in flow-induced residual stresses are assumed to be about an order of magnitude smaller than the thermally and pressure induced stresses due to almost instantaneous relaxation of the orientation of the polymer melt at high temperature and, therefore, they are often omitted in analyses [1,3,10].

2.1.2 Effect of Molding Conditions on the Dimensional Stability of Polymer Melts and Filled Polymer Systems

The melt temperature in the mold, mold surface temperature, cavity melt pressure, and fill rates or injection velocity are injection molding variables that can significantly affect the orientation and shrinkage distribution that develops during the filling, packing, and cooling stages. Therefore, these molding variables affect the residual stresses that

remain in an injection-molded part after it has been ejected from the mold, and thus, they affect the warpage. Some of the effects that the processing parameters have on the orientation and shrinkage are as follows:

Melt temperature. An increase in the melt temperature of the material yields a reduction in both orientation and shrinkage for many reasons. A hotter melt is less viscous than a colder one. Therefore, stresses that are generated by shearing and stretching of the polymeric material are reduced, which leads to a reduction in orientation. In general, a hotter melt freezes more slowly, allowing more time for additional material to enter the cavity of the mold in order to compensate for the shrinkage caused by cooling of the part and there is also more time for molecular relaxation of the polymer chains to occur before solidification of the molded part. In the case of semi-crystalline polymers, a higher melt temperature results in an increase in the cooling rate, which reduces the degree of crystallinity. A reduction in crystallinity yields a less dense material, and, therefore, less shrinkage occurs. The reduction in orientation and shrinkage with an increase in melt temperature leads to a reduction in residual stresses and, hence, warpage as the molded part cools.

Mold temperature. The mold temperature has little influence on surface orientation, but can have an effect on core orientation, shrinkage, and frozen-in pressure induced stresses. With a decrease in mold temperature, the molded part solidifies at a faster rate, which freezes-in a higher degree of orientation due to less opportunity for relaxation of orientation. The shrinkage depends on the material. Generally, for an amorphous polymer, the shrinkage increases with decreasing mold temperature. In this case, the cooling rate is increased leading to rapid volume changes and freezing of the gate in a much shorter time, which prevents additional material from entering the mold cavity to account for the volume changes. For semi-crystalline polymers, the shrinkage will depend on two factors. First, with a decrease in mold temperature, the cooling rate increases leading to freezing of the gate at a much shorter time resulting in an increase in shrinkage. However, the increase in cooling rate also results in a reduction in crystallinity and, hence, less shrinkage occurs. Therefore, if the reduction in molding

temperature is in a range where a considerable degree of crystallization can still occur before the gate freezes than the shrinkage will decrease due to an increase in cooling rate. However, if the mold temperature is in a range where some crystallization may still occur along with rapid freezing of the gate, then, the shrinkage will increase. Rapid cooling of the part also allows more of the molded part to solidify before the holding pressure is removed resulting in an increase in frozen-in pressure induced stresses. The increased orientation shrinkage, and locked in pressure induced stresses with a reduction in mold temperature leads to a general tendency for the injection-molded parts to warp.

Packing Pressure. An increase in packing pressure slightly increases the orientation but decreases shrinkage. Some re-orientation of the polymeric melt with an increase in packing pressure is due to flow of the melt that occurs during packing to compensate for shrinkage in the cavity of the mold. This was shown experimentally by use of birefringence measurements [11]. A small increase in birefringence with increasing packing pressure was reported in the core of the part, and, hence an increase in molecular orientation. At the lowest packing pressure, the core had a uniform brightness and there was no sign of molecular orientation. An increase in packing pressure allows for more material to enter the cavity of the mold and, hence, a reduction in shrinkage. Also, an increase in packing pressure results in higher compressive stresses that become frozen-in to the molded part, upon solidification [12]. Therefore, high packing pressures lead to a greater degree of warpage due to increased frozen-in pressure induced stresses.

Flow Rate. The fill rate seems to have little influence on the shrinkage of injection molded part but tends to promote a greater degree of warpage with a reduction in fill rate [10,11]. Fast fills tend to produce a much higher degree of orientation at the surface of the molded part relative to slow fills. This is due to the much greater extensional flow occurring at the advancing front as the fill rate increases. Also, for fast fills, the orientation in the bulk of the part is much lower relative to slow fills. This occurs for two reasons. First, higher rates of deformation are generated during fast fills. This leads to faster relaxation rates after cessation of the flow relative to slow fills, and hence, less orientation. Secondly, the melt cools more during slow fills, and therefore, it is more

viscous. This yields higher flow induced stresses, and thus, orientation. Therefore, filling at faster rates reduces core orientation, and consequently reduces warpage. In a paper by Huang and Tai [13], PC/ABS injection molded parts were generated with an end-gated mold that had a rectangular geometry. They showed that the warpage at the longest filling time, slowest fill rate (0.06 m/s), was about 8 times greater than at the shortest filling time, largest fill rate (1 m/s). In this work, the fill rate had a greater influence on the warpage than that of the melt temperature, mold temperature, and packing pressure.

In the case of filled polymer systems, the filler can have an effect on mold filling. In a paper by Folkes and Russell [12], mold filling of a PP/GF composite at a fiber loading of 20% by weight was investigated at two fill rates, 0.95 m/s and 0.017 m/s. At the fill rate of 0.95 m/s (fast fill), a high degree of molecular orientation was observed at the surface. This is due to the extensional flow occurring at the advancing front pushing the fibers towards the mold wall where it rapidly solidifies into a highly oriented state. In the core of the mold, small molecular orientation is observed. This was attributed to columnar spherulitic growth around the fibers and not flow induced orientation. At the fill rate of 0.017 m/s, the degree of molecular orientation at the surface is lower than what was observed at the faster fill rate. This is due to lower rates of deformation with a decrease in fill rate. They also found that the orientation of the core was higher at the slower fill rate relative to the faster fill rate. They observed that the layer that forms a boundary between the skin and core had a higher birefringence for the slow fill rate relative to the fast fill rate. In this region, there was no obvious change in fiber orientation. Therefore, they attributed the increase in birefringence to the fibers influencing the surrounding matrix to orient and align in the flow direction. By comparing the fiber filled system with the unfilled matrix, they deduced that the molecular orientation of the matrix is slightly influenced by orientation of the fibers. They suggest that as fiber concentration increases, the matrix orientation will be dominated by the orientation of the fibers.

2.1.3 Injection Molding Studies on the Dimensional Stability of Polymer Melts and Filled Polymer Systems

In a group of papers by Kikuchi and Koyama [15-18], the warpage of center-gated injection molded discs of unfilled Nylon 6,6, mineral filled Nylon 6,6, and fiber filled Nylon 6,6 were experimentally correlated to the anisotropy in the coefficient of linear thermal expansion (CLTE). They defined a parameter $R\alpha$, which is defined as the ratio of the CLTE in the flow direction to that of the transverse direction, α_{11}/α_{22}. The warpage of the base resin was insignificant ($0.2x10^{-3}$m) and had an $R\alpha$ of 1 (isotropic material). The mineral used for this study had an average aspect ratio of 4.0 and the glass fiber had an average aspect ratio of 55. Nylon 6,6/mineral and Nylon 6,6/GF composites had filler loadings of 40% by weight. The maximum warpage of the mineral filled system was $2.5x10^{-3}$m while the glass fiber filled material had a maximum deflection of $6.4x10^{-3}$m, which is two and a half times greater than that of the mineral filled composite. In general, much larger deflections (warpage) of molded parts for fiber filled systems relative to those of particulate filled systems are observed. The $R\alpha$ for the mineral filled system was 0.5 while it was smaller (0.4), and hence, slightly more anisotropic for the glass filled system. It is interesting to note that for a small difference in $R\alpha$ between the glass fiber and mineral filled system, there was a large difference in the magnitude of the warpage. However, the difference in $R\alpha$ between the mineral filled composite and base resin is large but the difference in the magnitude of the warpage is rather small. Also, the warpage of the glass fiber filled composite was about 30 times greater than the base resin even though the shrinkage decreased by about 20% in the flow direction with the addition of the fibers. In our opinion, the greater anisotropy and warpage of the fiber filled system is most likely due to orientation of the fibers in the flow direction, which in turn influences the orientation of the matrix, and a greater degree of inhibition of stress relaxation relative to the mineral and unfilled material rather than CLTE and shrinkage. They also reported that the warpage of an injection molded part decreased while $R\alpha$ increased towards 1 with increasing thickness. This is due to a more even orientation distribution in the core of the part as the thickness increases. The bulk of the part has more time to cool as the thickness increases, and therefore, the polymer chains have more time to relax before the part solidifies.

In a work done by Jeremy Panasewiecz [19], a glass fiber filled amorphous polymer was injection molded and left in the mold for approximately 30 seconds prior to ejection. A large amount of warpage occurred relative to the matrix. Then, using the same glass filled amorphous polymer, he injection molded another part using the same molding conditions but it was left in the mold overnight. The part was ejected from the molder the following day. This procedure resulted in no warpage of the molded part. This result cannot be explained by the anisotropy in the CLTE or density changes due to crystallization. By leaving the glass fiber filled amorphous polymer in the mold overnight, the CLTE in the flow and transverse direction should reach a state of equilibrium. Furthermore, density changes due to crystallization cannot occur in an amorphous polymer. Therefore, the only plausible explanation is that the polymer chains were allowed to fully relax when left in the mold overnight. Orientation of the glass fibers in the flow direction may cause the polymer chains to orient with them. Once the flow ceases, the polymer chains are allowed to relax, but this relaxation is impeded by the oriented glass fibers.

Thermal stresses are believed to arise as a consequence of thermal gradients that are present during solidification of the molded part. In an effort to verify this belief, Akay et al. [20] injection molded rectangular parts of two amorphous polymers, PC and ABS, by maintaining one half of the mold at a constant temperature and varied the temperature of the second half of the mold. This was done to force a non-uniform thermal distribution throughout the molded part. An unspecified commercial package was used to compare the experimental results with theory. The warpage increased in the length and the width of the part with an increase in temperature difference between the two halves of the mold for both the PC and ABS molded parts. This is to be expected because one side of the molded part solidifies faster than the other side does leading to a highly non-uniform orientation and density distribution throughout the molded part. The experimental and theoretical predictions were in qualitative agreement.

Fiber orientation structures and how it relates to warpage of injection molded short-glass fiber reinforced ribbed plates were investigated by Hine and Duckett [21]. The orientation distribution of the short-glass fibers was observed by using an optical image analysis. PBT, a semi-crystalline polymer, was used as the matrix. They found

that non-symmetric orientation layered structures lead to a significant amount of warpage. They proposed, just like Kikuchi and Koyama [15-18], that the driving force for warpage was the difference in thermal expansion in the flow and transverse direction due to the fiber orientation.

A more fundamental approach for measuring and predicting the warpage of an injection molded part is by relating the deformation of the molded part to the build-up of residual stresses during the molding process. Flow-induced residual stresses are due to frozen-in orientation of the macromolecules and thermally and pressure induced residual stresses are due to rapid inhomogeneous cooling of the molded part. Typically, the flow-induced stresses are assumed to be small due to rapid relaxation of orientation at the high temperatures employed during injection molding, and therefore, they are neglected.

Kabanemi et al. [22,23] numerically predicted thermally induced residual stresses for thermoviscoelastic materials by using a 3D finite element method. The material was assumed to be isotropic. Flow-induced residual stresses were neglected and only the cooling stage was modeled. In their model, the constraints imposed by the mold were not accounted for, and therefore, the material was free to contract in any direction. In essence, the effect of packing pressure is neglected, thus, frozen-in pressure induced stresses are also neglected. This results in a parabolic residual stress profile through the thickness of the molded part with compressive stresses at the skin and tensile stresses in the core, which is not observed experimentally for injection molded samples.

Titomanlio and Jansen [24] used a thermoelastic model accounting for the effect of packing pressure on the development of thermally and pressure induced residual stresses. The material was assumed to be isotropic and once again, flow induced residual stresses were neglected and only the packing and cooling stages were modeled. By using a thermoelastic model, stress relaxation is neglected, and thus, the residual stresses are over estimated throughout the thickness of the molded part. By accounting for compressibility of the melt due to the packing pressure, tensile stresses were observed near the surface followed by a compressive stress region and finally, tensile stresses in the core of the part. This generally observed experimentally. So, the numerical calculations were in qualitative agreement with experimental results but the magnitude of the stresses was over estimated because stress relaxation of the material is neglected.

To account for stress relaxation, Kamal et al. [2] and Zoetelief et al. [3] employed a thermoviscoelastic model obtained from a linearization of the compressible Leonov model to predict the residual stresses of PS and ABS as well as PS and HDPE injection molded parts, respectively. Flow-induced residual stresses were neglected. In all cases, the calculated residual stresses were in qualitative agreement with experiment but were still over estimated throughout the molded part. Zoetelief [3] compared the calculated residual stress distribution through the thickness of an injection molded part by using both the thermovisocelastic model and a thermoelastic model. The thermoviscoelastic model was quantitatively more accurate than the thermoelastic model because it took stress relaxation into account.

In a paper by Kwon and Lee [24], prediction of flow-induced residual stresses and birefringence of an isotropic material were taken into account by employing a non-linear viscoelastic Leonov model and the stress optic law, respectively. Thermally and pressure induced residual stresses during the packing and cooling stages were also taken into account. Unlike for the models mentioned earlier, the predicted residual stress distribution was actually underestimated by taking into account the flow-induced stresses. This was attributed to an underestimation of the thermally induced residual stresses.

For filled polymer systems, an isotropic model can not be employed. By introducing fillers to a thermoplastic matrix and applying a flow, the material properties become anisotropic because of the orientation of the fillers and the base resin in the direction of flow. Very few papers have been published on the modeling of filled polymer systems [1,25]. In a paper by Phan-Tien and Fan [1], thermally and pressure induced stresses of fiber reinforced plastics were predicted by using an anisotropic thermoviscoelastic model. Flow-induced residual stresses were neglected. Unfortunately, the model was not compared to experimental results. One would expect that the model would only qualitatively agree with experimental results by neglecting the flow-induced residual stresses.

In summary, warpage of polymer and reinforced polymer systems are due to frozen-in flow-induced residual stresses, thermally induced stresses, and pressure induced stresses as an injection molded part cools. The warpage of fiber filled polymer systems tends to be much greater than that of particulate filled or unfilled polymeric systems.

This was attributed to the difference in the CLTE between the flow and transverse direction caused by the orientation of the fiber. However, the anisotropy in the CLTE cannot explain why particulate reinforced systems exhibit much lower warpage than that of fiber filled systems, considering that the CLTE for particulates and fibers are of the same order of magnitude. Also, this mechanism cannot explain why a part produced from a glass fiber-filled polymer melt exhibits no warpage when left in a hot mold overnight but exhibits a large degree of warpage after being in the mold for approximately 30 seconds. The addition of fibers must in some way generate a higher degree of orientation of the polymer chains during the filling stage, while disrupting the stress relaxation of the polymer chains during the cooling stage relative to particle reinforced and unfilled systems. If this is true, then, frozen-in flow-induced residual stresses must be accounted for to accurately predict the dimensional stability of polymeric materials. Therefore, the effect that the addition of particulates and fibers has on the flow behavior of filled polymer melts must be investigated. In particular, differences in normal stress and stress relaxation behavior of particulate versus fiber filled systems must be examined.

2.2 Rheology of Filled Polymer Melts

This section is concerned with the effect of solid fillers on the rheology of polymeric fluids. The geometry of solid fillers taking into account particle shape, particle size, and aspect ratio is first discussed in section 2.2.1 as these factors affect the rheology of a filled polymer melt signficantly. Following this, the effect of fillers on the steady state and transient shear viscosity behavior of solid filled polymer melts is discussed in sections 2.2.1.1 and 2.2.1.2. The addition of fillers also has a significant effect on the elasticity of polymer melts. In particular, the effect of fillers on the normal stresses are discussed in section 2.2.2.1, storage modulus in 2.2.2.2, extrudate swell or die swell in section 2.2.2.3, and stress relaxation in section 2.2.3. Finally, the effect of fillers on the elongational viscosity will be discussed in section 2.2.4.

2.2.1 Filler Geometry

The rheological properties of solid filled polymer melts have received a substantial amount of attention throughout the last 30 to 40 years [26-73]. Solid fillers are added to polymer melts primarily to increase the stiffness or rigidity and/or reduce the cost of the blend.

Composites generated with solid additives can be divided into two broad categories: systems that have strong particle-particle interactions and systems where hydrodynamic interactions dominate, i.e. non-interacting particles. Solid additives that exhibit strong particle-particle interactions are commonly called particulates. Particulates are characterized by their small particle sizes (< 5 μm) and aspect ratio (length/diameter) and can be further subdivided into two groups based upon particle geometry (aspect ratio): isotropic and anisometric particles. Isotropic particulate fillers include calcium carbonate, titanium dioxide, and carbon black. These particles have a spherical geometry with an aspect ratio of approximately one and small average particle diameters that are typically less than one micron. Anisometric particulate fillers include talc, mica, and clay. These particles have a flaky or platelet geometry much like a quarter or dime, which typically have intermediate average particle diameters that are between 1-10 microns and aspect ratios on the order of 5-45 with the exception of nano-clays and nano-talcs. Nano-clays and nano-talcs have average particle diameters on the order of 100-200 nanometers and aspect ratios that can range from 15-60. The second class of solid additives is commonly referred to as fibers, and they are characterized by their large particle sizes and aspect ratios. Fibers are anisometric particles that have a rod-shaped geometry with average particle diameters on the order of 12 to 16 microns and aspect ratios on the order of 50 –150. Fiber fillers of commercial interest include aramid, carbon, and short-glass fibers. Glass beads that have an average particle diameter of 10 microns or greater are also catergorized in the second class of solid additives. Due to their large particle size, glass beads do not exhibit strong particle-particle interactions. They are isotropic particles that typically have a spherical geometry with an aspect ratio of approximately one. One should note that nano-particles, even with their small particle sizes, could fit in either one of the two major categories listed above. The particle-particle interactions of nano-particles are highly dependent upon the surface treatment used and polymer matrix that they are combined with [26]. The classification, filler,

geometry, and aspect ratio of solid additives that are of commercial interest are listed in Table 2.1. The addition of solid fillers often has a profound effect on the viscous and elastic behavior of polymeric melts [27].

2.2.2 Viscous Behavior of Filled Polymer Melts

2.2.2.1 Steady Viscous Behavior of Filled Polymer Melts

Particle size can have a significant effect on the steady shear viscosity of filled polymer melts [28-37]. Particles that have average particle diameters on the order of 5 microns or less (particulates) exhibit yield values particularly in the low shear rate region ($< 10^{-1}$ sec^{-1}) due to strong particle-particle interactions. Yield stresses, however, are not observed for particles where the average particle diameter exceeds 5 microns (fibers and large glass beads). Yield stresses have been attributed to inter-particle interaction to form a network or gel-like structure [28-31,33-35,37]. Agglomeration of the particles can also add to the observed yield stress [29,31,33]. The observed yield stress is associated with large increases in the shear viscosity at low shear rates. The magnitude of the viscosity increase is dependent on the particle size. As the particle size decreases, there is a subsequent increase in viscosity at an equivalent shear rate or stress. Suetsugu and White [29] have shown that for PS/$CaCO_3$ composites at a concentration of 30% by weight of $CaCO_3$ particles, the shear viscosity increased almost an order of magnitude when the particle size was reduced from 3 μm to 0.07 μm at a shear rate of 10^{-2} sec^{-1}. The effect of particle size on viscosity depends on the ability of particles to immobilize the molten polymer and, thus, restrict the volume of flowable melt [30,31]. As the particle size decreases (i.e., larger surface area), a greater amount of the melt becomes bound to the particles and is, thus, immobilized [31,32]. This leads to an increase in viscosity as the particle size decreases. As the shear rate increases, the network or gel-like structure is broken down and the viscosity converges to that of the unfilled matrix at high shear rates, regardless of the particle size [33, 38]. Therefore, particulate filled composites exhibit a monotonic increase in viscosity with decreasing shear in the low shear region (< 1 sec^{-1}). Once the gel-like structures are broken up, the viscosity decreases as the shear rate is

Table 2.1 – Typical fillers that are used to reinforce polymers

Classification	Filler	Geometry	Aspect Ratio
Partilculates	Carbon Black		
	Titanium dioxide	Spherical	≈ 1
	Calcium Carbonate	Spherical	≈ 1
	Glass Beads	Spherical	≈ 1
	Talc	Platelet	5-20
	Clays	Platelet	10-20
	Mica	Flake	25-50
Fibers	Aramid	Rod-like	50-100
	Cellulose	Rod-like	75-120
	Franklin	Rod-like	75-120
	Glass	Rod-like	50-150

further increased and starts to converge to that of the unfilled matrix at high shear rates (> 1 sec^{-1}). An example of this behavior is illustrated in Figure 2.2 [30]. In this figure, the steady shear viscosity for PS/calcium carbonate composites at various particle sizes is shown as a function of shear rate.

While the particle size exerts a major influence on the polymer melt rheology of particulate filled composites, the particle geometry can also have a significant effect [31]. Plate-like geometries, such as talc or clay, can significantly increase the viscosity relative to the incorporation of calcium carbonate or titanium dioxide fillers at low shear rates [39]. In Han's [39] experimental work, the viscosity is 2 times greater with the addition of talc particles over that of calcium carbonate fillers in a PP matrix at a concentration of 40% by weight and a shear rate of 10^{-2} sec^{-1}. This is attributed to the greater aspect ratio of the talc particles (≈ 5-10) over that of the calcium carbonate particles (≈ 1).

In addition to particle size and aspect ratio, the loading level or concentration of particles in a polymer matrix also has a significant effect on the rheology of particulate and fiber filled polymer melts. Typically, the addition of particulates and fibers increase the shear viscosity of the composite to that of the base resin at an equivalent level of shear rate or stress [27,29,30,34,35-45]. Usually, as the concentration is increased the effect of particles on the polymer melts becomes more pronounced. At low concentrations (10 % by weight or less), the addition of filler results in a small increase in viscosity, typically half order of magnitude or less, relative to the base resin. Also, a Newtonian plateau is still observed at low shear rates when the concentration is 10% by weight or below. For particulate filled composites where the particle size is below 10 microns, yield stresses are observed in the low shear rate region at concentrations higher than 10% by weight. This leads to significant increases in viscosity relative to the base resin, which can be as much as two to three orders of magnitude higher. The concentration at which one starts to observe yield stresses depends on the particle size. As particle size decreases, less concentration is required to observe yield stresses [42]. For example, for composites generated with nano-sized particles, a yield stress is observed at concentrations as low as 4% by weight. An example of steady shear viscous behavior for particle filled composites as a function of particle loading is shown in Figure 2.3. As the shear rate is increased, the effect of the particles on the shear viscosity is

minimized due to the break up of the network or gel-like structure and/or particle agglomeration that is responsible for the appearance of yield stresses [30,31,46]. At high shear rates, the shear viscosity of particulate filled melts converges to that of the matrix. Boaira and Chaffey [47] have reported this type of behavior for PP melts filled with mica particles. At high shear rates, the shear viscosity approached that of the neat PP resin due to realignment of the flaky particles into a more favorable orientation for flow. Hence, there was a greater predominance of viscous stresses over particle interactions as the shear rate was raised [31]. Shear thinning of various particulate filled systems has been observed to increase with increasing concentration of particles in the low shear rate region [27,48,49].

Sizing or coupling agents have been incorporated into both particle and fiber filled polymer melts for the purpose of reducing filler-filler interactions and at the same time improving filler-polymer bonding [50]. Addition of coupling agents has been known to significantly affect the shear viscosity of filled melts depending on how they alter the interactions between the polymer and solid additives [29,31,34,38,51]. In work performed by Suetsugu and White [29], calcium carbonate particles of various sizes were coated with stearic acid and melt blended with a polystyrene matrix. There was a significant reduction (almost an order of magnitude) in shear viscosity in the low shear rate region with the surface treated particles relative to the untreated particles. With decreasing particle size (3 μm to 0.07 μm), the observed viscosity reduction increases. Also, a Newtonian plateau region was observed at low shear rates for all particle sizes with the exception of particles that had an average diameter of 0.07 μms, which was not observed for untreated calcium carbonate particles. For this system, the reduction of shear viscosity was attributed to reduction in the strong particle-particle interactions between the calcium carbonate particles and enhanced compatibility between the polymer and filler leading to a reduction in particle agglomeration. The reduction of shear viscosity in the low shear rate region in the presence of a coupling agent has also been observed for composites of PP/talc [51] and PP/MgOH [6]. In both studies, less surface treatment was required to break up agglomerates, due to particle-particle interactions, as the particle size increased. For other systems the shear viscosity has actually increased

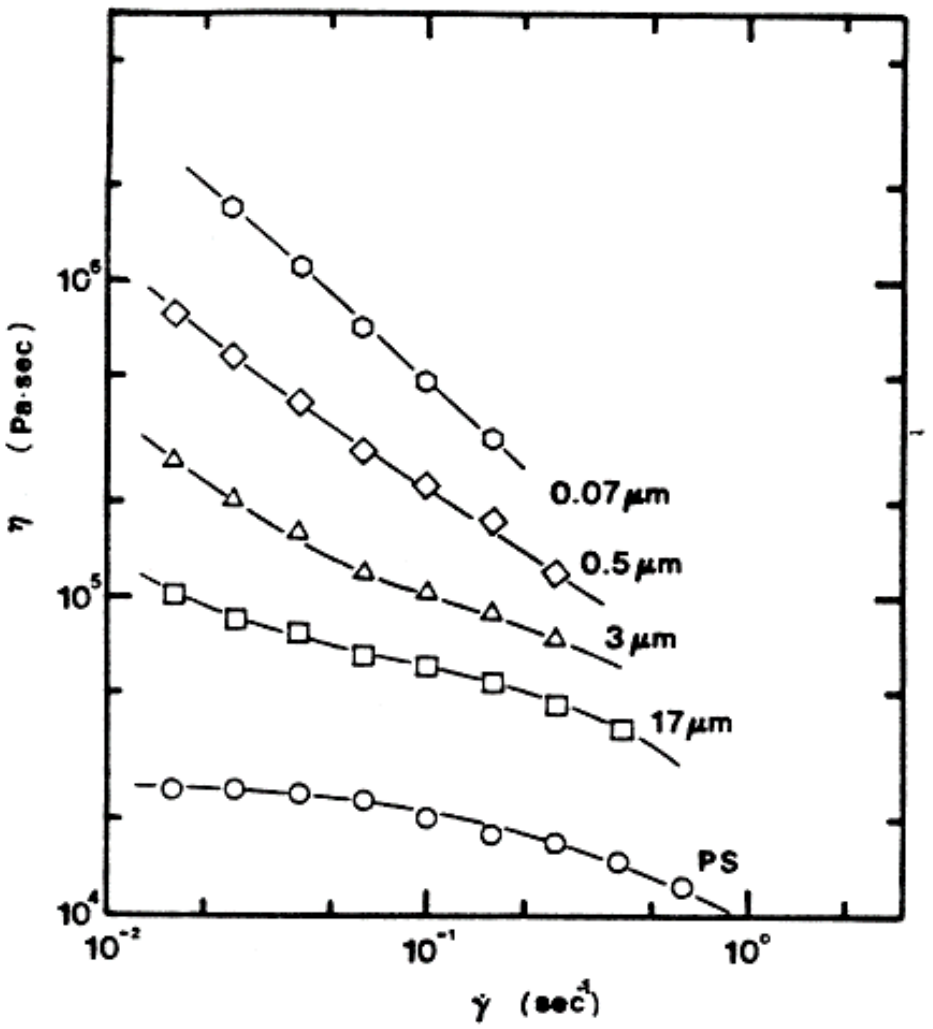

Figure 2.2 Steady shear viscosity of PS/$CaCO_3$ compounds ($\phi = 0.3$) as a function of shear rate at 180°C [29].

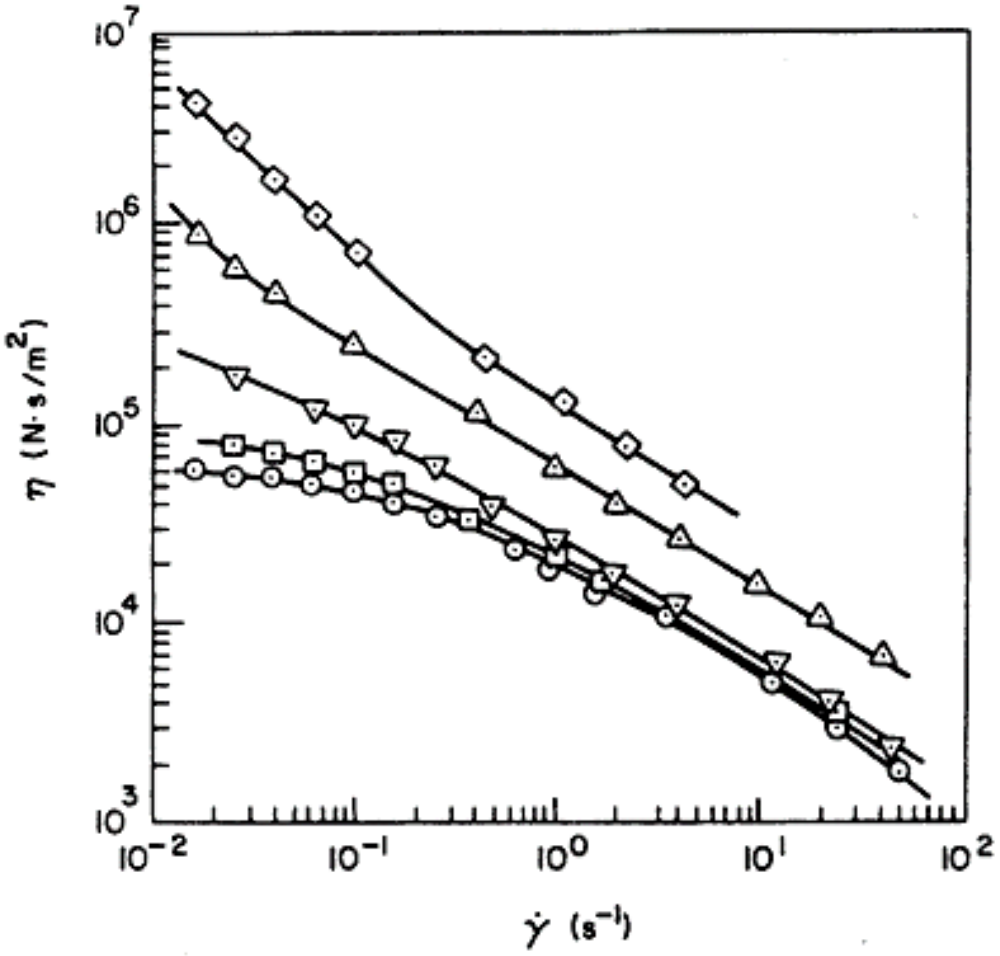

Figure 2.3 Steady state viscosity as a function of shear rate for carbon black filled polystyrene at 170°C [46].

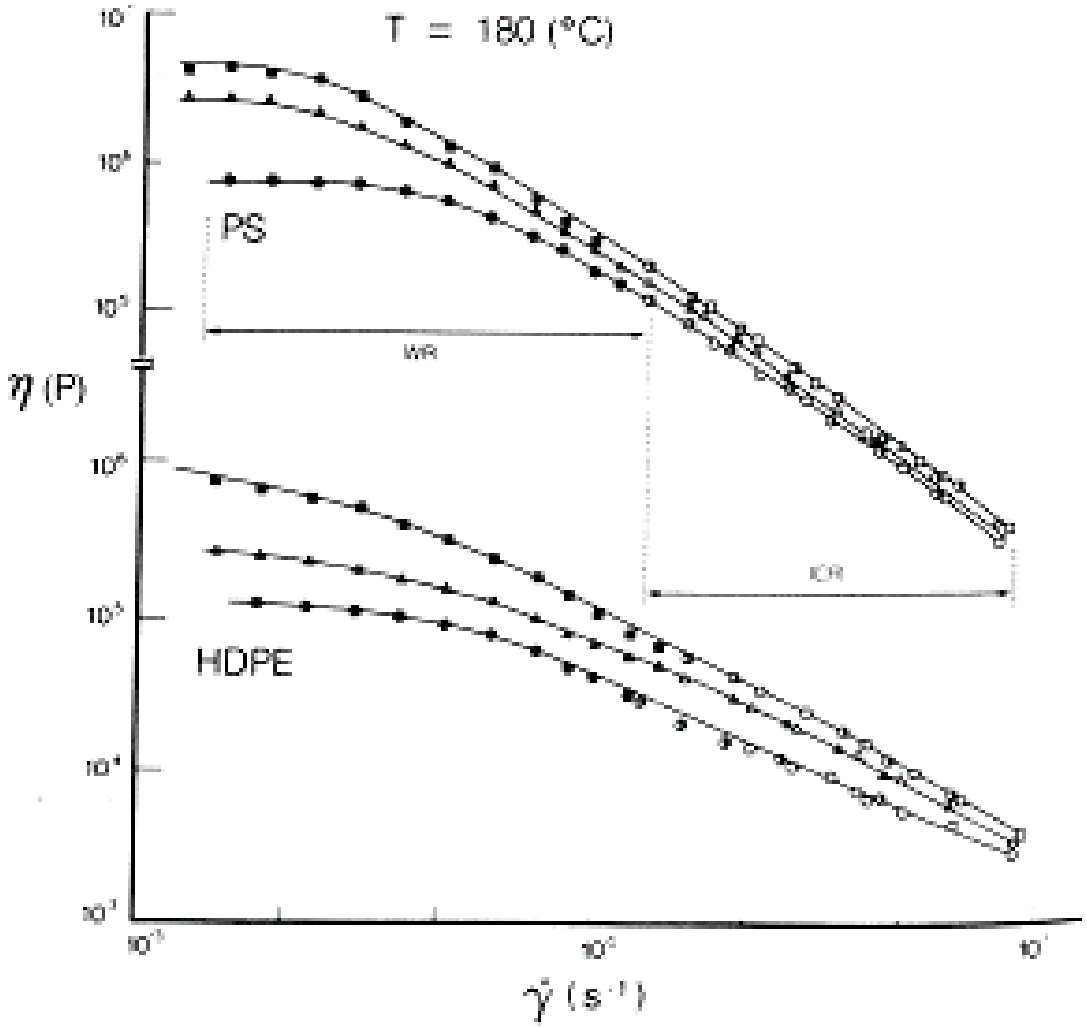

Figure 2.4 Flow curves for PS (upper diagram) and high-density PE (lower diagram) at 180°C filled with 0 (circle), 20 (triangle), and 40 (square) wt % of glass fibers [30].

with the addition of coupling agents [39,52]. For these systems, the increase in viscosity was attributed to enhanced adhesion between the filler and polymer.

For particles with an average particle size that exceeds 10 microns such as fibers and glass beads, strong particle-particle interactions are not observed and therefore, yield stresses are not observed at low shear rates. Thus, fiber filled systems exhibit Newtonian viscosities at low shear rates ($< 10^{-1}$ sec^{-1}), and a decrease in viscosity is observed as the shear rate is increased. Unlike with particulates, the particle size does not significantly influence the shear viscosity as long as it exceeds 10 microns in diameter, but the aspect ratio has a significant effect particularly at low shear rates (< 1 sec^{-1}). In a study by Cznarecki and White [28], the effect of fiber length was observed. They were able to reduce the fiber length, hence the aspect ratio, by increasing the mixing time of the fibers and the matrix in the compounding equipment. Increasing shear viscosity was observed at low shear rates with increasing aspect ratio, while maintaining a constant fiber concentration. Ramazani and Grmela [53] also reported an increase in shear viscosity with an increase in aspect ratio but the results were not shown.

As with particulate filled systems, the shear viscosity of fiber filled composites is strongly effected by the particle loading or concentration. As the concentration of fibers increase, the shear viscosity increases significantly at low shear rates (< 1 sec^{-1}) relative to the base resin, while at high shear rates the shear viscosity converges to that of the unfilled matrix [53-59]. In a study by Burrel [34], almost an order of magnitude increase in the zero shear viscosity was observed for PS and HDPE composites filled with 40% by weight of glass fibers (see figure 2.4). The higher viscosity at low shear rates has been attributed to the formation of a loose structure of fibers that are easily broken down by flow at high shear rates [2]. An alternate theory is that at low shear rates the matrix flows in between stationary fibers, which greatly impedes the flow of the polymer chains, and hence, leads to a large increase viscosity. At high shear rates, the fibers realign themselves and orient in the flow direction, which greatly reduces the resistance to flow of the polymer matrix. Thus, the viscosity converges to that of the matrix at high rates of shear.

Typically, sizing or coupling agents are added to fiber filled systems for the purpose of improving the mechanical properties by promoting better adhesion between

the fiber and the matrix. Generally, surface treated fibers lower the shear viscosity of fiber reinforced composites relative to untreated fibers [60-62]. The lowering of the viscosity can be attributed to enhanced compatibility (better adhesion) between the filler and the matrix, or lowering the interfacial tension between the phases.

2.2.2.2 Transient Viscous Behavior of Filled Polymer Melts

Very little research has been performed on the transient shear viscosity of particulate and fiber filled systems. For particulate filled systems particle size, particle loading, surface treatment, and rate of deformation have been shown to effect the transient shear viscosity [28,31,35]. In a study by Montes and White [36], the transient shear viscosity of rubber-carbon black compounds was investigated as a function of particle size and particle loading. At low shear rates (< 0.1 sec^{-1}), the transient shear viscosity increases monotonically until it reaches a steady value. At shear rates above 0.1 s^{-1}, an overshoot appears before the steady value is reached. Also, the time it takes to reach a steady state shear stress decreases with increasing shear rate. The magnitude of the overshoot and the time required to reach a steady value was dependent on both particle size and loading. As the average particle size of carbon black was reduced from 0.45 μm to 0.2 μm, the magnitude of the overshoot increased by about 30% at a shear rate of 1.54 sec^{-1}. Furthermore, the time it took to reach steady state increased. Also, as the particle loading increased while holding the average particle size constant, the magnitude of the stress overshoot and the time it took to reach steady state increased. At a particle size of 0.2 μm, the magnitude of the overshoot increased by about 25% and the time it took to reach steady state increased by 900 seconds at a concentration of 30% by weight relative to that of the matrix. Suh and White [37] observed similar transient behavior with PP/talc composites. The magnitude of the overshoot was much more pronounced as the loading level of talc increased. Also, the time it took to reach a steady state value increased by over 300s when the talc loading was increased by 40% relative to that of the matrix. In another study, Wang and Wang [38] investigated the transient shear behavior of calcium carbonate filled PP as a function of loading level for both surface treated and untreated particles. For their experiment, the shear rate was maintained at

0.05 sec^{-1}. At low concentrations of calcium carbonate particle (< 12% by weight), no stress overshoot was observed. At concentrations of 20% by weight a stress overshoot was observed, which increased with increasing concentration. The time it took to reach a steady value of stress increased with increasing concentration but it was much more pronounced once a stress overshoot was observed ($\geq$ 20% by weight). With the addition of a titanium coupling agent, the magnitude of the stress overshoot was reduced significantly and was more effective in reducing the stress overshoot as the concentration of calcium carbonate particles increased. The reduction in the overshoot was attributed to a decrease in particle-particle interactions. At a 30% by weight loading of calcium carbonate, the magnitude of the stress overshoot was reduced by 35%. The time it took to reach a steady value of stress was reduced by the addition of the coupling agent at a concentration of 30% by weight, but there was no significant reduction in the time it took to reach a steady value of stress at concentrations below 30% by weight. Based on the experimental observations, it has been hypothesized that the observed overshoot for particulate filled composites is due to a complete breakdown of the filler network or and/or agglomerated particles.

Fiber aspect ratio, fiber concentration, and rate of deformation have been found to affect the transient shear viscosity of fiber filled composites. In a study performed by Ramazani et al. [53], glass fibers were added to a suspension of 50% polyacrylamide and 50% glycerol/water mixture at fiber loadings of 10% and 15% by weight. Unlike with particulate filled composites, an overshoot is observed at low shear rates (< 0.1 sec^{-1}), which decreases with increasing shear rate. However, the time it takes to reach a steady state stress value decreases with increasing shear rate. This behavior is also observed for particlulate filled composites. The magnitude of the stress overshoot and the time it takes to reach a steady state shear stress increases as the fiber loading is increased. For particulate systems, the observed overshoot is attributed to the breakup of a gel-like structure formed by strong particle-particle interactions, but fibers are non-interacting particles so such a network structure is not formed. Instead, the observed overshoot is attributed to the initial fiber orientation of the material. As the shear rate is increased, the fibers orient in the flow direction, which reduces the resistance to flow. Hence, the observed overshoot decreases with increasing shear rate. Ramazani et. al. [53] also

showed that if a sample was pre-sheared before performing the rheological test than there was no observed overshoot before reaching a steady viscosity value. This was attributed to reorientation of the fibers in the flow direction before the test was performed. They also reported that an increase in aspect ratio increased the observed overshoot and the time required to reach a steady value but no results were shown. In a paper by Ausias et al. [58], similar transient viscous behavior was observed for PP melts filled with short-glass fibers at concentrations of 20% and 30% by weight. The average aspect ratio of the fibers was reported to be 25. The magnitude of the observed overshoot increased by about a factor of two with a 10% increase in fiber concentration and the time required to reach a steady value of stress increased by about 100 seconds. Once again, the observed overshoot was attributed to reorientation of the short-glass fibers.

2.2.3 Elastic Behavior of Filled Polymer Melts

2.2.3.1 Normal Stresses

The primary normal stress difference (N_1) of polymeric melts is greatly influenced by the addition of solid fillers especially in regard to which class of filler is added: particulates or fibers. The response of these materials depends on many variables, which include particle size and aspect ratio, concentration, and the rate of deformation. Understanding how N_1 is affected by these many variables has major significance because it is related to the state of orientation of the composites. The angle of orientation,θ, is related to N_1 by:

$$\theta = \frac{1}{2}\tan^{-1}\left(\frac{2\sigma}{N_1}\right) \qquad (2.1)$$

where σ is the shear stress [63]. For θ equal to 0^o, the particles are perfectly aligned in the flow direction and θ equal to 90^o, the particles are perfectly aligned in the transverse direction. Therefore, an increase in N1 at an equivalent level of stress indicates a higher state of orientation in the flow direction.

Particulate filled composites have qualitatively different N_1 behavior than their fiber filled counterparts. The addition of small particles (< 5 μm) reduces N_1 relative to

that of the matrix at an equivalent shear rate or stress [28,29,46]. N_1 also increases as the shear rate is increased (see figure 2.5). In a study by Czarnecki and White [28], particles of various sizes and morphologies were added to a PS matrix at a concentration of 20% by weight. As the particle size decreased, there was a corresponding decrease in N_1 at an equivalent level of stress. The addition of glass beads, which had a particle size on the order of 10 μm, only reduced N_1 slightly (< 5%). On the other hand, carbon black, titanium dioxide, and calcium carbonate particles that had particle diameters of 0.045 μm, 0.18 μm, and 0.5 μm, respectively, reduced N_1 by about almost 50% relative to that of the matrix. A further reduction in N_1 relative to the matrix was shown as the aspect ratio of the particles increased. For mica particles with an aspect ratio of 45, there was an order of magnitude reduction in N_1 relative to that of the matrix. Reduction in N_1 with a decrease in particle size was also shown for calcium carbonate particles suspended in a PS matrix [46]. With a decrease in particle size from 17 μm to 3 μm, there was about a 30% reduction in N1 at an equivalent stress. The reduction in N_1 for particulate filled systems is attributed to the appearance of yield stresses or increased system modulus [28]. As the particulate concentration increases, N_1 decreases. This was shown by Lobe and White [46] for composites consisting of carbon black particles in a PS matrix at various loadings of carbon black. There was almost a 60% reduction in N1 relative to the matrix when 20% by weight of carbon black particles were added to the PS matrix. As with viscosity, surface treatments can either increase or decrease the primary normal stress difference depending on the materials used [27,62,64].

Conversely, the addition of fibers to a polymer matrix increases N1 relative to that of the matrix at an equivalent shear rate or stress [53,54,57]. Just like in the case of particulate filled systems, N_1 increases with increasing shear rate (see figure 2.6). The increase of N_1 with increasing shear rate is attributed to an increase in orientation of the fibers and polymer chains in the flow direction. N_1 increases with fiber aspect ratio and concentration. Czarnecki and White [28] showed that the addition of glass and aramid fibers to a PS matrix at a concentration of 20% by weight increased the primary normal stress difference by a factor of two at an equivalent stress relative to the unfilled resin. Addition of cellulose fibers also increased N_1 but to a lesser effect due to a lower aspect ratio than that of the glass and aramid fibers. Kamal and Mutel [57] as well as White et

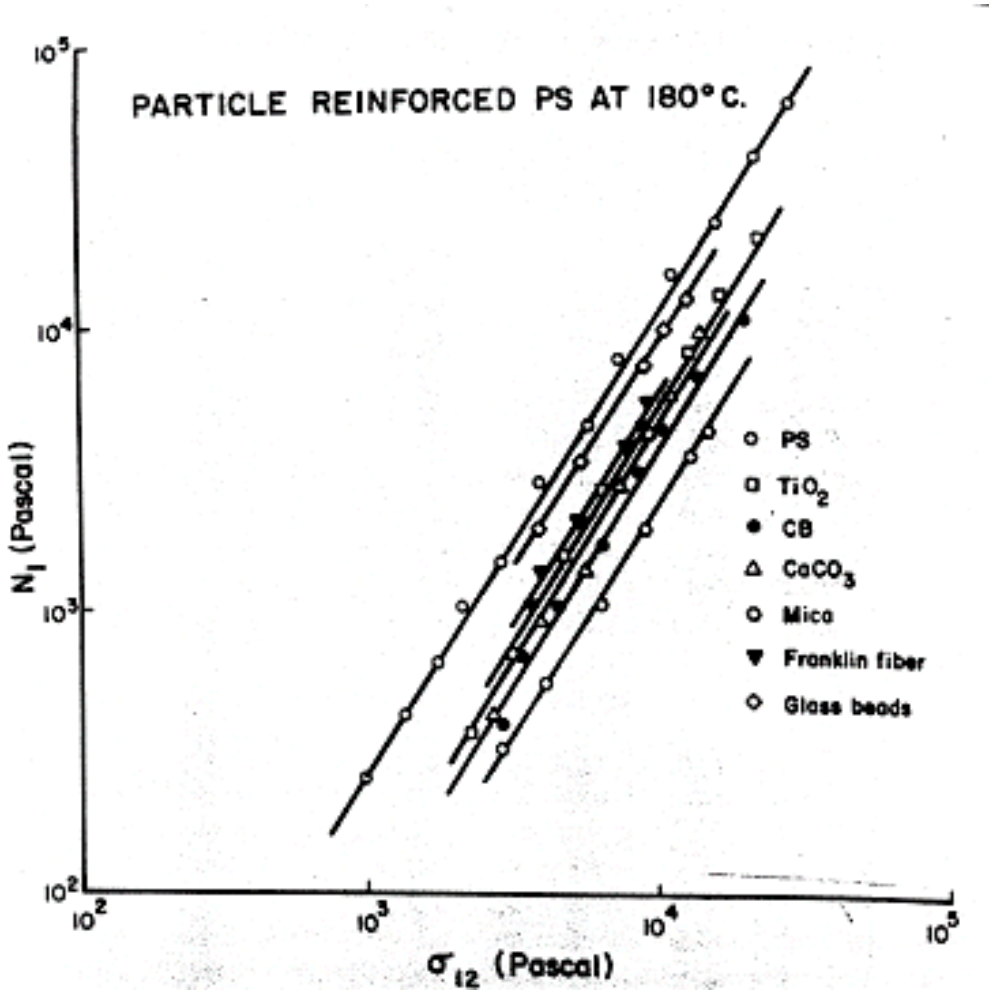

Figure 2.5 N_1 vs. σ_{12} for PS at 180°C reinforced with $\phi = 0.20$ of various particulate reinforcements [28].

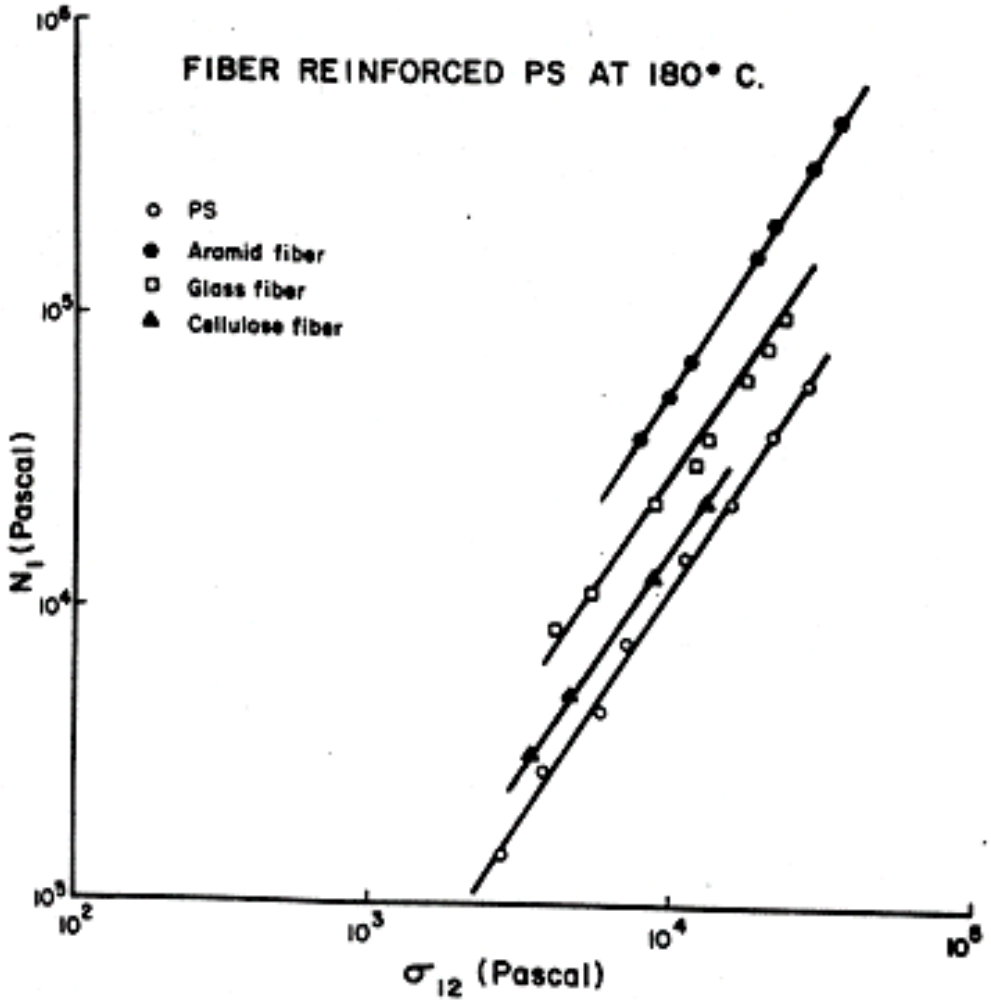

Figure 2.6 N_1 vs. σ_{12} for PS at 180°C reinforced with $\phi = 0.20$ of various fiber reinforcements [28].

al. [28] have shown that N_1 increases with an increase in fiber concentration for short-glass fiber filled PP and PC systems. For both the PP/GF and PC/GF system, there was almost an order of magnitude increase in N_1 relative to the matrix at a glass fiber loading of 40% by weight. N_1 has also been reported to increase with an increase in aspect ratio [53,58].

Very little data has been reported for the behavior of N_1^+, normal stress growth at the start up of steady shear flow. In a study by Han et al. [44], variations in N_1^+ of PC/clay nanocomposites were performed. For this system, there were no reproducible signals for N_1^+ during the transient shear flow experiments. This was attributed to the inelastic PC matrix that exhibited Newtonian behavior over the entire range of shear rates tested (0.04 –100 sec^{-1}). N_1^+ of short-glass fiber filled composites has been investigated by Ramazani et. al [53] and Mutel [65]. As in transient shear viscosity, η^+, an increase in fiber concentration and fiber aspect ratio results in an increase in an overshoot of $N1^+$ before reaching a steady value, which is attributed to fiber reorientation effects. With an increase in fiber concentration from 10% to 15% in a 50% polyacrlymide and 50% glycerol/water mixture, the stress overshoot increased by about 25%.

2.2.3.2 Storage Modulus

The elastic nature of filled polymer melts has also been investigated by determining the storage modulus (G') as a function of frequency. For particulate filled composites, much like the shear viscosity, particle concentration, particle size, surface treatments, and rate of deformation effect the storage modulus. The presence of yield stresses in particulate filled systems give rise to large increases in G' relative to that of the matrix at low frequencies and a plateau in the storage modulus is observed at high concentrations of particles (see Figure 2.7) [31,35,37,38,42,43,46]. Lobe and White [46] have shown as much as a two order of magnitude increase in storage modulus relative to a PS matrix when 25% by weight of carbon black particles were added at frequencies of 10^{-1} sec^{-1} or below. Typically, at low concentrations (< 15-20%), the storage modulus increases in the low frequency region but a plateau in the modulus is not observed. As the concentration of particles increase, the plateau in the storage modulus becomes

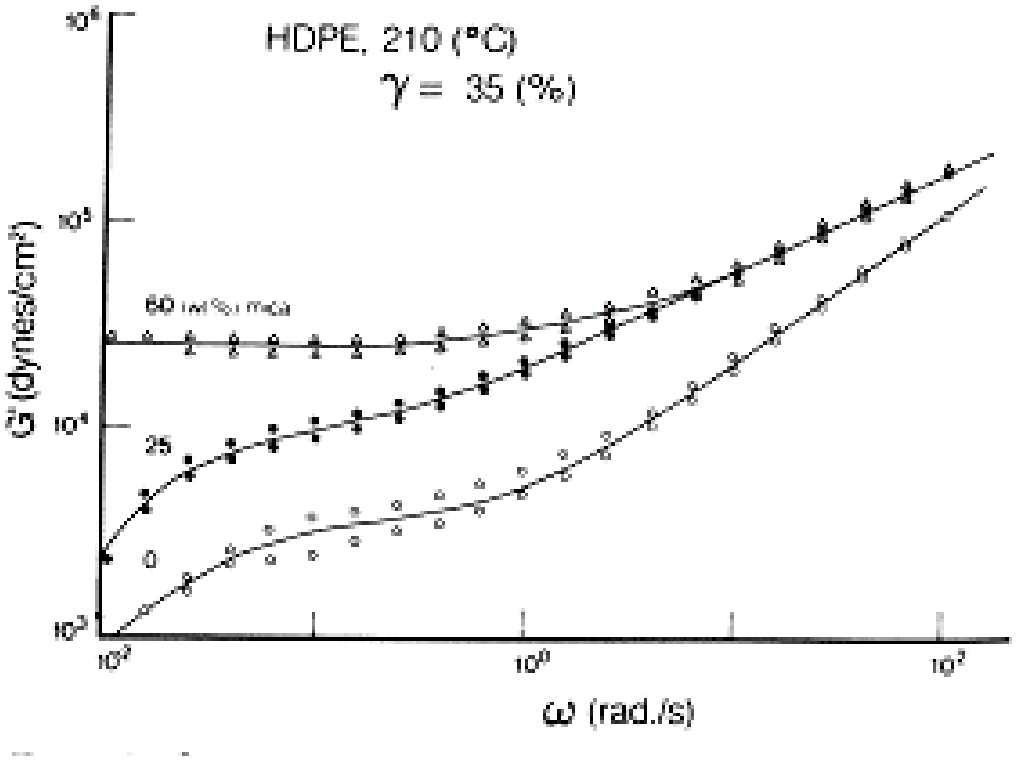

Figure 2.7 Storage modulus vs. frequency for high-density PE at 210°C and strain of 35%, filled with 0, 25, and 60 wt. % of mica [30].

clearly visible. One should note that the concentration at which one starts to observe the plateau in G' depends on the particle size, because it is attributed to the formation of agglomeration of particles and the formation of a gel-like structure. As with the steady shear viscosity for particulate filled composites, a decrease in the particle size leads to an increase in storage modulus at low frequencies, which becomes more evident as the particle loading increases [31,35,37]. In a study by Suh and White [37], the storage modulus increased by about 50% when the average particle size of talc particles was reduced from 9 μm to 2 μm in a HDPE matrix at a loading of 20% by weight at low frequency. When the talc loading was increased from 20% to 40% by weight in the same HDPE matrix, the difference in G' was further increased by an order of magnitude when the average particle size was reduced from 9 μm to 2 μm. Surface treatments aid in reducing the observed increase in storage modulus with the addition of particulates. This is attributed to a reduction in the particle-particle interactions. At high frequencies ($\omega > 1$ sec^{-1}), the storage modulus of particulate filled composites converges to that of the neat resin.

Fiber concentration, fiber aspect ratio and rate of deformation influence the storage modulus of fiber filled composites [53,54,56,57]. The storage modulus increases with an increase in fiber concentration and aspect ratio at low frequencies. As the frequency is increased, G' converges to that of the unfilled resin. In a study by Greene and Wilkes [56], short and long glass fibers were added to polypropylene, nylon 66, and polycarbonate resins at various fiber loadings. In all cases, the storage modulus increased with an increase in fiber concentration at low frequencies. A plateau in the storage modulus was observed when the loading of glass fibers was above 30% by weight. For the PP/GF composites at a fiber loading of 30% by weight and a frequency of 10^{-1} sec^{-1}, the long-glass fibers increased G' by about five times that of the base resin, whereas, short-glass fibers only increased G' by about three times. Therefore, the storage modulus increases with an increase in aspect ratio in the low shear rate region.

2.2.3.3 Die Swell or Extrudate Swell

Measurements of extrudate diameter as a polymer leaves a capillary have been used to study melt elasticity. For unfilled polymer melts, extrudate diameter is always

greater than that of the capillary and the ratio of the two is known as the die swell or extrudate swell coefficient (B). Both particulate and fiber filled systems reduce the die swell relative to the unfilled matrix [30,46,66-68]. The observed reduction in die swell is enhanced further with increasing concentration of filler. One would expect that a reduction in die swell with increased concentration might just be due to a dilution effect. However, Newman and Trementoozi [69] found a more rapid decline in die swell than a simple dilution of a polymer would indicate for systems of styrene acrylonitrile (SAN) filled with glass beads and calcium silicate. For SAN/GB and SAN/$CaSiO_3$, the die swell reduced by a factor of three with 30% by weight of glass beads and a factor of 2 with $CaSiO_3$ particles. Han [67] also found this to be the case for PP/talc composites. The addition of talc was found to reduce the entrance pressure drop in capillary flow (Bagley correction) and die swell compared to the unfilled PP resin. Lobe and White [46] also observed a reduction in die swell with an increase of carbon black concentration in a PS matrix. The die swell was reduced by 20% with the addition of 20% by weight of carbon black particles at a shear rate 10^3 s^{-1}. They also found that the die swell increased with increasing shear rate and the observed reduction in die swell with particulate concentration was more pronounced at high shear rates ($> 10^2$ s^{-1}). White and Oyanagi [70], Wu [71], and Crowson and Folkes [72] have shown similar observations with fiber filled composites.

The reduction of B with the addition of particulate and fiber fillers as the particle loading increases has been attributed to a hindrance of polymer chain mobility. As the polymer melt leaves the capillary, the polymer melt swells due to recovery of stored elastic energy, but the presence of the filler hinders chains from moving to the relaxed state they would attain in the unfilled melt. Lobe and White [46] proposed that the gel-like structure formed by strong particle-particle interactions are broken up by the high shear rates imposed during capillary flow. When the stresses induced by flow are removed, the gel-like structure can be easily reformed, which leads to a reduction in die swell. In other words, the hindrance of stress relaxation with the addition of particles and fibers leads to the reduction in die swell. If this is true, than particle size should also have an influence on the die swell of filled polymer melts.

2.2.4. Stress Relaxation of Filled Polymer Melts

2.2.4.1 Stress Relaxation after Cessation of Steady Shear Flow

The stress relaxation after cessation of steady shear flow, η^-, of both particulate and fiber filled composites are qualitatively the same but fibers seem to hinder polymer chain relaxation to a greater extent than particulate fillers. In a study performed by Pisipati [69], mineral and glass fiber mixtures were added to Nylon 6,6 at different mineral/glass fiber ratios while maintaining total particle loading at 20% by volume. It was found that the relaxation time of these composites decreased with an increase in shear rate. Furthermore, the relaxation time decreased with increasing mineral concentration (decrease in glass fiber content). Therefore, the glass fibers seemed to hinder the relaxation of the Nylon 6,6 to a greater extent than the mineral filler. The authors note that although the actual relaxation times are quite short, the difference between the two fillers is marked. Montes and White [36] have also performed stress relaxation studies on rubber/carbon black materials. They found that the stresses relaxed to zero when the concentration of the rubber particles was at 10% by weight or less. At concentrations above 10% by weight, the stresses relaxed to a finite value, which increased with increasing concentration. At a shear rate of 0.135 s^{-1}, the magnitude of the residual stress was an order of magnitude higher with an increase in carbon black loading from 20% to 30% by weight. They also found that the residual stress and relaxation time decreased with increasing shear rate.

2.2.4.2 Stress Relaxation after a Sudden Shearing Displacement

It has been found that the relaxation modulus, G(t), of both particulate and fiber filled composites are qualitatively the same. G(t) of particulate and fiber filled systems increase with increasing particle loading. Lobe and White [46] determined G(t) for a PS/carbon black composite system at various particle loadings. They found about an order of magnitude increase in G(t) when 25% by weight of carbon black particles were added relative to that of the unfilled PS resin at short times (< 1 sec). Furthermore, at

concentrations of 20% and 25% by weight of carbon black particles G(t) decreased to a finite value at long times (> 500 secs). The finite value at long times was about an order magnitude larger for the composite with the larger particle loading. Also, G(t) decreases with time at a much slower rate with an increase in loading. Utracki et. al. [30] have also shown similar behavior for mica and short-glass fiber filled PP composites. It was also reported that an increase in aspect ratio increased G(t) of the mica and short-glass fiber systems. As expected White et al. [36] have also shown that a reduction in particle size increases G(t) of rubber/carbon black materials. There was a 50% increase in G(t) at short times (< 1 sec) when the particle size decreased from 0.45 μm to 0.02 μm.

2.2.5 Elongational Flow of Filled Polymer Melts

The elongational flow of filled polymer melts has received little attention throughout the years. White et al. [29,37,46,73] has performed all reported data for elongational flow of filled polymers. As with steady-state shear viscosity, the elongational viscosity is dependent on particle size and aspect ratio, particle loading, surface treatment, and rate of deformation for filled polymer melts. Lobe and White [46] studied the effect of elongation rate and particle loading for PS/Carbon Black compsoite systems. For the PS matrix, the elongational viscosity was constant at low elongation rates ($E < 0.0063\ sec^{-1}$) and became unbound at higher rates of deformation. Thus the PS matrix exhibited strain-hardening behavior. With the addition of carbon black the elongational viscosity increased with increasing particle loading at an equivalent elongational rate. At an elongation rate of $0.0063\ sec^{-1}$, the steady state elongational viscosity increased by a factor of 20 at a particle loading of 20% by weight and a factor of 100 with only a further addition of 5% (25% by weight total) relative to the PS resin. Unlike with the PS matrix, constant elongation viscosities are achieved and that the values decrease with an increase in deformation rate. Suh and White [37] also observed similar behavior with PP/talc composites. However, in the case of PP/talc composites the samples would break before a steady elongational viscosity value was reached. This was most likely due to reorientation of the talc particles in the flow direction as the sample was being stretched or possibly by agglomeration of the talc particles.

Besides from particle loading, the particle size also affects the elongational viscosity. Suetsugu and White [29] performed viscosity measurements on PS/$CaCO_3$ composites with $CaCO_3$ particles of various sizes. As the particle size decreased from 17 to 0.07 μm, the elongational viscosity increased at a constant rate of deformation. There was a two order of magnitude increase in elongational viscosity between composites that had an average particle size of 17 μm versus an average particle size of 0.07 μm. As the rate of deformation increased the elongational viscosity decreased for all composites studied. The difference in magnitude of the elongational viscosity versus particle size is more pronounced at low deformation rates. Calcium carbonate particles were also surface coated with stearic acid. The extent of viscosity rise was reduced by the addition of the surface treatment at all rates of deformations and particle size.

The elongational viscosity of short-glass fiber filled polymer melts behaves similarly to particulate filled polymer melts [73]. As the fiber loading of filled PP melts increase, the elongational viscosity increases at an equivalent elongation rate. The extent of the increase in elongational viscosity for the fiber filled system was higher than that of the particulate filled composites. This may be attributed to the higher aspect ratio (≈ 100) over that of the small particulates that have an aspect ratio of approximately one.

In summary, the viscous, elastic, and elongational flow behavior of particulate and fiber filled polymer composites are a function of particle size, aspect ratio, concentration, and surface treatment. The addition of solid particles and an increase in aspect ratio increases the shear and elongational viscosity and of particulate and fiber polymer systems. Surface treatments can be added to reduce the particle-particle interactions and hence reduce the large increases in both the shear and elongational viscosity due to the addition of solid fillers. However, N_1, which is related to the state of orientation, increases for fiber filled systems but is reduced by the addition of particulates. Furthermore, the addition of particles and fibers increase the storage modulus for filled composites, while a reduction in die swell is observed. The reduction in die swell is attributed to the hindrance of stress relaxation due to the addition of particulates and fibers into polymer melts.

2.3 Rheological Modeling of Filled Polymer Melts

This section is concerned with theoretical predictions of the rheological behavior of filled polymer melts. Initially, theories predicting the viscosity of a particulate filled system in a Newtonian medium are described in section 2.3.1.1. The suspension viscosity for these systems depends on the volume fraction of the particulates and the geometry or shape of the filler. These models do not account for strong particle-particle interactions or shear rate dependence of the viscosity and, therefore, cannot be used to predict the viscoelastic behavior of filled polymer melts. Therefore, rheological models for particulate filled polymer melts are described in section 2.3.1.2.

The theoretical predictions for fiber filled systems are discussed in section 2.3.2. To accurately predict the rheological response of fiber filled suspensions, rheological constitutive equations must account for the orientation of the fibers due to flow and the fiber concentration. First, the different concentration regimes (dilute, semi-dilute, and concentrated) of fiber filled systems are described in section 2.3.2.1. This is followed by the modeling of the evolution of fiber orientation in the three concentration regimes (section 2.3.2.2). Once the evolution of fiber orientation is known, then its contribution to the flow behavior of the fluid must be determined. This is accomplished by rheological constitutive equations derived for fiber filled systems. These constitutive equations and their predictions for the flow behavior of fiber filled suspensions are described in section 2.3.2.3 and 2.3.2.4.

2.3.1 Rheological Modeling of Particulate Filled Polymer Melts

2.3.1.1 Particulate Filled Suspensions with a Newtonian Medium

Much of the work on the rheological modeling of fluids containing particles that are of small size and aspect ratio (particulates) has been performed in a Newtonian fluid or medium. Dating back to 1905, Einstein [37] proposed that the increase in viscosity with an increase in the volume fraction for infinitely dilute hard-sphere suspensions can be approximated by:

$$\mu/\mu_s = 1 + 2.5\phi \tag{2.1}$$

where μ is the viscosity of the suspension, μ_s is the viscosity of the suspending fluid, and ϕ is the volume fraction of the hard spheres. Simha [46, 37] later extended this hydrodynamic model to rigid dumbbells, ellipsoids of rotation, and rigid rods to account for the effect that the particle geometry (aspect ratio) has on the viscosity of dilute suspensions of particles. Furthermore, Simha [46, 74] used a cell model to account for concentrated hard sphere suspensions.

There are many other models for the suspensions of particulates in a Newtonian fluid in the literature [75-77]. The most successful models for predicting the viscosity of particulate filled suspensions as a function of concentration were proposed by Simha [74] (cell model theory), Mooney [78], and Quemada [79], which are:

Simha

$$\mu/\mu_s = 1 + 2.5\lambda\phi$$

$$\lambda = 4(1-Y^7)/(4(1+Y^{10}) - 25Y^3(1+Y^4) + 42Y^5) \qquad (2.2)$$

$$Y = (2(\phi_m/\phi)^{1/3} - 1)^{-1}$$

Mooney

$$\ln(\mu/\mu_s) = 2.5\phi/(1-\phi/\phi_m) \qquad (2.3)$$

Quemada

$$\mu/\mu_s = (1-\phi/\phi_m)^{-2} \qquad (2.4)$$

where ϕ_m is the maximum packing fraction, and it is related to the volume fraction of particles at the point when the suspension viscosity goes to infinity. Equation 2.4 has been used as a semi-empirical formula to account for particles of different size and aspect ratio [81]. ϕ_m is determined by centrifugation. By comparing the three models above with experimental data for suspensions of uniform spherical particles from 16 different laboratories, Utracki [55] showed that the order of accuracy of these models from most accurate to least is as follows: Simha, Mooney, and then Quemada.

These models, however, are limited to suspensions of non-interacting particles (> 10 μm in diameter). They also lose their validity when the particle concentration of the

suspension exceeds 30% by weight and/or is close to ϕ_m [34]. Even in a Newtonian medium, non-Newtonian shear-thinning behavior has been observed with the addition of small particles at high concentrations (> 30% by weight) and shear rates (> 1 sec^{-1}). To overcome this, Barnes [34, 81] with the help of the ideas from Highgate and Whorlow [82], showed that for a particulate filled suspension where the medium behaves like a power-law fluid, the exponent in equation 2.4 could be modified by raising it to the power of *n*, the power-law index. Therefore, the exponent –2 can be replaced by –2*n*. However, this model still cannot account for particle interactions. For suspensions or polymer melts that are filled with particles that have an average particle diameter less than 10 μm, yield stresses are observed at low shear rates (< 1 sec^{-1}). The observed yield stresses are due to strong particle-particle interactions.

2.3.1.2 Modeling of Particulate Filled Polymer Melts

There are two basic approaches to formulate the rheological behavior of filled systems: a generalized continuum theory approach, and a micro-mechanics approach. Continuum-based constitutive models are based on the theory of plasticity. In this case, the physical dimensions of the system are large enough so that the fluid properties can be thought of as varying continuously in space [83]. On the other hand, micro-mechanical based constitutive models are based on molecular theory.

Bingham [84] was the first researcher to propose a one-dimensional model to account for the observance of a yield stress in a viscous fluid by using a continuum theory approach. Hohenemser and Prager [85-87] extended the Bingham model to a three-dimensional constitutive equation, which was developed by Oldryod [85-88]. The modified three dimensional Bingham model for the flow of an incompressible viscoplastic fluid is given as:

$$\underline{\underline{D}} = 0 \qquad \text{for} \qquad \mathrm{Tr}\,\underline{\underline{P}}^2 < 2Y^2 \tag{2.5}$$

$$\frac{\mathrm{Tr}\,\underline{\underline{P}}^2 - Y}{\mathrm{Tr}\,\underline{\underline{P}}^2}\underline{\underline{P}} = 2\eta\underline{\underline{D}} \qquad \text{for} \qquad \mathrm{Tr}\,\underline{\underline{P}}^2 \geq 2Y^2 \tag{2.6}$$

where

$$\underline{\underline{P}} = \underline{\underline{\sigma}} - \frac{1}{3}\left(\mathrm{Tr}\,\underline{\underline{\sigma}}\right)\underline{\underline{I}} \tag{2.7}$$

$$\underline{\underline{D}} = \underline{\nabla v} + (\underline{\nabla v})^t \tag{2.8}$$

Here $\underline{\underline{\sigma}}$ is the extra stress tensor, $\underline{\underline{P}}$ is the deviatoric stress tensor, $\underline{\underline{D}}$ is the rate of deformation tensor, $\underline{\underline{I}}$ is the unit tensor, $\nabla\underline{v}$ is velocity gradient, $(\nabla\underline{v})^t$ is the transpose of the velocity gradient, η is the viscosity, and Y is a yield function. Slibar and Pasley [85-87] extended the above model to account for thixotropy, i.e. decrease in viscosity with time, by assuming that the yield value, Y, is a function of the rate of deformation tensor and deformation history:

$$Y = Y_{\max} - \frac{\int_{-\infty}^{t} D_2 e^{-a(t-s)} ds}{\beta + \int_{-\infty}^{t} D_2 e^{-a(t-s)} ds}(Y_{\max} - Y_o) \tag{2.9}$$

where $Y_{max,}$ Y_o, a, and β are model constants and D_2 is the second variant of the rate of deformation tensor. The model constant β accounts for the decay of Y from its maximum value Y_{max}. For the above model proposed by Slibar and Pasley, the specific form of Y is in the form of an integral model. There also have been various attempts to account for thixotropic characteristics by using one-dimensional kinetic equations [86,89-92]. Problems with these models occur when trying to reformulate the one-dimension kinetic equations into three-dimensional constitutive equations. The kinetic equations are

typically in differential form, which leads to difficult non-linearities as they imply convected derivatives. Non-linear transients are better handled by using an integral model [93-95]. Thus, the model developed by Slibar and Pasley was shown to be a more successful model.

White and Tanaka [87] also developed a three-dimensional constitutive model for concentrated suspensions of polymer melts that exhibit yield stresses by combining a von Mises yield criterion with a hereditary functional. The von Mises criterion is a specified yield surface, which is described mathematically as:

$$\sqrt{\frac{1}{2}\mathrm{Tr}\,\underline{\underline{P}}^2} \le \mathrm{Y} \tag{2.10}$$

The three-dimensional constitutive equation applying the von Mises criterion and a hereditary function is defined as:

$$\underline{\underline{P}} = \frac{Y}{\sqrt{\frac{1}{2}tr\,\underline{\underline{H}}^2}}\underline{\underline{H}} + \underline{\underline{H}} \tag{2.11}$$

where $\underline{\underline{H}}$ is defined as:

$$\underline{\underline{H}} = \int_0^\infty \left\{ m_1(s)(\underline{\underline{C}}^{-1} - \frac{1}{3}(tr\underline{\underline{C}}^{-1})\underline{\underline{I}}) - m_2(s)(\underline{\underline{C}} - \frac{1}{3}(tr\underline{\underline{C}})\underline{\underline{I}}) \right\} ds \tag{2.12}$$

where $m_1(s)$ and $m_2(s)$ are memory functions, $\underline{\underline{C}}^{-1}$ and $\underline{\underline{C}}$ are the Finger and Cauchy deformation tensors, and $\underline{\underline{H}}$ is a deviatoric hereditary function of the deformation history. Specifically, White and Tanaka [62] used a single integral formulation for the memory function $\underline{\underline{H}}$ with a Maxwellian relaxation modulus. Y was defined as:

$$Y(D_2,t) = Y_f + \beta D_2 - \left[\int_0^\infty \alpha D_2 e^{-\alpha D_2 s} ds \right](\beta D_2) \tag{2.13}$$

where α and β are constants and Y_f is the final yield value. This form of the yield function accounts for thixotropy by considering a time and rate of deformation dependent yield criterion.

Experimental data obtained with calcium carbonate and carbon black filled PS melts were compared to the predictions of the model developed above by Tanaka and White [83] and modified by Suetsugu and White [60] to account for thixotropy. For these particulate filled polymer melts, the ratio of the yield stress obtained in elongational flow to that of shear flow, Ye/Ys, was experimentally determined to be between 1.7-1.8. This suggests that using the von Mises criterion ($Ye/Ys = \sqrt{3}$) to specify the yield surface is applicable for these systems. The model predictions were in fairly good agreement with the steady and transient viscosity measurements at all particle loadings (30% by weight or less) and particle sizes (0.07 μm to 17 μm) investigated. One of the model parameters α is responsible for the overshoot decay observed in the start up of steady state shear flow. As observed experimentally for the overshoot, the optimum value of α decreased with decreasing particle size of the filler and increasing particle loadings. Model predictions of steady state elongational viscosity were in excellent agreement at low deformation rates ($< 10^{-1}$ sec^{-1}) but the upturn in elongational viscosity at high rates of deformation was not predicted. Disagreements in N_1 versus σ_{12} were observed at high stresses. The theoretical predictions were larger than the experimental values in the high stress region. The value of N_1 at fixed shear stress was lower than the value predicted. The authors suggest that better agreement may be obtained if a spectrum of relaxation times is used rather than the single relaxation time used. Recently, Suh and White [37] applied this model to a PS/talc composite. The model predictions were in excellent agreement with steady shear viscosity at all rates of deformation (10^{-4} to 10^{2} sec^{-1}) and for particle loadings of 20% and 40% by weight of talc.

2.3.2 Rheological Modeling of Fiber-Filled Suspensions

2.3.2.1 Concentration Regimes of Fiber Filled Suspensions

Fiber filled suspensions can be categorized into three concentration regimes according to the volume fraction, ϕ, and the aspect ratio, r of the fibers where the aspect ratio is defined as the length to diameter ratio of the fiber [1]. The fiber suspension is considered dilute if the product of the volume fraction and the aspect ratio squared is less than one, $\phi r^2 < 1$. In a dilute suspension, the fibers are able to freely rotate. A semi-dilute suspension in which the fibers only have two rotational degrees of freedom is defined as $1 < \phi r^2 < r$. Finally, the suspension with $\phi r < 1$ is called concentrated. In this regime the fibers can only rotate about their axis of symmetry, therefore, a fiber will not be able to rotate without the cooperative motion of surrounding fibers within the suspension. Most fiber suspensions of commercial interest are in the semi-dilute or concentrated regimes.

2.3.2.2 Modeling of Fiber Orientation

To accurately predict the rheological response of fiber filled suspensions, rheological constitutive equations must account for the orientation of the fibers due to flow and the fiber concentration. In 1922, Jeffrey solved the motion of a single rigid ellipsoidal particle immersed in Newtonian medium [1, 58, 96]. This model is valid for dilute suspensions of fibers, i.e. no fiber-fiber interactions, and is considered the starting point for most fiber orientation modeling. In order to describe a population of fibers with different orientations in any fluid element, an orientation distribution function can be used [58]. An orientation distribution function provides a direct measure of all fiber orientations relative to a specified direction, but these tend to be unwieldy for numerical simulations [55, 58]. So instead, orientation tensors are typically used to represent a quantitative measure of the fiber orientation in fiber filled suspensions.
The second and fourth order orientation tensor are defined as:

$$\underline{\underline{a}}_2 \Leftrightarrow a_{ij} = \int p_i p_j \Psi(\underline{p}) d\underline{p} \tag{2.14}$$

$$\underline{\underline{a}}_4 \Leftrightarrow a_{ijkl} = \int p_i p_j p_k p_l \Psi(\underline{p}) d\underline{p} \tag{2.15}$$

where $\underline{p}$ is an orientation vector for the main axis of the fiber (defined by Jeffrey [96]) and ψ is the probability distribution function of a fiber having an alignment in the direction of the director $\underline{p}$. Folgar and Tucker [1] modified Jeffrey's model by introduction of a rotary diffusion term, which takes into account fiber-fiber interactions. The evolution of the second order orientation tensor proposed by Folgar and Tucker [1] is given as:

$$\frac{d\underline{\underline{a}}_2}{dt} = -\frac{1}{2}(\underline{\underline{\omega}} \bullet \underline{\underline{a}}_2 - \underline{\underline{a}}_2 \bullet \underline{\underline{\omega}}) + \frac{1}{2}\lambda(\underline{\underline{D}} \bullet \underline{\underline{a}}_2 + \underline{\underline{a}}_2 \bullet \underline{\underline{D}} - 2\underline{\underline{\underline{\underline{D}}}}\underline{\underline{a}}_4) + 2C_I D_2(\underline{\underline{I}} - \alpha_o \underline{\underline{a}}_2) \quad (2.16)$$

$$\lambda = \frac{r^2 - 1}{r^2 + 1} \quad (2.17)$$

where $\underline{\underline{\omega}}$ is the vorticity tensor, r is the aspect ratio, α_o is a constant equal to 2 for two-dimensional orientation, and 3 for three-dimensional orientation, λ is a fiber shape factor, and C_I is a parameter to take into account fiber-fiber interactions in the case of semi-dilute suspensions. The rotary diffusion term (term on the far right of equation 2.16) extend the applicability of this model to the semi-dilute regime. It should be noted that Brownian motion is neglected in the evolution of the orientation tensor (equation 2.16). Furthermore, the Folger-Tucker model is de-coupled from the flow behavior of the suspending medium. The parameter C_I is isotropic and independent of the orientation state [1]. According to Ranganathan and Advani [97], C_I can be related to the fiber volume fraction, fiber aspect ratio, and the fiber orientation through an averaging of the fiber spacing between the test fiber and its nearest neighbors. Fan et al. [98] used a direct numerical simulation of fiber-fiber interactions to determine the phenomenogical parameter, C_I. The short-range interactions were modeled by lubrication forces, while the long-range interaction was calculated by using a boundary element method [1, 98, 99]. The hydrodynamic force and torque on each fiber was calculated to determine the motion of the fibers. However, this model is limited to shear flow.

The evolution of the second order orientation tensor described by equation 2.16 is in terms of the fourth order orientation tensor and, therefore, a closure approximation is needed to relate the fourth order orientation tensor in terms of the second order

orientation tensor. There have been many closure approximations proposed in the literature [96,100-103]. Hand [96] proposed a linear closure approximation. The linear closure approximation can exactly represent a state of an isotropic (random) orientation distribution. Doi [100], on the other hand, formulated a quadratic closure approximation. It is exact for a perfectly aligned orientation distribution. Therefore, Advani and Tucker [102-103] formulated a hybrid closure approximation by mixing the linear and quadratic approximations. However, a hybrid closure approximation predicts a higher degree of flow-induced orientation than what is observed in any flow field.

Doi [104] developed a molecular model for concentrated isotropic solutions of rod-like molecules, which are monodisperse in molecular weight. Doi [100] then extended the theory to more concentrated systems, which could become anisotropic at rest due to excluded volume effects. Doraiswamy and Metzner [105] then further extended it to fiber-filled systems. The orientation order parameter tensor, $\underline{\underline{S}}$, which describes the molecular orientation state of the system, is defined as:

$$\underline{\underline{S}} = \int_{\underline{p}} \psi(\underline{p},t)(p_i u_j - \frac{1}{3}\delta_{ij})du_i \tag{2.18}$$

where $\underline{p}$ is a unit vector that describes the molecular orientation of a rigid rod-like molecule, $\psi(\underline{p},t)$ is the orientation distribution function, and the integral is over the surface of a unit sphere, and δ_{ij} is the Kronecker delta. By using decoupling approximations for $\underline{\underline{S}}$ and averaging over the orientation distribution function $\psi(\underline{p},t)$, the time evolution of $\underline{\underline{S}}$ proposed by Doi [100] is given as:

$$\frac{\partial \underline{\underline{S}}}{\partial t} = \underline{\underline{F}}(\underline{\underline{S}}) + \underline{\underline{G}}(\underline{\underline{S}}) \tag{2.19}$$

where $\underline{\underline{F}}$ and $\underline{\underline{G}}$ represent the effects of Brownian motion and the macroscopic flow field on the rod orientation, respectively. They are given as [100]:

$$\underline{\underline{F}}(\underline{\underline{S}}) = -6\overline{D_r}\left[\left(1-\frac{C}{3}\right)\underline{\underline{S}} - C\left(\underline{\underline{S}}\bullet\underline{\underline{S}} - \frac{1}{3}\underline{\underline{I}}(\underline{\underline{S}}^2)\right) + C\underline{\underline{S}}(\underline{\underline{S}}^2)\right] \tag{2.20}$$

$$\underline{\underline{G}}(\underline{\underline{S}}) = \frac{1}{3}\left(\underline{\nabla v} + (\underline{\nabla v})^t\right) + \left(\underline{\nabla v} \bullet \underline{\underline{S}} + \underline{\underline{S}} \bullet \underline{\nabla v} - \frac{2}{3}\underline{\underline{I}}(\underline{\nabla v} : \underline{\underline{S}})\right) - 2(\underline{\nabla v} : \underline{\underline{S}})\underline{\underline{S}} \tag{2.21}$$

where

$$\overline{D_r} = D_r\left[1 - \frac{3}{2}\underline{\underline{S}}^2\right]^{-2} \tag{2.22}$$

$$S^2 = \underline{\underline{S}} : \underline{\underline{S}} \tag{2.23}$$

Here $\overline{D}_r$ is the pre-averaged rotary diffusion coefficient for a rod-like model, D_r is the rotary diffusion coefficient for a rod-like molecule in a concentrated isotropic solution, and C is a coefficient related to the potential of the rigid rods to organize into an ordered structure. This model describes the evolution of the orientation for a rigid rod at a molecular level for highly concentrated suspensions. It accounts for the effect of Brownian motion on the distribution function, ψ, the effect of the interaction potential between rods on there Brownian motion, and the effect of the macroscopic flow field. By accounting for the Brownian motion, Doi's evolution equation for the orientation order parameter tensor must be calculated simultaneously with the velocity and stress fields of the fluid. Doi also derived a constitutive equation in terms of the orientation order parameter tensor, $\underline{\underline{S}}$. This rheological constitutive equation will be further discussed in section 2.3.2.3.

2.3.2.3 Rheological Constitutive Equations and Model Predictions

Rheological constitutive equations for fiber filled systems are used to theoretically predict the flow behavior of these systems by accounting for the contribution of the fibers to the extra stress tensor in terms of fiber orientation and fiber concentration. Batchelor [58,106] proposed a modified Newtonian constitutive equation to account for the presence of fibers in a Newtonian medium, which is defined as:

$$\underline{\underline{\sigma}} = -P\underline{\underline{I}} + 2\eta_s \underline{\underline{D}} + \phi_o \sum \underline{\underline{\sigma}}_p \tag{2.24}$$

where $\underline{\underline{\sigma}}$ is the total stress tensor, P is the isotropic pressure, η_s is the viscosity of the suspending medium, ϕ_o is the volume fraction of a single fiber in the total volume, and $\underline{\underline{\sigma}}_p$ is the contribution to the bulk stress of a single particle. $\underline{\underline{\sigma}}_p$ is the stress that is given by the integral of the viscous stress over the particle surface. The summation is carried out on all the fibers in the volume. This model is a general equation for suspensions of long particles of any shape in an isotropic Newtonian fluid. However, application of this theory to concentrated suspensions is difficult, as knowledge of the local velocity field around every fiber is required in order to evaluate the macroscopic stress.

Ausias et al. [58] modified Batchelor's constitutive model by replacing the term on the far right of equation 2.24 with an extension of Erickson's theoretical model for anisotropic fluids and an orientation distribution function introduced by Lipscomb [58]. Erickson's [58] model for anisotropic fluids is given as:

$$\sigma_p = (\mu_1 + \mu_2 \underline{\underline{D}} : \underline{p}\,\underline{p})\,\underline{p}\,\underline{p} + 2\mu_3(\underline{\underline{D}} \bullet \underline{p}\,\underline{p} + \underline{p}\,\underline{p} \bullet \underline{\underline{D}}) \tag{2.25}$$

where $\underline{p}$ is a unit vector for the main axis of the fiber, and μ_1, μ_2, and μ_3 are rheological coefficients. The evolution of $\underline{p}$ is described by Jefferey's model [96]. An orientation distribution function was introduced by Lipscomb [58] in order to remove the summation in Batchelor's constitutive equation (equation 2.22):

$$\sum \underline{\underline{\sigma}}_p = n\phi_o \int \underline{\underline{\sigma}}_p \Psi(\underline{p}, t)\, d\,\underline{p} = \phi \left\langle \underline{\underline{\sigma}}_p \right\rangle \tag{2.26}$$

where n is the number density of fibers per unit volume and ϕ is volume fraction of fibers, and $\langle \underline{\underline{\sigma}}_p \rangle$ is the orientation-averaged fiber stress. By substituting equation 2.25 into equation 2.26 and introducing the orientation tensors, defined by equations 2.14 and 2.15, one gets:

$$\phi \left\langle \underline{\underline{\sigma}}_p \right\rangle = \mu_1 \underline{\underline{a}}_2 + \mu_2 \underline{\underline{D}} : \underline{\underline{a}}_4 + 2\mu_3(\underline{\underline{D}} \bullet \underline{\underline{a}}_2 + \underline{\underline{a}}_2 \bullet \underline{\underline{D}}) \tag{2.27}$$

Lipscomb [58] calculated the above coefficients by comparing constitutive models derived by Hand [107] and Giesekus [108] to equation 2.27. In doing so, he determined that:

$$\mu_1 \approx \mu_3 \approx 0 \qquad (2.28)$$

$$\mu_4 \approx \zeta\eta_s$$

where ζ is a function of the aspect ratio. The coefficients determined by Lipscomb are valid when the aspect ratio is greater than 10. By combining equations 2.24, 2.27, and 2.28 the stress tensor becomes:

$$\underline{\underline{\sigma}} = -PI + 2\eta_s \underline{\underline{D}} + \phi\left(4\eta_s \underline{\underline{D}} + \zeta(r)\eta_s \underline{\underline{D}} : \underline{\underline{a}}_4\right) \qquad (2.29)$$

where r is the average aspect ratio of the fibers (length/diameter).

For semi-dilute suspensions, Dinh and Armstrong [53] formulated a constitutive model by reformulating Batchelor's cell theory. Their model is identical to equation 2.29 with the exception of the third term. Also, the coefficient ζ in front of the fourth term is defined as an effective drag coefficient in the Dinh-Armstrong model, which depends on the fiber concentration and the spacing of the test fiber with its nearest neighbors. It can be shown that the third term is much smaller than the fourth term in equation 2.29. Therefore, Erickson's model and Dinh-Armstrong's model qualitatively predict the same flow behavior for dilute and semi-dilute fiber-filled suspensions. Other limitations of these models are that the particles must remain non-interacting and large enough so that Brownian motion can be neglected.

As discussed in section 2.3.2.2, Doi's molecular theory was extended by Doraiswamy and Metzner [107] to predict the rheological behavior of fiber-filled systems. The rheological constitutive model for the extra stress tensor, σ, in terms of S, which is given as:

$$\underline{\underline{\sigma}} = 3ck_BT\left[\underline{\underline{S}}\left(1-\frac{C}{3}\right) - C\left(\underline{\underline{S}}\bullet\underline{\underline{S}} - \frac{1}{3}\underline{\underline{I}}(\underline{\underline{S}}^2 + C\underline{\underline{S}}(\underline{\underline{S}}^2)\right)\right] + \frac{Ack_BT}{2D_r}\underline{\nabla v}\bullet\left(\left(\underline{\underline{S}}+\frac{1}{3}\underline{\underline{I}}\right)\left(\underline{\underline{S}}+\frac{1}{3}\underline{\underline{I}}\right)\right) \qquad (2.30)$$

where c is the number of rods per unit volume, k_B is the Boltzmann's constant, T is the temperature in Kelvin, and A is a coefficient, which is equal to the ratio of the diffusion coefficient of a rod-like molecule in concentrated isotropic solutions to that in dilute solutions. It should be noted that the last term in equation 2.28 was derived by applying a decoupling approximation for the fourth order moment of $\underline{p}$ and assuming uniaxial symmetry about the director [107].

2.3.2.4 Model Predictions of Fiber Filled Suspensions

In a paper by Ausias et al. [58], the transient shear viscosity of two glass-fiber reinforced polypropylenes at fiber loadings of 20% and 30% by weight were compared to the theoretical predictions of equation 2.29 and Dinh and Armstrong's model. The average aspect ratio of the fibers was measured at 25. Both models predict large stress overshoots but the model formulated by Dinh and Armstrong over predicts the magnitude of the overshoot at both glass-fiber loadings and it is more pronounced as the fiber loading increases. The model described by equation 2.29 accurately predicts the peak of the overshoot at both fiber loadings. However, for both models, the transient shear viscosity relaxes to a steady state value of viscosity at a much faster rate than what is observed experimentally. This is to be expected because the model employed is only valid for dilute suspensions where the suspension medium is Newtonian. For an average aspect ratio of 25 and a 6% volume fraction of glass fibers (20% by weight), the product of the aspect ratio and volume fraction is 1.5. This suggests that both of the PP/GF composites can be classified in the concentrated regime. Also, PP is highly viscoelastic, thus, the rheological response of the suspending medium is highly dependent on the shear rate. The magnitude of the observed stress overshoot is also predicted to increase with an increase in aspect ratio. This has also been observed experimentally [58]. The stress relaxation after cessation of flow was not reported. However, Viola and Baird [109] have shown that Erickson's model predicts instantaneous relaxation of stresses after cessation of flow, which is not experimentally observed for fiber-filled systems.

In a separate paper by Dinh and Armstrong [110], the steady shear viscosity behavior of glass filled honey suspensions was compared to their theoretical model. Three different fiber lengths were used 3.5 mm, 6.4 mm, and 12mm, respectively. Good agreement with the steady shear viscosity was observed for the suspension with the lowest aspect ratio. With an increase in the aspect ratio, the model overpredicts the steady shear viscosity. At intermediate values of shear strain, a finite normal force is predicted because of the preferred orientation acquired by the fiber. At large strains, the fibers become fully aligned in the flow direction. This reduces the tension on the fibers and the normal stresses disappear. Unfortunately, normal stress data was not reported or compared to the model due to excessive noise in the signal.

Becraft and Metzner [55] used the molecular theory of Doi for concentrated suspensions of rod-like molecules, modified by Doraiswamy and Metzner [107] to account for viscous dissipation at high rates of deformation. They employed the modified Doi's theory to predict steady shear viscosity of glass-filled polyethylene composites at concentrations of 10% and 40% by weight. Excellent agreement between the model predictions and experimental results for the steady shear viscosity were observed at high shear rates ($> 10^1$ sec^{-1}). At low rates of shear ($< 10^0$ sec^{-1}), the model predictions were still in good agreement with the experimental predictions. They also experimentally measured the coefficients of $\underline{\underline{S}}$. The coefficients of $\underline{\underline{S}}$ were experimentally determined by polishing cross sections of polymer extrudates at different fiber concentrations, which were then viewed with an optical microscope. Photographs of the images observed with the optical microscope were then analyzed numerically to compute fiber orientations and orientation distributions of the samples. Good agreement between theory and experiment was observed for S_{11}, which describes the orientation in the flow direction. However, S_{12}, which is a measure of the skewness of the orientation about the flow direction, was in poor agreement with the theory. S_{12} was experimentally shown to be approximately zero for 14 different sets of experimental data, whereas, Doi's theory significantly overpredicts this value. The theoretical prediction was thus simply incorrect. No transient or normal stress behavior was reported. However, for this model, it is expected that shear and normal stresses would not instantaneously relax to zero after cessation of flow [111].

In summary, most of the models, such as the one proposed by Ausias et al. [58] (equation 2.29), are modified Newtonian models that do not account for shear-thinning behavior, typically, observed for filled polymer systems. Furthermore, stress relaxation after cessation of flow instantaneously relaxes to zero. Therefore, these models are not useful for accurately predicting the orientation or residual stresses that develop during the cooling stage in injection molding. Therefore, these models cannot accurately predict the dimensional stability of molded parts. On the other hand, Doi's [100] molecular theory, which was extended by Doraiswamy and Metzner [87] to fiber-filled systems, does predict stress growth behavior of filled systems as shown by Wilson and Baird [111] and accurately predicts the S_{11} component of the orientation order parameter tensor, which describes the orientation in the flow direction. Further, the model should be able to account for stress relaxation of filled systems. Therefore, using an approach proposed by Wilson and Baird, Doi's molecular model modified by Doraiswamy and Metzner may be able to accurately predict the orientation and residual stresses that develop during the cooling stage of injection molding, and therefore, the dimensional stability of an injection-molded part.

2.4 Mechanical Properties of Particulate Filled Polymer Systems

This section is concerned with the mechanical properties of particulate filled polymer composites. Particulate fillers are added to polymer melts primarily to increase the stiffness or rigidity and/or reduce the cost of the blend. They have also been used to enhance the dimensional stability and the heat distortion temperature, while reducing mold shrinkage [112,113]. The tensile or flexural modulus as well as other important mechanical properties, i.e. tensile strength, tensile toughness and impact strength, of particulate filled polymer blends depends on particle size and aspect ratio, particle loading, surface characteristics and the degree of dispersion [2,31,114-119]. Typically, particulate fillers such as talc, mica, and calcium carbonate, are characterized by their small particle sizes (< 10 μm) and aspect ratios (diameter/thickness) that range from 1-45. However, in recent years, the development of nano-particles has lead to particulate fillers with even smaller particle sizes (on the order of 100-200 nanometers) and much larger aspect ratios (40-200). Therefore, the mechanical properties of micron sized

particulate filled systems with relatively low aspect ratios will be discussed in section 2.4.1, while the mechanical properties of nano-sized particulate filled systems with much larger aspect ratios will be discussed in 2.4.2.

2.4.1 Particulate Filled Polymer Systems Using Fine Particle Sizes

Particle loading and aspect ratio can significantly influence the tensile or flexural modulus of particulate filled polymer melts. Typically, with an increase in the volume fraction of particles, there is an increase in modulus [114-116]. Svehlova et al. [114] have shown that the tensile modulus of a PP/talc blend is roughly two times greater at a talc loading of 30% by weight relative to the unfilled PP matrix. However, at low particle loadings (3%-5% by weight of talc), only a 10%-20% increase in modulus was observed. Similar results were observed in mica filled PP blends [116] and calcium carbonate filled PP [117]. In the case of the PP/$CaCO_3$ composites, the modulus only increased by a factor of 1.5 (50%) relative to that of the matrix at 30% by weight of calcium carbonate, whereas, the modulus increased by a factor of three with the addition of 30% by weight of mica for the PP/Mica blend. Based on the results above, one can see that the aspect ratio or filler shape has a significant influence on the modulus of particulate filled systems. At 30% by weight of filler, the modulus decreased in the order mica > talc > calcium carbonate, which is in order of highest to lowest aspect ratio (40-45, 5-10, 1, respectively). McGenity [32] reported similar results for filled PP composites. He found that the modulus of the filled PP blends decreased in order of mica > talc > clay > calcium carbonate for volume fractions up to 20%, which is in the order of highest to lowest aspect ratio. Also, in a study by Mitsuishi [117], PP/$CaCO_3$ blends were generated with particles that were in the shape of spheres, cubes, or needles. The aspect ratio of the spheres and cubes was approximately 1 while the aspect ratio of the needles was between 5-10. He found that the modulus of the blends generated with the cubes or spheres were the same within experimental error while the blend generated with the higher aspect ratio needles was 60% greater than those generated by the spheres or cubes at a particle loading of 20% by weight.

Halpin and Tsai [117, 120, 121] developed an empirical model from the simple mixture rule to theoretically predict the modulus of particulate filled thermoplastics and was modified by Nielson [117] to include a particle packing factor:

$$E_c = \frac{1 + AB\phi}{1 - B\psi\phi} \tag{2.31}$$

where

$$B = \frac{\frac{E_f}{E_m} - 1}{\frac{E_f}{E_m} + A}$$

$$\psi = 1 + \frac{\phi(1 + \phi_m)}{\phi_m^2} \tag{2.32}$$

$A = \frac{(7 - 5\nu)}{(8 - 10\nu)}$ for spherical particles

$A = 2\frac{L}{D}$ for uniaxially oriented platelets, flakes, or fibers

Here E_c, E_f, E_m, ϕ, and ϕ_m are the modulus of the composite, modulus of the filler, modulus of the matrix, volume fraction of filler, and the maximum packing fraction, respectively. ν, L, and D are the Poisson ratio, the largest dimension of the filler, and the smallest dimension of the filler, respectively. For fibers, the L/D is the length/diameter, and for platelet or flaky fillers, the L/D is the diameter/thickness. The two assumptions of the model are that the perfect interfacial adhesion between the filler and matrix and that the filler particles are perfectly oriented in the flow direction. The model predicts that the modulus will increase with an increase in volume fraction. It also predicts that an increase in aspect ratio will increase rapidly at low aspect ratios say less than 20-25

(depends on the matrix and filler used), at which point a further increase in aspect ratio only results in a slight increase in modulus. In the study by Mitsuishi [117] mentioned above, the experimentally measured modulus for the composites generated with different shaped calcium carbonate particles were compared with the theoretical predictions of equation 2.31. Good agreement between the experimental results and theory were observed.

Particle size and degree of dispersion can also have a significant influence on the modulus of particulate filled systems. Gahleitner et al. [116] investigated the effect of particle size on the flexural modulus of PP/talc blends. The talc particle size for the generated PP/talc blends ranged from 2.2 μm to 14 μm while the talc loading was maintained at 30% by weight. The flexural modulus was observed to increase with decreasing particle size. They attributed this to an increase in relaxation time with a decrease in particle size. This allows for a higher degree of orientation to be locked into an injection molded part, and hence, higher modulus. In a separate paper by Gonzalez et al. [131], the effect of particle size and the degree of dispersion on the tensile modulus of PP/HDPE blends filled with $CaCO_3$ was investigated. In this case, the modulus increased with a decrease in particle size. They attributed this to better dispersion of the blends at the lower particle size. Particle agglomeration leads to coarser structures and a reduction in effective aspect ratio, thus, a reduction in modulus.

The effect of surface treatment on the modulus of filled thermoplastic composites has received attention in recent years [117,122,123]. Woodhams [122] found that mica increased the stiffness of PP but treatment with a bifunctional silane had no effect. Hancock [123], on the other hand, showed that a small reduction in the modulus occurred for stearate coated calcium carbonate particles in a PP matrix relative to the uncoated particles. Mitsuishi [117] also reported a slight reduction in modulus for surface treated particles relative to untreated particles of PP/$CaCO_3$ composites where the calcium carbonate particles were treated with a phosphate ester. The slight reduction in modulus has been attributed to a lubricating effect that the surface treatments have on the polymer chains. The effect of surface treatments seems to have little influence on the modulus of particulate filled polymer systems.

Unlike modulus, the tensile strength, tensile toughness, and impact strength are generally reduced with an increase in particle loading and aspect ratio. Typically, the impact strength, tensile strength and tensile toughness are significantly reduced at low particle loadings (< 10% by weight) while further addition of filler (> 10% by weight) leads to only slight reductions in their values [114,116,117,118]. For example, a 75% reduction in impact strength and a 35% reduction in tensile strength were observed with the addition of 10% by weight of mica particles in a PP matrix but at a mica loading of 40% by weight, the impact and tensile strength were further reduced by only 10% and 5%, respectively, relative to that of the PP matrix [115]. For calcium carbonate particles in a PP matrix, the impact strength and tensile strength were reduced by only 60% and 20%, respectively, at a particle loading of 40% by weight. Based on these results, one can infer that the aspect ratio has a significant influence on the strength and toughness of particulate filled polymer melts. In this case, an increase in aspect ratio reduces the strength and toughness of particulate filled polymer melts at an equivalent particle loading. There are several possible reasons for the reduction of these mechanical properties with the addition of particulates. First, an increase in particle loading allows for an increase in the number of polymer chains that can be absorbed on to the filler surface. The absorption of the polymer chains results in a shell of immobilized polymer chains around the filler particles [124]. Therefore, these polymer chains will be unable to deform under an applied load, which results in a more brittle material, and hence, a reduction in the toughness and impact strength. Secondly, agglomeration of particles significantly reduces both impact strength and toughness of particulate filled systems. The tendency of particles to agglomerate with each other increases with an increase in particle loading, especially when the polymer/matrix interactions are weak.

Particle size has a large impact on the strength and toughness of particulate filled systems. With a decrease in particle size, the tensile strength, tensile toughness, and impact strength increase as long as the presence of coarse particles or agglomeration of particles is not observed at an equivalent level of reinforcement. The impact strength of PP/talc blends at a talc loading of 30% by weight increased by 50% by reducing the average particle size of the talc from 14 μm to 2.2 μm [116]. A 30% increase in impact strength and a 20% increase in tensile toughness were observed by reducing the particle

size of calcium carbonate from 3.0 μm to 1.8 μm in filled PP/HDPE blends [118]. The increase in the mechanical properties with a reduction in particle size has been attributed to an increase in the surface area at the filler/matrix interface as well as a reduction in the average distance between the particles within the base resin [116].

Finally, the addition of coupling agents has also lead to an increase in the impact strength and tensile toughness of filled polymer systems by improving filler/polymer interactions, and hence, the degree of dispersion. Wah et al. [121] investigated the effect of a titanate coupling agent on the mechanical properties of PP/talc blends at two different talc particle sizes, 1.5 μm and 7.5 μm. It was found that the addition of titanate coupling agent improved the dispersion of the talc particles by increasing polymer/filler interactions. The increase in polymer/filler interactions results in better dispersion by reducing the aggregation of the filler. The talc with the average particle size of 7.5 μm generally promoted better filler dispersion relative to the 1.5 μm sized particles due to its larger particle size and smaller surface area. Therefore, a lesser amount of coupling agent was required to break up the formation of particle aggregates. The impact strength and tensile toughness both significantly increased with the addition of coupling agents due to the improved filler dispersion.

2.4.2 Nanocomposites

One would expect that filling polymer melts with nano-sized particles, which have average particle diameters that are an order of magnitude smaller than that of the fine particles and much larger aspect ratios, would lead to much improved mechanical properties over that of fine particles, especially at low particle loadings (< 5% by weight). Many researchers have investigated the effect of filler loading on the mechanical properties of nanocomposites [41,125-127]. Most of these studies have dealt with clay-based nanocomposites. In many cases, it has been shown that a marked increase in modulus (30%-70%) at low filler loadings (< 5% by weight) is observed relative to filled composites using fine particles due to their much larger aspect ratios (60-100 versus 5-40) as predicted by the Halpin-Tsai equations. Other factors such as increased surface area and better adhesion between that of the filler and polymer also play a role in the

improved mechanical properties when nanoparticles are used as opposed to micron-size particles. However, large improvements in the mechanical properties are only observed if the clay platelets are well dispersed and exhibit an exfoliated morphology within the polymer matrix. Due to strong particle-particle interactions, it is very difficult to achieve fully exfoliated morphology. Therefore, predicted modulus enhancements, which assume a fully exfoliated structure, by use of nano-particles are much higher than what is obtained experimentally.

The two morphologies that are observed for layered-silicate based nanocomposites can, in general, be defined as either intercalated or exfoliated. An intercalated structure results when the polymer penetrates into the galleries of the layered structure resulting in a highly ordered arrangement of alternating clay platelet and polymer layers. An exfoliated structure is formed when the layered silicates are delaminated. In this case individual silicate layers are completely dispersed in the continuous polymer matrix [125,126]. Therefore, an exfoliated structure results in enhanced mechanical properties relative to an intercalated structure due to an increase in the aspect ratio of the clay platelets. In order to achieve an exfoliated structure, it is necessary to break up the strong particle-particle interactions that are caused by small particle size and large surface area by enhancing the interactions between the polymer and filler. This can be accomplished by surface treating the clay platelets.

The mechanical properties of the polymer-layered silicates (PLS) are indicative of the morphological structure of the clay platelets. Therefore, the degree of dispersion (intercalated versus exfoliated), which depends on the polymer matrix and the applied surface treatment of the filler, influence the mechanical properties of PLS based nanocomposites. In a work done by Han et al. [41], the effect of surface treatment on the mechanical properties of PC/clay nanocomposites was investigated. The tensile modulus of the composites generated with the untreated clay platelets increased by approximately 16% relative to the unfilled PC matrix while the tensile strength remained the same at a clay loading of 4% by weight. However, the tensile modulus and tensile strength both increased considerably (75% and 40%, respectively) when the clay platelets were surface treated with a polar quaternary ammonium salt at the same level of reinforcement. The large increase in modulus and strength with the surface treated platelets was attributed to

fully exfoliated platelets. Hydrogen bonding between the carbonyl groups of the PC and the hydroxyl groups of the coupling agent resulted in the increase of the tensile properties. Typically, at low reinforcement (< 5% by weight) of conventional thermoplastic composites, the increase in modulus is relatively small (10%-30%) while the tensile strength tends to decrease. This shows that large improvements in the tensile modulus and strength can be obtained at much lower reinforcement levels relative to composites generated with fine particles as long as the nanoparticles are fully exfoliated.

Fornes et al. [127] investigated the effect of platelet loading and molecular weight on the tensile properties and the impact strength of Nylon-6/clay nanocomposites. The measured aspect ratio of the platelets dispersed in low molecular weight Nylon-6 (LMW) was approximately 120 for the entire range of clay loadings tested ($\leq$ 7% by weight) while the aspect ratio of the clay platelets was roughly 80 for the medium (MMW) and high (HWD) molecular weight Nylon-6 matrices. The tensile modulus and strength significantly increased with platelet loading for all clay loadings. At a loading of 5% by weight of clay, the tensile modulus and tensile strength increased by 65% and 30%, respectively, relative to the base resin for the HMW and MMW resin. However, at the same level of reinforcement, the modulus and strength only increased by 45% and 15%, respectively, for the LMW resin. This is an interesting result since the aspect ratio of the clay platelets was higher in the LMW resin relative to the HMW and MMW resin. By observing TEM images coupled with WAXD results of the composites, it was determined that the HMW and the MMW Nylon-6/clay composites had a greater degree of exfoliated clay platelets relative to the LMW Nylon-6/clay composite. Therefore, the higher tensile properties for the HMW and MWD resins were attributed to a higher degree of dispersion relative to the LMW resin. Impact strength of the composites was also measured. The impact strength of the HMW and MMW composites did not change with an increase in clay loading, whereas, the impact strength of the LMW composites gradually decreases with an increase in clay loading. The gradual decrease in impact strength of the LMW Nylon-6/clay composites may be due to the unexfoliated agglomerates of clay platelets as observed by the TEM images. Yoon et al. [128] reported similar results for the tensile properties of PC/clay nanocomposites as a function of platelet loading and molecular weight. However, they found that the impact strength was significantly reduced with an

increase in clay loading. Even with the addition of just 1.5% by weight of clay, the impact resistance was reduced by 95% relative to that of the base resin, PC. There are several possible reasons for the discrepancy in the impact behavior of PC and Nylon-6 nanocomposites filled with clay platelets. The main difference stems from the fact that the unfilled Nylon-6 resin is brittle in standard Izod impact tests, whereas, the unfilled PC resin remains ductile [127,128]. Addition of the clay particles leads to a rapid reduction in the ductility of the PC due to an immobilized polymer shell formed around the exfoliated platelets and/or unexfoliated agglomerates of the clay platelets.

In summary, 30%-70% increases in the modulus and strength of melt blended nanocomposites at low particle loadings (<5% by weight) are observed relative to conventional composites that are filled with fine particles due to their much larger aspect ratios and much smaller size. The increase in the modulus and strength are only observed if the silicate layers are exfoliated, and hence, well dispersed throughout the polymer matrix. Therefore, the replacement of particles in the micron size range with nanoparticles can result in a significant reduction in particle loading without a loss in stiffness and strength.

2.5 The Effect of Blending Sequence on the Morphology and Mechanical Properties of Filled Immiscible Blends

The morphological structure and mechanical properties of immiscible or partially miscible binary blends has been extensively studied for the last 40-50 years [129-146]. However, studies involving the incorporation of fillers into immiscisble binary blends and how it affects the morphology, and, therefore, the mechanical properties have been relatively infrequent [116,144,147, 149-155]. For immiscible binary blends, the composition of the components, component viscosity, the intensity of mixing, the applied flow field and compatibilization, among other factors, significantly influence the blend morphology and mechanical properties. A brief overview of the morphology and its influence on the mechanical properties of immiscible binary blends will be discussed in section 2.5.1. For ternary blends, the addition of fillers into immiscible binary blends leads to three possible morphological structures: filler particles and the minor phase are separately dispersed in the matrix (major phase), filler particles located at the interface of

the continuous phase and the dispersed minor phase, and the filler particles encapsulated by the minor. The location of the filler particles and its affect on the mechanical properties are strongly dependent on the blending sequence, intensity of mixing, and the surface treatments employed during the processing of the blends. There are two types of immiscisble ternary blends that have been investigated. The first type involves the combination of a thermoplastic polymer, an elastomer, and inorganic filler. By adding an elastomer to a thermoplastic polymer, the elongation at break and impact strength generally increases while the stiffness or rigidity decreases. The incorporation of inorganic filler is needed to account for the loss in stiffness due to the addition of the elastomer. In essence, a good balance of mechanical properties can be achieved with thermoplastic/elastomer/filler blends. The second type of ternary immiscible blends involves the blending of two thermoplastic polymers with filler. Incorporation of fillers is primarily used to increase the stiffness or rigidity and/or reduce the cost of the blend. The effectiveness of the filler in increasing the stiffness is highly dependent on how it affects the morphological structure of the blend. Therefore, the effect of blending sequence, intensity of mixing, and the surface treatments (interfacial interactions) employed during the processing of ternary blends on the location of the filler particles and hence its morphology and mechanical properties will be discussed in section 2.5.2.

2.5.1 Morphology and Mechanical Properties of Immsicible Binary Blends

The morphology of binary immiscible blends is dependent on the blend composition, viscosity ratio defined as the viscosity of the dispersed phase to that of the continuos phase, processing conditions (flow field, intensity of mixing and mixing time) and compatibillization. The domain size of the dispersed phase is affected by the phase content. Typically, as the concentration of the minor component increases, the domain size of the dispersed phase increases. This is due to greater coalescence between the droplets of the dispersed phase as the concentration increases [129-134]. The mechanical properties of the blend more reflect that of the continuous phase. As the concentration of the dispersed phase is increased, a transition zone exists where both phases can form a co-continuous phase structure. The importance of the co-continuous phase morphology

comes from the fact that there can be marked improvement in the mechanical properties, which reflect a balance in properties of both phases [135-138]. Finally, if the concentration of the dispersed phase is further increased phase inversion occurs. When phase inversion occurs, as the name suggests, the dispersed phase now becomes the continuous phase and the continuous phase is now the dispersed phase. The mechanical properties now reflect that of what was originally the dispersed phase. Mamat et al. [139] showed that at 70% by weight of ABS for blends of Nylon-6/ABS, the impact strength and elongation at break reached its peak value. At this concentration of ABS, a co-continuous morphology existed. Delimoy et. al [137] studied the phase morphology of PC/PBT blends. They showed that the domain size of the PBT phase increased with increasing concentration up to 40% by weight. A phase inversion was observed at 60% by weight of PBT. A co-continuous structure was not observed and no mechanical properties were reported. Finally, Zoldan et al. [130] showed that the domain size of EVOH increased with increasing concentration for PP/EVOH and EVA/EVOH blends. For the EVA/EVOH blends, the domain size of the dispersed phase increased from 0.5-2.0 μm to 9 um with an increase in EVOH content from 10-20% by weight.

Besides from concentration of the dispersed phase, the applied flow field can also significantly influence the domain size and shape of the dispersed phase and hence, the mechanical properties of immiscible binary blends. In an extensional flow field, such as that observed during mold filling of an injection molded part, the droplets of the dispersed phase are elongated without breaking up, and hence, oriented in the direction of flow. Whereas, for shear flow, the droplets are deformed first and then breakup once a critical deformation value is reached [130]. Benderly et al. [129] studied the morphological structure of PP/EVOH blends. They found that for injection molded parts, the bulk of the part contained spherical sized droplets for the dispersed phase while at the surface of the part, the dispersed droplets were elongated in the shape of long thread-like particles. This is caused by the fountain flow mechanism during mold filling. The deformable droplets appear to decelerate as it approaches the advancing front during mold filling and then the droplets stretch in an orthogonal direction towards the wall of the mold. The stretching generates considerable elongational deformation and, thus, as the droplets are laid up on the wall, they are rapidly solidified into a highly oriented state.

Hence, the extensional flow at the melt front leads to elongated droplets in the shape of thread-like particles at the surface of the molded part and the shear flow behind the melt front deforms and breaks up the droplets in the core. This skin/core morphology of the dispersed droplets has also been observed in many other studies [131-133]. It leads to a distribution of the mechanical properties throughout the molded part.

The development of the morphological structure during the melt blending process is also determined by the viscosity ratio, λ, defined as the viscosity of the dispersed phase relative to the continuous phase. Taylor [141,142] was the first to study the deformation and breakup of droplets in viscous fluids, which was later modified by Rumsheidt and Mason [143]. They found that the deformation and breakup of droplets within the dispersed phase could be classified into three regimes based upon λ as long as interfacial forces are not dominating over the hydrostatic forces. For λ less than 0.001, the droplets develop an ellipsoid shape without breaking and form a slender shape with pointed tips. The droplets are released at the tips due to flow. For λ on the order of 1, the droplets deform in an ellipsoidal shape and break once a critical shear rate is reached. However, if the shear rate has already exceeded the critical shear, a thread like shape is formed, which breaks into many small droplets after cessation of flow. For λ greater than 4, the droplets deform and do not break but orient into the flow direction. These models have been shown to agree qualitatively with experimental observations [129,144-146]. However, the domain size tends to be under predicted by Taylor's theory because it does not account for coalescence of the droplets. For example, the domain sizes for PP dispersed in Nylon 6 were larger than the domain sizes of Nylon 6 dispersed in PP [129]. This was attributed to the difference in λ. When PP was the dispersed phase, λ was approximately 5, whereas, λ is 0.2 when Nylon 6 is the dispersed phase. This was also found to be true for blends of Nylon-6/ABS. The ABS has a much higher viscosity than Nylon-6 [144]. Therefore, when the ABS was the dispersed phase, it was found that the domain size was larger than when the Nylon-6 was the dispersed phase. Sahnoune et al. [145] investigated binary blends of HDPE/PS. At a blend ratio of 75/25 HDPE/PS, the blend exhibited fibrillar morphology. They attributed the observed morphology to the viscosity ratio being much less 1. Typically, the tensile toughness, elongation at break, and impact properties are better for blends that have a viscosity ratio on the order of 1 due to the

deformation and breakup of the minor phase into fine well dispersed structures. On the other hand, fibrillar morphologies, which are observed for λ's much greater or much less than 1, tend to increase the modulus of immiscible binary blends in the direction of flow.

Finally, the morphological structure of immiscible binary blends can be affected by coupling agents or compatibillizers. While most polymer blends are immiscible, they can show improved mechanical properties. Hence, the term compatibility refers to immiscible blends that exhibit an improvement in the mechanical properties. In cases where this does not occur, techniques referred to as compatibllization are employed. Typically, block copolymers or graft polymers are added as coupling agents to the blends in order to improve the adhesion at the interface of the two phases, which leads to a finer dispersion of the minor phase. Sahnoune et al. [145] used a grafted triblock copolymer to improve the adhesion of HDPE/PS blends. By using the coupling agent, the tensile strength, elongation at break, and the impact strength increased but the tensile modulus decreased. This was attributed to finer dispersion of the PS phase relative to the uncompatibilized matrix. Favis [146] observed a similar result for PP/PC blends. For the uncompatibilized blend, the domain size of the dispersed phase increased with an increase in concentration of the minor phase. With the addition of a coupling agent, the domain size still increased, but was substantially less than the uncompatibilized blend. As mentioned earlier, coalescence of the droplets causes the increase in the domain size of the dispersed phase. Therefore, addition of the compatiblizer inhibits the coalescence of the droplets, which results in a reduction in domain size for the dispersed phase. The effect of coupling agents on the morphology of and hence, mechanical properties is very substantial for ternary blends where the third component is an inorganic filler.

2.5.2 Morphology and Mechanical Properties of Ternary Polymer Blends

For a filled immiscible blend, three possible morphologies may occur: filler particles and minor phase domains separately dispersed in the continuous matrix, filler particles encapsulated by the minor polymer phase, and filler particles located at the interface between the minor phase and the continuous matrix. Besides from the factors that influence the morphology, and therefore, the mechanical properties for binary blends,

filled immiscible blends are also substantially affected by the blending sequence. Though there are many factors that can contribute to the morphology and mechanical properties of ternary blends, this section will only be concerned with the effect of blending sequence, the intensity of mixing, surface treatment, and compatibilization.

The blending sequence employed in incorporating fillers with the binary blend can have a profound effect on the location of the filler particles, and hence, the morphological structure. Zheng and Li [147] investigated the effect of blending sequence for PP/Zinc-Neutralized Sulfonated Ethylene Diene Rubber (Zn-SEPDM)/$CaCO_3$ blends. For the first blend sequence (A), the Zn-SEPDM was blended with PP first and then blended with the $CaCO_3$ in a second step. Furthermore, the second blending sequence (B) involved blending the rubber with the calcium carbonate first and then blend the PP in a second step. It was found that for blend sequence B the impact strength and elongation at break was about 100% higher than that of blend sequence A at an equivalent loading of calcium carbonate for a particle loading range of 3-10% by weight. The large difference in impact strength and elongation at break was attributed to the placement of the inorganic filler within the blend. By blending the rubber with the calcium carbonate particles first, the filler became encapsulated within the dispersed rubber phase. However, by employing blend sequence A, the calcium carbonate particles and the rubber phase were separately dispersed within the continuous PP phase. Cheng et al. [148] also investigated the effect of blending sequence for ternary blends of PC/SAN/MBS, where MBS is methacrylated butadiene-styrene and the Acrylonitrile content in SAN was 25% by weight. They found that the highest impact strength was observed when SAN was blended with the MBS first. In this case, most of the modified rubber particles resided in the SAN phase, but there were still some particles at the interface between the SAN and PC phases as well as in the PC-rich phase. For the other blending sequences, the modified rubber particles were more concentrated at the interface or in the PC phase but had relatively the same impact strength (50% less than the above blending sequence). In a work by Kim and Lee [144], the blend sequencing of Nylon-6/Poly(styrene-co-maleic anhydride) (SMA)/ABS blends were investigated. It was found that blending of SMA and ABS first showed better dispersions or finer structures than blends where SMA and Nylon-6 were mixed first or for blends generated in one mixing

sequence. This was attributed to better interfacial adhesion at the interface between Nylon-6 and ABS. The mechanical properties were not reported. Finally, Benderly et al. [129] looked at the blending sequence of PP/Nylon-6 blends filled with short-glass fibers. They found that the blending sequence had no effect on the placement of the glass fibers. In all three mixing sequences, the glass fibers were encapsulated by the dispersed Nylon-6 phase. The encapsulation of the glass fibers reduced the amount of "free" Nylon-6 droplets that were dispersed in the continuous PP matrix, thus, reducing the degree of droplet coalescence. This led to the development of finer structures for the dispersed Nylon-6 phase. One would expect that the mechanical properties would increase due to the addition and encapsulation of the short-glass fibers, but they were not reported in this study.

The intensity of mixing can also have a significant affect on the morphology and mechanical properties of filled polymer blends and especially on the dispersion and attrition of the filler particles. Despite this fact, there have only been a few studies where the intensity of mixing has been investigated for ternary blends. In a recent study by Friedrich et al. [149], the morphological structure of PS/PMMA blends filled with glass spheres on the nano-size scale (250 nm) were investigated in both a single-screw extruder and a co-rotating twin-screw extruder. TEM images of the ternary blends were taken to view the morphological differences from using a single screw extruder versus the twin-screw extruder. TEM images of the blends showed that for lower intensity of mixing the nanoparticles were well dispersed and encapsulated in the PMMA phase. The encapsulation of the nanoparticles by the PMMA did not change for blends generated at a higher intensity of mixing (twin-screw extrusion). However, the domain size of the PMMA showed a marked increase with the higher intensity of mixing relative to the lower intensity of mixing. In both cases, a co-continuous morphology was observed. This suggests that at a higher intensity of mixing the mechanical properties should improve relative to a lower intensity of mixing. However, for the case of larger particles with high aspect ratios (> 1), such as mica, talc, and short-glass fibers, a higher intensity of mixing may lead to attrition of the particles and hence, a reduction in the mechanical properties relative to a lower intensity of mixing. Attrition of short-glass fibers and particulates have been shown to increase with increasing intensity of mixing for filled

polymer systems, so one would expect that this will occur for ternary blends as well [150,151]. In particular, Folkes [150] has shown that glass fibers that had an initial length of 6 mm were reduced down to an average size of 500 μm by using a co-rotating twin-screw extruder, whereas, the fibers were only reduced to 1.5 mm by use of a single-screw extruder for blends of PP/GF.

The mechanical properties of filled polymer/elastomer blends depend on the location of the filler particles within the blend. Surface treatments that are applied to filler particles and coupling agents can affect both interfacial interactions and compatibilization. Therefore, they can significantly affect the location of filler particles within a blend, and hence, the mechanical properties. For the case of polymer/elastomer binary blends, if the fillers are encapsulated by the elastomer then an increase in impact strength and elongation at break is typically observed with an increase in filler content, while the modulus and strength decrease [130, 151-153]. Encapsulation of the filler particles within the elastomeric phase acts to increase the effective volume fraction of the elastomeric phase, which results in the mechanical property changes observed above [151]. The filler particles can also be separately dispersed with the elastomer in a continuous thermoplastic matrix. In this case, the modulus and strength increase with an increase in filler content, while impact strength and elongation at break decreases. This result is typical for filled polymer melts. Qui et al. [154] investigated the mechanical properties of PP/elastomer blends as a function calcium carbonate loading level up to a particle loading of 30% by weight. They found that the modulus and strength of the blends only decreased by less than 5% with an increase in 30% by weight of $CaCO_3$ particles, whereas, the impact strength and the elongation at break increased by about a factor of 5. This was attributed to the encapsulation of the filler particles within the elastomeric phase. However, in a study by Kolarik et al. [116], unmodified and maleated PP were blended with Ethylene-Propylene (EPR) and surface treated calcium carbonate particles. Blends generated with unmodified PP exhibited higher modulus and lower impact strength relative to the blends generated with maleated PP. It was found that by using the compatibilizer (maleated PP), the phase structure was changed. With unmodified PP, the calcium carbonate particles were encapsulated by the EPR but the calcium carbonate particles and EPR were separately dispersed within the continuous PP

phase due to the compatibilizer. This is attributed to an increase in matrix/filler interaction induced by the coupling agent. Many research groups have reported similar results [151,152-154].

Incorporation of fillers into blends composed of two immiscible thermoplastic polymers is also strongly affected by surface treatments and coupling agents. Gonzalez et al. [154] investigated the influence of surface treatments on the morphology and mechanical properties of PP/HDPE blends filled with $CaCO_3$ particles. The particle loading of calcium carbonate was maintained at 30% by weight. The modulus increased by about 15% and the impact strength increased by 5% with surface treated particles relative to the untreated particles. The modulus and impact strength also increased with a decrease in particle size. SEM images confirmed that the filler particles were better dispersed with surface treatment relative to untreated particles and this lead to the increase in the mechanical properties. Ersoy and Nugay [155] evaluated the mechanical properties of PP/Nylon-6/talc blends as a function of talc loading. Maleated PP was also used as a compatibilizer. In this study, the majority of the talc particles were encapsulated within the Nylon-6 with and without compatibilizer. However, the domain size of the dispersed Nylon-6/talc phase decreased from about 15-30 μm to < 5 μm. The finer domain sizes formed by using the coupling agent were a result of better adhesion between the phases. This led to higher modulus (15% increase) and impact strength (18%) for the compatiblized blend relative to the uncompatibilized one at a talc loading of 10% by weight.

In summary, mechanical properties of filled immiscible blends is highly dependent upon the morphology. Several possible morphologies can occur, which depend on the location of the filler particles: encapsulated in the minor phase, separately dispersed with the minor phase in the continuous major phase, and between the interface of the minor and major component. The location of these particles can be affected by blending sequence, the intensity of mixing and surface treatments, which in turn affects the mechanical properties. Improved impact resistance has been observed when filler particles are encapsulated within the dispersed phase while the modulus tends to increase when the filler particles are separately dispersed within the continuous phase. Further, improvements in the mechanical properties can also be achieved by improving the

interfacial adhesion of the phase and promoting better filler/matrix interactions. Finally, an increase in the intensity of mixing can lead to co-continuous morphological structures, which have been shown to greatly enhance the properties of binary blends, but may also lead to severe attrition of the filler particles. The aspect ratio of the fillers is significantly reduced by attrition and hence, the increased stiffness or rigidity due to addition of the fillers is lost.

2.6. PC/PBT Blends

Blends based on polycarbonate (PC) and poly[butylene terephthalate] (PBT) have received much commercial attention for the last 20-30 years, especially in the automotive industry [156-165]. PC has a good balance of properties, which include high modulus and strength, heat deflection temperature, and toughness. However, it has poor solvent and hydrolysis resistance. Therefore, PBT is blended with PC to improve the chemical resistance of molded parts. It is well known that transesterification can occur during melt blending of PC/PBT [156-160]. Progressive transesterification results in the formation of block copolymers and finally into random copolymers. The extent of reaction for transesterification is temperature dependent. In general, a negligible amount of transesterification occurs in the temperature range of 260°C to 270°C at short residence times (< 10 minute) in the absence of a catalyst [158, 162]. Residence times during extrusion and injection molding are, typically, much less than 10 minutes and one would expect that the effect of interchange reactions on the miscibility, morphology and mechanical properties of PC/PBT blends would be negligible. However, residual catalyst that is used to promote the condensation reactions required to polymerize PBT also catalyzes the interchange reactions that are involved at the interface of the PC and PBT phase during melt blending. Therefore, in this section, the effect of transesterification and blend ratio on the miscibility, compatibility, morphology, and mechanical properties are discussed in sections 2.6.1, 2.6.2, and 2.6.3, respectively.

2.6.1 Miscibility and Compatibility

When blending two polymers, the resulting blend may form a single or multiphase mixture. A single-phase mixture is generated if the two polymers are miscible, whereas, multiphase mixtures form when the two polymers are partially miscible or immiscible. For a miscible system, only one Tg (glass transition temperature) is observed reflective of the single phase that is formed, and it is generally between the T_g's of the pure components. A partially miscible system exhibits two T_g's that are slightly shifted from that of the neat components. An immiscible system also exhibits two T_g's, but in this case, the two T_g's are exactly that of the neat components. The mechanical properties of partially miscible and miscible blends often offer advantages over the neat reasons. However, most polymer blends are immiscible. Because miscibility tends to improve the mechanical properties of polymer blends, there have been many attempts to improve the miscibility of immiscible polymer blends. This process is called compatibilization.

The state of miscibility of PC/PBT has been a controversial issue for many years [156-159]. Many research groups have reported that these blends are completely immiscible when solution cast by solvents [160,161], while varying degrees of partial miscibility have been reported when melt blended [160, 161-163]. The disagreements observed in the literature are attributed to interchange reactions that occur during the melt blending of PC/PBT blends. Wahrmund et al. [160] were the first to report partial miscibility of melt blended PC/PBT blends and that the degree of partial miscibility depended on the composition of the blend, i.e. the blend ratio of PC to PBT. They showed that the T_g of the PBT phase depends on whether it is in an amorphous or semicrystalline state. The T_g of the amorphous state is about 15°C lower than the T_g of the semicrystalline state. As the PC content increases the crystallization rate of PBT decreases, which results in a reduction in crystallinity. Therefore, the reduction in T_g of the PC-rich phase was attributed to the varying degrees of amorphous PBT in the PC-rich phase. However, in this study, a transesterification inhibitor was not used to stabilize the melt blends, and therefore, the varying degree of partial miscibility with blend ratio could also be attributed to differing degrees of block or random copolymer content formed by interchange reactions [157-159]. Hobbs et al. [163] investigated the miscibility of stabilized PC/PBT melt blends. The stabilized PC/PBT blends were also found to be

partially miscible. Even though inhibitors were used to prevent transesterification reactions from occurring, they may have not been completely suppressed, and thus, the observance of partial miscibility due to interchange reactions was still possible. Devaux et al. [159, 164] investigated solubility changes of PC/PBT blends at a blend ratio of 50/50 as a function of reaction time. The changes in solubility with reaction time were compared to blends with and without a transesterification inhibitor. At short reaction times, the solubility of the stabilized blend changed with time up to a critical reaction time. Once the critical reaction was reached, the solubility of the stabilized blend remained unchanged. This result suggests that the reaction rate of the interchange reaction is initially faster than the reaction between the catalyst and the stabilizer at short times, but at longer times the reaction between the catalyst and the stabilizer are dominant.

The role of the transesterification reactions on the compatability of PC/PBT blends is clearly identified by comparing the experimental results of work done by Tattum et al. [158] and Pompe et al. [159]. Tattum et al. [158] investigated the influence of transesterification on the compatibility of PC/PBT blends by incrementally increasing the amount of a titanium catalyst, thereby, increasing the reaction rate of the interchange reactions at a constant blend ratio of 50/50 PC/PBT. All the blends were mixed at 260°C in a Brabender plasticorder for 10 minutes. After 10 minutes, an inhibitor was added to quench the interchange reactions. The T_g values of the blends were determined by using solid state DMTA measurements. The results of the experiment are presented in Table 2.2. The T_g values of the neat components were 160°C and 80°C for PC and PBT, respectively. Two T_g values (95°C and 138°C) were observed for the blend that had no additional catalyst added. Hence, the PC/PBT blend is already partially miscible. This is attributed to the residual catalyst that is already present in the PBT phase. As the amount of catalyst increases, the T_g of the PC-rich phase shifts to lower and lower values while the T_g of the PBT-rich phase shifts to higher and higher values. Therefore, the compatibility improves due to an increase in the interchange reactions. Eventually, enough catalyst was added to promote complete miscibility of the PC/PBT blend. Only one T_g at 90°C was observed with the addition of 200 ppm of catalyst. Therefore, one can conclude that titanium catalysts, which increase the reaction rate of the interchange

Table 2.2 – Glass transition temperatures determined by dynamic mechanical thermal analysis for the pure homopolymers and catalyzed blends

Material	Tan δ peaks, °C
PC	160
PBT	80
0T*	95, 138
50T*	100, 136
100T*	110, 134
150T*	115,130
200T*	90

* Denotes level of titanate catalyst added in ppms

reactions, are compatibilizing agents for PC/PBT blends. In a separate study done by Pompe and Haubler [159], the miscibility of PC/PBT blends was investigated as a function of blend ratio. They found that the T_g of PC shifts to lower and lower values relative to the neat component as the PBT content is increased, while the T_g of PBT shifts to higher and higher values relative to the neat component. This is due to an increase in residual catalyst, and hence, an increase in the interchange reactions as the PBT content is increased. Furthermore, they were able to extrapolate the T_g values of the PC-rich phase and PBT-rich phase at 0% copolymer content (completely suppressed transesterification) by using NMR and DSC techniques. The extrapolated T_g values of the PC and PBT matched that of the neat components. Therefore, based on these experiments, it has been shown that the degree of miscibility for PC/PBT blends is determined by the degree of tranesterification that occurs. Complete suppression of transesterification results in an immiscible blend. Therefore, the degree of partial miscibility for these blends is determined by the extent of the interchange reactions and they can become completely miscible once a sufficient extent of reaction is achieved.

2.6.2 Morphology of PC/PBT Blends

The morphology of PC/PBT blends is affected by the composition of the blend and transesterification. Delimoy et al. [165] investigated the morphological structure of melt stabilized PC/PBT blends as a function blend composition. The blends were mixed in a Brabender Plasticorder for 5 minutes at 260°C. They were then compression molded for 2 minutes at the same temperature. This was followed by cooling under pressure in another cold press. At blend compositions in the range of 10% to 35% by weight of PBT, the PBT phase was dispersed in a continuous PC phase. The domain size of the PBT dispersed phase increased due to greater coalescence between the droplets as the concentration increased. The shape of the droplets is in the form of thread-like particles. In the composition range of 35% to 50% by weight of PBT, a co-continuous structure is observed. The PC and PBT phases exhibit a fibrillar morphology and it is difficult to distinguish the dispersed phase from the continuous phase. Finally, at concentrations of 50% by weight of PBT and higher, phase inversion occurs where the PC becomes the dispersed phase and PBT becomes the continuous matrix. The domain size of the

droplets is much larger when PC is dispersed in PBT relative to PBT dispersed in PC. This is attributed to λ being much larger than 1 for the case where PC is dispersed in PBT. When the dispersed phase has a higher viscosity than the continuous phase, it becomes more difficult for the domains to breakup. Since a co-continuous structure is observed for blends in the composition range of 35% to 50% by weight of PBT, the mechanical properties of the PC/PBT blends should be expected to reach a peak value within this range.

The effect of transesterification on the morphology of PC/PBT blends has been investigated by Tattum et al. [158]. The morphology of PC/PBT blends at a blend ratio of 50/50 was observed as a function of increasing titanium catalysts. The uncatalyzed blends exhibited a co-continuous structure where the PC and PBT phases exhibited a fibrillar morphology. This morphology was also observed by Delimoy et al. [148] at an equivalent blend ratio of 50/50. As the level of catalyst was increased, the co-continuous structure was maintained but at a reduced size scale. This is expected since the interchange reactions act as a compatibilizer for PC/PBT blends. However, once enough catalyst is added (200 ppm), the PC/PBT becomes completely miscible and so the co-continuous structure that is typically observed is reduced to a single phase. One would expect that the mechanical properties of the PC/PBT blends improve due to the compatibilizing affect of increased interchange reaction, but unfortunately, they were not reported. However, it is interesting to note that the solvent resistance of the PC/PBT blends is reduced with an increase in transesterification. Methylene-chloride, which is known to be insoluble in PBT, dissolved larger quantities of the PC/PBT blends when the amount of titanium catalyst added to the mixing step increased. Once, complete miscibility was achieved, the Methylene-chloride was able to completely dissolve the PC/PBT blend.

2.6.3 Mechanical Properties

To this date, the author has only been able to find one published paper on the mechanical properties of PC/PBT blends. Sanchez et al. [162] investigated the mechanical properties of stabilized PC/PBT blends as a function of composition. The tensile modulus as a function of PC content is shown in Figure 2.6. The tensile modulus

of the neat PC and PBT are 2.3 GPa and 1.8 GPa, respectively. The modulus increases with PC content up to about 80% by weight at which point an increase in PC content leads to a reduction in the modulus. The modulus of the blend is larger than either of the neat components in the composition range of 55% to 90% by weight of PC and it is below that of the neat PC in the composition range of 50% by weight of PC or below. The above results can be explained by the differences in morphological behavior that is observed as a function of composition for PC/PBT blends. In the composition range of 55% to 65% by weight of PC, a co-continuous morphology is observed, whereas at 65% by weight of PC or higher, finely dispersed PBT particles are observed in a continuous PC phase. On the other hand, when the PC content is below 50% by weight, the dispersed PC phase exhibits large domain sizes that are not dispersed well in the PBT continuous matrix. Finer domain structures that are well dispersed within a continuous phase or co-continuous morphologies tend to enhance the mechanical properties. The tensile strength and the elongation at break were also measured. For these properties the opposite trend was observed. The tensile strength and elongation at break both decreased with an increase in PC content.

In summary, transesterification leads to partial miscibility of PC/PBT blends and the formation of copolymers. The copolymers that are formed act as a compatibilizer for PC/PBT blends. A co-continuous morphology and/or small scale, well dispersed morphological structures are observed when the PC content is between 50%-90% by weight, which leads to enhanced mechanical properties. Compatibility due to the interchange reactions reduces the size scale of the dispersed PBT droplets in the composition range of 50%-90% by weight of PC. Compatibility due to interchange reactions may lead to improved mechanical properties but it is also reduces the solvent resistance of the blends because the block copolymer that is formed from the interchange reactions is not solvent resistance, which nullifies the main purpose for the incorporation of PBT into PC. Therefore, limiting the amount of copolymer formation due to the interchange reaction is necessary if these blends are going to be of any use for the automotive industry.

2.7 Research Objectives

The topics covered in the previous sections have shown that particle size and shape (aspect ratio) can have a significant affect on the flow behavior and dimensional stability of filled polymer composites. Warpage of filled polymer composites is attributed to frozen-in flow-induced stresses and thermally induced stresses. Typically, the frozen-in flow induced stresses are assumed to be an order of magnitude lower than that of thermally induced stresses, and therefore, they are often neglected. This is based on the assumption that stress relaxation upon cessation of flow is almost instantaneous. While the assumption of instantaneous relaxation of stresses upon cessation of flow may be true for unfilled materials, it has been shown to be untrue for particulate and fiber-reinforced systems. Furthermore, non-uniform thermally induced stresses generated during the cooling and solidification process in injection molding may be the primary cause for warpage in unfilled thermoplastic composites, the additional warpage observed for fiber-reinforced matrices cannot be accounted for by the mechanism of thermal stresses.

Besides from warpage, the addition of fillers also results in a reduction of tensile toughness and impact strength. In the case of ternary blends, the location of the particles within the binary blend promotes differences in the mechanical properties due to differences in the morphology of the generated blends. Improved impact resistance has been observed when filler particles are encapsulated within the dispersed phase while the modulus tends to increase when the filler particles are separately dispersed with the minor phase within the continuous phase. The location of these particles can be affected by blending sequence and the intensity of mixing, which in turn affect the mechanical properties. Therefore, maintaining the filler particles in a specific phase may allow for improvements in the mechanical properties for ternary blends, such as talc filled PC/PBT blends.

Finally, addition of fillers also increases the weight of a molded part relative to the unfilled blend due to the much larger densities of the fillers. Nano-particles can offer a higher stiffness to density ratio, i.e. specific modulus, opposed to that of fine particles. The increase in stiffness is highly dependent on the morphological structure of the nano-particles. Large increases in stiffness are observed for fully exfoliated nano-particles, whereas, only meager reinforcement occurs for filled blends where the nano-particles are

primarily intercalated. To achieve fully exfoliated structures surface treatments are applied to the nano-particles. Another method for dispersing nano-particles is also under investigation within our lab group by using supercritical CO_2 as a dispersing aid.

Since a large number questions remain concerning the origins of warpage, the effect of blend sequencing, and property enhancements that occur by using nano-particles opposed to fine particles, the research to be performed will investigate the following areas:

1) **Evaluate the role of the residual flow-induced stresses relative to that of thermally induced stresses, as governed by fiber concentration and aspect ratio, on the dimensional stability of injection-molded composites.**

2) **Establish the influence of blending sequence on the blend morphology and mechanical properties of particulate filled PC/PBT blends, focusing on the role of mixing intensity and sequencing on particle placement of the filled blends.**

3) **Determine if the use of nano-particles opposed to fine particles can allow lower loadings of reinforcement for filled PC/PBT blends while maintaining desired mechanical properties, such as stiffness, impact strength, and tensile toughness.**

2.8 References

1. Zheng, R., Kennedy, P., Phan-Tien, N., and Fan, X. J., "Thermoviscoelastic Simulation of Thermally and Pressure-Induced Stresses in Injection Moulding for the Prediction of Shrinkage and Warpage for Fibre-Reinforced Thermoplastics", *J. Non-Newtonian Fluid Mech.*, **84**, 159 (1999).

2. Kamal, M. R., Lai-Fook, R. A., and Hernandez-Aguilar, "Residual Thermal Stresses in Injection Moldings of Thermoplastic: A Theoretical and Experimental Study", *Polym. Eng. Sci.*, **42** (5), 1098 (2002).

3. Zoetelief, W. F., Douven, L. F. A., and Ingen Housz, A. J., "Residual Thermal Stresses in Injection Molded Products", *Polym. Eng. Sci.*, **36** (14), 1886 (1996).

4. Shen, Chang-Yu, and Li, Hai-Mei, "Numerical Simulation for Effects of Injection Mold Cooling on Warpage and residual Stresses", *Polym-Plast. Technol. Eng.*, **42** (5), 971 (2003).

5. Kwon, T. H., and Lee, Y. B., "Modeling and Numerical Simulation of Residual Stresses and Birefringence in Injection Molded Center-gated Disks", *Journal of Materials Processing Technology*, **111**, 214 (2001).

6. Bessell, T., Hull, D., and Shortall, J. B., "Interface morphology and mechanical properties of unidirectional fiber-reinforced nylon 6", *Faraday. Spec. D. Chem. Soc.*, **2**, 137 (1972).

7. Bessell, T., and Shortall, J. B., "Crystallization and Interfacial Bond Strength of Nylon 6 at Carbon and Glass-Fiber Surfaces", *J. Mater. Sci.*, **10**, 2035 (1975).

8. Folkes, M. J., and Russell, D. A. M., "Orientation Effects During the Flow of Short-fibre Reinforced Thermoplastics", *Polymer*, **21**, 1252 (1980).

9. Tadmor, Z., "Molecular Orientation in Injection Molding", *J. Appl. Polym. Sci.*, **18**, 1753 (1974).

10. Wimberger-Friedl, R., PhD thesis, Eindhoven University of Technology, The Netherlands (1990).

11. Sunderland, Paul, Yu, Wonjae, and Manson, Jan-Anders, "A Thermoviscoelastic Analysis of Process-Induced Internal Stresses in Thermoplastic Matrix Composites", *Polym. Comp.*, **22** (5), 579 (2001).

12. Choi, Du-Soon, and Im, Yong-Taek, "Prediction of Shrinkage and Warpage in Consideration of Residual Stress in Integrated Simulation of Injection Molding", *Composite Structures*, **47**, 655 (1999).

13. Liao, S. J., Chang, D. Y., Chen, H. J., Tsou, L. S., Ho, J. R., Yau, H. T., and Hsieh, W. H., "Optimal Process Conditions of Shrinkage and Warpage of Thin-Wall Parts", *Polym. Eng. Sci.*, **44**, 917 (2004).

14. Huang, Ming-Chih, and Tai, Ching-Chi, "The Effective factors in the Warpage Problem of an Injection-molded Part with a Thin Shell", *Journal of Materials Processing Technology*, **110**, 1 (2001).

15. Kikuchi, Hiroyuki, and Koyama, Kiyohito, "Material Anisotropy and Warpage of Nylon 66 Composites", *Polym. Sci. Eng.*, **34** (18), 1411 (1994).

16. Kikuchi, Hiroyuki, and Koyama, Kiyohito, "The Relation Between Thickness and Warpage in a Disk Injection Molded From Fiber Reinforced PA66", *Polym. Sci. Eng.*, **36** (10), 1317 (1996).

17. Kikuchi, Hiroyuki, and Koyama, Kiyohito, "Warpage, Anisotropy, and Part Thickness", *Polym. Sci. Eng.*, **36** (10), 1326 (1996).

18. Kikuchi, Hiroyuki, and Koyama, Kiyohito, "Generalized Warpage Parameter", *Polym. Sci. Eng.*, **36** (10), 1309 (1996).

19. Panasiewicz, Jeremy, Daimler-Chrysler, *Private Communications*.

20. Akay, M., and Ozden, S., "Prediction of Process-Induced Warpage of Injection Molded Thermoplastics", **36** (13), 1839 (1996).

21. Duckett, R. A., and Hine, P. J., "Fiber Orientation Structures and Mechanical Properties of Injection Molded Short Glass Fiber Reinforced Ribbed Plates", **25** (3), 237 (2004).

22. Kabanemi, K. K., and Crochet, M. J., "Thermoviscoelastic Calculation of Residual Stresses and Residual Shapes of Injection Molded Parts", *Int. Polym. Process.*, **7**, 60 (1992).

23. Kabanemi, K. K., Vaillancourt, H., Wang, H., and Salloum, G., "Residual Stresses, Shrinkage, and Warpage of Complex Injection Molded Products: Numerical Simulation and Experimental Validation", *Polym. Eng. Sci.*, **38**, 21 (1998).

24. Pontes, A. J., Oliveira, M. J., and Pouzada, A. S., "Studies on the Influence of the Holding Pressure on the Orientation and Shrinkage of Injection Molded Parts", *SPE ANTEC* Tech. Paper, **48**, (2002).

25. Foss, Peter H., “Coupling of Flow Simulation and Structural Analysis for Glass-Filled Thermoplastics”, *Polym. Comp.*, **25** (4), 343 (2004).

26. Lee, K. M., and Han, C. D., “Rheology of Organoclay Nanocomposites: Effects of Polymer Matrix/Organoclay Compatibility and the Gallery Distance of Organoclay”, *Macromolecules*, **36**, 7165 (2003).

27. Young, R., PhD thesis, “Processing Behavior of Thermoplastics Reinforced with Melt Processable Glasses” Virginia Polytechnic Institute, (1999).

28. Czarnecki, Lech, Tanaka, Hideho, and White, James L., “Experimental Studies of the Influence of Particle and Fiber Reinforcement on the Rheological Properties of Polymer Melts”, *Rubber Chemistry and Technology*, **53**, 823 (1980).

29. Suetsugu, Yoshiyuki, and White, James L., “The Influence of Particle Size and a Surface Coating of calcium Carbonate on the Rheological Properties of Its Suspensions in Molten Polystyrene”, *J. Appl. Polym. Sci.*, **28**, 1481 (1983).

30. Fisa, B. and Utracki, L. A., “Rheology of Fiber- or Flake-Filled Plastics”, *Polym. Comp.*, **3**, 193 (1982).

31. Hornsby, P. R. and Mthupha, A., “Rheological Characterization of Polypropylene Filled with Magnesium Hydroxide”, *Journal of Materials Science*, 29, 5293 (1994).

32. Rothon, R., “Particulate-Filled Polymer Composites”, Longman Scientific and Technical, England, 1995.

33. Lobe, V. M. and White, J. L., “An Experimental Study of the Influence of Carbon Black on the Rheological Properties of a Polystyrene Melt”, *Polym. Eng. Sci.*, **18**, 617, (1979).

34. Barnes, H., “A Review of the Rheology of Filled Viscoelastic Systems”, *Appl. Rheol.*, **11,** 89 (2001).

35. Gahleitner, M., Bernreitner, K. and Neibl, W., “Correlations Between Rheological and Mechanical Properties of Mineral Filled polypropylene Compounds”, *J. Appl. Polym. Sci.*, **53**, 283 (1994).

36. Montes, Sergio, White, James L., and Nakajima, Nobuyuki, “Rheological Behavior of Rubber Carbon Black Compounds in Various Shear Flow Histories”, *J. Non-Newtonian Fluid Mech.*, **28**, 183 (1988).

37. Suh, Chang Ho, and White, James L., “Talc-thermoplastic compounds: Particle Orientation in the Flow and Rheological Properties”, *J. Non-Newtonian Fluid Mech.*, **62**, 175 (1996).

38. Wang, Yeh and Wang, Jyun-Jye, “Shear Yield Behavior of Calcium Carbonate-Filled Polypropylene”, *Polym. Eng. Sci.*, **39** (1), 190 (1999).

39. Han, C. D., “Multiphase Flow in Polymer Processing”, Academic, London, 1981, p. 100.

40. Utracki, L. A., “Flow and Flow Orientation of Composites Containing Anisometric Particles”, *Polym. Comp.*, **7**, 274 (1986).

41. Gu, Shu-Ying, Ren, Jie, and Wang, Qin-Feng, “Theology of Poly(Propylene)/Clay Nanocomposites”, *J. Appl. Polym. Sci.*, **91**, 2427 (2004).

42. Lee, K. M., and Han, C. D., “Effect of Hydrogen Bonding on the Rheology of Polycarbonate/Organoclay Nanocomposites”, *Polymer*, **44**, 4573 (2003).

43. Incarnato, I., Scarfato, P., Scatteia, L., and Acierno, D., “Rheological Behavior of New Melt Compounded Copolyamide Nanocomposites”, *Polymer*, **45**, 3487 (2004).

44. Solomon, Michael J., Almusallam, Abdulwahab S., Seefeldt, Kurt F., Somwangthanaroj, Anongnat, and Varadan, Priya, “Rheology of Polypropylene/Clay Hybrid Materials”, *Macromolecules*, **34**, 1864 (2001).

45. Gelfer, M., Song, H. H., Liu, L., Avila-Orta, C., Yang, L., Si, M., Hsiao, B. S., Chu, B., Rafailovich, M., and Tsou, A., “Manipulating the Microstructure and Rheology in Polymer-Organoclay Composites”, *Polym. Eng. Sci.*, **42**, 1841 (2002).

46. Lobe, Vincent M., and White, James L., “An Experimental Study of the Influence of Carbon Black on the Rheological Properties of a Polystyrene Melt”, *Polym. Eng. Sci.*, **19** (9), 617 (1979).

47. Boaira, M. S., and Chaffey, C. E., “Effects of Coupling Agents on the Mechanical and Rheological Properties of Mica-Reinforced Polypropylene”, *Polym. Eng. Sci.*, **17,** 713 (1977).

48. Kataoka, T., Kitano, T., Sasahara, M., and Nishijima, K., “Viscosity of Particle Filled Polymer Melts” *Rheol. Acta.*, **17**, 149 (1978).

49. Kataoka, T., Kitano, T., Oyanagi, Y., and Sasahara, M., “Viscous Properties of Calcium Carbonate Filled Polymer Melts”, *Rheol. Acta.*, **18**, 635 (1979).

50. Plueddemann, E. P., and Stark, G. L., “Additives for Plastics,” Seymour, R. B., ed., Academic Press, New York, (1979).

51. Wah, C. A., Choong, L. Y., and Neon, G. S., “Effects of Titanate Coupling Agent on the Rheological Behaviour, Dispersion Characteristics and Mechanical Properties of Talc Filled Polypropylene”, *Eur. Polym. J.*, **36**, 789 (2000).

52. Scherbakoff, N. and Ishida, H., "Dynamic Mechanical Properties of a Polystyrene/Poly(methyl methacrylate)/Glass Beads System", *Polym. Mater. Sci. Eng.*, **65**, 337 (1991).

53. Ramazani, A., Ait-Kadi, A., and Gremela, M., "Rheology of Fiber Suspensions in Viscoelastic Media: Experiments and Model Predictions", *J. Rheol.*, **45** (4), 945 (2001).

54. Kim, Jin Kon, and Song, Ju Ho, "Rheological Properties and Fiber Orientation of Short Fiber-Reinforced Plastics", *J. Rheol.*, **41** (5), 1061 (1997).

55. Becraft, M. L., and Metzner A. B., "The rheology, Fiber Orientation, and Processing Behavior of Fiber-Filled Fluids", *J. Rheol.*, **36** (1), 143 (1992).

56. Greene, Joseph P., and Wilkes, James O., "Steady-State and Dynamic Properties of Concentrated Fiber-Filled Thermoplastics", *Polym. Eng. Sci.*, **35** (21), 1670 (1995).

57. Mutel, A. T., and Kamal, M. R., "The Effect of Glass Fibers on the Rheological Behavior of Polypropylene Melts Between Rotating Parallel Plates", *Polym. Comp.*, **5** (1), 29 (1984).

58. Ausias, G., Agassant, J. F., and Vincent, M., "Rheology of Short Glass Fiber Reinforced Polypropylene", *J. Rheol.*, **36** (4), 525 (1992).

59. Burrell, H., "Pigment wetting parameter", *A.C.S. Div. Org. Coatings Plast., Preprints*, **35**, 18 (1975).

60. Minagawa, N. and White, J. L., "The Influence of Titanium Dioxide on the Rheological and Extrusion Properties of Polymer Melts", *J. Appl. Polym. Sci.*, **20**, 501 (1976).

61. Han, C. D., "Rheological Properties of Calcium Carbonate-Filled Polypropylene Melts", *J. Appl. Polym. Sci.*, **18**, 821 (1974).

62. Han, C. D., Weghe, T. V. D., Shete, P., and Haw, J. R., "Effects of Coupling Agents on the Rheological Properties, Processability, and Mechanical Properties of Filled Polypropylene", *Polym. Eng. Sci.* **20**, 925 (1980).

63. Baird, D. G., and Collias, D., "Polymer Processing", John Wiley and Sons, Inc., New York, (1998).

64. Tanaka, H. and White, J. L., "Experimental Investigations of Shear and Elongational Flow Properties of Polystyrene Melts Reinforced with Calcium Carbonate, Titanium Dioxide, and Carbon Black", *Polym. Eng. Sci.*, **20** (14), 949 (1980).

65. Mutel, A. T., “Rheological Behavior and Fiber Orientation in Simple Flows of Glass Fiber Filled Polypropylene Melts”, PhD thesis, McGill University, (1989).

66. White, J. L., “Processability of Rubber and Rheological Behavior”, *Rubber Chem. Technol.*, **50**, 163 (1977).

67. Goel, D. C., “Effect of Polymeric Additives on the Rheological Properties of Talc-Filled Polypropylene. *Polym. Eng. Sci.*, **20**, 198 (1980).

68. Crowson, R. J., Folkes, M. J., and Bright, P. F., “Rheology of Short Glass Fiber-Reinforced Thermoplastics and Its Application to Injection Molding. I. Fiber Motion and Viscosity Measurement,” *Polym. Eng. Sci.*, **20**, 934 (1980).

69. Pisipati, R. M., “A Rheological Characterization of Particle and Fiber Filled Nylon 6,6 Melts and Its Application to Weld-Line Formation in Molded Parts”, PhD thesis, Virginia Polytechnic Institute, (1983).

70. Chan, Y., White, J. L., and Oyanagi, Y., “A Fundamental Study of the Rheological Properties of Glass-Fiber-Reinforced Polyethylene and Polystyrene Melts”, *J. Rheol.*, **22**, 507, (1978).

71. Wu, S. *Polym. Eng. Sci.*, **19**, 638 (1979).

72. Crowson, R. J., and Folkes, M. J., Rheology of Short Glass Fiber-Reinforced Thermoplastics and Its Application to Injection Molding. II. The Effect of Material Parameters”, *Polym. Eng. Sci.*, **20**, 934 (1980).

73. Knutsson, B. A., White, J. L., and Abbas, K. B., “Rheology”, Academic Press, New York, (1980).

74. Simha, R., “A Treatment of the Viscosity of Concentration Suspensions”, *J. Appl. Phys.*, **23**, 1020 (1952).

75. Rutgers, I. R., “Relative Viscosity and Concentration,” *Rheo. Acta*, **2**, 305 (1962).

76. Smith, T. L., *J. Paint Techn.*, “Rheological Properties of Dispersions of Particulate Solids in Liquid Media”, **44**, 71 (1972).

77. Jefferey, D. J., and Acrivos, A., “The Rheological Properties of Suspensions of Rigid Particles”, *AICHE J.*, **22**, 417 (1976).

78. Mooney, M., “The Viscosity of a Concentrated Suspension of Spherical Particles”, *J. Colloid Sci.*, **6**, 162 (1951).

79. Quemada, D., "Viscosity of suspensions modeled with a shear-dependent maximum packing fraction", *Rheo. Acta*, **16**, 82 (1977).

80. Utracki, L. A., and Simha, R., “Viscosity of Polymer Solutions: Scaling Relationships”, *J. Rheol.*, **25**, 329 (1981).

81. Barnes, H. A., “A Handbook of Elementary Rheology”, The University of Wales Institute of Non-Newtonian Fluid Mechanics, Aberystwyth, (2000).

82. Highgate, D. J., and Whorlow, R. W., “Rheological Properties of Suspensions of Spheres in Non-Newtonian Media”, *Rheol. Acta*, **9**, 569 (1970).

83. White, F. M., “Fluid Mechanics”, McGraw-Hill Inc., New York, (1994).

84. Bingham, E. C., “Fluidity and Plasticity”, McGraw Hill Book Company, New York, (1922).

85. Suetsugu, Hyuki, and White, James L., “A Theory Thixotropic Plastic Viscoelastic Fluids with a Time-Dependent yield Surface and Its Comparison to Transient and Steady State Experiments on Small Particle Filled Polymer Melts”, *J. Non-Newtonian Fluid Mech.*, **14**, 121 (1984).

86. Sobhanie, Mohammed, Isayev, Avraam I., and Fan, Yiyan, “Viscoelastic Plastic Rheological Model for Particle Filled Polymer Melts”, *Rheol Acta*, **36**, 66 (1997).

87. White, James L. and Tanaka, Hideho, “Comparison of a Plastic-Viscoelastic Constitutive Equation with Rheological Measurements ona Polysyrene Melt Reinforced with Small Particles”, *J. Non-Newtonian Fluid Mech.*, **8**, 1 (1981).

88. Hohenesmer, K., and Prager, W., *Z. Angnew. Math. Mech.*, **12**, 216 (1932).

89. Goodeve, C. F., and Whitfield, G. W., “The Measurement of Thixotropy in Absolute Units”, *Trans. Farad. Soc.*, **34**, 511 (1938).

90. Hahn, S. J., Ree, T., and Eyring, H., “A Theory of Thixotropy and Its Application to Grease. *Ind. Eng. Chem.*, **51**, 856 (1959).

91. Ruckenstein, E., and Mewis, J., *J. Colloid. Intern. Sci.*, **44**, 552 (1973).

92. Cheng, D. C. H., and Evans, F., “Phenomenological Characterization of the Rheological Behavior of Inelastic Reversible Thixotropic and Antithixotropic Fluids”, *J. Appl. Phys.*, **16**, 1599 (1965).

93. Chen, L. J., and Bogue, D. C., “Time-Dependent Stress in Polymer Melts and Review of Viscoelastic Theory”, *Trans. Soc. Rheol.*, **16**, 59 (1972).

94. White, J. L., “Processability of Rubber and Rheological Behavior”, *Rubber Chem. Technol.*, **50**, 163 (1977).

95. Bird, R. B., Armstrong, R. C., and Hassager, O., “Dynamics of Polymeric Liquids”, John Wiley and Sons, New York, (1987).

96. Chung, Du Hwan, and Kwon, Tai hun, “Invariant-based Optimal Fitting Closure Approximation for the Numerical Prediction of Flow-Induced Fiber Orientation”, *J. Rheol.*, **46** (1), 169 (2002).

97. Ranganathan, S., and Advani, S. G., “Fiber-Fiber Interactions in Homogeneous Flows of Non-Dilute Suspensions”, *J. Rheol.*, **35**, 1499 (1991).

98. Fan, X. J., Phan-Tien, N., and Zheng, R., “A Direct Simulation of Fibre Suspensions”, *J. Non-Newtonian Fluid Mech.*, **74**, 113 (1998).

99. Yamane, Y., Kaneda, Y., and Doi, M., “Numerical Simulation of Semi-Dilute Suspensions of Rodlike Particles in Shear Flow, *J. Non-Newtonian Fluid Mech.*, **54**, 405 (1994).

100. Doi, M., “Molecular Dynamics and Rheological Properties of Concentrated Solutions of Rodlike Polymers in Isotropic and Liquid Crystalline Phases”, *J. Polym. Sci., Polym. Phys. Ed.*, **19**, 229 (1981).

101. Lipscomb, G. G., Denn, M. M., Hur, D. U., and Boger, D., “The Flow of Fiber Suspensions in Complex Geometries”, *J. Non-Newtonian Fluid Mech.*, **26**, 297 (1988).

102. Advani, S. G., and Tucker III, C. L., “The Use of Tensors to Describe and Predict Fiber Orientation in Short Fiber Composites”, *J. Rheol.*, **31**, 751 (1987).

103. Advani, S. G., and Tucker III, C. L., “Closure Approximations for Three-Dimensional Structure Tensors”, *J. Rheol.*, **34**, 367 (1990).

104. Doi, M., and Edwards, S. F., “Theory of Polymer Dynamics”, Claredon Press, Oxford, (1986).

105. Doraiswamy, D. and Metzner, A. B., “The Rheology of Polymeric Liquid Crystals”, *Rheol. Acta*, **25**, 580 (1986).

106. Batchelor, G. K., “The Stress System in a Suspension of Force-Free Particles”, *J. Fluid Mech.*, **41**, 545 (1970).

107. Doraiswamy, D. and Metzner, A. B., “The Rhology of Polymeric Liquid Crystals”, *Rheol. Acta*, **25**, 580 (1986).

108. Giesekus, H., “Elasto-Viskose Flussigkeiten, fur die in Stationaren Schichstromungen Samtliche Normalspannungskompinenten Verschieden Gross Sind”, *Rheol. Acta*, **2**, 50 (1962).

109. Viola, G. G., and Baird, D. G., “Studies on the Transient Shear Flow Behavior of Liquid Crystalline Polymers”, *J. Rheol.*, **30** (3), 601 (1986).

110. Derjaguin, B., *Trans Faraday Soc.*, **36**, 203 (1940).

111. Wilson, Thomas S., and Baird, D. G., “Transient Elongational Flow Behavior of Thermotropic Liquid Crystalline Polymers”, *J. Non-Newtonian Fluid Mech.*, **44**, 85 (1992).

112. Baker, R. A., Koller, L. L., and Kummer, P. E., “Handbook of Filler for Plastics”, Van Nostrand Reinhold, New York, (1987).

113. Hoffman, H., Grellmann, W., and Zilvar V., “Polymer Composites”, Academic Press, New York, (1986).

114. Svehlova, Vitezslava, and Poloucek, Eduard, “Mechanical Properties of talc-filled PP”, *Die Angewandte Makromolekulare Chemie*, **214**, 91 (1994).

115. Pastorini, M. T., and Nunes, R. C. R., “Mica as a Filler for ABS/Polycarbonate Blends”, *J. Appl. Polym. Sci.*, **74**, 1361 (1999).

116. Gahleitner, M., Bernreitner, K. and Neibl, W., “Correlations Between Rheological and Mechanical Properties of Mineral Filled polypropylene Compounds”, *J. Appl. Polym. Sci.*, **53**, 283 (1994).

117. Mitsuishi, Kazuta, “Mechanical Properties of Poly(propylene) Filled with Calcium Carbonate of Various Shape”, *Die Angewandte Makromolekulare Chemie*, **248**, 73 (1997).

118. Mareri, P., Bastide, S., Binda, N., and Crespy, A., “Mechanical Behaviour of Polypropylene Composites Containing Fine Minearal Filler: Effect of Filler Surface Treatment”, *Composites Science and Technology*, **58**, 747 (1998).

119. Maiti, S. N., and Sharma, K. K., “Studies on Polypropylene Composites Filled with Talc Particles”, *J. Mater. Sci.*, **27**, 4605 (1992).

120. Li, Zhigang, and Narh, K. A., “Experimental Determination and Numerical Prediction of Mechanical Properties of Injection Molded Self-reinforcing polymer Composites”, *Composites: Part B*, **32**, 103 (2003).

121. Brune, Douglas A., and Bicerano, Jozef, "Micromechanics of Nanocomposites: Comparison of Tensile and Compressive Elastic Moduli, and Prediction of Effects of Incomplete Exfoliation and Imperfect Alignment on Modulus", *Polymer*, **43**, 369 (2002).

122. Maine, F. W., and Shepard, P. D., "Mica reinforced plastics. Review", *Composites*, **5** (5), 193 (1974).

123. Hancock, M., Tremayne, P., and Rosevear, D. J., *J. Polym. Sci.*, **18** (11), 3211 (1980).

124. Maiti, S. N., and Sharma, K. K., "Studies on Polypropylene Composites Filled with Talc Particles", *J. Mater. Sci.*, **27**, 4605 (1992).

125. Wu, Dezhen, Wang, Xiaodong, Song, Yongzhi, and Jin, Riguang, "Nanocomposite of Poly(vinyl chloride) and Nanometric Calcium Carbonate Particles: Effects of Chlorinated Polyethylene on Mechanical Properties, Morphology, and Theology", *J. Appl. Polym. Sci.*, **92**, 2714 (2004).

126. Alexandre, Michael, Dubois, Philippe, Sun, Tao, Garces, M., Jerome, Robert, "Polyethylene-layered Silicate Nanocomposites Prepared by the Polymerization-filling Technique: Synthesis and Mechanical Properties", *Polymer*, **43**, 2123 (2002).

127. Fornes, T. D., Yoon, P. J., Keskkula, H., and Paul, D. R., "Nylon 6 Nanocomposites: the Effect of Matrix Molecular Weight", *Polymer*, **42**, 9929 (2001).

128. Yoon, P. J., Hunter, D. L., and Paul, D. R., "Polycarbonate Nanocomposites. Part 1. Effect of Organoclay Structure on Morphology and Properties", *Polymer*, **44**, 5323 (2003).

129. Benderly, D., Siegmann, A. and Narkis, M., "Polymer Encapsulation of Glass Filler in Ternary PP/PA6/Glass Blends", *Polymer Composites*, **17** (1), 86 (1996).

130. Zoldan, J., Siegmann, and A., Narkis, M., "Encapsulation During Melt Processing of Ternary Immiscible Polymer Blends", *J. of Polym. Eng.*, **23** (2), 119 (2003).

131. Gonzalez-Nunez, R., Favis, B. D., Carreau, P. J., and Lavalle, C., "Factors Influencing the Formation of Elongated Morphologies in Immiscible Polymer Blends During Melt Processing", *Polym. Eng. Sci.*, **33**, 851 (1993).

132. Utacki, L. A., "Polymer Alloys and Blends", Hanser Publishers, Munich, (1989).

133. Favis, B. D., Willis, J. M., "Phase Size/Composition Dependence in Immiscible Blends: Experimental and Theoretical Considerations", *J. Polym. Sci., Polym. Phys.*, **28**, 2259 (1990).

134. Serpe, G., Jarrin, J., and Dawans, F., "Morphology-Processing Relationships in Polyethylene-Polyamide Blends", *Polym. Eng. Sci.*, **30**, 553 (1990).

135. Cook, W. D., Zhang, T., Moad, G., van Deipen, G., Cser, F., Fox, B., and O'Shea, M., "Morphology-Property Relationships in ABS/PET blends. II. Influence of Processing Conditions on Structure and Properties", *J. Appl. Polm. Sci.*, **62**, 1699 (1996).

136. Hourston, D. J., Schafer, F-U, "Poly(ether urethane)/Poly(ethyl methacrylate) IPNs with High Damping Characteristics: The Influence of the Crosslink Density in Both Networks", *Polymer*, **37**, 3521 (1996).

137. Yang, Y., Westerweele, E., Zhang, C., Smith, P., and Heeger, A. J., "Enhanced Performance of Polymer Light-Emitting Diodes Using High-Surface Area Polyaniline Network Electrodes", *J. Appl. Polym. Sci.*, **77**, 694 (1995).

138. Nunes, S. P., "Recent Advances in the Controlled Formation of Pores in Membranes", *TRIP*, **5**, 187 (1997).

139. Mamat, A., Vu-Khanh, T., Cigana, P., and Favis, B. D., "Impact Fracture Behavior of Nylon-6/ABS blends", *J. Polym. Sci., Polym. Phys.*, **35**, 2583 (1997).

140. Inberg, J. P. F., and Gaymans, R. J., "Co-continuous Polycarbonate/ABS Blends", Polymer, 43, 2425 (2002).

141. Taylor, G. I., "The Viscosity of a Fluid Containing Small Drops of Another Fluid", *Proc. Roy. Soc.*, **A138**, 41 (1932).

142. Taylor, G. I., "The Formation of Emulsions in Definable Fields of Flow", *Proc. Roy. Soc.*, **A146**, 501 (1934).

143. Rumscheidt, F. D., and Mason, S. D., "Particle Motion in Sheared Suspensions XII", *J. Coll. Sci.*, **16**, 238 (1961).

144. Kim, B. K., and Lee, Y. M., "Physical Properties of ABS/SMA/Nylon-6 Ternary Blends: Effect of Blending Sequence", *Polymer*, **34** (10), 2075 (1993).

145. Sahnoune, P., Lopez Cuesta, J. M., and Crespy, A., "Improvement of the Mechanical Properties of an HDPE/PS Blend by Compatibilization and Incorporation of $CaCO_3$", *Polym. Eng. Sci.*, **43** (3), 647 (2003).

146. Favis, B. D., "Polymer Alloy and Blends: Recent Advances", *Can. J. Chem. Engr.*, **69**, 619 (1991).

147. Zheng, Mingjia, and Li, Huilin, "Study on Isotactic Polypropylene/Zinc-Neutralized Sulfonated Ethylene Propylene Diene Monomer Rubber/$CaCO_3$ Ternary Blends", *J. Appl. Polym. Sci.*, **91**, 1635 (2004).

148. Cheng, T. W., Keskkula, H., and Paul, D. R., "Property and Morphology Relationships for Ternary Blends of Polycarbonate, Brittle Polymers, and an Impact Modifier", *Polymer*, **33** (8), 1606 (1992).

149. Steinmann, Sandra, Gronski, Wolfram, and Friedrich, Christian, "Influence of Selective Filling on Rheological Properties and Phase Inversion of Two-phase Polymer Blends", *Polymer*, **43**, 4467 (2002).

150. MacKenzie, B. T., "Filler Effects and Treeing Phenomena in Laboratory Models and Cable Sections", *Ann. Rep. Conf. Elec. Insul. Dielec. Phenomena*, 232 (1972).

151. Kylma, Janne, and Seppala, Jukka, "Ternary-Phase Poly(ester-urethane)/Elastomer/Filler Composites", *J. Appl. Polym. Sci.*, **79**, 1531 (2001).

152. Stamhuis, J. E., "Mechanical Properties and Morphology of Polypropylene Composites III. Short Glass Fiber Reinforced Elastomer Modified Polypropylene", *Polymer Composites*, **9** (4), 280 (1988).

153. Qiu, Gui-Xue, Raue, Frank, and Ehrenstein, Gottfried W., "Mechanical Properties and Morphologies of PP/mPE/Filler Composites", *J. Appl. Polym. Sci.*, **83**, 3029 (2002).

154. Gonzalez, J., Albano, C., Ichazo, M., and Diaz, B., "Effects of Coupling Agents on Mechanical and Morphological Behavior of the PP/HDPE Blend with Two Different $CaCO_3$", *Eur. Polym. J.*, **38**, 2465 (2002).

155. Ersoy, O. G., and Nugay, N., "Effect of Inorganic Filler Phase on Mechanical and Morphological Properties of Binary Immiscible Polymer Blends", *Polymer Bulletin*, **49**, 465 (2003).

156. Wahrmund, D. C., Paul, D. R., and Barlow, J. W., "Polyester-Polycarbonate Blends. I. Poly(butylene Terephthalate)", *J. Appl. Polym. Sci.*, **22**, 2155 (1978).

157. Wilkinson, A. N., and Tattum, S. B., "Melting, Reaction, and Recrystallization in a Reactive PC-PBT Blend", *Polymer*, **38**, 1923 (1997).

158. Tattum, S. B., Cole, D., and Wilkinson, A. N., "Controlled Tranesterification and Its Effects on Structure Development in Polycarbonate-Poly(Butylene Terephthalate) Melt Blends", *J. Macromol.Sci.-Phys. B.*, **39** (4), 459 (2000).

159. Hobbs, S. Y., Groshans, V. L., Dekkers, M. E. J., and Shultz, A. R., *Polymer Bulletin*, "Partial Miscibility of Poly(butylene terephthalate)/Bisphenol A Polycarbonate Melt Blends", **17**, 335 (1987).

160. Hanrahan, B. D., Angeli, S. R., and Runt J., "Miscibility and Melting in Poly(Butylene Terephthalate)/Polt(Bisphenol A-Carbonate) Blends", *Polymer Bulletin*, **14**, 399 (1985).

161. Hobbs, S. Y., Dekkers, M. E. J., and Watkins, V. H., "The Morphology and Deformation Behavior of Poly(Butylene Terephthalate)/BPA Polycarbonate Blends", *Polymer Bulletin,* **17**, 341 (1987).

162. Sanchez, P., Remiro, P. M., and Nazbal, J., "Physical Properties and Structure of Unreacted PC/PBT Blends", *J. Appl. Polym. Sci.*, **50**, 995 (1993).

163. Delimoy, D., Bailly, C., Devaux, J., and Legras, J., "Morphological Studies of Polycarbonate-Poly(butylene terephthalate) Blends by Transmission Electron Microscopy", *Polym. Eng. Sci.*, **28**, 104 (1988).

164. Devaux, J. Godard, P., and Mercier, J. P., "Bisphenol-A Polycarbonate-Poly(Butylene Terephthalate) Transesterification. II. Structure Analysis of the Reaction Products by IR and H and C NMR", *J. Polym. Sci.*, **20**, 1881 (1982).

165. Delimoy, D., Goffaux, B., Devaux, J., and Legras, R., "Thermal and Morphological Behaviors of Bisphenol A Polycarbonate/Poly(Butylene Terephthalate) Blends", *Polymer*, **36**, 3255 (1995).

3.0 Flow-Induced Warpage of Injection Molded TLCP Fiber Reinforced Polypropylene Composites

W.S. DePolo and D.G. Baird
Department of Chemical Engineering and Macromolecules and Interfaces Institute, Virginia Polytechnic Institute and State University, Blacksburg, VA 24061-0211

(ABSTRACT)

Warpage in injection molded fiber reinforced thermoplastics is primarily believed to be due to residual thermal stresses associated with shrinkage (density changes) and thermal contraction (coefficient of thermal expansion) of the parts and that flow-induced stresses generated during mold filling do not play a significant role. Injection molded plaques of polypropylene (PP) reinforced with pregenerated thermotropic liquid crystalline polymer (TLCP) micro-fibrils were generated as a function of TLCP concentration and the fiber aspect ratio of the TLCP fibrils in order to investigate the role of the residual flow-induced stresses relative to that of the thermal stresses on the warpage. In an effort to relate the material parameters to warpage, the rheological behavior of these fiber-filled systems was investigated. Estimations of the flow-induced and thermally induced residual stresses during mold filling of the generated TLCP/PP composites were made. Results show that warpage of the molded parts increased with an increase in TLCP concentration, while the thermally induced residual stresses decreased. On the other hand, the flow-induced stresses increased with an increase in fiber concentration. The studies on PP reinforced with pregenerated TLCP micro-fibrils suggest that warpage is associated with enhanced flow induced orientation in the presence of high aspect ratio fibrils and increased frozen-in flow-induced residual stresses due to increased relaxation times (this is not the only cause, but is a significant factor). It is expected that the results reported here can be extended to glass-reinforced PP composites as well.

3.1 Introduction

Warpage and dimensional stability of fiber-reinforced thermoplastics have drawn much attention in recent years [1-7]. This is especially the case for the automotive industry where there is an ongoing desire for more fuel efficient cars by replacing high-density metallic parts with lower density fiber-reinforced thermoplastics. Reinforcement with high aspect ratio fibers is required to increase the stiffness and strength of the thermoplastic. However, when reinforced thermoplastics are injection molded to produce flat panels, such as for use in the exterior of cars, there is a considerable tendency for the part to not remain flat when removed from the mold. Both warpage (a bend around the centerline) and twist (a bend around the diagonal) of the part are observed. Furthermore, it is observed that warpage and twist of thermoplastics reinforced with low aspect ratio particulates, such as mineral or talc, are considerably less than that for systems reinforced with high aspect ratio fibers, such as glass or carbon fibers. For example, Kikuchi and Koyama [1-4] injection molded center-gated discs of mineral filled Nylon 6,6 and glass fiber filled Nylon 6,6 at filler loadings of 40% by weight. The mineral used for the study had an average aspect ratio of 4.0, while the glass fibers had an average aspect ratio of 55. It was observed that the warpage of the higher aspect ratio glass fibers was two and a half times greater than that of the mineral filled system.

The most common belief is that warpage is caused by an imbalance in the residual stresses that remain in an injection molded part after it has been ejected from the mold and cooled down to ambient temperatures. These residual stresses originate from two main sources: (primarily) thermally induced stresses and (secondarily) frozen-in flow-induced stresses [5,8-12]. Thermally induced stresses are associated with differential shrinkage and thermal contraction (coefficient of linear thermal expansion, CLTE) during non-uniform cooling of the molded part, both inside and after ejection from the mold. The flow-induced stresses are associated with the viscoelastic behavior of the melt during mold filling. During the filling stage, the viscoelastic flow of the melt promotes orientation (alignment in the direction of flow) of polymer chains due to the high shear and elongational deformation rates that are developed. The rate of stress relaxation of the oriented macromolecules once flow is stopped seems to be retarded by the presence of the fibers, and, hence, stress is not completely relaxed due to rapid solidification of the

molded part. Therefore, flow-induced stress becomes locked into the molded part. In the case of polymer composites, the reinforcing filler will further inhibit the oriented polymer chains from relaxing, which leads to a greater buildup of frozen-in flow-induced residual stresses. Typically, the frozen-in flow-induced residual stresses are assumed to be at least an order of magnitude smaller than the thermally induced stresses due to almost instantaneous relaxation of the orientation of the polymer melt at high temperature and, therefore, they are often omitted in analyses [5,8-14].

Although thermally induced stresses generated during the cooling and solidification process may be the primary cause for warpage in un-reinforced composites, the additional warpage observed for fiber-reinforced matrices cannot be accounted for merely by the mechanism of residual thermal stresses for various reasons. For example, the warpage of fiber-reinforced composites is generally much greater than that of the neat resin even though the shrinkage is significantly less in the fiber-reinforced composites. In fact, neat polymers typically do not warp to any measurable extent even though they shrink significantly on cooling. Furthermore, if low aspect ratio particles are used to reinforce the same neat resin, then the warpage is found to be significantly less relative to the fiber-reinforced system even though the reduction in shrinkage is similar. In the work performed by Kikuchi and Koyama [1-4], the warpage of the glass fiber reinforced Nylon 6,6 was thirty times greater ($6.4x10^{-3}$m) than that of the neat resin ($0.2x10^{-3}$m), while the shrinkage of the glass fiber reinforced composite was reduced by 20% relative to the matrix. A mineral filled composite containing low aspect ratio particles had much lower warpage ($2.5x10^{-3}$m) than the glass filled composite but a similar reduction in shrinkage was observed. The warpage was attributed to increasing anisotropy in the CLTE with increasing filler aspect ratio. The anisotropy of the CLTE, which is defined as the ratio of the CLTE in the flow direction to that of the transverse direction, was 1.0 for the unfilled matrix, 0.5 for the mineral filled Nylon 6,6 and 0.4 for the glass fiber filled Nylon 6,6. It is interesting to note that for a small difference in the anisotropy of the CLTE between the glass fiber and mineral filled system, there was a large difference in the magnitude of the warpage. However, the difference in the anisotropy of the CLTE between the mineral filled composite and base resin is large, but the difference in the magnitude of the warpage is rather small.

It is our belief that the greater anisotropy and warpage of the fiber filled system is most likely due to an increase in the orientation of the polymer chains, and, hence stresses, as well as to a greater degree of inhibition of stress relaxation relative to the mineral filled and unfilled systems rather than residual thermal stresses (CLTE and shrinkage). The high aspect ratio fibers promote increased chain alignment and, therefore, orientation, and increased relaxation times, thereby retarding the process of stress relaxation on cessation of the filling process. As the polymer melt cools inside the mold, frozen-in flow-induced stresses are generated. If any imbalance in the cooling process of the part occurs, then one can expect a non-uniform variation in relaxation of stresses and, therefore, an increase in warpage of fiber-reinforced thermoplastics.

Warpage of injection-molded plaques that are reinforced with high aspect ratio fibers is of primary interest in this paper. In particular, our goal is to evaluate the role of the residual flow-induced stresses relative to the thermal stresses on the warpage of injection molded rectangular plaques consisting of polypropylene (PP) reinforced with pregenerated micro-fibrils of a thermotropic liquid crystalline polymer (TLCP). Although, we are primarily interested in the effect that pregenerated TLCP micro-fibrils have on the warpage of PP composites, it is expected that the results will be applicable to other high aspect ratio reinforcing fibers such as glass. It is apparent that the addition of fibers and an increase in the aspect ratio of the fibers that are used to reinforce thermoplastics enhance the degree of warpage of injection-molded parts. Although, it is widely believed that warpage is caused by residual thermal stresses (shrinkage and anisotropy of the CLTE), we show that the effect of residual stresses generated during melt flow cannot be overlooked. In this paper, we investigate the effect of the TLCP micro-fibril concentration and aspect ratio on the warpage of the TLCP/PP composites.

3.2 Experimental

3.2.1 Materials

The thermotropic liquid crystalline polymer used in this work is HX3000 provided by DuPont and the thermoplastic matrix used is a polypropylene (PP) homopolymer Profax 6823 provided by Basell. The HX3000 is composed of unspecified

ratios of terephthalic acid, 4-hydroxybenzoic acid, hydriquinone and hydroquinone derivatives [15,28-31]. The solid density is 1.38 g/cm^3, its melting temperature is 320°C, and there is no discernable glass transition temperature. The PP used for composite generation is Profax 6823 and it has a melting temperature of 165°C, a melt flow rate of 0.5g/min, a solid density of 0.902 g/cm^3 and a weight average molecular weight of 600,000. This PP was selected because of the loss of some MW during the process by which the pre-generated microfibrils were created as discussed below.

3.2.2 Composite Strand Generation

Pregenerated strands of HX3000/PP at a composition of 55% by weight of HX3000 were extruded using a patented dual extrusion process consisting of two Killion extruders each with 1" barrels and a mixing head [15-19]. The mixer assembly consisted of a mixing head including three helical elements and a Koch static mixer with four elements. The HX3000 was melt processed in one of the extruders at a process temperature between 350°C to 360°C, while the thermoplastic matrix (PP) was melt processed in a second extruder at a processing temperature in the range of 260°C to 270°C. Gear pumps were used to control the flow rate of each stream produced by the two extruders and, hence, the final concentration of the generated composite strand. Once the TLCP passed through the gear pump, its melt temperature was dropped to 340°C, while the PP stream was increased to 290°C after passing through the gear pump of the second extruder. The TLCP stream was then joined with the PP stream from the second extruder before passing through the mixing head. The combined TLCP/PP stream passed through the mixing head to further divide the TLCP fibers into smaller layers. Upon exiting the mixers, the strands were drawn at a draw ratio in the range of 50 to 56, quenched in a cooling bath, and then chopped into 3, 6, or 12 mm pellets. Sabol et al. [15] have shown that the generated TLCP micro-fibrils are nearly continuous in the strand. Therefore, it is believed that the aspect ratio (L/D) of the generated micro-fibrils is increased with an increase in the pellet length of the chopped strand. The pellets could then be processed at a temperature where the PP melted but not the TLCP microfibrils as discussed next.

3.2.3 Injection Molding

The 6 mm pellets containing 55% by weight of TLCP that were generated by the dual extrusion process were further diluted to loadings of 10, 20, 30, and 40 wt% TLCP by dry blending them with PP (Profax 6823) as the diluting agent in a mechanical mixer. The 3 and 12 mm pellets containing 55% by weight of TLCP were also further diluted to a loading of 30 wt% TLCP by dry blending them with the PP as the diluting agent. The dry-blended composites were then injection molded using an Arburg Allrounder Model 221-55-250 injection-molding machine. The Arburg Allrounder has a 22 mm diameter screw, a check ring non-return valve, and an insulated nozzle that is 2 mm in diameter [16]. The composites were injection molded, using a melt temperature of 210°C, a mold temperature of 70°C, a hold pressure of 100 bars, and a screw speed of 200 RPMs, into a rectangular end-gated mold with dimensions of 80 mm by 76 mm by 1.6 mm.

In order to maintain uniform cooling of the part while it was in the mold, both sides of the mold were heated by using cartridge heaters, two for each side, equidistant from one another at approximately 20 mm and 60 mm from the bottom of the mold. Furthermore, the mold was allowed to heat for 5 hrs prior to molding to ensure thermal equilibrium. The first 10-15 molded plaques during each molding run were also discarded to allow the mold to reach an equilibrium temperature.

3.2.4 Warpage and Shrinkage Testing

Warpage and twist measurements of the 80 mm by 76 mm plaques were performed by using a Trans-Tek Model 1003 Linear Variable Displacement Transducer. The warpage and twist measurements were normalized to a 914 mm by 914 mm plaque in accordance with ASTM standard D229-96. The percent warpage was calculated by the following equation:

$$W_{36} = \left(914 \frac{D}{L^2} \right) \mathrm{X}\, 100 \qquad (3.1)$$

where W36 is the percent warp or twist that is observed for a molded part that is 914 mm in length, D is the maximum deviation in millimeters that is observed from the molded parts originally flat shape, and L is the length in millimeters of the dimension along which the warp or twist is observed. A minimum of 10 samples was tested, and the average value and standard deviation were calculated from the data.

The shrinkage measurements in the flow and transverse direction of the molded plaques were made in accordance with ASTM standard D955-00. The percent mold shrinkage was calculated from the following equation:

$$MS = \left(\frac{DC - DS}{DC} \right) \mathrm{X}\, 100 \qquad (3.2)$$

where MS is the percent mold shrinkage that is observed, DC is the dimension of the mold cavity in millimeters, and DS is the dimension of the specimen. A minimum of 10 samples was tested, and the average value and standard deviation were calculated from the data.

3.2.5 Dynamic Mechanical Thermal Analysis of Solid Plaques

Dynamic mechanical thermal analysis (DMTA) of the TLCP/PP composites was measured in the flow and transverse direction on rectangular strips cut from the plaques using a Rheometrics RMS-800. Along with measurements of the storage (G') and loss (G") moduli, the CLTE was also measured. When using a torsional rectangular geometry, the Rheometrics RMS-800 contains a function called auto-tension, which maintains a small tension on the samples as it expands during heating. When auto-tension is enabled, the displacement of a sample can be measured as the material is heated from an initial testing temperature. Therefore, the CLTE of a sample can be measured experimentally within the range of temperatures tested. To perform the tests, rectangular strips approximately 75 mm long by 8 mm wide were cut near the center of the plaques. Once the strips were mounted in the rheometer, G', G", and the change in length as a function of temperature were measured. The temperature range of 30°C to 120°C was investigated at a temperature ramp rate of 5°C/min under a continuous nitrogen atmosphere. For each composite generated, three samples were tested to check

for reproducibility. The CLTE of each composite generated was determined by plotting the change in length normalized to the initial length at 30°C as a function of temperature. The slope of the line is the CLTE for that material, and it has units of (mm/mm)/ °C.

3.2.6 Rheological Measurements of the Composite Melts

The complex viscosity, $|\eta^*|$, and storage modulus, G', of the TLCP/PP composites in the melt state were measured using a Rheometrics RMS-800 with 25 mm diameter plates. Specimens that were 1.6 mm thick were prepared by cutting 25 mm diameter disks from the center of the injection molded plaques. The tests were performed at a melt temperature of 210°C and a strain of 5% under nitrogen. A minimum of 3 samples was tested to check for reproducibility.

3.3 Results and Discussion

3.3.1 Effect of TLCP Concentration on Dimensional Stability

Concentration effects on the dimensional stability of the TLCP/PP composites were investigated by varying the loading level of TLCP (0%, 10%, 20%, 30%, 40%). For the concentration study, a starting pellet length of 6mm was used for all generated composites. In Fig. 3.1, the warpage and twist of the injection molded TLCP/PP plaques are shown as a function of the TLCP loading. Generally, the warpage and twist both increase with an increase in concentration of TLCP up to about 30 wt% of TLCP. Beyond 30 wt% of TLCP, the increase in warpage and twist relative to the unfilled PP matrix remains unchanged with further addition of the TLCP fibers, 16% warp and 14% twist, respectively. It is also worth noting that there is a significant jump in the level of warpage and twist from a 10% to a 20% loading level of TLCP (4% to 12% change in warpage).

To determine the origins of the warpage and twist that are observed in the molded plaques of PP reinforced with TLCP fibers, the effect of shrinkage on TLCP concentration was first investigated and the results are shown in Fig. 3.2. As the concentration of TLCP increases, the shrinkage in the flow and transverse direction decreases. Furthermore, the anisotropy in the shrinkage in the transverse and flow

direction also decreases as the concentration of TLCP is increased. This is a very interesting result because it shows that shrinkage due to crystallization and non-uniform cooling is not an important contributor to warpage for these fiber reinforced materials. If anything, the reduction in the anisotropy between the flow and transverse shrinkage with an increase in fiber loading should reduce the warpage of the molded plaques if shrinkage is the cause.

Next, the thermal expansion and CLTE as a function of TLCP loading were investigated because the anisotropy in the CLTE has been correlated to warpage of injection-molded plaques by many authors [1-4]. These material properties are shown in the flow direction (Fig. 3.3) and the transverse direction (Fig. 3.4) as a function of TLCP concentration in the temperature range of 30°C to 120°C. The numerical values on the right hand side of Fig. 3.3 and Fig. 3.4 are the CLTE values (mm/mm/°C) determined by the slopes of the lines within the temperature range of 60°C to 120°C. We note that the CLTE values of the TLCP/PP composites are similar to those found in the literature for short-glass fiber reinforced PP. In the flow direction, the thermal expansion and CLTE decrease with an increase in fiber loading. Even though the CLTE values only decrease slightly with an increase in the TLCP concentration, there are still significant reductions in the overall dimensional change of the molded plaques with an increase in fiber loading. At a 20 and 40 wt% loading of TLCP, the dimensional change in the flow direction is reduced by 30% and 50%, respectively, relative to the base resin (PP) at a temperature of 120°C. However, in the transverse direction, an increase in TLCP fiber concentrations has little to no influence on the thermal properties of the TLCP/PP molded plaques. This leads to a significant increase in the anisotropy in the CLTE with increasing fiber concentration. This is also a very interesting result because it shows that the dimensional change and the anisotropy in the CLTE are still greatly increasing between TLCP loadings of 20 to 40 wt%, while the warpage ceases to increase further at a loading of 30 wt% and only slightly increases by 4% in the concentration range of 20 to 40 wt%. This suggests that the anisotropy in the residual thermal stresses cannot account for the observed plateau in the warpage as the TLCP fiber concentration is increased.

In order to determine the effects of TLCP concentration on the viscoelastic flow behavior of the composite melts, the storage modulus (G') as a function of frequency for

all tested loading levels of TLCP is shown in Fig. 3.5 at a temperature of 210°C. As the loading level of TLCP increases, the magnitude of G' also increases in the low frequency region (long relaxation times). At the 30 and 40 wt% loading of TLCP, G' in the low frequency region is a little more than an order of magnitude larger than that of the matrix, and a plateau at high loadings can be observed. The observed plateau at the high TLCP loadings is indicative of a yield stress. For the 10 wt% loading, there is only a slight increase in the storage modulus in the low frequency region. This increase in G' is believed to affect the stress relaxation of the composite as it is indicative of enhanced long relaxation times. As the magnitude of G' increases, stress relaxation is inhibited and, therefore, a greater degree of flow-induced stresses are frozen into the part. If the magnitude in G' at the low frequency region is truly indicative of an increase in relaxation times and, therefore, an increase in residual stresses, then by inspection of Fig. 3.5, one would expect that warpage and twist would increase as the loading level increases up to about 30 to 40 wt% of TLCP. These results are in qualitative agreement with the observed warpage of the TLCP/PP composites. The magnitude of G' in the low frequency region of the unfilled matrix and the 10 wt% TLCP reinforced plaques are very close to each other, as is the observed warpage. There is a significant jump in the magnitude of G' in the low frequency region, which correlates with the large increase in the observed warpage from 4% to 12%, when the level of fiber reinforcement is increased from 10 to 20 wt% of TLCP. The lack of increase in the observed warpage when the fiber reinforcement is increased from 30 to 40 wt% of TLCP is consistent with the lack of increase in the magnitude of G' at low frequencies.

3.3.2 Effect of Aspect Ratio on Dimensional Stability

The dependence of fiber aspect ratio on warpage was also investigated by varying the pellet lengths of the TLCP/PP fiber composites (3, 6, and 12 mm), while maintaining the TLCP reinforcement level at 30% by weight (Fig. 3.6). The unfilled PP matrix has a small percentage of warpage, but with the addition of fiber reinforcement, the warpage increases dramatically from an average value of 1.5% to 16%. The warpage of the TLCP/PP composites generated with the 3 mm and 6 mm pellets is approximately the

same at an average value of 16%, while the warpage of the composites generated with the 12 mm pellets is much larger having an average value of 26%.

In Fig. 3.7, the dependence of fiber aspect ratio on shrinkage is shown. The flow direction shrinkage significantly decreases with the addition of TLCP fibers but there is little change with increasing fiber aspect ratio. However, the shrinkage in the transverse direction slightly decreases with an increase in fibril aspect ratio, even though there is an increase in warpage. This shows that the warpage increases with a reduction in shrinkage, and therefore, shrinkage cannot be a major contributor to the warpage of fiber-reinforced composites.

The thermal expansion and the CLTE values are shown in the flow direction (Fig. 3.8) and the transverse direction (Fig. 3.9) for the TLCP/PP composites in the temperature range of 30°C to 120°C. In the flow direction, the thermal expansion and CLTE decrease with an increase in fiber aspect ratio and, as observed in the case of TLCP concentration, the aspect ratio of the fibers had little to no influence on the thermal properties in the transverse direction. Therefore, the anisotropy in the thermal properties increases with an increase in aspect ratio. It is interesting to note that there is very little difference in the dimensional change and CLTE values of the composites generated with 3 mm and 6 mm pellets relative to those generated with the 12 mm pellets. These results are in qualitative agreement with the observed warpage.

Finally, the dependence of fiber aspect ratio on G' is presented in Fig. 3.10. The magnitude of G' increases at low frequencies for the 12 mm long pellets relative to that of the values for the 3 and 6 mm fibers, but there is no increase in G' between the 3 and 6 mm long pellets. The lack of increase in warpage (see Fig. 3.6) in going from the 3 to 6 mm long pellets is consistent with the G' values. Whereas, the composites generated with starting pellet lengths of 12 mm show an increase in storage modulus in the low frequency region indicating an increase in the long relaxation time, which is consistent with the increase in warpage.

3.3.3 Estimation of Thermally Induced Stresses

In order to estimate the residual thermal stresses that are locked into the molded parts upon ejection from the mold and the subsequent cooling to ambient temperature,

Hooke's law was applied, which assumes that there is a linear relationship between the stress and the strain. Assuming the flow direction is x and the transverse direction is y then the thermal stress in the flow direction is given by:

$$\sigma_{xx} = E_{\|}\varepsilon_{xx} \tag{3.3}$$

where σ_{xx} is the residual thermal stress, $E_{\|}$ is Young's Modulus, and ε_{xx} is the thermal strain. Eq. (3.3) can be applied to the transverse direction to calculate σ_{yy} using the appropriate values of $E_{\perp}$ and ε_{yy}. The Young's Modulus at ambient temperature was approximated as 3G', where G' is the storage modulus.

The thermal strain imposed on a solid object can also be expressed as:

$$\varepsilon_{xx} = \alpha_{\|}(\Delta T) \tag{3.4}$$

where $\alpha_{\|}$ is the CLTE and ΔT is the change in temperature. Eq. (3.4) can be applied to the transverse direction to calculate ε_{yy} using the appropriate value of $\alpha_{\perp}$. The CLTE of the TLCP/PP composites was measured by running DMTAs of the solid plaques as described in the experimental section. As a first approximation, the change in temperature is represented by the temperature difference of the mold to that of the ambient air.

3.3.4 Estimation of the "Frozen-in" Flow-Induced Stresses

Flow-induced stresses are generated during mold filling due to the high shear and elongational deformation rates that are developed during the viscoelastic flow of the composite melt. The generated stresses are subsequently locked into the molded part due to rapid solidification. The flow behavior during mold filling is further complicated by the fountain flow effect as described by Tadmor [20]. Using axes attached the fluid and moving with the average velocity, Tadmor describes the kinematics of the advancing front as a stagnation flow where the particles appear to decelerate as they approach the advancing front and then the particles stretch in an orthogonal direction towards the wall of the mold. The stretching generates considerable orientation, and, thus, as the particles

are laid up on the wall, they are rapidly solidified into a highly oriented state. Hence, the extensional flow at the melt front leads to a higher state of orientation at the surface of the molded part than in the core.

In order to simplify the complex flow behavior that is typically observed during mold filling, it is assumed that the flow behavior of the melt into the rectilinear end-gated mold can be represented by parallel-plate pressure driven flow. A power-law model is used to model the shear rate dependent viscosity and is defined as:

$$\eta = m\left|\dot{\gamma}\right|^{n-1} \tag{3.5}$$

where η is the viscosity, $\dot{\gamma}$ is the shear rate, n is the power-law index and m is the consistency. With these assumptions, the additional orientation that is generated by the extensional flow at the melt front during mold filling is neglected. Based on the above assumptions, the governing fluid flow equations become:

$$Q = \frac{WH^2}{2(s+2)}\left(\frac{H\Delta P}{2mL}\right)^s \tag{3.6}$$

$$\dot{\gamma}_w = \left(\frac{H\Delta P}{2mL}\right)^s \tag{3.7}$$

$$\tau_w = \frac{H\Delta P}{2L} \tag{3.8}$$

where Q is the volumetric flow rate of the viscoelatic fluid, ΔP is the pressure drop, $\dot{\gamma}_w$ is the shear rate at the wall, τ_w is the shear stress at the wall of the mold, H is the thickness of the mold, L is the length of the mold, and s is the reciprocal of the power-law index, n [21]. The height and thickness of the mold are known values and the power-law parameters m and n are determined by fitting Eq. (3.5) with experimental viscosity-shear

rate data that is obtained by performing the rheological measurements of the composite melts as described in the experimental section. Therefore, the pressure drop can be obtained by using Eq. (3.6) if the volumetric flow rate of the fluid is experimentally determined. The volumetric flow rate was experimentally determined by assuming a constant screw injection speed and dividing the total volume, which consists of the volume of the mold, sprue, and gate, by the fill time. The fill time is the time for the polymer to flow from the entrance of the mold to the point where the mold is filled, and it is calculated from the injection time by subtracting the time the screw advances from the retracted position to the point where the polymer composite begins to enter the mold. Once the pressure drop is known, the shear stress at the wall can be calculated by using Eq (3.8).

In addition to the shear stress, the primary normal stress difference, N_1, also contributes to the overall buildup of stress during mold filling of the composite melt. N_1 was estimated by using the White-Metzner model [21] and for steady shear flow it is expressed as:

$$N_1 = 2\eta\lambda\dot{\gamma}^2 \qquad (3.9)$$

where λ is the relaxation time of the polymer chains, and it is a function of shear rate. In order to accurately predict N_1, it is necessary to fit λ to experimental results. N_1 is very difficult to measure for reinforced composites but, for a number of polymers, N_1 is approximately two times the storage modulus, G' [21]. Therefore, as a first approximation, one can calculate the relaxation time at any given frequency (or shear rate) by substituting 2G' for N_1 in Eq. (3.9), provided that the G' is known. However, shear rates much greater than 100 s^{-1} are typically reached during mold filling [20]. To estimate the relaxation time at high rates of shear, Read and Baird [22] found that by rearranging Eq. (3.9) in terms of λ and taking the natural log of both sides, one gets a curve that can be fit by a power-law model. Once the power-law parameters are determined, the relaxation time of the polymer composites can be estimated at the high rates of shear that are generated during mold filling. Because the shear rate during mold filling can be calculated by using Eq. (3.7), one can estimate N_1. By calculating N_1 using

this method, it is assumed that N_1 was approximated by 2G' at high shear rates. It has been shown that at high frequencies G' levels off while N_1 continues to increase as the shear rate increases [23]. Therefore, N_1 is underestimated by using 2G' at high rates of shear, which should lead to an underestimation of the flow-induced stresses that are generated during mold filling. Finally, the total flow-induced stresses at the mold wall, that are generated during mold filling, can be estimated by calculating the principal stress difference, $\Delta\sigma$, which in shear flow is expressed as:

$$\Delta\sigma = \sqrt{4\tau_w^{\,2} + N_1^2} \tag{3.10}$$

3.3.5 Thermally induced and flow-induced residual stresses of the injection molded composites

In order to calculate the residual thermal stresses, the CLTE and G' at ambient temperature were measured. The CLTE values in the flow and transverse direction of the TLCP/PP composites that were generated using a starting pellet size of 6 mm at the various TLCP loadings are presented in Fig. 3.3 and Fig. 3.4. In addition to the thermal expansion and CLTE values of the generated composites, G' at 30°C was also measured by running the DMTA of the solid plaques, and the results are shown in Table 3.1 for the flow and transverse direction. With the CLTE values, G' at 30°C, and the mold temperature of 70°C, the residual thermal stresses in the flow and transverse direction were calculated by using Eq. (3.3) and Eq. (3.4). The results will be presented later.

In order to calculate the flow-induced stresses, the volumetric flow rate and the power-law parameters of the generated TLCP/PP composites were determined experimentally. The fill time and the volume of the mold, including the sprue and gate, were constant at 1.5 seconds and 14820 mm^3, respectively, during injection molding of the TLCP/PP composites that were generated using a starting pellet size of 6 mm at the various TLCP concentrations. Hence, the volumetric flow rate of the composite melts was the same at 9.88E-6 m^3/s for all injection molding runs.

In Fig. 3.11, the complex viscosity, $|\eta^*|$, as a function of frequency for all tested loading levels of TLCP is shown at a temperature of 210°C. The power-law parameters for each composite are also shown in Fig. 3.11, and they were obtained by fitting Eq. (3.5) to the high frequency region of the viscosity-frequency curves. As expected, $|\eta^*|$ in the low frequency region increases with an increase in fiber loading and the increase in viscosity becomes more pronounced with an increase in concentration of the TLCP fibrils. At low concentrations (20 % by weight or less), the addition of the TLCP fibers results in a small increase in viscosity, typically half an order of magnitude or less, relative to the base resin. Also, a Newtonian plateau is still observed at low shear rates when the concentration is 10% by weight or below. At the high fiber loadings, $|\eta^*|$ in the low frequency region is about an order of magnitude larger than that of the base resin. Also, there is no observance of a Newtonian plateau, which is indicative of a yield stress at the high TLCP concentrations. In the high frequency region, $|\eta^*|$ of the TLCP/PP composite melts converges to that of the matrix. Although the viscosity curves begin to merge at high frequency, there is still a significant increase in the viscosity with an increase in fiber loading. These results suggest that during mold filling the shear stress at the wall of the mold will increase with an increase in TLCP concentration.

The flow-induced stresses, $\Delta\sigma$, of the injection molded TLCP/PP plaques that were generated using a starting pellet size of 6 mm at the various TLCP loadings were calculated by using Eqs. (5-10), and the results are presented in Table 3.2 along with the thermally induced stresses in the flow, $\sigma_{F,}$ and transverse direction, σ_T. Generally, the flow-induced residual stresses increase with an increase in concentration of TLCP up to 30 wt% of TLCP, whereas the thermally induced residual stresses decrease in the flow direction due to the significant reduction in thermal expansion and shrinkage attributed to the incorporation of the TLCP fibers. Beyond 30 wt% of TLCP, both the flow-induced and thermally induced stresses remain unchanged with further addition of the TLCP fibers. It is interesting to note that the warpage of the molded parts increases with increasing TLCP concentration even though the thermally induced stresses are reduced. Furthermore, the ratio of the magnitude of the flow-induced stress to that of the thermally induced stress are within an order of magnitude of one another and, as the concentration of the TLCP increases, this ratio decreases until it plateaus at a TLCP concentration of

30% by weight. The ratio of the magnitude of the flow-induced stresses to that of the thermally induced stresses would even be further reduced if the additional flow-induced stresses that are generated by the advancing front were taken into account. This is especially the case for fiber filled polymer systems, where the fountain flow effect leads to highly oriented fibers at the surface of the molded part.

There are two possible reasons for the observed increase in warpage with increasing TLCP concentration: 1) the anisotropy between the thermally induced residual stresses in the flow and transverse direction is increased and 2) the greater generation of orientation of the polymer chains as well as the increased inhibition of stress relaxation of these chains. If the increase in warpage were truly due to the increase in the anisotropy, then one would expect that the warpage of the molded plaques would continue to increase with an increase in the fiber loading, but this is not the case. At TLCP loadings of 30 and 40 wt% of TLCP, the magnitude of the flow-induced and thermally induced residual stresses that are locked into the molded parts are nearly equivalent, which results in warpage values that are nearly equivalent within experimental error. These results correlate well with the observed warpage and twist of the TLCP/PP composites and show that the flow-induced stresses may have a more significant impact on the warpage of fiber reinforced injection molded parts than previously thought. Therefore, to accurately predict the warpage of fiber reinforced injection molded parts, the flow-induced residual stresses must be accounted for**.**

3.4 Conclusions

This study was concerned with ascertaining the main causes of the enhanced warpage observed for injection thermoplastics reinforced with high aspect ratio fibers. In this case, the warpage of PP composites reinforced with TLCP fibers was investigated and correlated to enhanced flow-induced residual stresses in the presence of the high aspect ratio fibers. The increase in warpage was attributed to an inhibition of stress relaxation of the polymer chains and greater generation of frozen-in flow induced stresses with an increase in the concentration of the fibers. As the concentration of fibers increased, the warpage increased up to a TLCP loading of 30% by weight at which point

a plateau was reached, where further addition of the TLCP fibers had no affect on the warpage. The observed plateau in the warpage could not be accounted for by changes in the thermally induced residual stresses. The shrinkage and the thermal expansion of the TLCP/PP composites were significantly reduced in the presence of the fibers with the decrease being enhanced by further addition of the TLCP fibers. Therefore, the warpage increased with an increase in TLCP concentration, while the thermally induced residual stresses decreased. On the other hand, the flow-induced stresses increased with an increase in fiber concentration. This suggests that, for fiber-filled thermoplastics, the flow-induced stresses may have a more significant impact on the warpage than previously thought. Therefore, in order to accurately predict the warpage of fiber reinforced thermoplastics, the flow-induced residual stresses must be accounted for.

3.5 Acknowledgements

The authors would like to gratefully acknowledge the support from the DaimlerChrysler Challenge Fund. We also appreciate DuPont for donating the TLCPs.

3.6 References

1. H. Kikuchi and K. Koyama, *Polym. Sci. Eng.*, **34(18)**, 1411 (1994).

2. H. Kikuchi and K. Koyama, *Polym. Sci. Eng.*, **36(10)**, 1317 (1996).

3. H. Kikuchi and K. Koyama, *Polym. Sci. Eng.*, **36(10)**, 1326 (1996).

4. H. Kikuchi and K. Koyama, *Polym. Sci. Eng.*, **36(10)**, 1309 (1996).

5. R. Zheng, P. Kennedy, N. Phan-Tien, and X.J. Fan, *J. Non-Newtonian Fluid Mech.*, **84**, 159 (1999).

6. P.J. Hine and R.A. Duckett, *Polym. Compos.*, **25(3)**, 237 (2004).

7. P.H. Foss, *Polym. Compos.*, **25(4)**, 343, (2004).

8. M.R. Kamal, R.A. Lai-Fook, and J.R.Hernandez-Aguilar, *Polym. Eng. Sci.*, **42(5)**, 1098 (2002).

9. D. Choi and Y. Im, *Composite Structures*, **47**, 655 (1999).

10. C. Shen and H. Li, *Polymer-Plastics Technology and Engineering*, **42(5)**, 971 (2003).

11. W.C. Bushko and V.K. Stokes, *Polym. Sci. Eng.*, **35(4)**, 351 (1995).

12. W.C. Bushko and V.K. Stokes, *Polym. Sci. Eng.*, **36(3)**, 322 (1996).

13. W.F. Zoetelief, L.F.A. Douven, and A.J. Ingen Housz, *Polym. Eng. Sci.*, **36(14)**, 1886 (1996).

14. R. Wimberger-Friedl, PhD thesis, Eindhoven University of Technology, The Netherlands (1990).

15. E.A. Sabol, A.A. Handlos, and D.G. Baird, *Polym. Compos.*, **16**, 330 (1995).

16. D.G. Baird, W. Huang, and J. Huang, *J. of Injection Molding Technology*, **5(4)**, 233 (2001).

17. A.A. Handlos and D.G. Baird, *Int'l. Polym. Process.*, **XI**, 1 (1996).

18. D.G. Baird and A.M. Sukhadia, U.S. Patent, 5,225,488 (1993).

19. A.A. Handlos and D.G. Baird, *Int'l Polym. Process.*, **VII**, 218 (1992).

20. Z. Tadmor, *J. Appl. Polym. Sci.*, **18**, 1753 (1974).

21. D.G. Baird and D.I. Collias, *Polymer Processing*, John Wiley & Sons, Inc., New York (1998).

22. M. Read, Ph.D. Dissertation, Virginia Polytechnic Institute and State University, Blacksburg, VA (1986).

23. R.B. Bird, R.C. Armstrong, and O. Hassager, *Dynamics of Polymeric Liquids*, John Wiley and Sons, New York (1987).

Table 3.1: Storage modulus at 30°C as a function of TLCP concentration (6 mm pellet length).

TLCP Concentration (% by weight)	Flow (Pa)	Transverse (Pa)
0	1.54E8	1.58E8
10	1.82E8	1.78E8
20	2.05E8	2.03E8
30	2.15E8	1.95E8
40	2.56E8	2.35E8

Table 3.2: Estimations of Flow and Thermally Induced Residual Stresses as a function of TLCP concentration (6 mm pellet length).

TLCP Concentration (% by weight)	$\Delta\sigma$ (Pa)	σ_F (Pa)	σ_T (Pa)	Ratio of $\sigma_F/\Delta\sigma$	Ratio of σ_F/σ_T
0	7.79E5	4.38E6	4.64E6	5.63	1.06
10	9.32E5	4.27E6	5.33E6	4.58	1.25
20	1.08E6	3.90E6	5.74E6	3.63	1.47
30	1.52E6	3.64E6	5.37E6	2.4	1.47
40	1.52E6	3.29E6	6.14E6	2.16	1.7

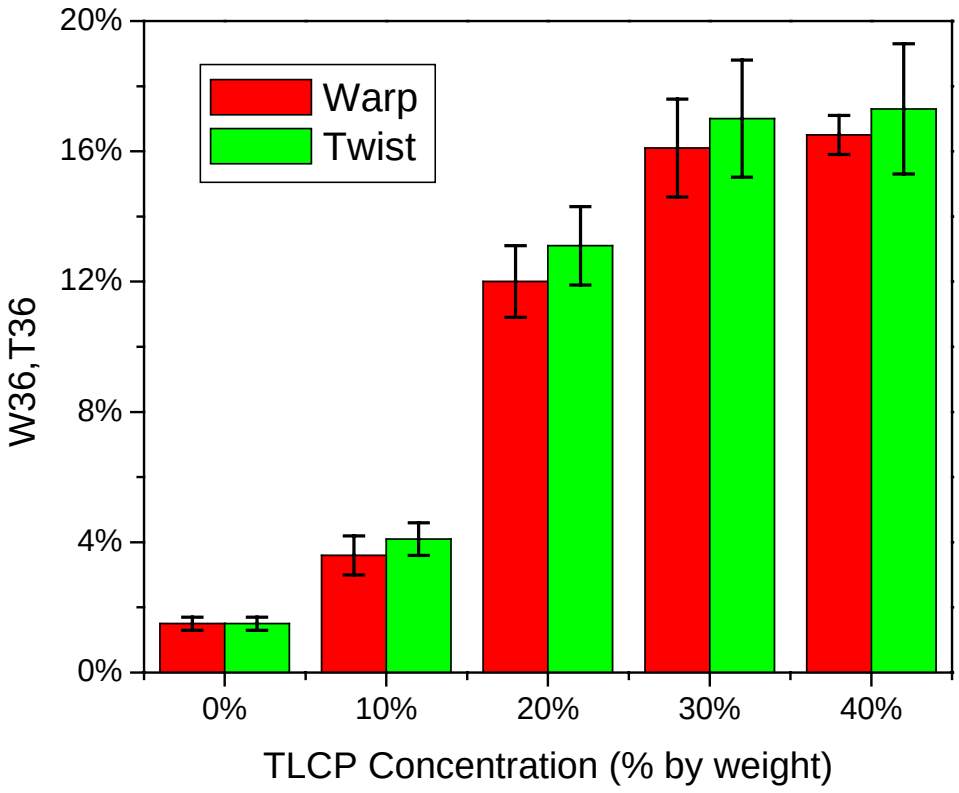

Figure 3.1: Warpage and twist of TLCP/PP composites as a function of TLCP concentration. The TLCP/PP composites were generated with pellets that were 6 mm in length.

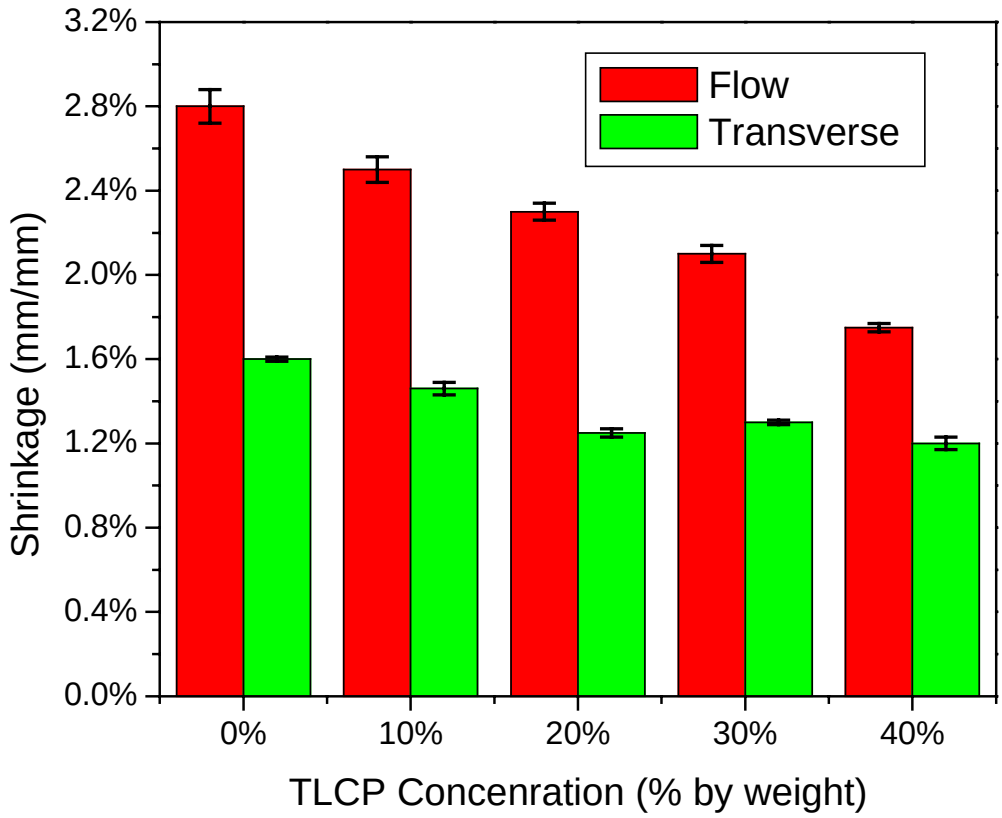

Figure 3.2: Flow and transverse direction shrinkage of TLCP/PP composites as a function of TLCP concentration. The TLCP/PP composites were generated with pellets that were 6 mm in length.

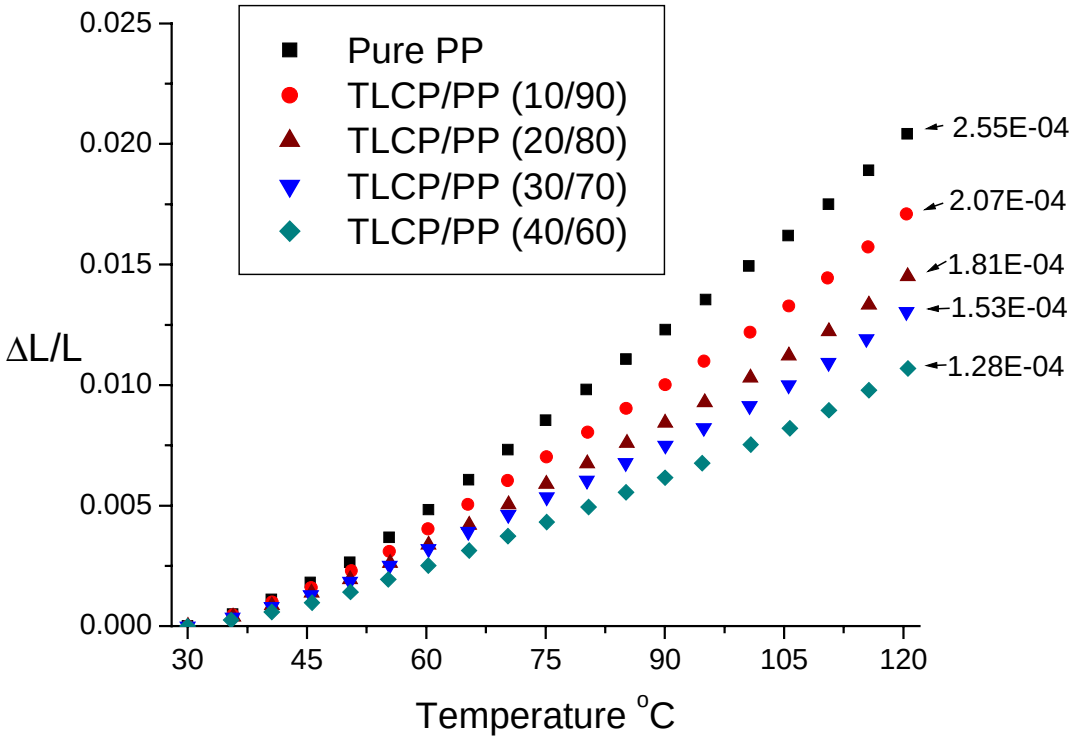

Figure 3.3: Thermal strain (mm/mm) and CLTE values (mm/mm/°C) in the flow direction of the TLCP/PP composites as a function of TLCP concentration. The TLCP/PP composites were generated with pellets that were 6 mm in length. A temperature ramp of 5°C/min was applied.

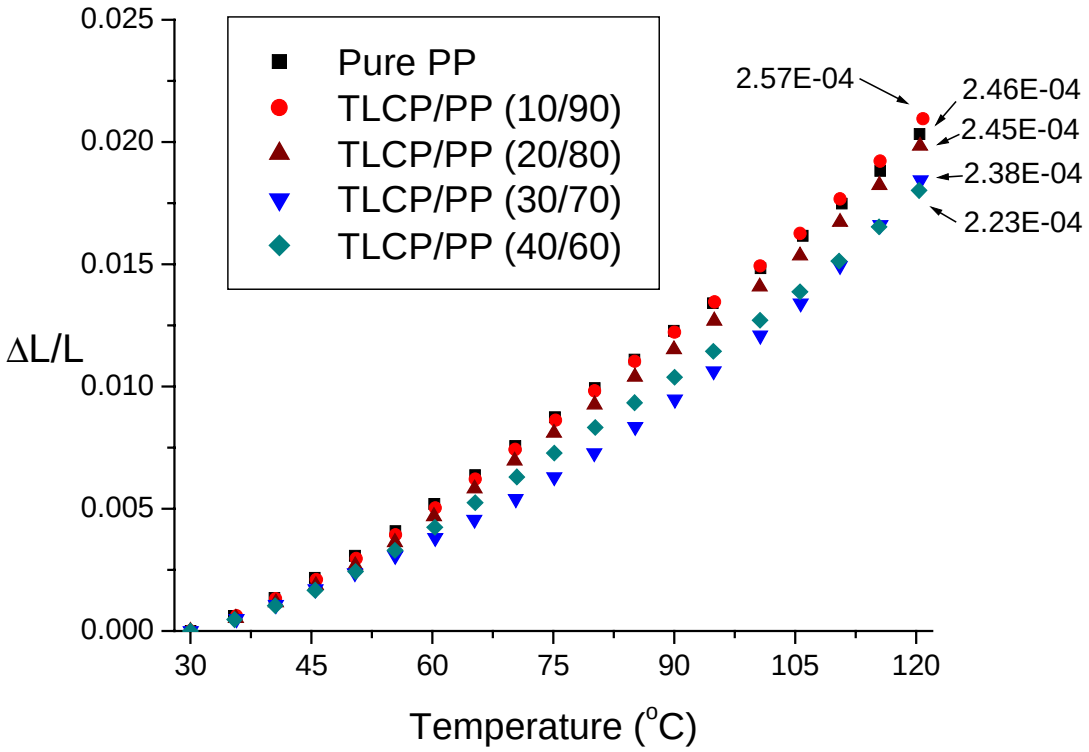

Figure 3.4: Thermal strain (mm/mm) and CLTE values (mm/mm/°C) in the transverse direction of the TLCP/PP composites as a function of TLCP concentration. The TLCP/PP composites were generated with pellets that were 6 mm in length. A temperature ramp of 5°C/min was applied.

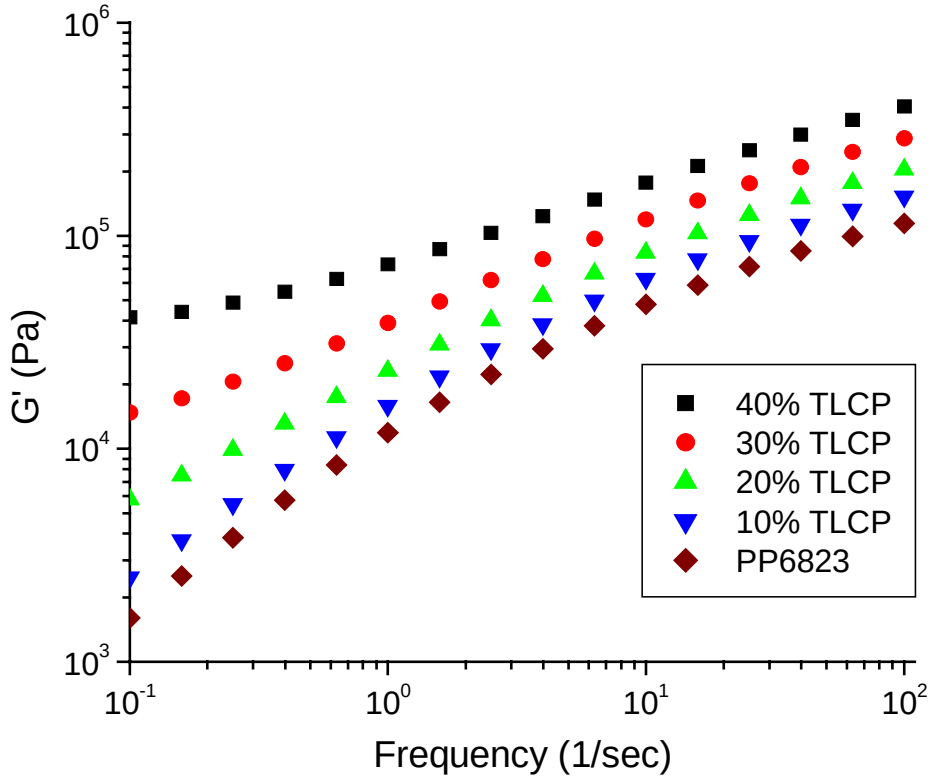

Figure 3.5: Storage modulus as a function of frequency of the TLCP/PP composites for different TLCP loadings at a melt temperature of 210°C. The TLCP/PP composites were generated with pellets that were 6 mm in length.

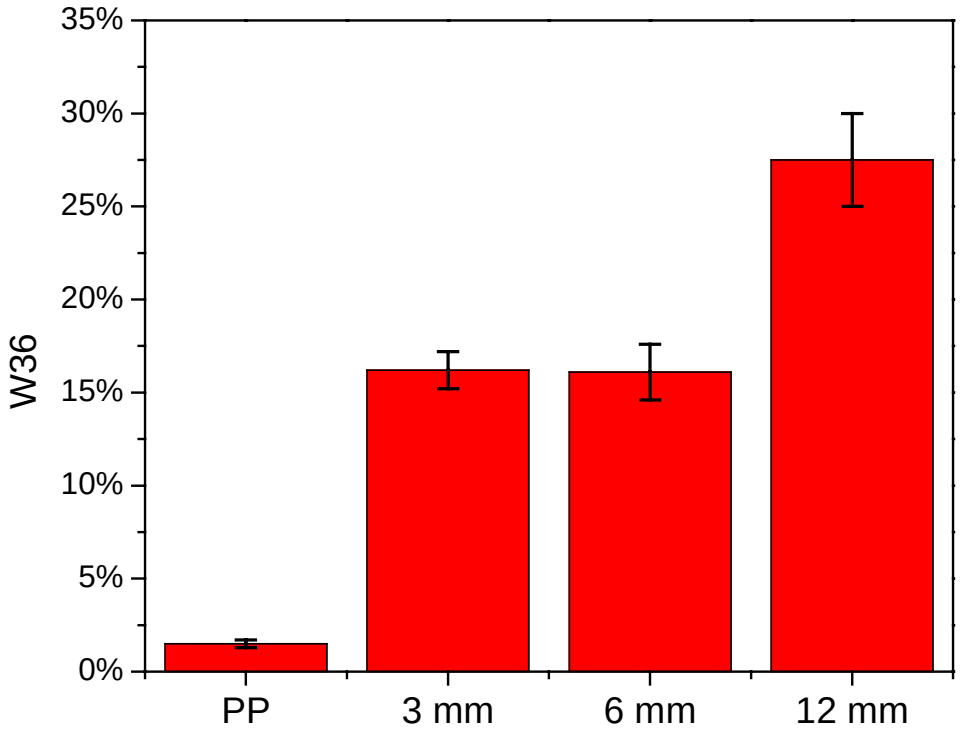

Figure 3.6: Warpage of unfilled PP and TLCP/PP composites as a function of starting pellet length. Concentration of TLCP in PP is 30 wt%.

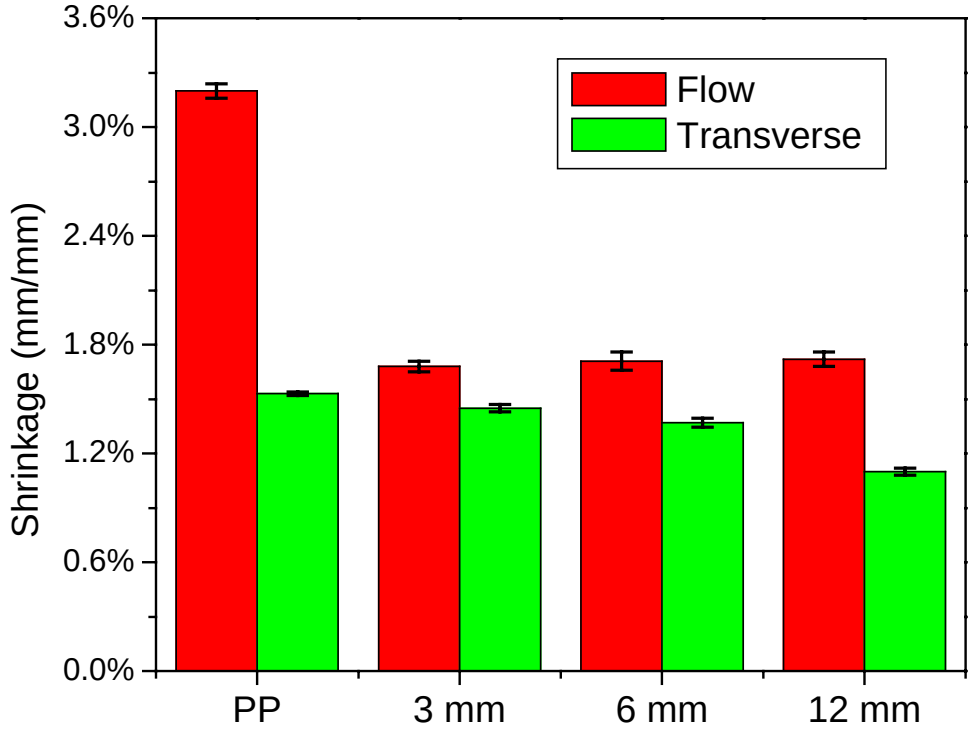

Figure 3.7: Flow and transverse direction shrinkage of unfilled PP and TLCP/PP composites as a function of starting pellet length. Concentration of TLCP in PP is 30 wt%.

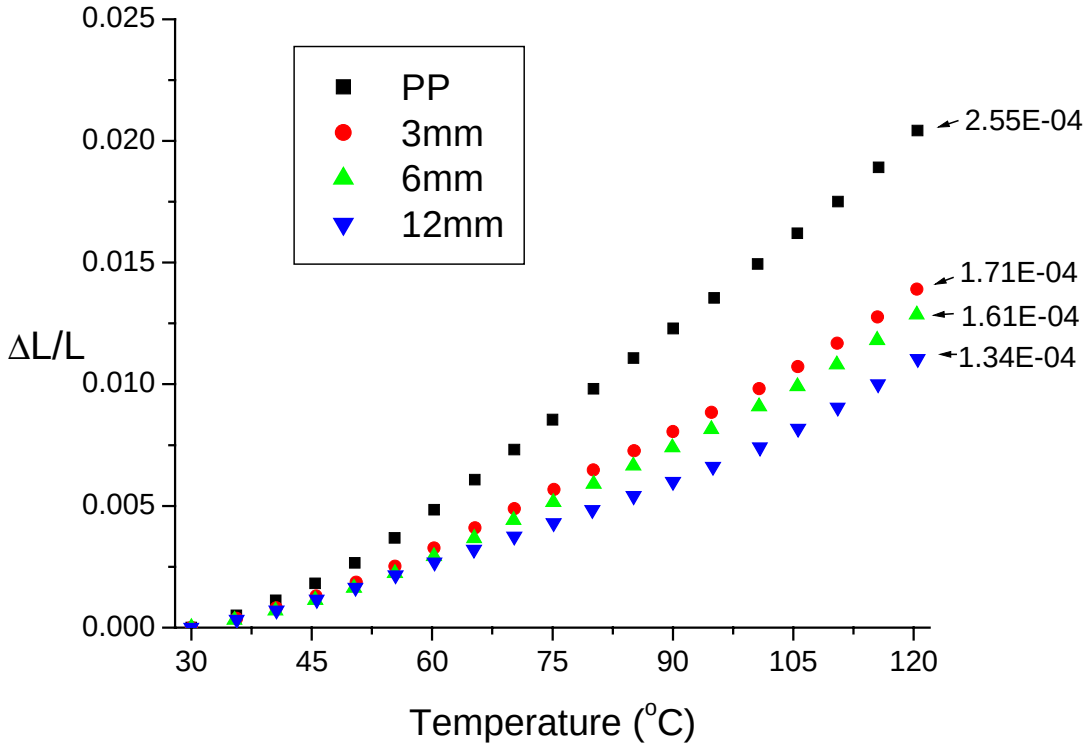

Figure 3.8: Thermal strain (mm/mm) and CLTE (mm/mm/°C) values in the flow direction of unfilled PP and the TLCP/PP composites as a function of starting pellet length. Concentration of TLCP in PP is 30 wt%. A temperature ramp of 5°C/min was applied.

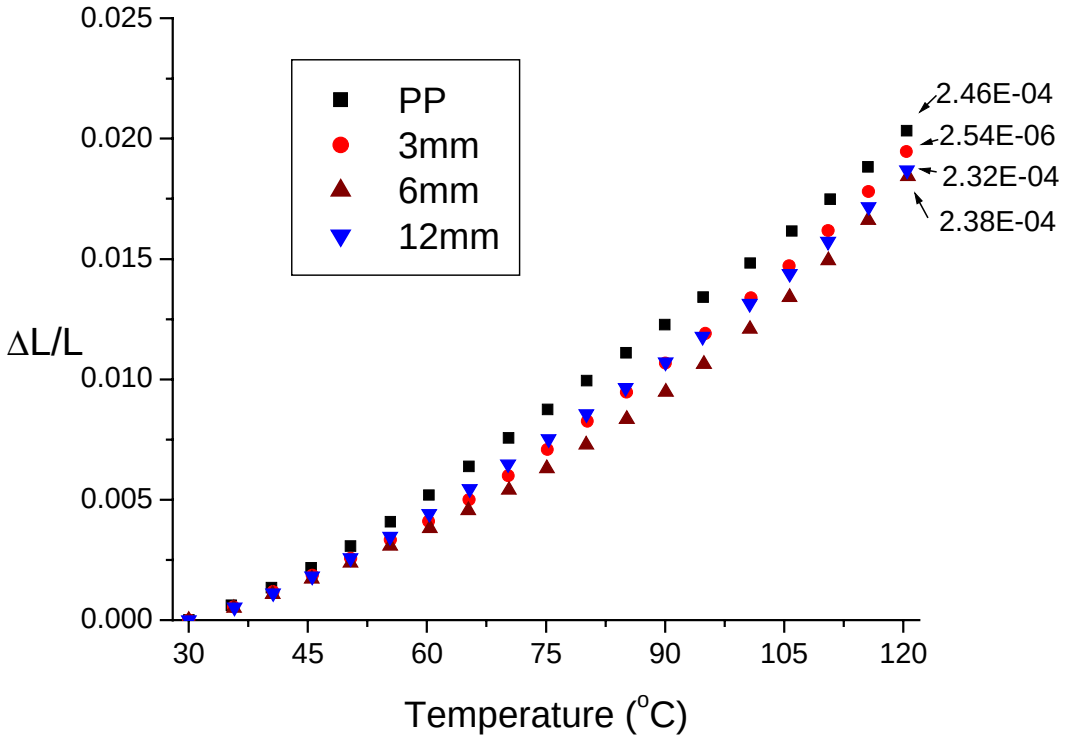

Figure 3.9: Thermal strain (mm/mm) and CLTE values (mm/mm/°C) in the transverse direction of unfilled PP and the TLCP/PP composite as a function of starting pellet length. Concentration of TLCP in PP is 30 wt%. A temperature ramp of 5°C/min was applied.

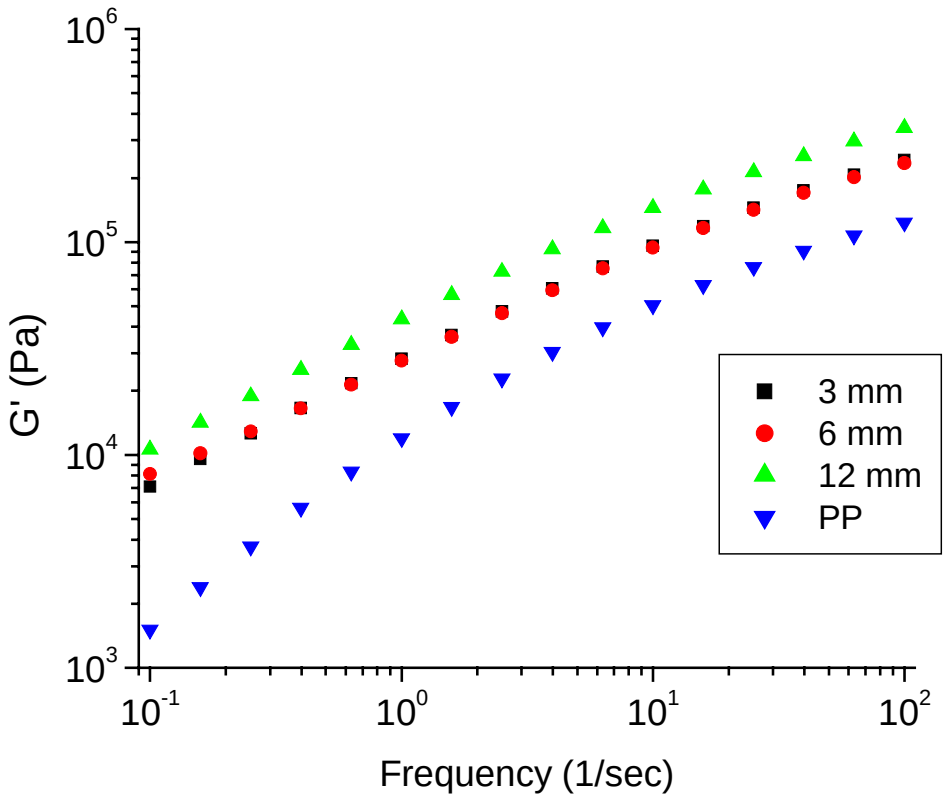

Figure 3.10: Storage modulus as a function of frequency of unfilled PP and the TLCP/PP composites for different starting pellet lengths at a melt temperature of 210°C. Concentration of TLCP in PP is 30 wt%.

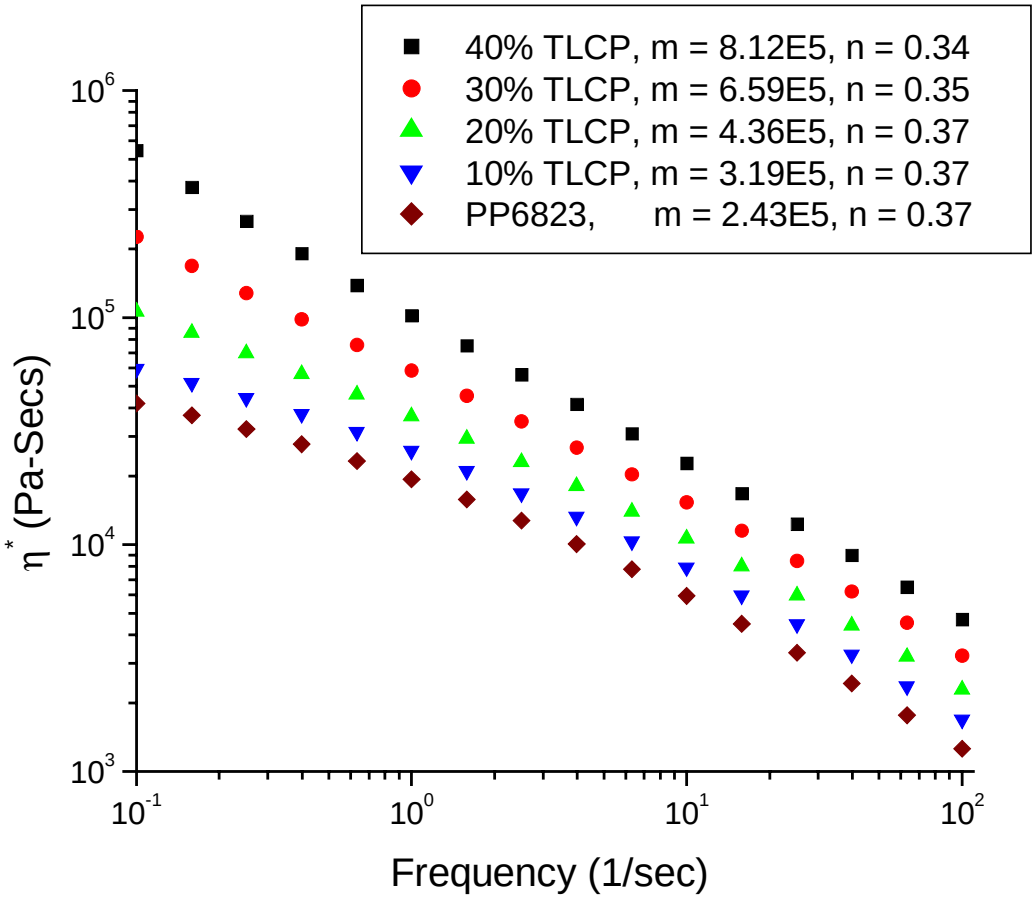

Figure 3.11: Complex viscosity as a function of frequency of the TLCP/PP composites for different TLCP loadings at a melt temperature of 210°C. The TLCP/PP composites were generated with pellets that were 6 mm in length.

4.0 Effect of Blending Sequence on the Dimensional Stability and Properties of Talc Reinforced PC/PBT Composites

W.S. DePolo and D.G. Baird
Department of Chemical Engineering and Macromolecules and Interfaces Institute, Virginia Polytechnic Institute and State University, Blacksburg, VA 24061-0211.

(ABSTRACT)

Ternary blends based on polycarbonate (PC), poly[butylene terephthalate] (PBT), and talc are typically mixed in one step having a talc composition in the range of 6–12% by weight. The addition of the talc particles gives rise to increased flexural modulus in the range of 3 GPa and reduced thermal expansion, which is advantageous for the production of exterior body panels. However, at these high talc loading levels, the tensile toughness and impact strength are significantly reduced. In an effort to improve the dimensional stability and the tensile toughness of the ternary blends while maintaining the modulus, three different blending sequences of the above ternary composite were prepared: melt blend PBT with talc first and then dry blend the PC with the PBT/talc (PPT-PBT), melt blend the PC, PBT, and talc in one step (PPT-All), and melt blend PC with talc first and then dry blend PBT (PPT-PC). It was found that the blending sequence had a significant influence on the tensile toughness while maintaining a flexural modulus of 3.0 GPa. The ternary composites compounded and injection molded by using blending sequence PPT-PBT had approximately a 10% and 65% greater tensile toughness relative to that of the samples prepared by using blending sequences PPT-All and PPT-PC, respectively. The higher toughness observed for samples prepared by using blending sequence PPT-PBT was attributed to encapsulation of the talc particles within the PBT phase and better dispersion of the talc particles within the PC/PBT matrix.

4.1 Introduction

Ternary blends based on polycarbonate (PC), poly[butylene terephyhalate] (PBT), and talc have been receiving much commercial attention in recent years, especially in the automotive industry. PC has a good balance of properties, which include high modulus and strength, heat deflection temperature, and tensile toughness. However, it has poor solvent and hydrolysis resistance [1]. Therefore, PBT is blended with PC to improve the chemical resistance of molded parts.

PC/PBT blends by themselves do not have high enough modulus for use in the manufacture of car door panels and, hence, some type of reinforcement is required to increase the modulus. Typically, short-glass fiber reinforcements are used to increase the modulus for car door applications. However, short-glass fiber composites are injection molded to produce panels, there is a considerable tendency for the part to warp. This is attributed to thermally induced stresses (shrinkage and coefficient of linear thermal expansion, CLTE) and "frozen-in" orientation, associated with large increases in the normal stresses during melt flow of the reinforced blends relative to that of the matrix [2-7]. On the other hand, mineral reinforcements (low aspect ratio particles), such as talc, do not generate large normal stresses and in some instances have lower normal stresses than that of the matrix [8]. Therefore, talc is being used as reinforcement due to its ability to increase the modulus of the PC/PBT blends while maintaining and possibly improving the dimensional stability of flat panels produced by means of injection molding.

Although the addition of particulates, such as talc, gives rise to an increase in the modulus, there is also a subsequent decrease in the impact strength and/or tensile toughness [9-13]. Typically, the impact strength and/or tensile toughness are significantly reduced at low particle loadings (< 10% by weight) while further addition of filler (> 10% by weight) leads to only slight reductions in their values [9,11-13]. For example, a 75% reduction in impact strength was observed with the addition of 10% by weight of mica particles in a PP matrix but at a mica loading of 40% by weight, the impact was further reduced by only 10% relative to that of the PP matrix [10]. For calcium carbonate particles in a PP matrix, the impact strength and tensile strength were

reduced by 60% and 20%, respectively, at a particle loading of 40% by weight. Futhermore, the impact strength and tensile toughness of PP/talc blends at a talc loading of 30% by weight were reduced by 50% and 70%, respectively, relative to the base resin [11]. There are several possible reasons for the reduction of these mechanical properties with the addition of particulates. First, an increase in particle loading allows for an increase in the number of polymer chains that can be absorbed on to the filler surface. The absorption of the polymer chains results in a shell of immobilized polymer chains around the filler particles [14]. Therefore, these polymer chains will be unable to deform under an applied load, which results in a more brittle material, and hence, a reduction in the toughness and impact strength. Secondly, agglomeration of particles significantly reduces both impact strength and toughness of particulate filled systems. The tendency of particles to agglomerate with each other increases with an increase in particle loading, especially when the polymer/matrix interactions are weak.

Traditionally, ternary blends of PC, PBT, and talc are mixed in a one step process but there has been evidence in recent years that blending sequence can have a significant influence on the morphological structure (location of the reinforcing filler) and, hence, the mechanical properties (ie. modulus, strength, and toughness) of ternary blends [1, 15-21]. For example, Zheng and Li [15] investigated the effect of blending sequence for PP/Zinc-Neutralized Sulfonated Ethylene Diene Rubber (Zn-SEPDM)/$CaCO_3$ blends. For the first blend sequence (A), the Zn-SEPDM was blended with PP first and then blended with the $CaCO_3$ in a second step. Furthermore, the second blending sequence (B) involved blending the rubber with the calcium carbonate first and then blending the PP in a second step. It was found that for blend sequence (B) the impact strength and elongation at break of the samples was about 100% higher than that of the samples prepared by using blend sequence (A) at an equivalent loading of calcium carbonate for a particle loading range of 3-10% by weight. The large difference in impact strength and elongation at break was attributed to the placement of the inorganic filler within the blend. By blending the rubber with the calcium carbonate particles first, the filler became encapsulated within the dispersed rubber phase. However, by employing blend sequence A, the calcium carbonate particles and the rubber phase were separately dispersed within the continuous PP phase.

Cheng et al. [1] investigated the effect of blending sequence for ternary blends of PC/SAN/MBS, where MBS is methacrylated butadiene-styrene and the acrylonitrile content in SAN (styrene-acrylonitrile) was 25% by weight. They found that the highest impact strength was observed when SAN was blended with the MBS first. In this case, most of the modified rubber particles resided in the SAN phase, but there were still some particles at the interface between the SAN and PC phases as well as in the PC-rich phase. For the other blending sequences, the modified rubber particles were more concentrated at the interface or in the PC phase but had relatively the same impact strength (50% less than the above blending sequence).

In a work by Kim and Lee [16], the blend sequencing of nylon-6/poly(styrene-co-maleic anhydride) (SMA)/ABS blends was investigated. It was found that blending of SMA and ABS first showed better dispersions or finer structures than blends where SMA and nylon-6 were mixed first or for blends generated in one mixing sequence. This was attributed to better interfacial adhesion at the interface between nylon-6 and ABS. The mechanical properties were not reported.

Benderly et al. [17] investigated the blending sequence of PP/nylon-6 blends filled with short-glass fibers. They found that the blending sequence had no effect on the placement of the glass fibers. In all three mixing sequences, the glass fibers were encapsulated by the dispersed nylon-6 phase. The encapsulation of the glass fibers reduced the amount of "free" nylon-6 droplets that were dispersed in the continuous PP matrix, thus, reducing the degree of droplet coalescence. This led to the development of finer structures for the dispersed Nylon-6 phase. One would expect that the mechanical properties would increase due to the addition and encapsulation of the short-glass fibers, but they were not reported in this study.

Hobbs et al. [18,19] and Delimoy et al. [20] investigated PC/PBT blends with an impact modifier. With these systems, the impact modifier was primarily located in the PC phase, which increased the impact strength of the composites. In this work, the effect of blending sequence was not investigated.

Finally, Li et al. [21] investigated on how the blending sequence of PBT, maleic anhydride grafted poly(ethylene-co-vinyl acetate) (EVA-g-MAH), and organically modified montmorillonite (organoclays) composites influenced their structure and

properties. They found that in a two-step blending sequence the organoclays stayed in the PBT phase while in the one step process the organocalys were mixed evenly in both the PBT and EVA-g-MAH phase. Samples generated by means of the two-step procedure had much greater impact strength, which was attributed to the organoclays being distributed solely in the PBT phase.

The effect of blending sequence on the dimensional stability, i.e. coefficient of linear thermal expansion (CLTE), and the mechanical properties of ternary blends based on PC, PBT, and talc is of primary interest in this paper. In particular, our goal is to evaluate the role that blending sequence has on the particle placement of the filled blends and how the structure-property relationships correlate with the melt rheology of the PC and PBT components. In this study, three different blending sequences of the PC/PBT/talc composite were prepared: (1) PBT and talc were first melt blended in an extruder and, then, in a second-step, the PBT/talc composites were dry blended with PC and melt processed in an injection molder, (2) PC and talc were first mixed in an extruder and, then, in a second step, the PC/talc composites were dry blended with PBT and melt blended in the injection molding process, and (3) the PC, PBT, and talc were all melt blended in an extruder and, then, in a second-step, the PC/PBT/talc composites were further blended during the injection molding process.

4.2 Experimental

4.2.1 Materials

The PC used in these experiments was Lexan 101, which was provided by GE. It has a solid density of 1.20 g/cm^3, melt flow rate of 0.7g/min at 300°C, and a glass transition temperature of 160°C. The PBT used was Celanex 1600A, which was provided by Ticona. It has a solid density of 1.31 g/cm^3 and a glass transition temperature of 55°C.

The talc used in this study was Cimpact 699 provided by Luzenac. Cimpact 699 consists of talc particles with a disc shaped geometry that have an average aspect ratio on the order of 5-10, where the aspect ratio is defined as the ratio of the disc diameter to the thickness of the plate. The average particle size of the talc is 1.5 microns and the loose

bulk density is between 0.1-0.15 g/cm^3. The chemical formula for talc is $Mg_3(Si_4O_{10})(OH)_2$ and the chemical structure of the talc particles is comprised of a layer of magnesium-oxygen/hydroxyl octahedral sandwiched between two layers of silicon-oxygen tetrahedral [22]. The basal surface of the talc particles does not contain any hydroxyl groups or active ions and, therefore, it is chemically inert. Cimpact699 was chosen because of its small average particle size. In studies performed by Hancock [23] and Abolins [24], maximum values of toughness were obtained for fillers with the smallest average particle sizes provided that there were no coarse particles present and the dispersion of the particles was good. No additives were used in the melt processing steps, such as an inhibitor for the interchange reactions that may occur with PC and PBT. However, based on previous studies, uncatalyzed blends of PC and PBT were found to have negligible amounts of transesterification products at the processing conditions employed for this study [20, 25-26]. The overall residence time of the melt blends in the compounding and injection molding steps combined was less than 5 minutes for this study. It was shown by Nazabal et al. [25] that a negligible amount of interchange reactions occurred for blends of PC and PBT when mixed in a batch reactor at a residence time of 8 minutes or less.

4.2.2 Compounding and Injection Molding of PC/talc and PBT/talc Blends

Prior to melt processing, the PC, PBT, and talc were all dried in a vacuum oven for at least 14 hours at a temperature of 120°C. In preparation of the PC/talc and PBT/talc composites, the dried pellets of PC or PBT were first mechanically mixed with the talc particles at talc concentrations of 8 and 16 wt% and then compounded with a single-screw Killion extruder that had a 25 mm diameter barrel and a L/D of 30. The die was cylindrical with L/D of 2.5 and diameter of 3 mm. The screw speed was maintained at 20 rpm and the process temperature was 320°C for the PC/talc composites and 250°C for the PBT/talc composites. Upon exiting the die, the composite strands were quenched in a water bath and then chopped into 6 mm long pellets.

After compounding, the PC/talc and PBT/talc composites were then injection molded using an Arburg Allrounder Model 221-55-250 injection-molding machine. The Arburg Allrounder had a 22 mm diameter screw, a check ring non-return valve, and an insulated nozzle that was 2 mm in diameter [27]. The composites were injection molded at a melt temperature of 320°C and 250°C for the PC/talc and PBT/talc composites, respectively, a mold temperature of 100°C, a holding pressure of 100 bars, and a screw speed of 200 RPMs, into a rectangular end-gated mold with dimensions of 80 mm by 76 mm by 1.6 mm.

4.2.3 Compounding and Injection Molding of PC/PBT/talc Blends

Prior to melt processing, the PC, PBT, and talc were all dried in a vacuum oven for at least 14 hours at a temperature of 120°C. The compounding and injection-molding step was performed using the same extruder and injection molder as described in the previous section. During compounding of the blends, the screw speed was maintained at 20 rpms. During injection molding of the blends, a melt temperature of 270°C, a mold temperature of 100°C, and a holding pressure of 100 bars were maintained.

The PC/PBT/talc composites were pre-mixed as summarized in Table 4.1 and the details of the sequential blending process are described as follows. For blending sequence (PPT-PBT), the PBT was first mechanically mixed with the talc particles and then melt blended in the extruder at a melt temperature of 250°C. The PBT/talc composites were then dry-blended with PC and injection molded. For blending sequence (PPT-PC), the PC was first mechanically mixed with the talc particles and then blended in the single-screw extruder at a melt temperature of 320°C. The PC/talc composites were then dry-blended with PBT and injection molded. For the blending sequence (PPT-All), PC, PBT, and talc were all mechanically mixed together and then melt blended in the extruder at a melt temperature of 270°C. The PC/PBT/talc composites were then further mixed in the injection molder. The final composition of the PC/PBT/talc composites had a PC/PBT blend ratio of 50/50 (by weight) and a talc loading level of 8 wt%, regardless of the blending sequence employed.

4.2.4 Dynamic Mechanical Thermal Analysis of Molded Plaques

Dynamic mechanical thermal analysis (DMTA) of the composites was performed using a Rheometrics RMS-800 rheometer. Along with measurements of the storage (G') and loss (G") moduli, the CLTE was also measured. When using a torsional rectangular geometry, the Rheometrics RMS-800 contains a function called auto-tension, which maintains a small tension on the samples as it expands during heating. When auto-tension is enabled, the displacement of a sample can be measured as the material is heated from an initial testing temperature. Therefore, the CLTE of a sample can be measured experimentally within the range of temperatures tested. To perform the tests, rectangular strips approximately 75 mm long by 8 mm wide were cut near the center of the plaques. Once the strips were mounted in the rheometer, G', G", and the change in length as a function of temperature was measured. The temperature range of 30°C to 100°C was investigated at a temperature ramp rate of 5°C/min under a continuous nitrogen atmosphere. For each composite generated, three samples were tested to check for reproducibility. The CLTE of each composite generated was determined by plotting the change in length normalized to the initial length at 30°C as a function of temperature. The slope of the line is the CLTE for that material, and it has units of (mm/mm)/ °C.

4.2.5 Dynamic Mechanical Thermal Analysis of the PC and PBT Components

The complex viscosity, $|\eta^*|$, of the pure PC and PBT components in the melt state was measured using a parallel-disk rheometer (Rheometrics RMS-800) with 25 mm diameter plates. The temperature range of 250°C to 300°C was investigated at a temperature ramp rate of 5°C/min, frequency of 1 rad/s, gap size of 1 mm and strain of 5% under a continuous nitrogen atmosphere. A minimum of 3 samples was tested to check for reproducibility.

4.2.6 Degradation of PBT

To check for degradation of PBT at elevated temperatures, $|\eta^*|$ of the PBT was measured using a parallel-disk rheometer (Rheometrics RMS-800) with 25 mm plates at a frequency of 1 rad/s, gap size of 1 mm, and strain of 5% for 30 minutes. Tests were performed at 260°C and 270°C under nitrogen. A minimum of 3 samples was tested to check for reproducibility.

4.2.7 Mechanical Properties

Flexural and tensile properties of the composites were tested by using an Instron mechanical tester, model 4204. Test specimens were prepared by cutting rectangular strips approximately 75 mm long by 8 mm wide near the center of the molded plaques. Flexural specimens were tested in accordance with ASTM standard D790 while the tensile specimens were tested at a crosshead speed of 1.27 mm/min in accordance with ASTM standard D2256. An extensiometer, Instron model 2630-25, was also used for all tensile tests to provide an accurate measure of the tensile modulus. A minimum of 5 samples was tested in the flow direction, and an average value and standard deviation were calculated from the data.

4.2.8 Transmission Electron Microscopy (TEM)

The morphology of the PC/PBT/talc composites was characterized by means of transmission electron microscopy using a Philips EM420T. The acceleration voltage used was 100kV. Ultra-thin sections of the injection-molded plaques were cut at room temperature using a Reichert-Jung Ultracut E Microtome fitted with a 35° diamond knife. The ultra-thin sections were recovered on 300 mesh Cu grid. Delimoy et al. [20] reported that the natural phase contrast between the PC and PBT phases is weak. Therefore, to improve the phase contrast, the samples were stained by exposing them to RuO_4 vapors for approximately 15 minutes following the procedure described by Delimoy et al. [20]. In this study, the specimen blocks were cut near the center of the molded plaques and microtomed sections were cut perpendicular to the flow direction.

4.3 Results and Discussion

4.3.1 Effect of concentration on the thermal expansion and toughness of PC/talc and PBT/talc composites

The effect of talc concentration on the thermal expansion of the PC/talc and PBT/talc composites was investigated by varying the talc loading level (8%, and 16% by weight). In Fig. 4.1, the thermal expansion and coefficient of linear thermal expansion, CLTE, of the PC/talc and PBT/talc composites is illustrated as a function of talc content over the temperature range of 30°C to 100°C. The numerical values on the right hand side of Fig. 4.1 are the CLTE values (mm/mm/°C), which were determined by the slopes of the lines within the temperature range of 40°C to 100°C. The CLTE and the overall dimensional change of the unfilled PBT are much greater than that of the unfilled PC. The large difference in the thermal properties between unfilled PC and PBT is due to PBT's low glass transition temperature of 50°C to 55°C relative to that of PC, which is 160°C. With an increase in talc loading, the CLTE and the overall dimensional change of the talc filled PC and talc filled PBT composites decrease, but the magnitude of the decrease is much more pronounced for the PBT/talc composites relative to that of the PC/talc composites over the temperature range studied. For example, at a talc loading of 8% by weight, the CLTE of the PBT/talc composite is reduced by 18% relative to the base resin while the CLTE of the PC/talc composite is only reduced by half as much (9%) relative to its base resin. Furthermore, the overall dimensional change of the PBT/talc and PC/talc composites at a talc loading of 8% by weight and a temperature of 100°C is reduced by 20% and 8%, respectively, relative to the values of the neat resin components. It is also interesting to note that the overall dimensional change of the PBT/talc composite at a talc loading of 16% by weight is 30% greater than that of the unfilled PC.

In Fig. 4.2, the effect of concentration on the tensile toughness of the PBT/talc and PC/talc are shown as a function of talc concentration (0%, 8%, and 16% by weight). The tensile toughness of the unfilled PC (24 MPa) is approximately 25% greater than that of the unfilled PBT (17.5 MPa). However, with the addition of talc, the filled PBT composites retain its initial tensile toughness to a greater extent than the filled PC composites. In fact, at an equivalent concentration of talc (8% or 16% by weight), the

tensile toughness of the filled PBT composites is greater than that of the filled PC composites even though the tensile toughness of the PBT is initially lower than that of the PC. At the highest talc concentration, the PC/talc and PBT/talc composites lose more than 90% of their initial tensile toughness. At the lower talc concentration (8% by weight), on the other hand, PBT retains approximately 30% of its original toughness, whereas the PC only retains 10% of its original toughness.

These results suggest that the dimensional stability and tensile toughness of ternary blends consisting of PC, PBT, and talc can potentially be improved by maintaining the talc particles within the PBT phase for various reasons. First of all, the reduction in the CLTE and overall dimensional change with the addition of talc is much more pronounced in PBT/talc composites relative to that of the PC/talc composites. Secondly, with the addition of talc, the talc filled PBT composites retain its initial toughness to a much greater extent than that of the filled PC composites. Because, it is possible that a simple simultaneous mixing of the PC, PBT, and talc may not produce the desired phase morphology (keeping the talc in the PBT phase), the effect of blend sequencing on the dimensional stability and the structure-property relationships of ternary blends consisting of PC, PBT, and talc are investigated in the sections that follow.

4.3.2 Thermal Expansion and Mechanical Properties of PC/PBT/talc composites

The effect of blending sequence on the thermal expansion of the ternary PC/PBT/talc composites was investigated by varying the blend preparation protocol as summarized in Table 4.1. The final composition of the blends consisted of a PC/PBT blend ratio of 50/50 (by weight) and a talc concentration of 8% by weight. In Fig. 4.3, the thermal expansion and CLTE of the PC/PBT/talc composites are illustrated as a function of blending sequence in the temperature range of 30°C to 100°C. With the addition of talc particles, the CLTE and the magnitude of the dimensional change at 100°C decreased by approximately 10% and 20%, respectively, relative to that of the unfilled PC/PBT matrix. However, the mixing sequence had no significant influence on the CLTE or the thermal expansion of the PC/PBT/talc composites. The magnitude of

the dimensional change at 100°C of the ternary blends was reduced by 8% when the PC was blended with the talc particles first (PPT-PC), while it was reduced by 12% when the other two mixing sequences were employed (PPT-PBT and PPT-All) relative to that of the PC/PBT matrix. It is possible that the slightly greater CLTE and thermal expansion observed for the blends prepared by blending sequence PPT-PC are due to a larger number of talc particles within the PC phase and, hence, an increase in the number of filler-PC contacts.

In Table 4.2, the mechanical properties of the PC/PBT matrix and the ternary blends are summarized. The PC/PBT matrix had a flexural and tensile modulus of 2.4 GPa, whereas the ternary blends with a talc loading level of 8% by weight had a flexural modulus and tensile modulus on the order of 2.9 to 3.1 GPa, which corresponds to a 20% to 25% increase in modulus. Similar trends were also observed for the flexural and tensile strength. The flexural and tensile strength of the PC/PBT matrix was 65 MPa and 40 MPa, respectively, whereas the ternary blends had a flexural and tensile strength in the order of 80 GPa and 50 GPa, respectively, which corresponds to a 20% increase in strength. The variations in flexural and tensile properties, such as modulus and strength were only slightly affected by varying the blend sequencing. Typically, the properties varied by less than 3% with the exception of the tensile toughness. Cheng et al. [1] have observed similar behavior for ternary blends consisting of PC, brittle polymers such as polystyrene (PS), and methacrylated butadiene-styrene (MBS). The blend sequencing had very little influence on the tensile properties. Tensile toughness of the materials was not reported but they found that the impact strength was significantly influenced by the blending sequence.

In Fig. 4.4, the tensile toughness at break of the ternary blends as a function of blending sequence including the PC/PBT matrix is shown. The tensile toughness of the PC/PBT matrix was approximately 20 MPa. With the addition of talc particles, the tensile toughness was significantly reduced for the samples obtained by means of all three blending sequences (by 50% of its original value or greater) but the blending sequence did affect the tensile toughness of the ternary blends. The samples prepared by the two-step mixing sequence PPT-PBT had on average a tensile toughness that was 10% greater than that of the samples generated by the conventional one-step mixing sequence

PPT-All and 65% greater than that of the samples mixed using the two-step blending sequence PPT-PC.

There are many possible reasons for the greater tensile toughness observed for samples generated by blending protocol PPT-PBT relative to the samples generated by the other two blending protocols, PPT-All and PPT-PC. First of all, it is possible that the talc particles have more contact and/or they are encapsulated with the PBT phase due to pre-melt-blending the talc with PBT first rather than when combining the PC, PBT, and talc in one mixing step or melt blending the PC with the talc first. Secondly, the development of the phase structure during the melt blending process is affected by the viscosity ratio, λ, defined as the viscosity of the dispersed phase relative to the continuous phase. The difference in the viscosity of the two components at the processing temperature employed may result in a preferred morphological state. Finally, it is possible that degradation of PBT may occur at the high processing temperatures that were employed during the extrusion and injection molding of the ternary composites, see Table 4.1. Therefore, in the following sections, the phase morphology of the ternary blends as observed by TEM and the melt rheology of the PC and PBT components are investigated.

4.3.3 Morphology of PC/PBT/talc composites

In Fig. 4.5, images obtained by means of transmission electron microscopy (TEM) for the ternary blends are shown as a function of the mixing sequence. In these micrographs, the talc particles are black and have particle diameters that range from 0.5 μm to 2-3 μm, while the plate thickness ranges from 0.2-0.3 μm. The PC phase is a dark gray due to staining with the RuO_4 vapors, while the PBT phase is white or a light shade of gray. The samples prepared by blending sequence PPT-PC have the lowest observed tensile toughness. This is due to poor mixing between the PC phase and the PBT phase, large agglomeration of the talc particles as well as a greater amount of talc particle contacts with the PC phase relative to the samples generated by the other two blending sequences. There are large domains of PC that are void of PBT, and in these large domains the talc particles are only contacting the PC phase. One can also see much larger agglomerates of

the talc particles in the composites generated by blend sequence PPT-PC relative to the other two blending sequences. This significantly contributes to a reduction in tensile toughness, because it has been shown that the toughness decreases with the addition of coarse particles. The tensile toughness value of the blend generated by blend sequence PPT-All is approximately 10% lower relative to the blend generated by using blend sequence PPT-PBT. In this case, however, the dispersion between the talc particles and the PC and PBT phase are unaffected by the blending protocol. For the samples prepared by the mixing sequence PPT-PBT and PPT-All, the phase morphology seems to have a co-continuous structure where the domain size of the two phases are similar. In both cases, some agglomeration of the talc particles are observed, which contribute to a reduction in the tensile toughness, but not nearly to the extent that is observed when the PC is melt blended with the talc particles first. It is possible that degradation of the PBT may contribute to the reduction in tensile toughness of the samples prepared by using the blending sequence PPT-All relative to that of the samples generated by using the blending sequence PPT-PBT. When the blending sequence PPT-All is employed, the PBT is processed at 270°C in both the extrusion and molding steps, but it only sees 270°C in the molding step when blend sequence PPT-PBT is used. This observation will be discussed later in more detail.

Photographs of the ternary blends are shown at a higher magnification in Fig. 4.6. One can see that the talc particles are encapsulated within the PBT phase and have limited contact with the PC phase, if the talc particles are small enough. Even in the case where the samples are prepared by using blending sequence PPT-PC, the talc particles are preferentially in the PBT phase. Based on the observed phase morphology, it is now apparent why the blend sequencing has no significant influence on the coefficient of linear thermal expansion of the ternary blends. The talc particles have limited contact with the PC phase when blending protocol PPT-PBT or PPT-All is used. The slight increase in the thermal expansion of the samples generated by using blend sequence PPT-PC is attributed to the large domains of PC that are void of PBT in which the talc particles are only contacting the PC phase.

4.3.4 Role of Rheology on Phase Morphology

Rheological properties of blends can have a significant influence on the observed phase morphology and, hence, the mechanical properties [17, 28-30]. In particular, the domain size of the phases is significantly affected by the viscosity ratio, λ, defined as the viscosity of the dispersed phase relative to the continuous phase. For λ on the order of unity, the droplets are able to deform into fibrils and then break-up into evenly dispersed droplets once a critical shear rate is reached. Generally, this leads to better dispersion between the two phases. However, if the viscosity ratio of the two materials deviates to values much higher or lower than unity, the droplets are unable to deform, which leads to poor dispersion of the two phases. In Fig. 4.7, the dynamic viscosity, $|\eta^*|$, of the PC and PBT components is illustrated as a function of temperature. The viscosity curves of PC and PBT are used to determine λ (PC/PBT) within the temperature range of 250°C to 300°C (Fig. 4.8). The viscosity ratio of PC to PBT is between 3.3 at 250°C and rises to about 12.0 at 300°C. The large increase in viscosity ratio at temperatures above 280°C is due to a serious increase in the rate of degradation of the PBT. A minimum of 2.6 in the viscosity ratio is observed at 270°C, which is the molding temperature employed during the processing of the ternary blends. The viscosity ratio of 2.6 is on the order 1.0, and, therefore, the droplets are expected to deform into fibrils and then break-up into dispersed droplets. However, in the case of the PC/PBT/talc composites, a fibrillar phase morphology is observed (see Fig. 4.5 and Fig. 4.6). These results suggest that the shear rates generated during compounding of the ternary blends are not great enough to break-up the elongated droplets and, hence, a fibrillar phase morphology is observed. A fibrillar phase morphology for unfilled PC/PBT blends at a blend ratio of 50/50 by weight was also observed by Delimoy et al. [20]. A single-screw extruder was also used in that study.

At 270°C, the viscosity of the PC phase is approximately 2.6 times greater than that of the PBT phase. This suggests that the affinity of the talc particles for the PBT phase is kinetically driven by the much lower observed viscosity of the PBT phase relative to that of the PC phase at 270°C. It is also possible that the affinity of the talc particles for the PBT phase is thermodynamically driven by polymer-filler interactions

but, in this case, the basal surface of the talc particles does not contain any hydroxyl groups or active ions. Therefore, the surface of the talc particles is chemically inert and, hence, the talc particles are encapsulated within the PBT phase due to the lower viscosity of the PBT phase relative to that of the PC phase at 270°C.

4.3.5 PBT Degradation at Elevated Temperatures

Another issue that needs to be addressed is the issue of possible degradation of PBT at the melt temperatures that are employed during the compounding and molding of the ternary blends (Table 4.1). The suggested temperature range for processing of the PBT used in this study is normally between 240°C and 260°C. The upper temperature range of the PBT is limited due to degradation of the polymer above 260°C. Degradation of the PBT can adversely affect the mechanical properties of the PC/PBT blends, especially the tensile toughness. To test for degradation, the magnitude of the complex viscosity, $|\eta^*|$, of the PBT was measured at a constant shear rate for 30 minutes. $|\eta^*|$ as a function of time at 260°C and 270°C is shown in Figure 4.9. The PBT degrades immediately and loses about 50% of its initial viscosity in 15 minutes at 270°C. Degradation corresponds to a reduction in molecular weight, hence a reduction in the tensile toughness. However, at 260°C the melt viscosity is stable for about 10 minutes. This result suggests that the lower tensile toughness observed for the samples prepared by blending sequence PPT-All relative to that of the samples generated by bending sequence PPT-PBT is a result of the thermal history of the samples. When blending sequence PPT-All is used, the PBT is processed at 270°C in both the extrusion and molding steps. Whereas, the PBT is compounded with the talc particles at a melt temperature of 250°C, and hence, only sees 270°C in the molding step when blend sequence PPT-PBT is employed.

4.4 Conclusions

The effect of blending sequence on the dimensional stability and the property-structure relationships of PC/PBT/talc composites was investigated. It was found that the

coefficient of linear thermal expansion was reduced by 10% with the addition of 8% by weight of talc particles but was unaffected by the blending sequence employed. Furthermore, the flexural and tensile properties, i.e. modulus and strength, were not significantly influenced by the blending protocol employed but the tensile toughness, on the other hand, was significantly affected. The samples generated by using a two-step blending procedure in which PBT was blended with talc first (PPT-PBT) had on average a tensile toughness that was 10% greater to that of the samples that were generated by the conventional one-step mixing sequence PPT-All and 65% greater to that of the samples generated by the two-step mixing sequence PPT-PC. The higher tensile toughness that was observed for the samples prepared by using blending sequence PPT-PBT was attributed to encapsulation of the talc particles within the PBT phase, better dispersion of the talc particles within the PC/PBT matrix, and better dispersion between the PC and PBT phase. The large reduction in tensile toughness that was observed for samples generated by using blending sequence PPT-PC was attributed to agglomeration of the talc particles, which was not observed with the samples generated by using the other two blending sequences, and the increase in PC-talc contacts due to poor dispersion between the PC and PBT phase. The slight reduction in tensile toughness for samples prepared by using blending sequence PPT-All relative to that of the samples prepared by using blending sequence PPT-PBT was attributed to degradation of the PBT component at 270°C.

4.5 Acknowledgements

The authors would like to gratefully acknowledge the support from the DaimlerChrysler Challenge Fund. We would also like to thank Luzenac for donating the Cimpact699 talc particles and Steve McCartney at the Materials Research Institute in Blacksburg, VA for photographing and developing the images obtained by means of transmission electron microscopy (TEM).

4.6 References

1. T.W. Cheng, H. Keskkula, and D.R. Paul, *Polymer,* **33**, 1606 (1992).

2. R. Zheng, P. Kennedy, N. Phan-Tien, and X.J. Fan, *J. Non-Newtonian Fluid Mech.*, **84**, 159 (1999).

3. M.R. Kamal, R.A. Lai-Fook, and J.R.Hernandez-Aguilar, *Polym. Eng. Sci.*, **42(5)**, 1098 (2002).

4. D. Choi and Y. Im, *Composite Structures*, **47**, 655 (1999).

5. C. Shen and H. Li, *Polymer-Plastics Technology and Engineering*, **42(5)**, 971 (2003).

6. W.C. Bushko and V.K. Stokes, *Polym. Sci. Eng.*, **35(4)**, 351 (1995).

7. W.C. Bushko and V.K. Stokes, *Polym. Sci. Eng.*, **36(3)**, 322 (1996).

8. R.M. Pisipati, Ph.D. Dissertation, Virginia Polytechnic Institute and State University, Blacksburg, VA (1983).

9. V. Svehlova and E. Poloucek, *Die Angewandte Makromolekulare Chemie*, **214**, 91 (1994).

10. M.T. Pastorini and R.C.R. Nunes, *J. Appl. Polym. Sci.*, **74**, 1361 (1999).

11. M. Gahleitner, K. Bernreitner, and W. Neibl, *J. Appl. Polym. Sci.*, **53**, 283 (1994).

12. K. Mitsuishi, *Die Angewandte Makromolekulare Chemie*, **248**, 73 (1997).

13. P. Mareri, S. Bastide, N. Binda, and A. Crespy, *Composites Science and Technology*, **58**, 747 (1998).

14. S.N. Maiti, and K.K. Sharma, *J. Mater. Sci.*, **27**, 4605 (1992).

15. M. Zheng, and H. Li, *J. Appl. Polym. Sci.*, **91**, 1635 (2004).

16. B.K. Kim, and Y.M. Lee, *Polymer*, **34(10),** 2075 (1993).

17. D. Benderly, A. Siegmann, and M. Narkis, *Polymer Composites*, 17 (1), 86 (1996).

18. S.Y. Hobbs, M.E.J. Dekkers, and V.H. Watkins, *J. Material Science,* **23**, 1219 (1988).

19. M.E.J. Dekkers, S.Y. Hobbs, and V. H. Watkins, *J. Material Science*, **23**, 1225, (1998).

20. D. Delimoy, C. Bailly, J. Devaux, and R. Legras, *Polym. Sci. Eng.*, **28**, 104 (1988).

21. X. Li, H. Park, J. Lee, and H. Chang-sik, *Polym. Sci. Eng.*, **42**, 2156 (2002).

22. Talc Mineralogy Bulletin from Luzenac.

23. M. Hancock, P. Tremayne, and D.J. Rosevear, *J. Polym. Sci.*, **18**, 3211 (1980).

24. V. Abolins, US Patent 4,317,761 (1992).

25. P. Sanchez, P.M. Remiro, and J. Nazabal, *J. Appl. Polym. Sci.*, **50**, 995 (1993).

26. G. Pompe, and L. Haubler, *J. of Polym. Sci.: Part B: Polym. Phys.*, 35, 2161 (1997).

27. D.G. Baird, W. Huang, and J. Huang, *J. of Injection Molding Technology*, **5(4)**, 233 (2001).

28. B.K. Kim and Y.M. Lee, *Polymer*, **34(10)**, 2075 (1993).

29. P. Sahnoune, J.M. Lopez-Cuesta, and A. Crespy, *Polym. Eng. Sci.*, **43(3)**, 647 (2003).

30. B.D. Favis, *Can. J. Chem. Engr.*, **69**, 619 (1991).

Table 4.1: Processing Methodology (extrusion and injection molding) for PC/PBT/talc composites

Blend	*Extrusion Cycle*	*Extrusion Melt Temp*	*Injection Molding cycle*	*Injection Molding Melt Temp*
PC/PBT	PC + PBT	270°C	PC/PBT	270°C
PPT-PBT	PBT + Talc	250°C	(PBT/Talc) + PC	270°C
PPT-PC	PC + Talc	320°C	(PC/Talc) + PBT	270°C
PPT-All	PC + PBT + Talc	270°C	PC/PBT/Talc	270°C

Table 4.2: Mechanical Properties of the PC/PBT matrix and the ternary PC/PBT/talc composites

Material	*Flexural Modulus (GPa)*	*Flexural Strength (MPa)*	*Tensile Modulus (GPa)*	*Tensile Strength (MPa)*	Tensile Toughness *(MPa)*
PC/PBT	2.4 ($\pm$ 0.12)	65 ($\pm$ 2.2)	2.4 ($\pm$ 0.15)	40 ($\pm$ 1)	20 ($\pm$ 2.0)
PPT-PBT	2.9 ($\pm$ 0.15)	78 ($\pm$ 2.1)	2.9 ($\pm$ 0.12)	50 ($\pm$ 2)	12 ($\pm$ 0.9)
PPT-PC	3.1 ($\pm$ 0.10)	81 ($\pm$ 2.2)	2.9 ($\pm$ 0.11)	49 ($\pm$ 1)	10 ($\pm$ 1.2)
PPT-All	3.0 ($\pm$ 0.05)	82 ($\pm$ 2.0)	2.9 ($\pm$ 0.13)	45 ($\pm$ 2)	4 ($\pm$ 0.5)

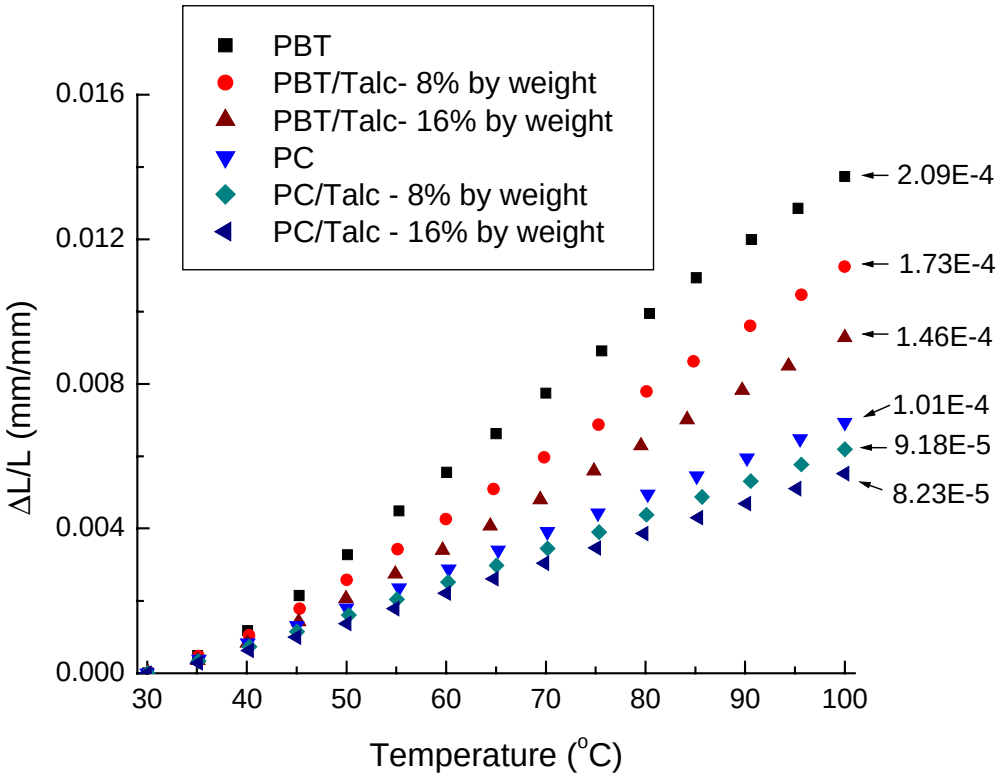

Figure 4.1: Thermal strain (mm/mm) and CLTE values (mm/mm/°C) of the PC/talc and PBT/talc composites as a function of talc concentration. A temperature ramp of 5°C/min was applied.

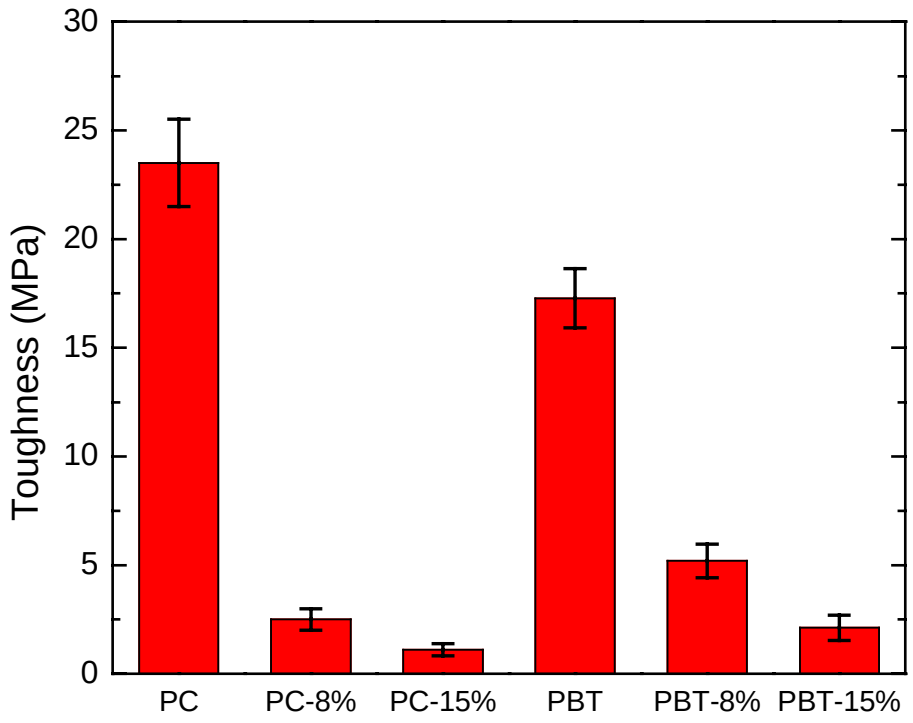

Figure 4.2: Comparison of tensile toughness as a function of talc concentration for PC/talc and PBT/talc composites.

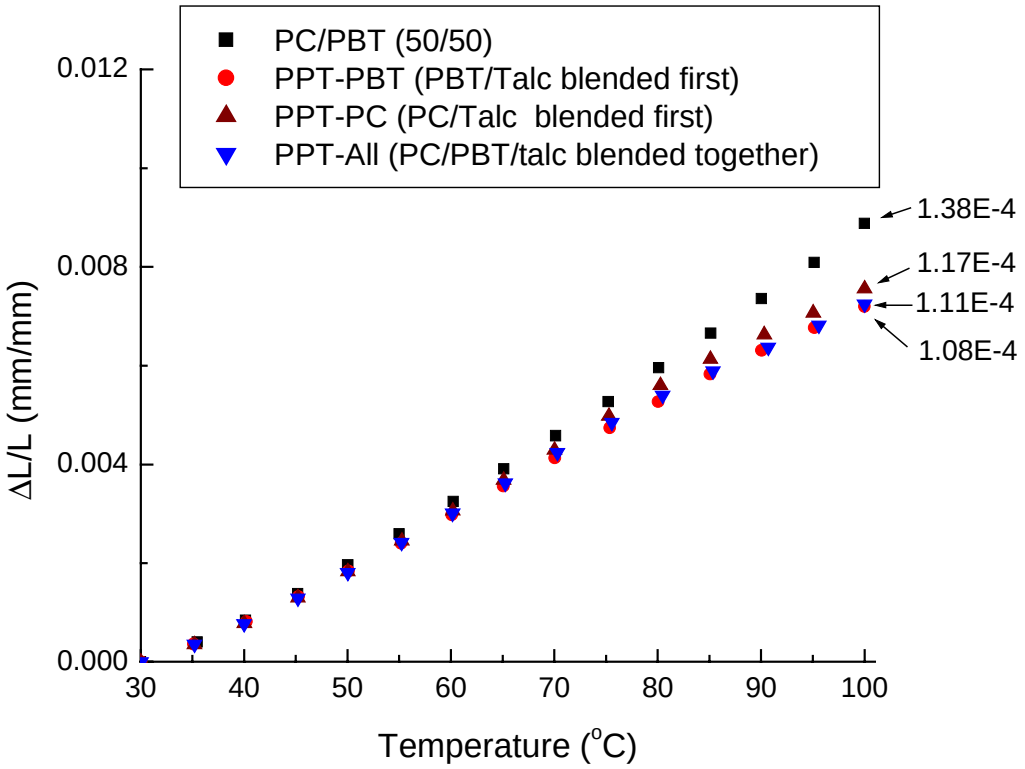

Figure 4.3: Thermal strain (mm/mm) and CLTE values (mm/mm/^{o}C) of the PC/PBT/talc composites as a function of blending sequence. The final composition of the ternary blends consists of a PC/PBT blend ratio of 50/50 by weight and a talc concentration of 8% by weight. The thermal strain and CLTE of the PC/PBT matrix is also included for comparative purposes. A temperature ramp of 5°C/min was applied.

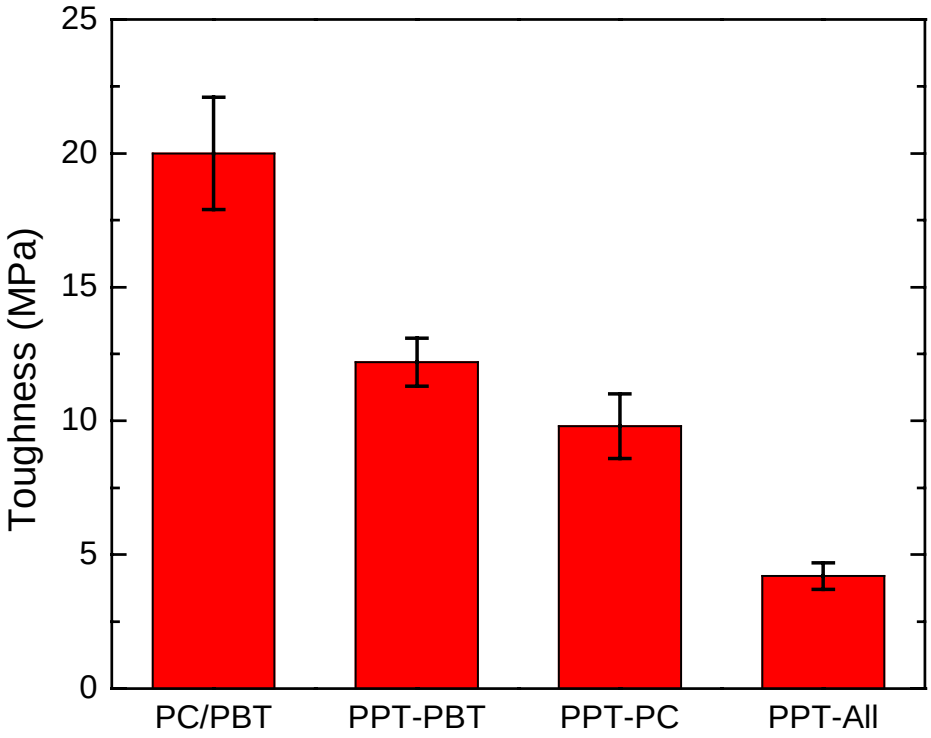

Figure 4.4: Comparison of tensile toughness as a function of blending sequence for the ternary PC/PBT/talc composites. The final composition of the ternary blends consists of a PC/PBT blend ratio of 50/50 by weight and a talc concentration of 8% by weight. The tensile toughness of the PC/PBT matrix is also included for comparative purposes.

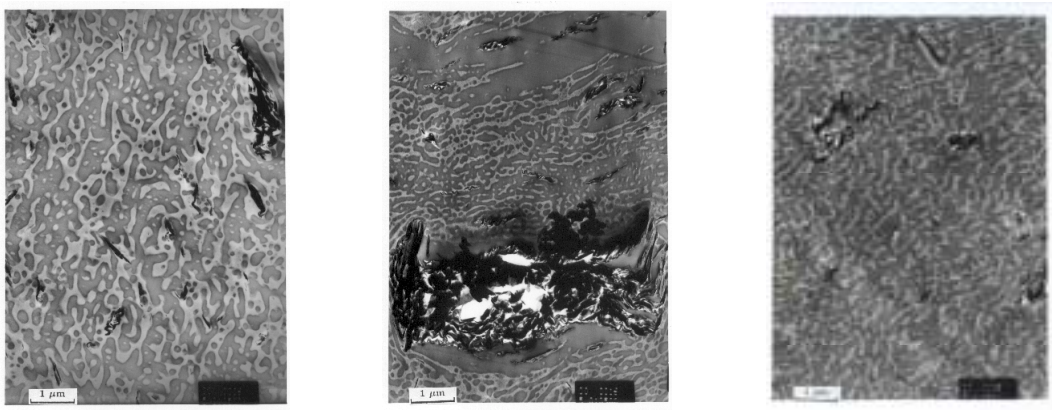

(a) (b) (c)

Figure 4.5: Transmission electron photomicrographs of PC/PBT/talc blends as a function of blending sequence: (a) PPT-PBT; (b) PPT-PC; (c) PPT-All. The dark gray phase is PC, the white or light gray phase is PBT, and the black platelets are the talc particles.

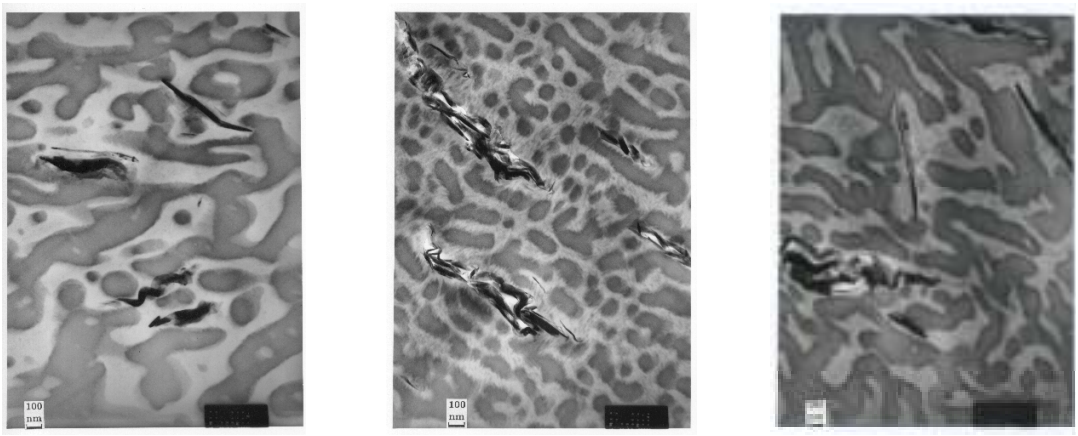

(a) (b) (c)

Figure 4.6: Transmission electron photomicrographs of PC/PBT/talc blends as a function of blending sequence at a higher magnification: (a) PPT-PBT; (b) PPT-PC; (c) PPT-All. The dark gray phase is PC, the white or light gray phase is PBT, and the black platelets are the talc particles.

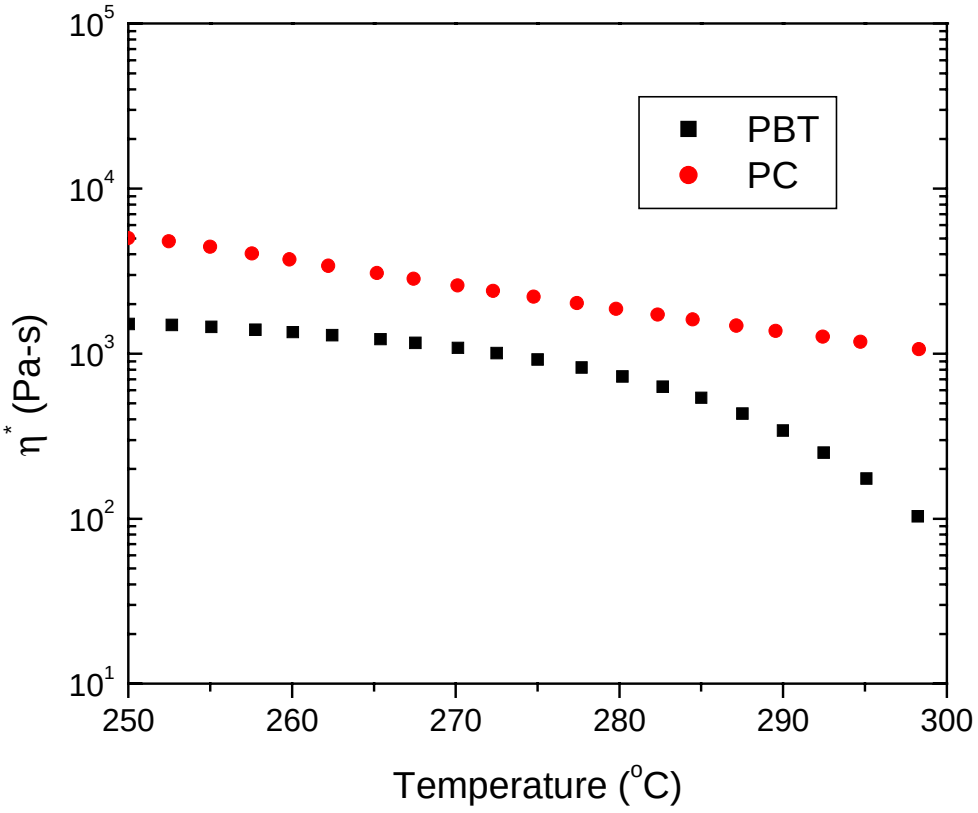

Figure 4.7: Complex viscosity as a function of temperature for PC and PBT. The temperature range of 250°C to 300°C is investigated at a temperature ramp rate of 5°C/min, a frequency of 1 rad/s, and a strain of 5% under a continuous nitrogen atmosphere.

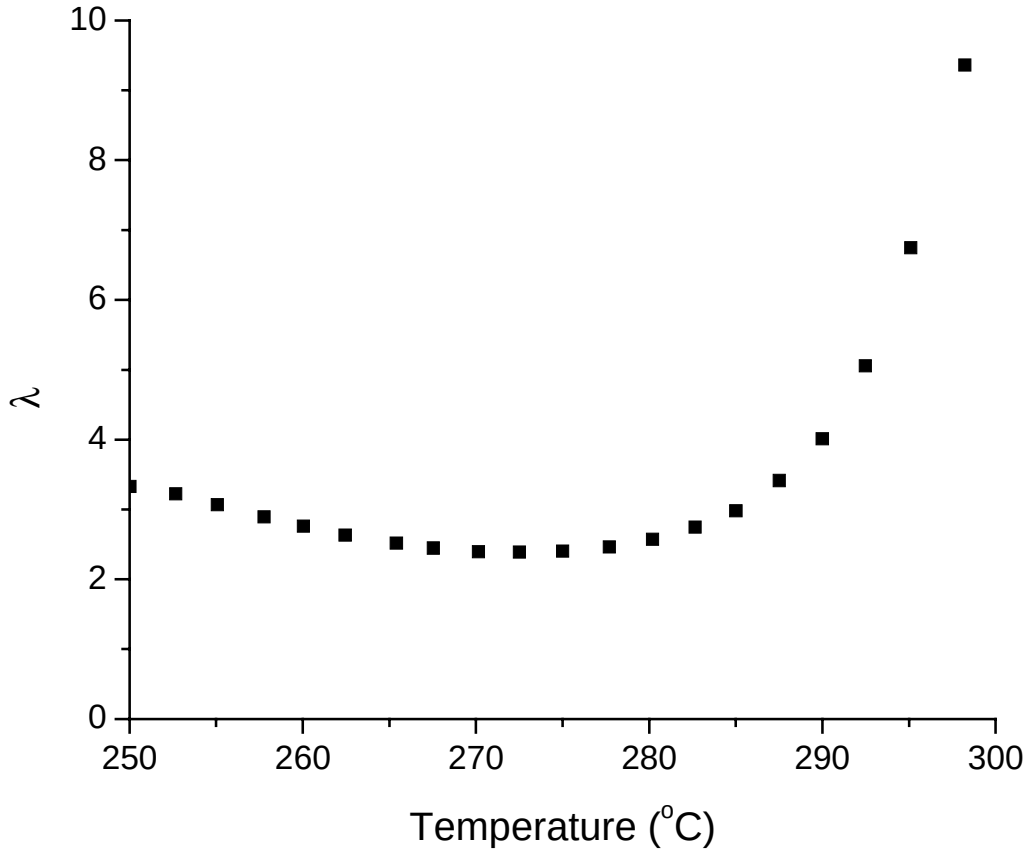

Figure 4.8: Viscosity ratio (PC/PBT) as a function of temperature. Viscosity measurements are investigated in the temperature range of 250°C to 300°C at a temperature ramp rate of 5°C/min, a frequency of 1 rad/s, and a strain of 5% under a continuous nitrogen atmosphere.

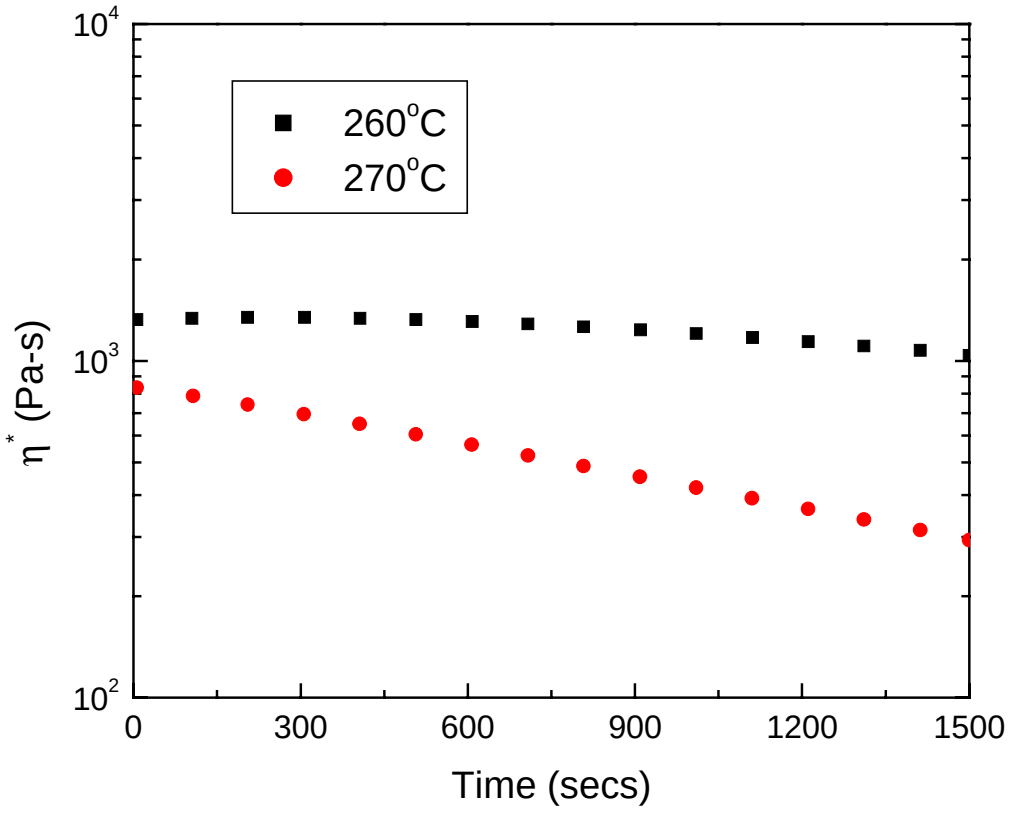

Figure 4.9: Complex viscosity as a function of time for PBT at 260°C and 270°C. A frequency of 1 rad/s and a strain of 5% under a continuous nitrogen atmosphere were applied.

5.0 Particulate Reinforced PC/PBT Composites, Part 1: Effect of Particle Size (Nano-talc Versus Fine Talc Particles) on Dimensional Stability and Properties

W.S. DePolo and D.G. Baird
Department of Chemical Engineering and Macromolecules and Interfaces Institute, Virginia Polytechnic Institute and State University, Blacksburg, VA 24061-0211.

(ABSTRACT)

The effect of particle size (nano-talc versus fine talc) on the dimensional stability, mechanical properties, and morphology of composites consisting of polycarbonate (PC), poly[butylene terephyhalate] (PBT), and talc was investigated at various talc loadings. It was found that by using nano-talc as opposed to fine talc particles, the level of talc reinforcement could be reduced from 6 to 1 wt% without sacrificing the dimensional stability, i.e. CLTE and shrinkage of injection molded plaques, or flexural modulus of the PC/PBT/talc composites at a PC to PBT blend ratio of 60/40 by weight or greater. Further benefits included a 14% increase in flexural strength, 50% increase in the tensile toughness and 3% reduction in the density of the PC/PBT/talc composites. The improved stiffness is attributed to the higher aspect ratio (diameter/thickness of the platelets) of nano-talc (20-25) relative to that of the fine talc (5-10). An increase in the flexural modulus of the PC/PBT/talc composites with an increase in nano-talc loading was observed even though there was evidence of significant degradation in molecular weight of the PC/PBT matrix. Possible degradation in the molecular weight of the PC/PBT matrix was supported by a significant reduction in the storage modulus and complex viscosity at high frequencies of the composites generated with the nano-talc relative to that of the unfilled matrix.

5.1 Introduction

Binary blends based on polycarbonate (PC) and poly[butylene terephyhalate] (PBT) containing talc have been receiving much commercial attention in recent years, especially in the automotive industry. PC has a good balance of properties, which include high modulus and strength, heat deflection temperature, and tensile toughness. However, it has poor solvent and hydrolysis resistance [1]. Therefore, PBT is blended with PC to improve the chemical resistance of molded parts.

PC/PBT blends by themselves do not have high enough stiffness for use in the manufacture of car door panels and, hence, some type of reinforcement is required to increase the modulus. Typically, fiber reinforcements, such as short-glass fiber, can be used to increase the modulus of the PC/PBT blends, reduce the thermal expansion, and reduce the shrinkage of injection molded parts but this may lead to a significant degree of warpage and surface roughness. Warpage is attributed to thermally induced stresses (shrinkage and coefficient of linear thermal expansion, CLTE) and "frozen-in" orientation, associated with large increases in the normal stresses during melt flow of the reinforced blends relative to its matrix [2-7]. On the other hand, particulate reinforcement does not generate large normal stresses and in some instances has lower normal stresses than those of the matrix [8]. Therefore, particulate fillers are more suited for the purpose of increasing the modulus, reducing thermal expansion, and reducing the shrinkage of molded parts for the use of exterior car door panels [9,10]. They provide adequate stiffness for vertical panels ($\geq$ 2.75 GPa) but not for horizontal panels ($\approx$ 7.0 GPa).

Typically, with an increase in the volume fraction of particles, there is an increase in modulus, but the level of reinforcement (concentration) that is required to achieve a specified stiffness by use of particulate fillers is highly dependent on the particle size [11-15]. For example, Gahleitner et al. [12] investigated the effect of particle size on the flexural modulus of talc filled polypropylene (PP) composites. Fine talc particles in the size range from 2.2 μm to 14 μm in diameter were used, while the talc loading was maintained at 30% by weight. The flexural modulus of the composites was observed to increase with decreasing particle size. They attributed this to an increase in relaxation time with a decrease in particle size. This allows for a higher degree of orientation to be

locked into an injection molded part, and hence, higher modulus. In a separate paper by Gonzalez et al. [13], the effect of particle size and the degree of dispersion on the tensile modulus of PP and high-density polyethylene (HDPE) blends filled with calcium carbonate ($CaCO_3$) was investigated. In this case, the modulus also increased with a decrease in particle size. They attributed this to better dispersion of the blends at the lower particle size. Particle agglomeration leads to coarser structures and a reduction in effective aspect ratio, thus, a reduction in modulus.

Along with particle size, the aspect ratio or filler shape can also significantly affect the level of reinforcement that is required to achieve a specific stiffness. Svehlova et al. [14] have shown that the tensile modulus of a PP/talc blend is roughly two times greater at a talc loading of 30% by weight relative to that of the unfilled PP matrix. However, at low particle loadings (3%-5% by weight of talc), only a 10%-20% increase in modulus was observed. Similar results were observed in mica filled PP blends [12] and calcium carbonate filled PP [15]. In the case of the PP/$CaCO_3$ composites, the modulus only increased by a factor of 1.5 (50%) relative to that of the matrix at 30% by weight of calcium carbonate, whereas, the modulus increased by a factor of three with the addition of 30% by weight of mica for the PP/Mica blend. Based on the results above, one can see that the aspect ratio or filler shape has a significant influence on the modulus of particulate filled systems. At 30% by weight of filler, the modulus decreased in the order mica > talc > calcium carbonate, which is in order of highest to lowest aspect ratio (40-45, 5-10, 1, respectively). In a study by Mitsuishi [15], PP/$CaCO_3$ composites were generated with particles that were in the shape of spheres, cubes, or needles. The aspect ratio of the spheres and cubes was approximately one while the aspect ratio of the needles was on the order of 5-10. He found that the modulus of the blends generated with the cubes or spheres was the same within experimental error. The blend generated with the higher aspect ratio needles was 60% greater than that of the blends generated by the spheres or cubes at a particle loading of 20% by weight.

In the study by Mitsuishi [15] mentioned above, the experimentally measured modulus for the composites generated with different shaped calcium carbonate particles was compared with theoretical predictions first proposed by Halpin and Tsai [15-17]. Halpin and Tsai [15-17] developed an empirical model from the simple mixture rule to

theoretically predict the modulus of particulate and fiber filled thermoplastics and the model was later modified by Nielson [16] to include a particle packing factor. There are two assumptions of the model: 1) there is perfect interfacial adhesion between the filler and matrix and 2) the filler particles are perfectly oriented in the flow direction. The model predicts that the modulus will increase with an increase in volume fraction. It also predicts that an increase in aspect ratio will increase rapidly at aspect ratios of 100 or less (depends on the matrix and filler used), at which point a further increase in aspect ratio only results in a slight increase in modulus. With an aspect ratio of 100 or greater, the modulus of the composites still increases proportionally with the particle loading. Good agreement between the experimental results and theory was observed in the study mentioned above [15].

Many researchers have investigated the effect of filler loading on the mechanical properties of nanocomposites [18-21]. Most of these studies have dealt with clay-based nanocomposites. In many cases, it has been shown that a marked increase in modulus (30%-70%) at low filler loadings (< 5% by weight) is observed relative to that of filled composites using fine particles due to their much larger aspect ratios (60-100 versus 5-40). However, large improvements in the mechanical properties are only observed if the clay platelets are well dispersed and exhibit an exfoliated morphology within the polymer matrix. In work done by Han et al. [21], the effect of surface treatment on the mechanical properties of PC/clay nanocomposites was investigated. The tensile modulus of the composites generated with the untreated clay platelets increased by approximately 16% relative to that of the unfilled PC matrix while the tensile strength remained the same at a clay loading of 4% by weight. However, the tensile modulus and tensile strength both increased considerably (75% and 40%, respectively) when the clay platelets were surface treated with a polar quaternary ammonium salt at the same level of reinforcement, i.e. 4% by weight. The large increase in modulus and strength with the surface treated platelets was attributed to fully exfoliated platelets. Hydrogen bonding between the carbonyl groups of the PC and the hydroxyl groups of the coupling agent resulted in the increase of the tensile properties. Typically, at low reinforcement (< 5% by weight) of conventional thermoplastic composites, the increase in modulus is relatively small (10%-30%) while the tensile strength tends to decrease. This shows that large improvements in the tensile

modulus and strength can be obtained at much lower reinforcement levels relative to composites generated with fine particles as long as the nanoparticles are fully exfoliated.

Although the addition of particulates gives rise to an increase in the modulus, there is also a subsequent decrease in the impact strength and/or tensile toughness as well as an increase in the weight of the molded parts relative to that of the unfilled blend [11-14, 22]. The increase in weight is due to the higher density of the fillers relative to those of the thermoplastics. Densities for fillers range from 2.0 – 2.8 g/cm^3, whereas, the density of polymers typically range from 0.8-1.4 g/cm^3. Added weight and a reduction in impact resistance are not desirable for automotive purposes.

The effect of talc loading and particle size/aspect ratio on the dimensional stability, i.e. coefficient of linear thermal expansion (CLTE) and shrinkage, and the mechanical properties of composites based on PC, PBT, and talc are of primary interest in this paper. In particular, our goal is to determine if the use of nano-particles opposed to fine particles can allow lower loadings of reinforcement for filled PC/PBT blends while maintaining the desired mechanical properties (stiffness and tensile toughness) and dimensional stability (CLTE and shrinkage) of flat panels produced by means of injection molding.

5.2 Experimental

5.2.1 Materials

The PC used in these experiments was Lexan 101, which was provided by GE. It has a solid density of 1.20 g/cm^3, melt flow rate of 0.7g/min at 300°C, and a glass transition temperature of 160°C. The PBT used was Celanex 1600A, which was provided by Ticona. It has a solid density of 1.31 g/cm^3 and a glass transition temperature of 55°C. Fine talc particles (Cimpact 699) provided by Luzenac and nano-talcs provided by Nanova were used in this study. The fine talc particles had a disc shaped geometry that have an average aspect ratio on the order of 5-10, where the aspect ratio is defined as the ratio of the disc diameter to the thickness of the plate and an average particle diameter of 1.5 μm. The chemical formula and chemical structure of the fine talc particles are

described elsewhere [23]. The nano-talc also had a disc shaped geometry but the average aspect ratio and particle diameter were on the order of 20-25 and 70-150 nanometers, respectively. It should be noted that the fine talc particles were not surface treated, while the nano-talc particles were treated with a proprietary surface treatment (Nanova). No additives were used in the melt processing steps, such as an inhibitor for the interchange reactions that may occur with PC and PBT. However, based on previous studies, uncatalyzed blends of PC and PBT were found to have negligible amounts of transesterification products at the processing conditions employed for this study [24-26]. The overall residence time of the melt blends in the compounding and injection molding steps combined was less than 5 minutes for this study. It was shown by Nazabal et al. [26] that a negligible amount of interchange reactions occurred for blends of PC and PBT when mixed in a batch reactor at a residence time of 8 minutes or less.

5.2.2 Compounding and Injection Molding of PC/PBT and PC/PBT/talc Blends

Prior to melt processing, the PC, PBT, and talc (fine or nano) were all dried in a vacuum oven for at least 14 hours at a temperature of 120°C. In preparation of the PC/PBT blends, the dried pellets of PC and PBT were first mechanically mixed at various blend ratios of PC-to-PBT (40/60, 50/50, 60/40, and 70/30 by weight). For the case of the PC/PBT/talc composites, dried pellets of PC and PBT at a blend ratio of 60/40 (PC/PBT by weight) were dry blended with the fine or nanotalc particles at talc concentrations of 3 and 6 wt%. PC/PBT/talc composites were also mixed at 1 wt% with the nano-talc particles. Once dry blending was complete, the PC/PBT blends and PC/PBT/talc composites were melt blended by using a single-screw Killion extruder that had a 25 mm diameter barrel and a L/D of 30. The die was cylindrical with L/D of 2.5 and diameter of 3 mm. The screw speed was maintained at 20 rpm and the melt temperature was 260°C with a temperature profile of 220/240/260/260°C from hopper to the exit of the die. Upon exiting the die, the composite strands were quenched in a water bath and then chopped into 6 mm long pellets.

After compounding, the pellets were dried in the vacuum oven for at least another 14 hours at 120°C prior to injection molding. After drying, the PC/PBT blends and PC/PBT/talc composites were injection molded using an Arburg Allrounder Model 221-55-250 injection-molding machine. The Arburg Allrounder had a 22 mm diameter screw, a check ring non-return valve, and an insulated nozzle that was 2 mm in diameter [27]. The composites were injection molded at a melt temperature of 260°C, a mold temperature of 100°C, a holding pressure of 100 bars, and a screw speed of 200 RPMs, into a rectangular end-gated mold with dimensions of 80 mm by 76 mm by 1.6 mm.

5.2.3 Dynamic Mechanical Thermal Analysis of Molded Plaques

Dynamic mechanical thermal analysis (DMTA) of the PC/PBT blends and the PC/PBT/talc composites was performed using a Rheometrics RMS-800 rheometer. Along with measurements of the storage (G') and loss (G") moduli, the coefficient of linear thermal expansion (CLTE) was also measured. When using a torsional rectangular geometry, the Rheometrics RMS-800 contains a function called auto-tension, which maintains a small tension on the samples as it expands during heating. When auto-tension is enabled, the displacement of a sample can be measured as the material is heated from an initial testing temperature. Therefore, the CLTE of a sample can be measured experimentally within the range of temperatures tested. To perform the tests, rectangular strips approximately 75 mm long by 8 mm wide were cut near the center of the plaques. Once the strips were mounted in the rheometer, G', G", and the change in length as a function of temperature were measured. The temperature range of 30°C to 100°C was investigated at a temperature ramp rate of 5°C/min under a continuous nitrogen atmosphere. For each composite generated, three samples were tested to check for reproducibility. The CLTE of each composite generated was determined by plotting the change in length normalized to the initial length at 30°C as a function of temperature. The slope of the line is the CLTE for that material, and it has units of (mm/mm)/ °C.

5.2.4 Mold Shrinkage Measurements of Injection Molded Plaques

The shrinkage measurements in the flow of the molded plaques were made in accordance with ASTM standard D955-00. The percent mold shrinkage was calculated from the following equation:

$$MS = \left(\frac{DC - DS}{DC} \right) \mathrm{X}\, 100 \qquad (5.1)$$

where MS is the percent mold shrinkage that is observed, DC is the dimension of the mold cavity in millimeters, and DS is the dimension of the specimen. A minimum of 10 samples was tested, and the average value and standard deviation were calculated from the data.

5.2.5 Mechanical Properties

Flexural and tensile properties of the composites were tested by using an Instron mechanical tester, model 4204. Test specimens were prepared by cutting rectangular strips approximately 75 mm long by 8 mm wide near the center of the molded plaques. Flexural specimens were tested in accordance with ASTM standard D790 while the tensile specimens were tested at a crosshead speed of 1.27 mm/min in accordance with ASTM standard D2256. An extensiometer, Instron model 2630-25, was also used for all tensile tests to provide an accurate measure of the tensile modulus. A minimum of 5 samples was tested in the flow direction, and an average value and standard deviation were calculated from the data.

5.2.6 Transmission Electron Microscopy (TEM)

The morphology of the PC/PBT/talc composites was characterized by means of transmission electron microscopy using a Philips EM420T. The acceleration voltage used was 100kV. Ultra-thin sections of the injection-molded plaques were cut at room temperature using a Reichert-Jung Ultracut E Microtome fitted with a 35° diamond knife. The ultra-thin sections were recovered on 300 mesh Cu grid. Delimoy et al. [24] reported that the natural phase contrast between the PC and PBT phases is weak. Therefore, to

improve the phase contrast, samples were stained by exposing RuO_4 vapors for approximately 15 minutes following the procedure described by Delimoy et al. [24]. In this study, the specimen blocks were cut near the center of the molded plaques and microtomed sections were cut perpendicular to the flow direction.

5.2.7 Rheological Measurements of the Composite Melts

Dynamic oscillatory shear flow measurements of the PC/PBT/talc composites and the PC/PBT matrix in the melt state were obtained using a parallel-disk rheometer (Rheometrics RMS-800) with 25 mm diameter plates. The complex viscosity, $|\eta^*|$, and storage modulus, G', were investigated in a frequency range of 0.1 to 100 rad/s at a melt temperature of 260°C under a continuous nitrogen atmosphere. A strain of 5% was maintained to ensure that the measurements were taken within the linear viscoelastic region. Test specimens that were 1.0 mm thick were prepared by compression molding the generated pellets into 25 mm diameter disks at 260°C. A minimum of 3 samples was tested to check for reproducibility.

5.3 Results and Discussion

5.3.1 Effect of Blend Ratio (PC to PBT) on the Dimensional Stability of PC/PBT Blends

The effect of blend ratio on the dimensional stability, i.e. coefficient of linear thermal expansion (CLTE) and mold shrinkage, of the PC/PBT blends was investigated by varying the blend ratio of PC to PBT (40/60, 50/50, 60/40, and 70/30 by weight). In Fig. 5.1, the thermal expansion and CLTE of the PC/PBT blends are illustrated as a function of blend ratio over the temperature range of 30°C to 100°C. The thermal expansion and CLTE of unfilled PC and PBT are also shown for comparative purposes. The numerical values on the right hand side of Fig. 5.1 are the CLTE values (mm/mm/°C), which were determined by the slopes of the lines within the temperature range of 40°C to 100°C. The CLTE and the overall dimensional change of the neat PBT are much greater than that of the neat PC. The large difference in the thermal properties

between unfilled PC and PBT is due to PBT's low glass transition temperature of 50°C to 55°C relative to that of PC, which is 160°C. With an increase in PC content, the CLTE and the overall dimensional change of the blends decrease, but the magnitude of the decrease is much more pronounced when the PBT phase is dominant relative to that of the PC phase over the temperature range studied. Once the PC phase is the dominant phase on a per volume basis, the reduction in the thermal expansion and CLTE is relatively unchanged with any further increase in PC concentration. For example, at a PC concentration of 70% by weight, the CLTE of the PC/PBT blend is reduced by 18% and 12% relative to that of the PC/PBT blends at a PC content of 40% and 50% by weight, respectively. However, the CLTE of the blend at a PC concentration of 70% by weight is only reduced by less than 1% relative to that of the blend at a PC concentration of 60% by weight. Furthermore, at a PC concentration 60% and 70% by weight, the overall dimensional change at a temperature of 100°C is reduced by 26% and 20% relative to that of the blends at a PC concentration of 40% and 50% by weight, respectively. The results suggest that the PC phase controls the dimensional stability of PC/PBT blends due to its high glass transition temperature relative to that of the PBT.

The shrinkage in the flow direction of the injection molded PC/PBT blends is illustrated as a function of blend ratio in Fig. 5.2. Similar trends are observed for the shrinkage of the molded PC/PBT blends. The shrinkage of the neat PBT is approximately 70% greater than that of the neat PC. The large difference in the shrinkage between the PC and PBT is due to crystallization of the PBT during injection molding. The PC resin is amorphous and, hence, no crystallization takes place when molding the neat PC. With an increase in PC content, the shrinkage of the blends decrease, but the magnitude of the decrease is much more pronounced when the PBT phase is dominant relative to that of the PC phase. Once the PC phase is the major phase, the reduction in the shrinkage is relatively unchanged with any further increase in PC concentration. It is interesting to note that the shrinkage of the blends at a PC content of 60% by weight or greater is equivalent (< 1% difference) to that if the neat PC. This is further evidence that PC controls the dimensional stability of the PC/PBT blends.

These results suggest that the dimensional stability of PC/PBT blends is controlled by the PC phase and that there is no significant advantage in terms of

dimensional stability in using a blend ratio of PC to PBT that is greater than 60/40. Although the mechanical properties of the blends are not reported here, it has been shown by Nazabal et al. [26] that the tensile properties, i.e. modulus and strength, of uncatalyzed PC/PBT blends are maximized at a blend ratio of 75/25 (PC/PBT). However, the difference in tensile modulus and strength of the PC/PBT blends at a blend ratio of 75/25 to that of 60/40 was insignificant (< 3%). Therefore, composites consisting of PC, PBT, and talc (fine particles and nanoparticles) are generated at a blend ratio of 60/40 (PC/PBT) in the sections that follow unless otherwise specified. A blend ratio of 60/40 is used for two reasons. First of all, there is no significant advantages in dimensional stability or mechanical properties when a blend ratio greater than 60/40 is used. Secondly, a further increase in the PC content (> 60 wt%) may result in a reduction of the solvent and hydrolysis resistance of the PC/PBT blends due to a reduction in PBT concentration. Solvent and hydrolysis resistance is necessary for use in the manufacture of exterior car door panels.

5.3.2 Effect of Talc Concentration and Particle Size/Aspect Ratio on the Dimensional Stability of PC/PBT/talc Composites

The effect of talc concentration on the dimensional stability of the PC/PBT/talc composites was investigated by varying the loading level of talc (3 and 6 wt%). Particle size and aspect ratio of the composites were investigated by combining the PC/PBT blends with either fine talc particles (1.5 μm in diameter and an aspect ratio of 5-10) or nanotalc particles (70-150 nm in diameter and an aspect ratio of 20-25) at the talc loadings mentioned above. In Fig. 5.3, the thermal expansion and CLTE of the PC/PBT/talc composites (fine talc particles) are illustrated as a function of talc concentration in the temperature range of 30°C to 100°C. Data for PC/PBT/talc composites generated with nanoparticles was omitted for clarity. With the addition of talc particles, the CLTE and the magnitude of the dimensional change at 100°C remained unchanged relative to that of the unfilled PC/PBT matrix, regardless of particle size (fine versus nano). Similar trends were also observed with the shrinkage of the molded panels. The mold shrinkage in the flow direction of the generated plaques was approximately

1.45% ($\pm$ 0.2%) at all talc concentrations investigated. Particle size also had no influence on the shrinkage of the generated plaques. This is an interesting result because it suggests that a reduction in talc content will have no affect on the dimensional stability of the PC/PBT blends at a blend ratio of 60/40 or greater.

5.3.3 Mechanical Properties of PC/PBT/talc Composites

In Fig. 5.4, the effect of talc concentration on the flexural modulus of the PC/PBT/talc composites is investigated by varying the loading level of talc (3 and 6 wt%). PC/PBT/talc composites are also generated with 1 wt% of the nano-talc particles. The PC/PBT matrix has a flexural modulus of 2.1 GPa. With the addition of talc (fine particles or nanoparticles), the flexural modulus increases with an increase in talc loading. In the case of the fine talc particles, there is a linear increase in the flexural modulus and at a talc loading of 6% by weight, the flexural modulus is 2.43 GPa, which corresponds to a 17% increase in modulus relative to that of the unfilled PC/PBT matrix. For the composites generated with nanoparticles opposed to fine particles, there is initially a significant increase in the flexural modulus relative to that of the PC/PBT matrix at a talc loading of 1% by weight. However, with further addition of nano-talc, the flexural modulus only increases slightly. For example, the flexural modulus at a nano-talc loading of 1% is 2.45 GPa (17% increase relative to that of the PC/PBT matrix), whereas, at a nano-talc loading of 6% by weight, the modulus is only 2.53 GPa (20% increase relative to that of the PC/PBT matrix), which corresponds to a 3% increase in modulus. It should also be noted that the flexural modulus is always greater for the composites generated with the nano-talc particles as opposed to those of the fine talc particles, regardless of talc concentration. Furthermore, at a nano-talc loading of 1 wt%, the flexural modulus of the composite is equivalent to that of the PC/PBT/talc composite generated with fine talc particles at a talc loading of 6 wt%. The greater flexural modulus observed for the composites generated with the nano-talc particles as opposed to fine talc particles is attributed to the higher aspect ratio of the nano-particles (20-25) relative to that of the fine talc particles (5-10). These results are in qualitative agreement with the

Halpin-Tsai equations [15-17], which predict an increase in modulus with an increase in aspect ratio up to an aspect ratio on the order of 100.

Talc concentration has little influence (< 3%) on the flexural strength of the ternary composites, but the particle size and/or aspect ratio does. The flexural strength of the PC/PBT matrix is 65 MPa. With the addition of fine talc particles, the flexural strength of the ternary blends is approximately 70 MPa while it is approximately 80 MPa when nano-talc particles are used. This corresponds to a 10% increase in flexural strength when fine particles are used and 24% increase in flexural strength when nano-talc particles are used relative to that of the unfilled PC/PBT blend.

Finally, the tensile toughness as measured by the area under the stress-strain curve of the PC/PBT matrix and the PC/PBT/talc composites is illustrated in Fig. 5. As expected, the tensile toughness of the composites is reduced with an increase in talc concentration. However, the composites generated with the nano-talc particles retain the initial tensile toughness of the unfilled PC/PBT matrix to a greater extent than that of the composites generated with the fine talc particles, with an exception occurring at a nano-talc loading of 6% by weight. For instance, at nano-talc loadings of 3% by weight or less, the tensile toughness of the composites is 36% greater than that of the composites generated with fine talc particle at an equivalent level of reinforcement. On the other hand, at a nano-talc loading of 6% by weight, the tensile toughness of the molded plaques is reduced by 99% relative to that of the unfilled PC/PBT matrix and by 90% relative to that of the molded plaques generated with fine talc particles at an equivalent concentration of talc. The greater tensile toughness observed for the molded plaques generated with the nano-talc as opposed to fine talc is attributed to the reduction in particle size when using the nanoparticles. A reduction in the particle size leads to an increase in the surface area at the filler/matrix interface as well as a reduction in the average distance between the particles within the base resin and, hence, an increase in tensile toughness [12]. Hancock [28] and Abolins [29] have reported similar observations. They found that maximum values of toughness were obtained for fillers with the smallest average particle sizes provided that there were no coarse particles present and the dispersion of the particles was good. The findings by Hancock and Abolins [28-29] suggest that the extreme reduction in the tensile toughness of the

composites generated at a nano-talc loading of 6% by weight is most likely due to the presence of large agglomerates of the nano-particles. The phase morphology and the dispersion of the talc particles within the PC/PBT matrix will be discussed in more detail in a later section.

By using nano-talc particles opposed to fine talc particles, the level of talc reinforcement can be reduced from 6 to 1 wt% without sacrificing the dimensional stability or flexural modulus of the PC/PBT/talc composites. Further benefits include a 14% increase in flexural strength and a 120% increase in the tensile toughness. A reduction in the level of talc reinforcement also leads to a reduction in the density of the PC/PBT/talc composites and, hence, a reduction in the overall weight of the molded part. The weight savings that are gained by reducing the loading level of talc are discussed in the following section.

5.3.4 Density Savings

In Fig. 5.6, the flexural modulus of the composites and the PC/PBT matrix is illustrated as a function of solid density. The numerals refer to the concentration of the talc particles in percent by weight of the composites, 0 refers to the unfilled PC/PBT matrix. The solid densities of the PC, PBT, and talc (fine particles and nanoparticles) are 1.2, 1.31, and 2.75 g/cm^3, respectively. The density of the composites is estimated by assuming that the component volumes are additive. Therefore, a simple averaging formula is used to calculate the solid density of the mixtures. The flexural modulus along with the density of the composites increases with an increase in the talc concentration. Due to the large difference in density of the talc particles relative to that of the PC and PBT components, a small increase in talc concentration leads to a significant increase in the density of the talc filled composites relative to that of the unfilled PC/PBT matrix. At a talc loading of 6% by weight, the density increases by approximately 3.5% relative to that of the unfilled matrix (from 1.241 g/cm^3 to 1.284 g/cm^3). By observation of Fig. 5.6, it is clear that the level of talc reinforcement can be reduced from 6 to 1 wt% without sacrificing the flexural modulus of the PC/PBT/talc composites with the use of nano-talc particles as opposed to fine talc particles. With the 83% reduction in talc concentration,

the density is reduced from 1.284 g/cm^3 to 1.248 g/cm^3, which corresponds to a 3% reduction in density relative to that of the unfilled PC/PBT matrix (1.241 g/cm^3).

5.3.5 Morphology of the PC/PBT/talc Composites

In Fig. 5.7, images obtained by means of transmission electron microscopy (TEM) for the composites are shown at a talc concentration of 6 wt% of fine talc particles and talc concentrations of 3% and 6% by weight of nano-talc . In these micrographs, the talc particles are black and have particle diameters that range from 0.5 μm to 2-3 μm for the fine particles and 70-150 nm for the nano-talc particles, while the plate thickness ranges from 0.2-0.3 μm and 6-8 nm, respectively. The PC phase is a dark gray due to staining with the RuO_4 vapors, while the PBT phase is white or a light shade of gray. The composites prepared at a nano-talc loading of 6% by weight have the lowest observed tensile toughness, which is reduced by approximately 96% relative to that of the unfilled PC/PBT matrix. The extreme reduction in the tensile toughness is due to agglomeration of the nano-talc particles, see Figs. 5.7(c) and 5.7(d). This significantly contributes to a reduction in tensile toughness, because it has been shown that the toughness decreases with the addition of coarse particles [28-29]. With the exception of the composites generated at a nano-talc loading of 6% by weight, the tensile toughness of the composites produced with the smaller sized nano-particles is greater than that of the composites produced with the fine particles. In this case, the greater observed tensile toughness of the composites generated with the nano-talc particles is due to the smaller particle size of the talc and better dispersion of the nano-talc particles within the PC/PBT matrix. Some agglomeration of the talc particles is observed when fine particles are used as opposed to nano-particles, which contribute to the greater reduction in the tensile toughness that is observed, but not nearly to the extent that is observed at a nano-talc loading of 6% by weight.

A fibrillar phase morphology is observed for the PC/PBT/talc composites (see Fig. 5.7), where the PBT droplets deformed into fibrils within the continuous PC phase. In a separate study, the authors [30] found that the viscosity ratio of the PC/PBT at 260°C is 2.6, which is on the order of 1.0. Therefore, the PBT droplets are expected to deform

into fibrils and then breakup into dispersed droplets, but in this case the stretched PBT fibrils do not break-up and, hence, the observed fibrillar phase morphology. These results suggest that the shear rates generated during compounding of the composites are not great enough to break-up the elongated droplets and, hence, a fibrillar phase morphology is observed. A fibrillar phase morphology for unfilled PC/PBT blends at a blend ratio of 60/40 by weight was also observed by Delimoy et al. [24]. A single-screw extruder was also used in that study. The domain size and phase structure seems to be unaffected by the talc concentration or particle size, i.e fine talc versus nano-talc.

Photographs of the composites are shown at a higher magnification in Fig. 5.8. One can see that the talc particles are encapsulated within the PBT phase, if agglomeration of the talc particles is not present. When fine talc particles are used to reinforce the PC/PBT matrix, the talc particles are mainly encapsulated within the PBT phase and have limited contact with the PC phase. In some cases, however, the diameter and thickness of the fine talc particles is greater than that of the PBT phase and, therefore, the talc particles have some contact with the PC phase. With nano-talc particles, on the other hand, the diameter and thickness are much smaller than that of the PBT phase. This leads to complete isolation of the talc particles from the PBT phase. In a separate study, the authors [30] found that encapsulation of the talc particles improves both tensile toughness and dimensional stability of talc filled PC/PBT blends. Therefore, it is possible that the complete isolation of the nano-talc particles from the PC phase may also contribute to the higher tensile toughness that is observed when nano-talc particles are used as opposed to fine talc particles, at an equivalent level of talc reinforcement.

5.3.6 Rheology of Composite Melts

Although particulate fillers are added to polymer melts to increase the stiffness or rigidity and/or reduce the cost of the blend, they also can have a significant affect on the rheological properties and, hence, the ability to process the composites. Rheological properties are also sensitive to small changes in the morphological state and to the molecular weight of the materials. Recently, Han et al. [21] and Yoon et al. [31] have observed a reduction in the storage modulus, G', relative to that of the matrix at high

frequencies for PC nanocomposites. Yoon et al. [31] attributed the reduction in G' at high frequencies to degradation in the molecular weight of the PC matrix with the addition of nano-clay.

In order to determine the effects of talc concentration and particle size on the viscoelastic flow behavior of the composite melts, G' and $|\eta^*|$ of the composites and the PC/PBT matrix are illustrated in Fig. 5.9 and Fig. 5.10 at 260°C (i.e., the melt processing temperature of the materials). As the talc concentration increases, the magnitude of G' increases in the low frequency region (long relaxation times). However, the increase in the magnitude of G' in the low frequency region is more pronounced when nano-talc is used to reinforce the PC/PBT matrix relative to that of the fine talc. The greater increase in G' at low frequencies when the nano-talc is used as opposed to the fine talc is due to the increased surface area of the nano-talc and adhesion between the nano-talc and the PC/PBT matrix. Similar results have been reported by many other authors [12, 32-33]. A decrease in the particle size leads to an increase in G' at low frequencies, which becomes more evident as the particle loading increases. It is interesting to note that with an increase in talc loading from 3% to 6% by weight, the magnitude of G' at low frequencies increases by a greater extent when fine talc is used as opposed to the nano-talc, which is unexpected. At a nano-talc loading of 6% by weight, it should be expected that the magnitude of G' in the low frequency region would be much larger than that of the composites generated at a nano-talc loading of 3% by weight due to the differences in the morphology. Agglomeration of the nano-talc particles, which tends to increase G' at low frequencies, is observed at a talc loading of 6 wt% (see Figure 5.7(d)), but it is not observed at a talc loading of 3 wt% (see Figure 5.7(c)). It is possible that the lack of a significant increase in G' at low frequencies may be due to significant degradation of the PC/PBT matrix promoted by the surface treatment that is applied to the nano-talc particles.

The rheological behavior of G' at low frequencies is in good agreement with the observed flexural modulus of the composites. An increase in G' at low frequencies is indicative of an increase in the long relaxation times of the material and, therefore, inhibits stress relaxation of the polymer chains. This allows for a higher degree of orientation to be locked into an injection molded part, and hence, higher modulus. For

example, the flexural modulus of the composites generated with the fine talc particles increases with an increase in talc loading while G' at low frequencies also increases with an increase in talc loading. Furthermore, the flexural modulus and G' at low frequencies of the composites generated with nano-talc are greater than that of the composites generated with fine talc particles.

In the high frequency region, the magnitude of G' converges to that of the PC/PBT matrix when the fine talc particles are used, regardless of talc loading (see Fig 5.9). This is typical behavior for particulate filled composites. However, in the case of the nanofilled PC/PBT composites, the magnitude of G' in the high frequency region is a half an order of magnitude lower than that of the PC/PBT matrix at a loading of 3 wt%. With an increase in talc loading to 6 wt%, the magnitude of G' at high frequencies is further reduced and is approximately an order of magnitude lower than that of the PC/PBT matrix. Similar results have been observed for PC composites filled with nano-clay particles [31]. Yoon et al. [31] attributed the reduction in G' at high frequencies to a reduction in the molecular weight of the PC matrix. The degree of molecular degradation was found to be dependent on the surface treatment that was applied to the nano-clay particles. Based on their results, it is plausible that the reduction in G' at high frequencies with an increase in nano-talc loading is due to a reduction in the molecular weight of the PC/PBT matrix, which seems to be enhanced by the surface treatment that is used to prevent agglomeration of the nano-talc. Degradation of the surface treatment at the high temperatures employed during the compounding and molding of the composites as well as the presence of hydroxyl groups may contribute to the significant reduction in the molecular weight of the PC/PBT matrix. In the case of the fine talc, the magnitude in G' at high frequency is not reduced but equivalent to that of the matrix up to a loading of 6 wt%. The lack of reduction in G' at high frequencies may be due to the fact that the fine talc particles are not surface treated.

The complex viscosity, $|\eta^*|$, of the PC/PBT/talc composites decreases with an increase in talc concentration, but the magnitude of the decrease is much more pronounced when the nano-talc particles are used relative to that of the fine talc particles. The viscosity at a frequency of 1 rad/s is reduced by 18% and 30% at fine talc loadings of 3 and 6 wt% relative to that of the PC/PBT matrix, while it is reduced by 70% and 90% at

nano-talc loadings of 3 and 6 wt% relative to that of the PC/PBT matrix. The extreme reduction in the viscosity that is observed when nano-talc particles are used is most likely due to a decrease in molecular weight of the matrix. Even though there is a significant reduction in viscosity and most likely in molecular weight with an increase in talc concentration, the flexural modulus of the filled composites still increases with an increase in talc concentration. It is also interesting to note that a yield stress is observed at a nano-talc loading of 6 wt%, whereas, one is not observed at a nano-talc loading of 3 wt% or for the composites generated with the fine particles. These results are in good agreement with the observed phase morphology of the composites. The presence of a yield stress at a nano-talc loading of 6 wt% is attributed to agglomeration of the talc particles that is observed in Figs. 5.7(c), 5.7(d), and 5.8(c), while the lack of an observed yield stress at a nano-talc loading of 3 wt% is attributed to good dispersion of the talc particles within the PC/PBT matrix as observed in Figs. 5.7(b) and 5.8(b).

5.4 Conclusions

The effect of talc concentration and particle size on the dimensional stability, structure-property relationships, and rheological behavior of PC/PBT/talc composites was investigated. By using nano-talc as opposed to fine talc particles, the level of talc reinforcement could be reduced from 6 to 1 wt% without sacrificing the dimensional stability, i.e. CLTE and shrinkage of the molded plaques, or flexural modulus of the PC/PBT/talc composites at a PC to PBT blend ratio of 60/40 or greater. Further benefits include a 14% increase in flexural strength, a 120% increase in the tensile toughness and a 3% reduction in the density of the PC/PBT/talc composites. The flexural modulus of the composites increased with an increase in talc concentration and particle size even though the viscosity was significantly reduced due to a loss of molecular weight of the PC/PBT matrix. A severe reduction in tensile toughness of the composites generated at a nano-talc loading of 6 wt% was observed and attributed to agglomeration of the talc particles, which was not observed at a nano-talc loading of 3 wt%. The tensile toughness of the composites produced with the fine talc particles was lower than that of the composites generated with nano-talc (3 wt% or less) due to some agglomeration of the

talc particles. It is also interesting to note that the PC phase controls the dimensional stability of PC/PBT blends, once the PC content is greater than 60% by weight. There is no further reduction in CLTE or mold shrinkage with addition of talc particles once the PC to PBT blend ratio is 60/40 or greater.

5.5 Acknowledgements

The authors would like to gratefully acknowledge the support from the DaimlerChrysler Challenge Fund. We would also like to thank Luzenac for donating the Cimpact699 talc particles, Nanova for donating the nano-talc particles and Steve McCartney at the Materials Research Institute in Blacksburg, VA for photographing and developing the images obtained by means of transmission electron microscopy (TEM).

5.6 References

1. T.W. Cheng, H. Keskkula, and D.R. Paul, *Polymer,* **33**, 1606 (1992).

2. R. Zheng, P. Kennedy, N. Phan-Tien, and X.J. Fan, *J. Non-Newtonian Fluid Mech.*, **84**, 159 (1999).

3. M.R. Kamal, R.A. Lai-Fook, and J.R.Hernandez-Aguilar, *Polym. Eng. Sci.*, **42(5)**, 1098 (2002).

4. D. Choi and Y. Im, *Composite Structures*, **47**, 655 (1999).

5. C. Shen and H. Li, *Polymer-Plastics Technology and Engineering*, **42(5)**, 971 (2003).

6. W.C. Bushko and V.K. Stokes, *Polym. Sci. Eng.*, **35(4)**, 351 (1995).

7. W.C. Bushko and V.K. Stokes, *Polym. Sci. Eng.*, **36(3)**, 322 (1996).

8. R.M. Pisipati, Ph.D. Dissertation, Virginia Polytechnic Institute and State University, Blacksburg, VA (1983).

9. R.A. Baker, L.L. Koller, and P.E. Kummer, "Polymer Composites", Van Nostrand Reinhold, New York, (1987).

10. H. Hoffman, W. Grellmann, and V. Zilvar, "Polymer Composites", Academic Press, New York, (1986).

11. M.T. Pastorini and R.C.R. Nunes, *J. Appl. Polym. Sci.*, **74**, 1361 (1999).

12. M. Gahleitner, K. Bernreitner, and W. Neibl, *J. Appl. Polym. Sci.*, **53**, 283 (1994).

13. R. Gonzalez-Nunez, B.D. Favis, P.J. Carreau, and C. Lavalle, *Polym. Eng. Sci.*, **33**, 851 (1993).

14. V. Svehlova and E. Poloucek, *Die Angewandte Makromolekulare Chemie,* **214**, 91 (1994).

15. K. Mitsuishi, *Die Angewandte Makromolekulare Chemie*, **248**, 73 (1997).

16. Z. Li and K.A. Narh, *Composites: Part B*, **32**, 103 (2003).

17. D.A. Brune and J. Bicerano, *Polymer*, **43**, 369 (2002).

18. D. Wu, X. Wang, Y. Song, and R. Jin, *J. Appl. Polym. Sci.*, **92**, 2714 (2004).

19. M. Alexandre, P. Dubois, T. Su, M. Garces, and R. Jerome, *Polymer*, **43**, 2123 (2002).

20. T.D. Fornes, P.J. Yoon, H. Keskkula, and D.R. Paul, *Polymer*, **42**, 9929 (2001).

21. K.M. Lee and C.D. Han, *Polymer*, **44**, 4573 (2003).

22. P. Mareri, S. Bastide, N. Binda, and A. Crespy, *Composites Science and Technology*, **58**, 747 (1998).

23. W.S. DePolo and D.G. Baird, *Polym. Eng. Sci.*, Submitted September (2005).

24. D. Delimoy, C. Bailly, J. Devaux, and R. Legras, *Polym. Sci. Eng.*, **28**, 104 (1988).

25. G. Pompe, and L. Haubler, *J. of Polym. Sci.: Part B: Polym. Phys.*, **35**, 2161 (1997).

26. P. Sanchez, P.M. Remiro, and J. Nazabal, *J. Appl. Polym. Sci.*, **50**, 995 (1993).

27. D.G. Baird, W. Huang, and J. Huang, *J. of Injection Molding Technology*, **5(4)**, 233 (2001).

28. M. Hancock, P. Tremayne, and D.J. Rosevear, *J. Polym. Sci.*, **18**, 3211 (1980).

29. V. Abolins, US Patent 4,317,761 (1992).

30. W.S. DePolo and D.G. Baird, *Polym. Sci. Eng.*, Submitted September (2002).

31. P.J. Yoon, D.L. Hunter, and D.R. Paul, *Polymer*, **44**, 5341 (2003).

32. P.R Hornsby and A.Mthupha, *Journal of Materials Science*, **29**, 5293 (1994).

33. C.H. Suh, and J.L. White, *J. Non-Newtonian Fluid Mech.*, **62**, 175 (1996).

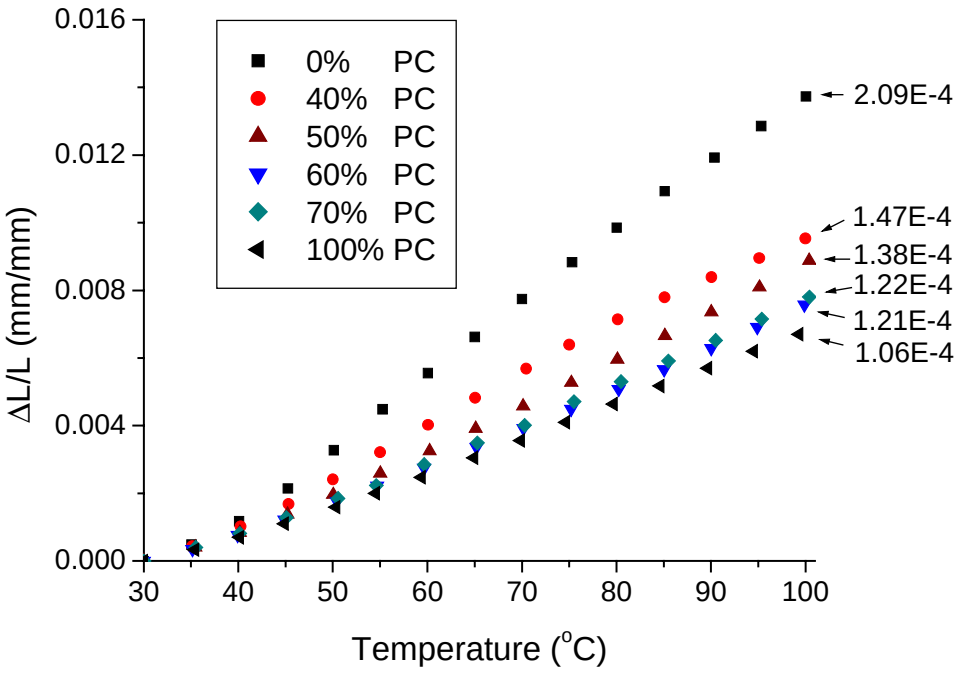

Figure 5.1: Thermal strain (mm/mm) and CLTE values (mm/mm/°C) of PC/PBT blends as a function of PC concentration, i.e. blend ratio of PC to PBT. A temperature ramp of 5°C/min was applied.

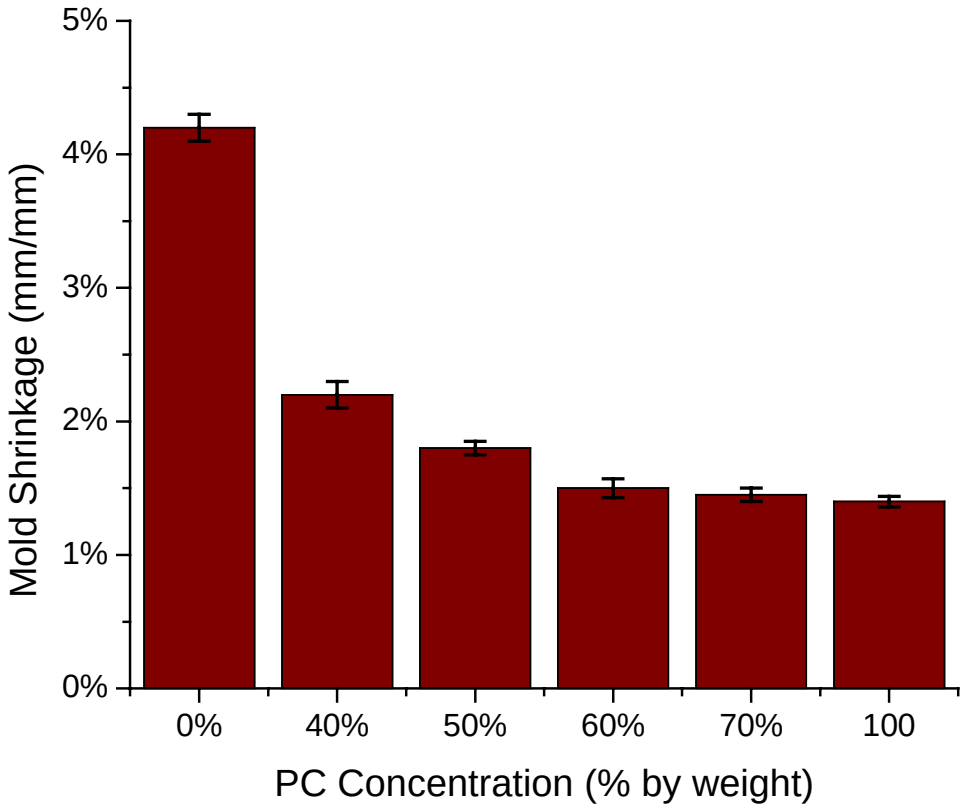

Figure 5.2: Comparison of mold shrinkage for PC/PBT blends as a function of PC concentration (wt%), i.e. blend ratio of PC to PBT.

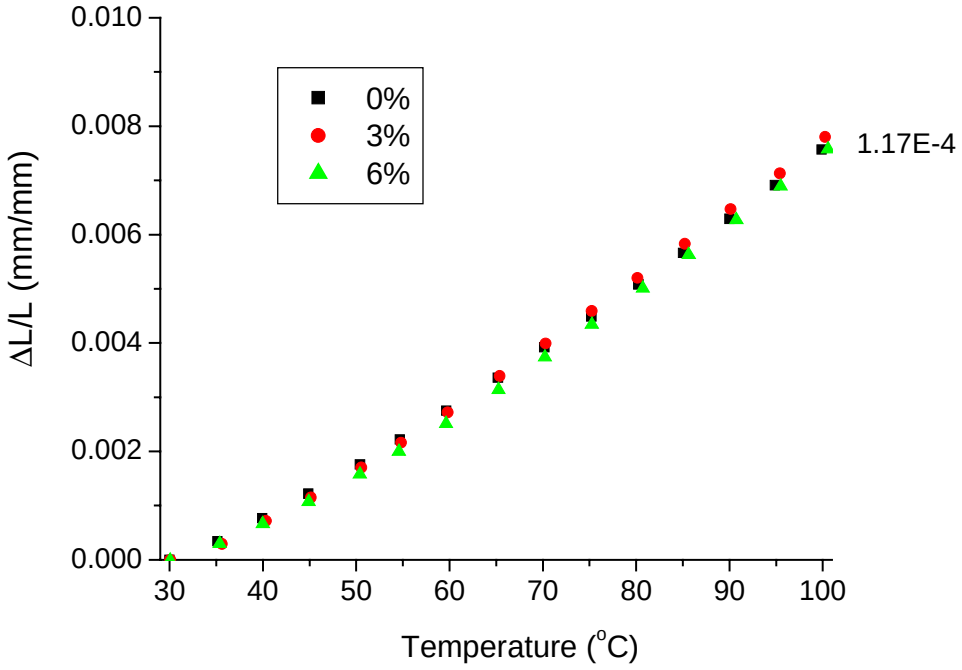

Figure 5.3: Thermal strain (mm/mm) and CLTE values (mm/mm/°C) of PC/PBT/talc composites as a function of fine talc concentration (wt%). The PC/PBT blend ratio is 60/40 by weight. A talc loading of 0% by weight refers to the PC/PBT matrix. A temperature ramp of 5°C/min was applied.

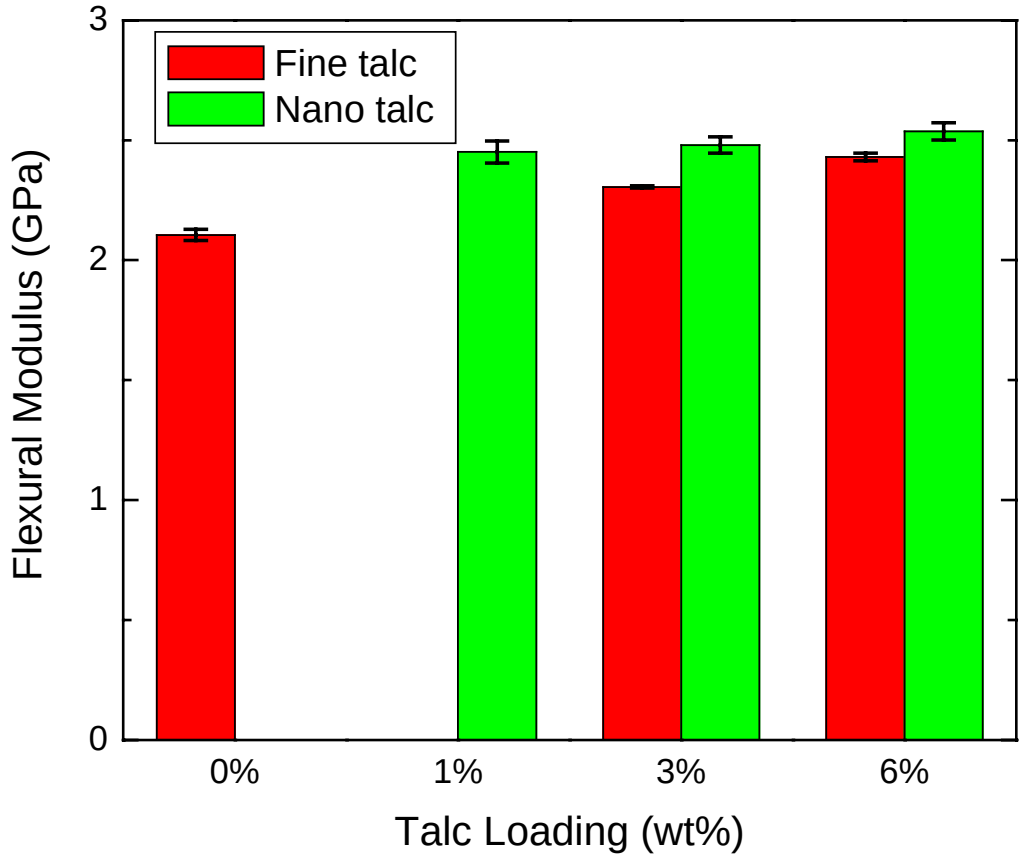

Figure 5.4: Comparison of flexural modulus as a function of talc loading (fine talc versus nano-talc) for ternary PC/PBT/talc composites. The PC/PBT blend ratio is 60/40 by weight. A talc loading of 0% by weight refers to the PC/PBT matrix.

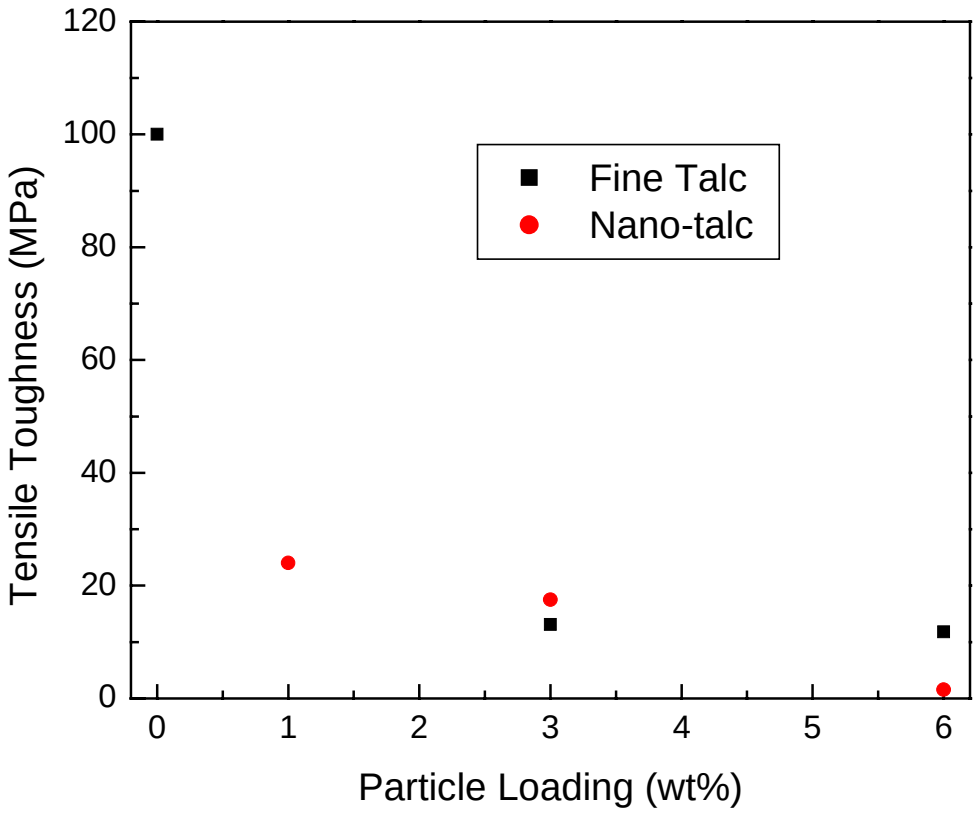

Figure 5.5: Comparison of tensile toughness as a function of talc loading (fine talc versus nano-talc) for ternary PC/PBT/talc composites. The PC/PBT blend ratio is 60/40 by weight. A talc loading of 0% by weight refers to the PC/PBT matrix.

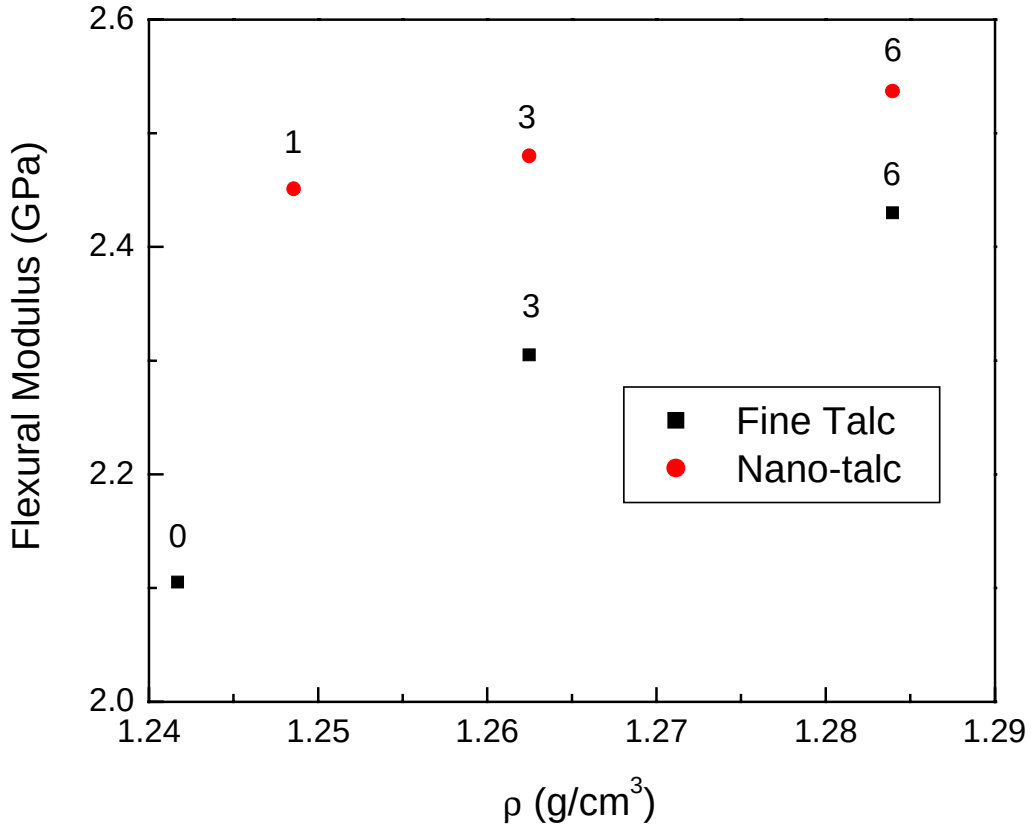

Figure 5.6: Comparison of flexural modulus as a function of density for ternary PC/PBT/talc composites. The numerals correspond to the talc loading in percentage by weight. Zero refers to the unfilled PC/PBT matrix, which has a PC/PBT blend ratio of 60/40 by weight.

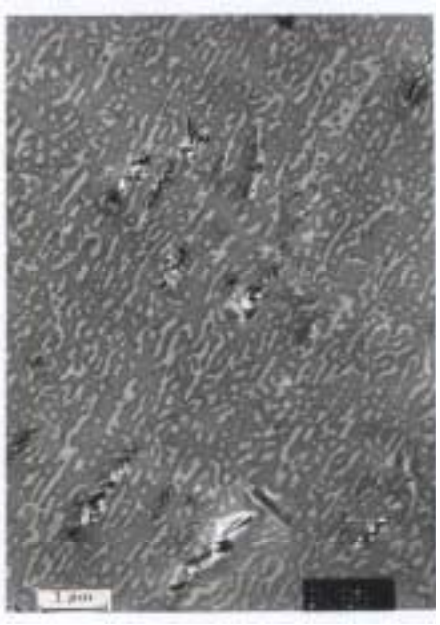

(a)

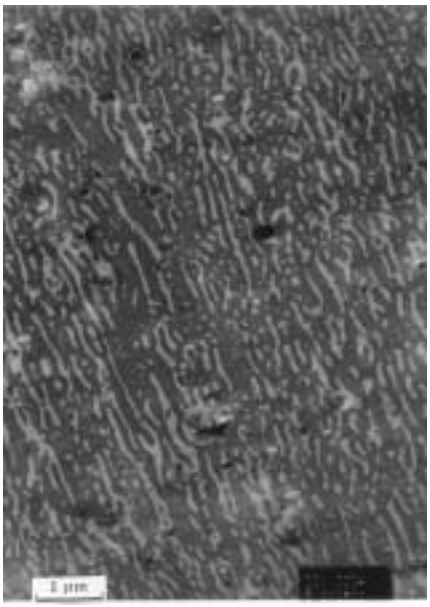

(b)

(c)

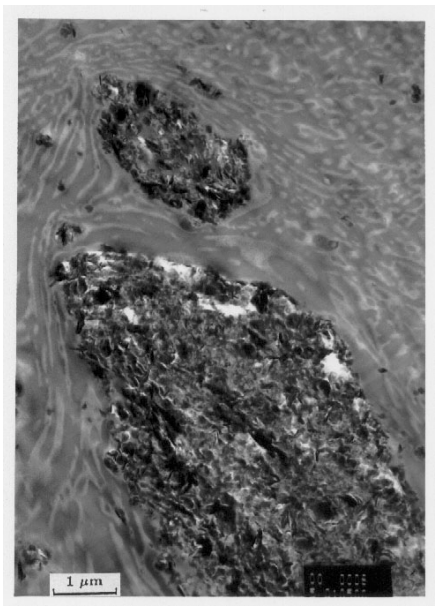

(d)

Figure 5.7: Transmission electron photomicrographs of PC/PBT/talc composites as a function of talc particle size and loading: (a) 6 wt% fine talc; (b) 3 wt% nano-talc; (c) 6 wt% nano-talc; (d) 6 wt% nano-talc (higher magnification). The dark gray phase is PC, the white or light gray phase is PBT, and the black platelets are the talc particles.

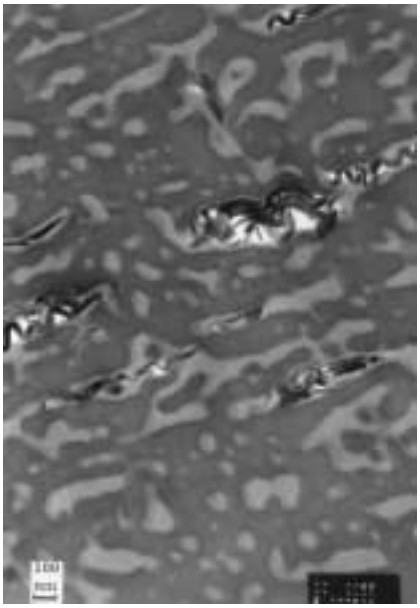

(a)

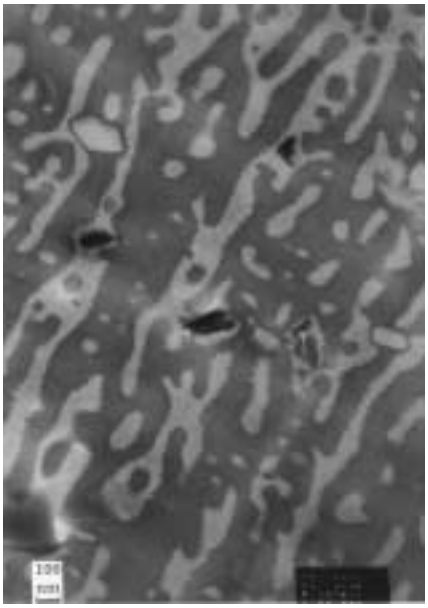

(b)

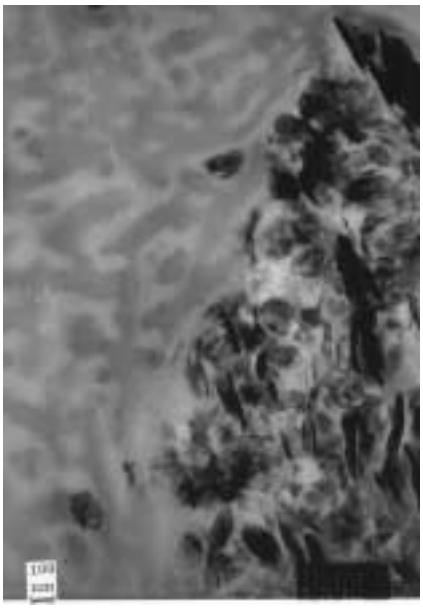

(c)

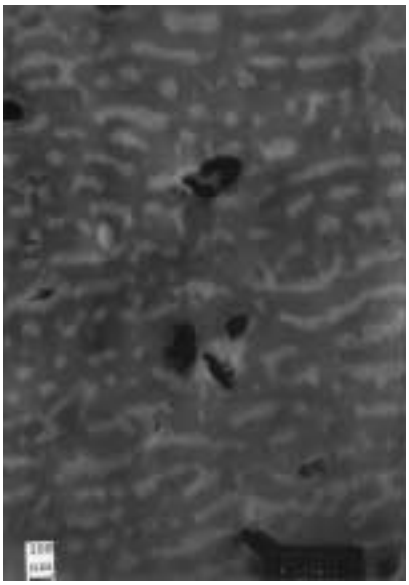

(d)

Figure 5.8: Transmission electron photomicrographs of PC/PBT/talc composites as a function of talc particle size and loading at a higher magnification: (a) 6 wt% fine talc; (b) 3 wt% nano-talc; (c) 6 wt% nano-talc; (d) 6 wt% nano-talc (higher magnification). The dark gray phase is PC, the white or light gray phase is PBT, and the black platelets are the talc particles.

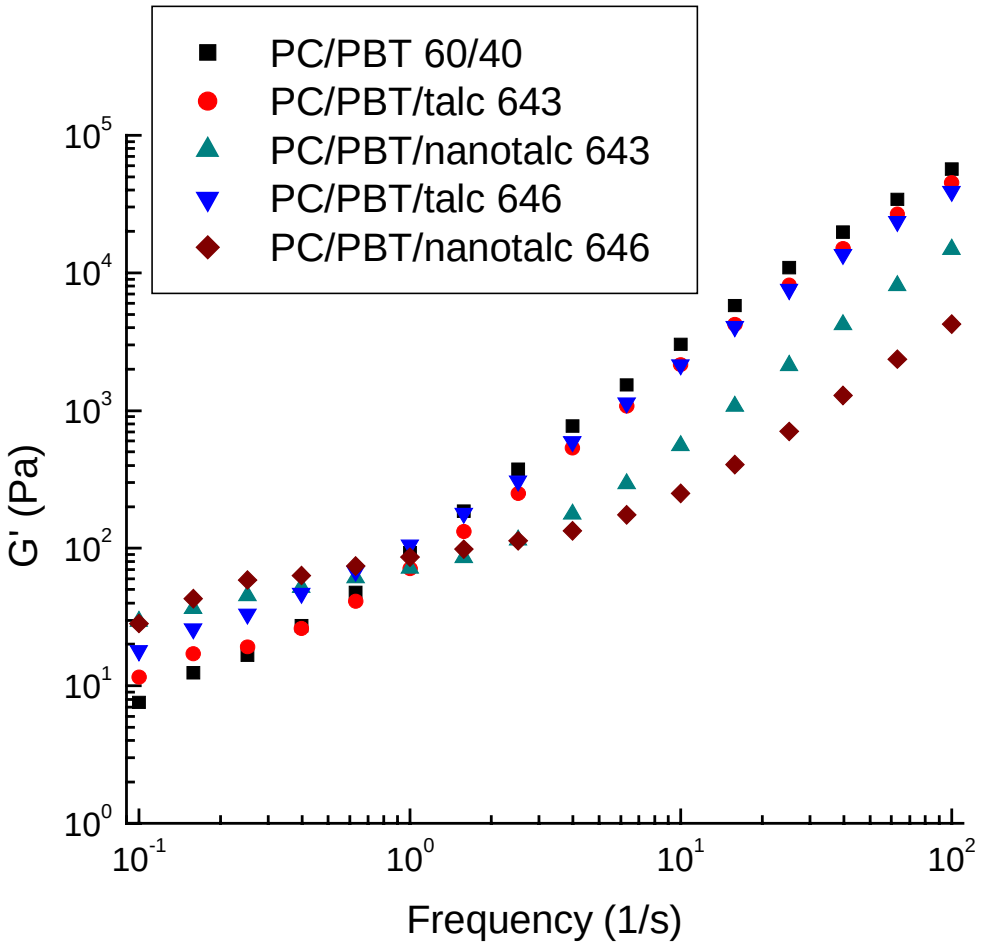

Figure 5.9: Comparison of storage modulus, G', as a function of talc loading (fine talc versus nano-talc) for ternary PC/PBT/talc composites at a temperature of 260°C and a strain of 5% under nitrogen.

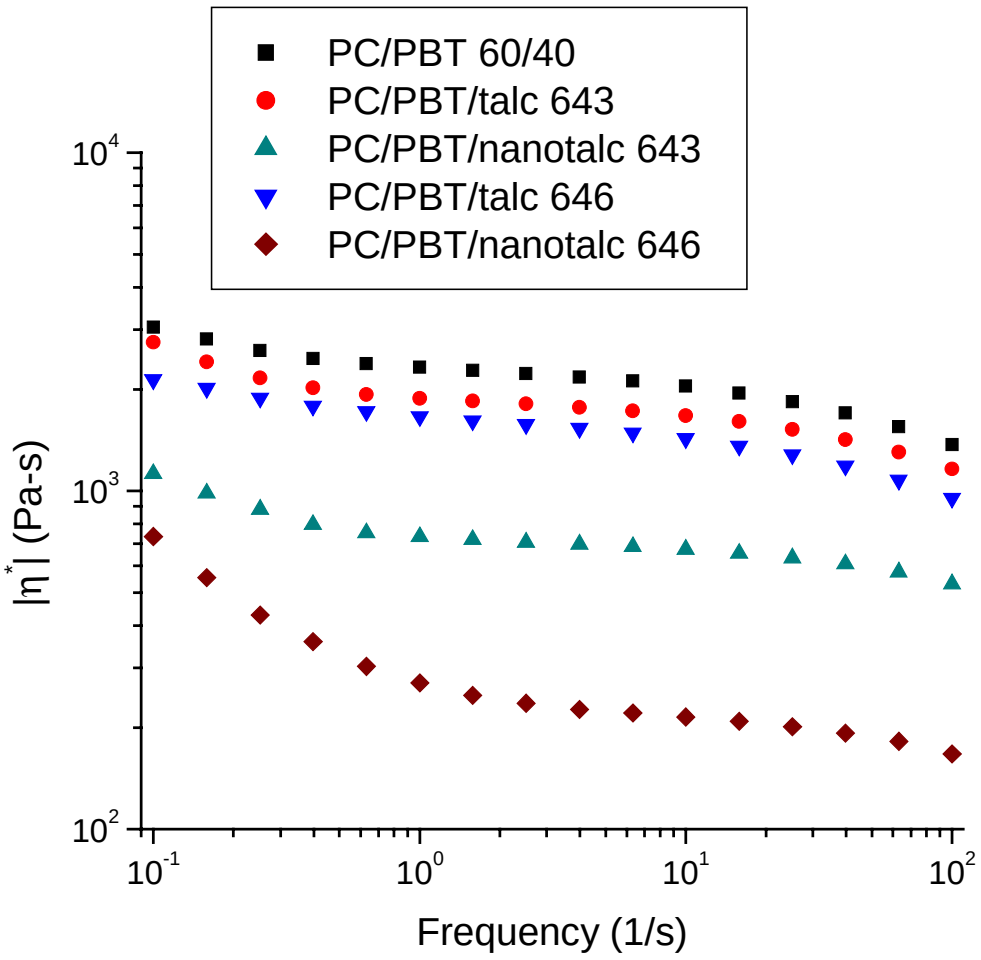

Figure 5.10: Comparison of complex viscosity, $|\eta^*|$, as a function of talc loading (fine talc versus nano-talc) for ternary PC/PBT/talc composites at a temperature of 260°C and a strain of 5% under nitrogen.

6.0 Particulate Reinforced PC/PBT Composites, Part 2: Effect of Nano-clay Particles on Dimensional Stability and Structure-Property Relationships

W.S. DePolo and D.G. Baird
Department of Chemical Engineering and Macromolecules and Interfaces Institute, Virginia Polytechnic Institute and State University, Blacksburg, VA 24061-0211

(ABSTRACT)

The effect of organoclay loading and surface treatment on the dimensional stability, structure-property relationships, and rheological behavior of nanocomposites consisting of polycarbonate (PC), poly[butylene terephyhalate] (PBT), and nano-clay was investigated at various clay loadings and with various surface modifiers for the nano-clay particles. It was found that by using an organoclay formed with a polar amine compound that contained two hydroxyl end groups (Cloisite 30B) as opposed to nano-talc, the flexural strength and tensile toughness of the nanocomposites increased by 12% and 27%, respectively, at a particle loading of 1 wt% without sacrificing the flexural modulus of the nanofilled PC/PBT blends. The flexural and tensile modulus of the nanocomposites increased with an increase in particle loading even though the viscosity was reduced due to a loss of molecular weight of the PC/PBT and/or an increase in the compability of the interface between the PC and PBT phase, which varied with organoclay structure. Possible loss of the molecular weight of the PC/PBT matrix was supported by a significant reduction in the storage modulus and complex viscosity at high frequencies of the composites generated with nano-clay relative to that of the unfilled matrix. The largest enhancement in flexural and tensile modulus was observed for nanocomposites prepared by using an organoclay that was formed with a polar amine compound that contained two hydroxyl end groups (Cloisite 30B). This was due to hydrogen bonding between the carbonyl group of the PC phase with that of the hydroxyl end groups located on the surface of the chemically modified clay platelets. However, the highest tensile toughness was observed for nanocomposites generated by using an organoclay that was formed with a non-polar amine compound that contained two long alkyl groups (Cloisite 20A). This was attributed to the formation of a single-phase

mixture, which leads to the highest degree of dispersion of the clay platelets relative to that of the other organoclays.

6.1 Introduction

In a previous paper [1], the effect of particle size (nanoparticles versus micron-size particles) on the dimensional stability and structure-property relationships of talc reinforced PC/PBT blends was evaluated. It was shown that by using nano-talc as opposed to fine talc particles, the level of talc reinforcement could be reduced from 6 to 1 wt% without sacrificing the dimensional stability, i.e. CLTE and shrinkage of injection molded plaques, or flexural modulus of the PC/PBT/talc composites at a PC to PBT blend ratio of 60/40 by weight or greater. Further benefits included a 14% increase in flexural strength, 50% increase in the tensile toughness and 3% reduction in the density of the PC/PBT/talc composites. The improved stiffness was attributed to the higher aspect ratio of the nano-talc (20-25) relative to that of the fine talc (5-10). An increase in the flexural modulus of the PC/PBT/talc composites with an increase in nano-talc loading was observed even though there was evidence of significant degradation in molecular weight of the PC/PBT matrix. Possible degradation in the molecular weight of the PC/PBT matrix was supported by a significant reduction in the storage modulus and complex viscosity at high frequencies of the composites generated with the nano-talc relative to that of the unfilled matrix. It was also interesting to note that the PC phase controlled the dimensional stability of PC/PBT blends, once the PC content was greater than 60% by weight. There was no further reduction in CLTE or mold shrinkage with addition of talc particles once the PC to PBT blend ratio was 60/40 or greater.

Our intent in this paper is to report results on further improvement in the mechanical properties of the PC/PBT blends by reinforcing the blends with nano-clay particles as opposed to nano-talc particles. Some possible advantages in replacing the nano-talc particles with nano-clay particles include: 1) nano-clay particles have an average aspect ratio (diameter/thickness of platelets) on the order of 100-150 whereas the nano-talc particles only have an average aspect ratio on the order of 20-25 and 2) the density of the nano-clay particles is approximately 2.0 g/cm^3 while the nano-talc particles have a density of 2.75 g/cm^3. The greater aspect ratio of the nano-clay particles can lead to enhanced flexural and/or tensile modulus of the PC/PBT blends relative to that of the nano-talc particles at an equivalent level of reinforcement. Also, the lower density of the

nano-clay particles results in a reduction in the overall weight of the particulate reinforced PC/PBT blends at an equivalent level of reinforcement.

However, large improvements in the mechanical properties for blends reinforced with nanoparticles are only, typically, observed if the platelets are well dispersed and exhibit an exfoliated morphology as opposed to an intercalated morphology within the polymer matrix. An intercalated structure results when the polymer penetrates into the galleries of the layered structure resulting in a highly ordered arrangement of alternating clay platelet and polymer layers. An exfoliated structure is formed when the layered silicates are delaminated. In this case individual silicate layers are completely dispersed in the continuous polymer matrix [2,3]. Therefore, an exfoliated structure results in enhanced mechanical properties relative to an intercalated structure due to an increase in the aspect ratio of the platelets. In order to achieve an exfoliated structure, it is necessary to break up the strong particle-particle interactions by enhancing the interactions between the polymer and filler. This can be accomplished by using a coupling agent or surface treating the platelets.

For the thermoplastics of interest in this paper, PC and PBT, only nanocomposites consisting of PC and nano-clay particles has been investigated [4,5]. In work done by Han et al. [4], the effect of surface treatment on the mechanical properties of PC/clay nanocomposites was investigated. The chemically modified clay consisted of a polar quaternary ammonium salt. The tensile modulus of the composites generated with the untreated clay platelets increased by approximately 16% relative to that of the unfilled PC matrix while the tensile strength remained the same at a clay loading of 4 wt%. However, the tensile modulus and tensile strength both increased considerably (75% and 40%, respectively) when the clay platelets were surface treated with the polar quaternary ammonium salt at the same level of reinforcement. The large increase in modulus and strength with the surface treated platelets was attributed to fully exfoliated platelets. Hydrogen bonding between the carbonyl groups of the PC and the hydroxyl groups of the coupling agent resulted in the increase of the tensile properties.

Yoon et al. [5] reported similar results for the tensile properties of PC/clay nanocomposites as a function of clay loading and molecular weight. The nano-clay particles were chemically modified using various surface treatments. It was shown that

the tensile modulus of PC/clay nanocomposites increased by 33% relative to that of the unfilled PC matrix when a polar quaternary ammonium salt was used to surface treat the clay particles while the modulus of the PC/clay nanocomposites only increased by approximately 20% relative to that of the PC matrix when non-polar quaternary ammonium salts were used to surface treat the clay particles. Nanocomposites with clay particles possessing no surface treatment had a tensile modulus that was only 10% greater than that of the unfilled PC matrix. The large increase in modulus that was observed for the nanocomposites where the clay particles were surface treated with a polar quaternary ammonium salt was attributed to partially exfoliated clay platelets.

In particular, our goal in this paper is to determine if the use of nano-clay particles as opposed to nano-talc particles can increase the desired mechanical properties (stiffness and tensile toughness) at an equivalent level of reinforcement while maintaining dimensional stability of flat panels produced by means of injection molding. Furthermore, we investigate whether the phase structure of the PC/PBT blends is altered by the applied surface modification of the nano-clay. Throughout the paper we use the properties of the PC/PBT/nano-talc composites generated in our previous paper as a basis for comparison [1].

6.2 Experimental

6.2.1 Materials

The PC used in these experiments was Lexan 101, which was provided by GE. It has a density of 1.20 g/cm^3 at room temperature, melt flow rate of 0.7g/min at 300°C, and a glass transition temperature of 160°C. The PBT used was Celanex 1600A, which was provided by Ticona. It has a density of 1.31 g/cm^3 at room temperature and a glass transition temperature of 55°C.

Four different types of chemically modified nano-clay particles provided by Southern Clay Products under the tradename Cloisite were used in this study and there structures are illustrated in Fig. 6.1 [6]. The clay platelets have an average aspect ratio on the order of 100-150, where the aspect ratio is defined as the ratio of the length to the

thickness of the plate, an average length of 100-150 nanometers, and an average plate thickness of one nanometer [6]. For Cloisite 15A and Cloisite 20A, the natural sodium montmorillonite (Cloisite Na^+) was modified with the same surfactant, (2MT2HT): dimethyl, dihydrogenatedtallow, quaternary ammonium chloride, with the chemical structure shown in Fig. 6.1(a). N^+ denotes the quaternary ammonium chloride and HT denotes long alkyl chains from hydrogenated tallow (~ 65% C18, 30% C16, and 5% C14). The modifier concentration for Cloisite 15A and Cloisite 20A was 125 meq/100g clay and 95 meq/100g clay, respectively. For Cloisite 25A (Fig. 6.1(b)), the natural sodium montmorillonite was modified with the surfactant, (2MHTL8): dimethyl, hydrogenated tallow, 2-ethylhexyl, quaternary ammonium methyl sulfate, at a modifier concentration of 95 meq/100g clay. Finally, for Cloisite 30B (Fig. 6.1(c)), the natural sodium montmorillonite was modified with the surfactant, (MT2EtOH): methyl, tallow, bis-2-hydroxyethyl, quaternary ammonium chloride, at a modifier concentration of 90 meq/100 g clay. T represents long alkyl chains from natural tallow oil (~ 65% C18, 30% C16, and 5% C14). It is important to note that the surface modifiers used to produce Cloisite 15A, 20A, and 25A are non-polar quaternary ammonium salts that consist of long alkyl chains, whereas the surface modifier used to produce Cloisite 30B is a polar quaternary ammonium salt consisting of hydroxyl groups. The hydroxyl groups of the polar quaternary salt allow for hydrogen bonding with the carbonyl group of the PC. Therefore, the surface modification with the polar quaternary salt is expected to improve the dispersion of the nano-clay platelets to a greater extent than the clay platelets surface modified with the non-polar quaternary ammonium salts. For simplicity, the surface modified nano-clay particles will be refered to as ‘organoclays’ and the different organoclay structures will be identified by its tradename, i.e. Cloisite 15A, Cloisite 20A, Cloisite 25A, and Cloisite 30B.

No additives were used in the melt processing steps, such as an inhibitor for the interchange reactions that might occur with PC and PBT under some conditions. It is well known that transesterification can occur during melt blending of PC and PBT [7-11]. Progressive transesterification results in the formation of block copolymers and finally into random copolymers. However, based on previous studies, uncatalyzed blends of PC and PBT were found to have negligible amounts of transesterification products at the

processing conditions employed for this study [12-14]. The overall residence time of the melt blends in the compounding and injection molding steps combined was less than 5 minutes for this study. It was shown by Nazabal et al. [14] that a negligible amount of interchange reactions occurred for blends of PC and PBT when mixed in a batch reactor at a residence time of 8 minutes or less. It should be noted that residual catalyst that is used to promote the condensation reactions required to polymerize PBT also catalyzes the interchange reactions that are involved at the interface of the PC and PBT phase during melt blending. Furthermore, the extent of copolymer formation due to the interchange reactions can have a significant influence on miscibility, morphology and mechanical properties of PC/PBT blends 8-11,13-15].

6.2.2 Compounding and Injection Molding of PC/PBT/nano-clay Composites

Prior to melt processing, the PC, PBT, and organoclays were all dried in a vacuum oven for at least 14 hours at a temperature of 120°C. For the nano-clay loading study, dried pellets of PC and PBT at a blend ratio of 60/40 (PC/PBT by weight) were dry-blended with Cloisite 30B at nano-clay concentrations of 1, 2, 3 and 6 wt%. Cloisite 30B was chosen because Han [4] and Yoon [5] showed that the greatest enhancement in the modulus of PC nanocomposites was greatest when hydroxyl groups were present on the surface modifier. To investigate the effects of organoclay structure on the properties of the nano-clay reinforced PC/PBT composites, dried pellets of PC and PBT at the same blend ratio were mechanically mixed with Cloisite 15A, 20A, 25A, and 30B at a clay loading of 2 wt%. Once dry blending was complete, the nanocomposites were melt blended by using a single-screw Killion extruder that had a 25 mm diameter barrel and a L/D of 30. The die was cylindrical with L/D of 2.5 and diameter of 3 mm. The screw speed was maintained at 20 rpm and the melt temperature was 260°C with a temperature profile of 220/240/260/260°C from hopper to the exit of the die. Upon exiting the die, the composite strands were quenched in a water bath and then chopped into 6 mm long pellets.

After compounding, the pellets were dried in the vacuum oven for at least another 14 hours at 120°C prior to injection molding. After drying, the nanocomposites were injection molded using an Arburg Allrounder Model 221-55-250 injection-molding machine. The Arburg Allrounder had a 22 mm diameter screw, a check ring non-return valve, and an insulated nozzle that was 2 mm in diameter [16]. The composites were injection molded at a melt temperature of 260°C, a mold temperature of 100°C, a holding pressure of 100 bars, and a screw speed of 200 RPMs, into a rectangular end-gated mold with dimensions of 80 mm by 76 mm by 1.6 mm.

6.2.3 Dynamic Mechanical Thermal Analysis of Molded Plaques

Dynamic mechanical thermal analysis (DMTA) of the nanocomposites was performed using a Rheometrics RMS-800 rheometer. Along with measurements of the storage (G') and loss (G") moduli, the thermal expansion of the nanocomposites was also measured. When using a torsional rectangular geometry, the Rheometrics RMS-800 contains a function called auto-tension, which maintains a small tension on the samples as it expands during heating. When auto-tension is enabled, the displacement of a sample can be measured as the material is heated from an initial testing temperature. Therefore, the thermal expansion of a sample can be measured within the range of temperatures tested. To perform the tests, rectangular strips approximately 75 mm long by 8 mm wide were cut near the center of the plaques. Once the strips were mounted in the rheometer, G', G", and the change in length as a function of temperature were measured. The temperature range of 30°C to 160°C was investigated at a temperature ramp rate of 5°C/min under a continuous nitrogen atmosphere. For each composite generated, three samples were tested to check for reproducibility.

6.2.4 Mechanical Properties

Flexural and tensile properties of the nanocomposites and the PC/PBT matrix were tested by using an Instron mechanical tester, model 4204. Test specimens were prepared by cutting rectangular strips approximately 75 mm long by 8 mm wide near the

center of the molded plaques. Flexural specimens were tested in accordance with ASTM standard D790 while the tensile specimens were tested at a crosshead speed of 1.27 mm/min in accordance with ASTM standard D2256. An extensiometer, Instron model 2630-25, was also used for all tensile tests to provide an accurate measure of the tensile modulus. A minimum of 5 samples was tested in the flow direction, and an average value and standard deviation were calculated from the data.

6.2.5 Transmission Electron Microscopy (TEM)

The morphology of the nanocomposites was characterized by means of transmission electron microscopy using a Philips EM420T. The acceleration voltage used was 100kV. Ultra-thin sections of the injection-molded plaques were cut at room temperature using a Reichert-Jung Ultracut E Microtome fitted with a 35° diamond knife. The ultra-thin sections were recovered on 300 mesh Cu grid. Delimoy et al. [14] reported that the natural phase contrast between the PC and PBT phases is weak. Therefore, to improve the phase contrast, samples were stained by exposing them to RuO_4 vapors for approximately 15 minutes following the procedure described by Delimoy et al. [14]. In this study, the specimen blocks were cut near the center of the molded plaques and microtomed sections were cut perpendicular to the flow direction.

6.2.6 Rheological Measurements of the Composite Melts

Dynamic oscillatory shear flow measurements of the nanocomposites and the PC/PBT matrix in the melt state were obtained using a parallel-disk rheometer (Rheometrics RMS-800) with 25 mm diameter plates. The complex viscosity, $|\eta^*|$, and storage modulus, G', were investigated in a frequency range of 0.1 to 100 rad/s at a melt temperature of 260°C under a continuous nitrogen atmosphere. A strain of 5% was maintained to ensure that the measurements were taken within the linear viscoelastic region. Test specimens that were 1.0 mm thick were prepared by compression molding the generated pellets into 25 mm diameter disks at 260°C. A minimum of 3 samples was tested to check for reproducibility.

6.3 Results and Discussion

6.3.1 Effect of Organoclay Structure on the Miscibility of PC/PBT/nano clay Composites

The effect of organoclay structure on the miscibility of the PC/PBT/nano-clay composites was investigated at a nano-clay loading of 2 wt%. In Fig. 6.2, tan δ, which is defined as the ratio of the loss modulus to that of the storage modulus (G"/G'), of the nanocomposites, the PC/PBT matrix, and PC is illustrated as a function of organoclay structure in the temperature range of 30°C to 180°C. A peak in tan δ is indicative of the glass transition temperature, T_g, of a material. When blending two polymers, the resulting blend may have one T_g, which is indicative of a miscible system, or two T_gs, which is indicative of an immiscible or partially miscible system. A partially miscible system exhibits two T_gs that are slightly shifted from that of the neat components. An immiscible system also exhibits two T_gs, but in this case, the two T_gs are exactly that of the neat components. By using dynamic mechanical thermal analysis, it is difficult to ascertain the T_g of the PBT rich phase, but the T_g of the PC rich phase is clearly visible. The T_g of the pure PBT (not shown) is 55°C while the T_g of the pure PC is 160°C. The T_g of the PC rich phase is shifted downward by 28°C to a value of 132°C when the PC and PBT are melt blended at a blend ratio of 60/40 (PC/PBT) by weight, which is indicative of a partially miscible system. Partial miscibility when PC and PBT are melt blended has also been reported by many other research groups, but to varying degrees of partial miscibility [11, 13-15]. The disagreements observed in the literature are attributed to the interchange reactions that occur during the melt blending of PC/PBT blends. However, Hobbs et al. [15] showed that partial miscibility of PC/PBT blends is still observed when a stabilizer, such as an inhibitor for the interchange reactions, is introduced. It was shown that even though inhibitors were used to prevent transesterification reactions from occurring, they were not completely suppressed, and thus, the observance of partial miscibility due to interchange reactions was still possible. As mentioned in the experimental section, an inhibitor was not used to suppress the

interchange reactions at the interface between the PC and PBT phase and, therefore, the observance of a partially miscible system is most likely due to the interchange reactions.

The organoclay structure also has a strong influence on the miscibility of the PC/PBT blends (see Fig. 6.2). With the addition of the organoclays, the T_g of the PC rich phase is shifted downward relative to that of the unfilled PC/PBT matrix, but the extent of the shift is dependent on the organoclay structure. The T_g of the PC rich phase for the nanocomposites, PC/PBT matrix, and PC is summarized in Table 6.1. The largest shift downward in T_g of the PC rich phase is observed when the PC/PBT matrix is melt blended with Cloisite 20A. In this case, the T_g of the PC rich phase is reduced by 30°C relative to that of the unfilled PC/PBT matrix to a value of 102°C. The smallest shift downward in T_g of the PC rich phase (by 6°C) is observed when the PC/PBT matrix is melt blended with Cloisite 25A. The composites generated with the other two organoclays fall within these limits. These results suggest that the organoclays (Cloisite 15A and Cloisite 20A) with two long alkyl groups from hydrogenated tallow improve the compatibility of the PC and PBT phase to a much greater extent than that of the other two organoclays. The organoclays Cloisite 30B and Cloisite 25A improve the compatibility of the PC and PBT phase to a similar extent, but the compatibility of the two phases is slightly better when Cloisite 30B is used. The enhanced compatiblility of the PC and PBT phase by using Cloisite 30B as opposed to Cloisite 25A is most likely do to the polar organoclay structure of the Cloisite 30B since the alkyl chain length of the two organoclays are similar. It is also possible that the enhanced compatibility of the PC and PBT phase with the addition of organoclays may be due to an increase in the formation of block copolymers, which are generated by the interchange reactions, at the interface between the PC and PBT phase. It should be noted that in our previous work [1], the T_g of the PC rich phase was unaffected with the addition of nano-talc particles and, therefore, the surface modification of the nano-talc particles had no influence on the miscibility of the PC and PBT phase.

Based on the above results, the varying degrees of miscibility of the PC/PBT blends reinforced with the various organoclays can have a significant affect on the dimensional stability, i.e. thermal expansion, of the nanocomposites in the temperature range of interest (30°C to 100°C). Therefore, the effect of organoclay structure on the

dimensional stability of the PC/PBT/nano-clay composites will be investigated in the following section.

6.3.2 Effect of Organoclay Structure on the Dimensional Stability of PC/PBT/nano-clay Composites

The effect of organoclay structure on the dimensional stability, i.e. thermal expansion, of the PC/PBT/nano-clay composites was investigated at a nano-clay loading of 2 wt%. In Fig. 6.3, the thermal expansion of the nanocomposites is illustrated as a function of organoclay structure over the temperature of 30°C to 100°C. The thermal expansion of the PC/PBT matrix at a blend ratio of 60/40 (PC/PBT) by weight is also shown for comparative purposes. Typically, the addition of particulate fillers results in a reduction in the thermal expansion. However, it was shown in our previous work [1] that at a PC/PBT blend ratio of 60/40 by weight or greater the addition of talc particles had no influence on the dimensional stability of talc reinforced PC/PBT blends. This was attributed to the high T_g of the PC rich phase, which was approximately 132°C, as well as the phase inversion that occurs once the blend ratio of PC/PBT is equal to or greater than 60/40 by weight. Once phase inversion occurs, the PBT phase is dispersed within the continuous PC phase. In this case, the thermal expansion of the nanocomposites increases with the addition of organoclay and the extent of the increase is significantly affected by the organoclay structure. In fact, the increase in the thermal expansion with organoclay structure is in good agreement with the reduction in the T_g of the PC rich phase as observed in the previous section. For example, the overall dimensional change at 100°C is greatest for the nanocomposites generated with Cloisite 20A (≈ 60% greater than that of the unfilled matrix) while it is lowest and similar to that of the unfilled PC/PBT matrix (< 3%) for the nanocomposites generated with Cloisite 25A. The significant increase in the thermal expansion of the nanocomposites generated with Cloisite 20A is due to the 30°C reduction in the T_g of the PC rich phase relative to that of the unfilled PC/PBT matrix. Furthermore, the T_g of the PC rich phase for the nanocomposites generated with Cloisite 25A is only reduced by 6°C relative to that of the unfilled matrix and has a value of 126°C. These results suggest that the dimensional

stability of PC/PBT/nano-clay composites is dominated by the T_g of the PC rich phase, and, therefore the degree of miscibility between the PC and PBT phase.

6.3.3 Effect of Organoclay Concentration on the Mechanical Properties of PC/PBT/Cloisite 30B Composites

The effect of organoclay concentration on the flexural (see Fig 6.4(a)) and tensile modulus (see Fig. 6.4(b)) of PC/PBT/nano-clay composites is investigated by varying the loading level of Cloisite 30B (1, 2, 3 and 6 wt%). In Fig. 4(a), the effect of nano-talc loading on the flexural modulus of PC/PBT/nano-talc composites, obtained from our previous paper [1], is also added for comparative purposes. The PC/PBT matrix has a flexural modulus of 2.1 GPa. With the addition of organoclay or nano-talc, the flexural modulus increases with an increase in particle loading, but the increase in modulus with particle loading is more pronounced when the organoclay is used. In both cases, there is initially a significant increase in the flexural modulus relative to that of the unfilled PC/PBT matrix at a nanoparticle loading of 1 wt%. However, with further addition of nano-talc, the flexural modulus of the nanocomposites only increases slightly. On the other hand, the flexural modulus of the nanocomposites generated with organoclay continues to significantly increase with an increase in organocaly loading. For example, the flexural modulus at a nanoparticle loading of 1 wt% is 2.45 GPa and 2.5 GPa for the nanocomposites generated with nano-talc and organoclay, respectively, which corresponds to a 17% and 20% increase in modulus relative to that of the PC/PBT matrix. At a nano-talc loading of 6 wt%, the flexural modulus of the nanocomposites is only 2.53 GPa (20% increase in modulus relative to that of the PC/PBT matrix), which corresponds to a 3% increase in modulus relative to that of the nanocomposite at a nano-talc loading of 1 wt%. However, at an organoclay loading of 6 wt%, the flexural modulus is 2.8 GPa (34% increase in modulus relative to that of the PC/PBT matrix), which corresponds to a 14% increase in modulus relative to that of the nanocomposite generated at 1 wt%. The flexural modulus of the nanocomposites generated with the organoclay is always greater than that of the nanocomposites generated with the nano-talc at an equivalent level of reinforcement. The greater flexural modulus for the nanocomposites generated with the organoclay as opposed to the nano-talc is attributed to the higher aspect ratio of the

organoclays (100-150) relative to that of the nano-talc (20-25). These results are in qualitative agreement with the Halpin-Tsai equations [17-19], which predict an increase in modulus with an increase in aspect ratio up to an aspect ratio on the order of 100.

The tensile modulus of the nanocomposites increases with an in increase in organoclay loading, see Figure 6.4(b). There is a linear increase in the tensile modulus with an increase in particle loading. At an organoclay loading of 6 wt%, the tensile modulus of the nanocomposite is increased by 60% relative to that of the unfilled PC/PBT matrix. Similar results have been reported by Yoon et al. [5] and Han et al. for PC nanocomposites, where the PC was reinforced with Cloisite 30B. Yoon et al. observed a linear increase in the tensile modulus with organoclay loading up to an organoclay loading of 4.5 wt%. Also, at an organoclay loading of 3 wt%, the tensile modulus of the PC nanocomposite was 2.98 GPa, which correlated to a 28% increase in the modulus relative to that of the PC matrix. In our case the tensile modulus of the PC/PBT/Closite 30B nanocomposite at an equivalent level of reinforcement is 2.1 GPa, which corresponds to a 40% increase in the tensile modulus of the nanocomposite relative to that of the nanoclay. Han et al. [4] reported a 75% increase in the tensile modulus at an organoclay loading of 4.5 wt%. The increase in tensile modulus with an increase in organoclay loading was attributed to partial exfoliation of the clay platelets, which was enhanced by the presence of hydrogen bonding between the carbonyl groups in PC with the hydroxyl groups residing at the surface of the oraganoclay (Cloisite 30B). These results suggest that the increase in tensile modulus with the addition of Cloisite 30B for the PC/PBT/nano-clay can be attributed to improved dispersion of the clay platelets promoted by hydrogen bonding between the PC phase and the organoclay. The morphology of the nanocomposites will be discussed in more detail in a later section.

Organoclay concentration has little influence (< 2%) on the flexural or tensile strength of the nanocomposites. The flexural and tensile strength of the PC/PBT matrix are 65 MPa and 40 MPa, respectively. With the addition of organoclay, the flexural and tensile strength of the nanocomposites are approximately 85 MPa and 50 MPa, respectively, which corresponds to a 30% and 25% increase in flexural and tensile strength relative to that of the unfilled matrix. Similar results on the effect of nano-talc concentration on the flexural strength of PC/PBT/nano-talc composites were recently

reported by the authors [1]. In this case, the flexural strength of the nano-talc reinforced PC/PBT blends were 80 MPa, which corresponded to a 23% increase in flexural strength relative to that of the unfilled PC/PBT matrix.

Finally, the tensile toughness as measured by the area under the stress-strain curve of the PC/PBT matrix and the nanocomposites as a function of organoclay or nano-talc loading is illustrated in Fig. 6.5. As expected, the tensile toughness of the nanocomposites is reduced with an increase in particle loading. However, the nanocomposites generated with the organoclay retain the initial tensile toughness of the unfilled PC/PBT matrix to a much greater extent than that of the nanocomposites generated with the nano-talc. For instance, at an organoclay loading of 1 wt%, the tensile toughness of the nanocomposite is reduced by 50% relative to that of the PC/PBT matrix while the tensile toughness of the nano-talc reinforced nanocomposite at the same level of reinforcement is reduced by approximately 78% relative to the observed tensile toughness of the unfilled matrix. The greater tensile toughness observed for the molded plaques generated with the organoclay as opposed to that of the nano-talc can be attributed to improved compatibility that is observed between the PC and PBT phase, as observed by the downward shift in the Tg of the PC rich phase (see, Fig. 6.2), and improved polymer/filler interactions due to hydrogen bonding of the PC phase with the surface of the Cloisite 30B. Other factors such as particle placement, i.e. the location of the particles within the PC/PBT matrix, and morphological structure of the PC and PBT phase themselves could play a critical role on the tensile toughness of the nanocomposites. Therefore, the morphology of the nanocomposites will be discussed in a later section.

There are several advantages in using Cloisite 30B to reinforce PC/PBT blends as opposed to the nano-talc. At an organoclay loading of 1 wt%, the flexural modulus, flexural strength and tensile toughness are increased by 1%, 12% and 120%, respectively, relative to that of the nanocomposites generated with nano-talc at an equivalent level of reinforcement. However, due to the improved compatibility of the PC and PBT phase with the addition of the organoclay, the Tg of the PC rich phase is shifted downward from 130°C to 112°C, which leads to an increase in the overall dimensional change of the organoclay reinforced nanocomposites in the temperature range of 30°C to 100°C.

Because the organoclay structure has been known to have a significant affect on the properties and morphology of PC nanocomposites, the effect of organoclay structure on the properties and morphology of the nanocomposites will be discussed in the following sections [4,5].

6.3.4 Effect of Organoclay Structure on the Mechanical Properties of PC/PBT/nano-clay Composites

The effect of organoclay structure on the mechanical properties of PC/PBT/nano-clay composites is investigated by varying the structure of the organic amine compound used to form the organoclays (Cloisite 15A, 20A, 25A, and 30B) at an organoclay loading of 2 wt%. The results are summarized in Table 6.2. The unfilled PC/PBT matrix is also included for comparitive purposes. The chain length of the alkyl groups and the concentration of the modifier seem to have little influence (< 3%) on the flexural modulus or flexural strength of the nanocomposites. However, the polarity of the organic amine compound used to form the organoclay affects to some extent both the flexural modulus and strength of the nanocomposites. The flexural modulus and strength of the non-polar organoclays (Coisite 15A, 20A, and 25A) are approximately 2.5 GPa and 80 MPa, respectively, while the flexural modulus and strength of the polar organoclay (Cloisite 30B) are 2.66 GPa and 85 MPa, which corresponds to a 5% increase in modulus and strength relative to that of the non-polar oraganoclays.

The effect of organoclay structure on the tensile modulus (see Fig 6.6(a)) and tensile toughness (see Fig. 6.6(b)) of PC/PBT/nano-clay composites is investigated. The PC/PBT matrix is included for comparative purposes. The tensile modulus of the PC/PBT matrix is approximately 2.2 GPa. With the addition of organoclay, there is an increase in the tensile modulus relative to that of the unfilled PC/PBT matrix, but the extent of the increase is strongly affected by the organoclay structure. The largest increase in tensile modulus is observed when the clay platelets are surface modified with an organic amine compound that contains two hyroxyl end groups (Cloisite 30B). In this case, the tensile modulus of the nanocomposite increases by approximately 30% relative to that of the unfilled PC/PBT matrix with just an addition of 2% by weight of the organoclay. Furthermore, the chain length of the alkyl groups also has an influence on

the tensile modulus of the nanocomposites. For instance, the organic amine group that has two long alkyl groups from hydrogenated tallow (Cloisite 20A) has a tensile modulus of 2.42, which corresponds to a 10% increase in the modulus relative to that of the unfilled matrix. On the other hand, the tensile modulus of the nanocomposites generated with the organoclay (Cloisite 25A) that contains only one long alkyl group from hydrogenated tallow and a smaller hydrocarbon chain is only 2.32 GPa, which corresponds to just a 5% increase in the modulus of the nanocomposite relative to that of the unfilled PC/PBT matrix. These results suggest that the nanoparticles are exfoliated to a greater extent when the organoclay Cloisite 30B is used relative to that of the other organoclays.

The tensile toughness of the nanocomposites is also significantly influenced by the structure of the organoclay, (see Fig. 6.6(b)). With the addition of organoclay, the tensile toughness of the nanocomposites is reduced relative to that of the unfilled matrix. However, the nanocomposites generated with Cloisite 20A, which has the two long alkyl groups from the hydrogenated tallow, retain the initial tensile toughness of the unfilled PC/PBT matrix to a much greater extent than that of the composites generated with the other organoclays. For example, the tensile toughness of the nanocomposites retains approximately 86% of the initial tensile toughness that is observed for the unfilled PC/PBT matrix when Cloisite 20A is used as the reinforcing agent, while the tensile toughness is reduced on the order of 60% to 70% relative to that of the unfilled PC/PBT matrix when the other organoclays are used as the reinforcing agent. It is also interesting to note that the tensile toughness of the nanocomposites generated with Cloisite 30B is the lowest even though it has the greatest tensile modulus. There are a few possible reasons for the lack of significant reduction in tensile toughness observed for the nanocomposites that are generated with Cloisite 20A. First of all, the organic amine compound used to form Cloisite 20A improved the compatibility between the PC and PBT phase to the greatest extent relative to that of the other organoclays, as indicated by the greatest downward shift in Tg of the PC rich phase (see Fig. 6.2 and Table 6.1). Secondly, the clay platelets may have been dispersed within the PC/PBT matrix to a greater degree when the nanocomposites are generated with Cloisite 20A as opposed to the other organoclays. However, this possibility contradicts the findings that the greatest

improvement in the tensile modulus was observed for the nanocomposites generated with Cloisite 30B. In order to clear up this issue, the effect of organoclay structure on the phase morphology of the PC/PBT blends and the dispersion of the organoclays within the PC/PBT matrix will be discussed next.

6.3.5 Effect of Organoclay Structure on the Morphology of PC/PBT/nano-clay Composites

Based on the above findings, the organoclay structure is expected to have some effect on the phase structure of the PC and PBT phase as well as the dispersion of the organclays within the PC/PBT matrix. In Fig. 6.7 and Fig. 6.8, images of the injection molded samples obtained by means of transmission electron microscopy (TEM) for the nanocomposites are shown as a function of organoclay structure at an organoclay concentration of 2 wt%. In these micrographs, the organoclays are black. The PC phase is a dark gray due to staining with the RuO_4 vapors, while the PBT phase is white or a light shade of gray. With the exception of the nanocomposites generated with Cloiste 20A, a fibrillar phase morphology is observed, where the PBT droplets deformed into fibrils within the continuous PC phase. The domain size, i.e. the thickness of the PBT fibrils, is significantly affected by the organoclay structure. The average thickness of the PBT fibrils are on the order of 90-100 nm, 75-80 nm, and 40-50 nm when the PC/PBT blends are reinforced with Closite 25A, 30B, and 15A, respectively. The reduction in the size scale of the PBT fibrils with organoclay structure is directly related to the observed increase in compatibility as indicated by the downward shift in the T_g of the PC rich phase. For instance, the average thickness of the PBT fibrils is reduced from 90-100 nm to 40-50 nm while the reduction in the T_g of the PC rich phase is increased by 20°C when the nanocomposites are generated with Cloisite 15A as opposed to 25A. In the case of the nanocomposites generated with Cloisite 20A, only a single-phase mixture is observed, which is indicative of a miscible blend. Similar results have been reported by Tattum et al. [9] for unfilled PC/PBT blends that were catalyzed by using a titanium catalyst. They found that uncatalyzed blends exhibited a co-continuous structure where the PC and PBT phases exhibited a fibrillar morphology. As the level of catalyst was increased, the co-continuous structure was maintained but at a reduced size scale. This is

expected since the interchange reactions act as a compatibilizer for PC/PBT blends. However, once enough catalyst was added (200 ppm), the PC/PBT became completely miscible and so the co-continuous structure that was typically observed was reduced to a single phase. These results suggest that the structure of the organic amine compound that is used to form the organoclays in some way promotes transesterification at the interface between the PC and PBT phase. If this is true, then the extent of reaction is also influenced by the chemical structure of the organoclays.

Besides from the morphological structure of the PC and PBT phase, the organoclay structure also has an influence on the dispersion of the organoclays and the location of the reinforcing filler. The nanocomposites prepared with Cloisite 20A have the highest observed tensile toughness at a value of 92 MPa while the nanocomposites generated with the other organoclays have a similar tensile toughness that ranges between 30-40 MPa. If a fibrillar phase morphology is observed (Cloisite 15A, 25A, and 30B), there is a mixture between partially exfoliated clay platelets, fully exfoliated clay platelets and agglomerates with diameters and length scales on the order of 2-3 ums can be observed. However, if a single-phase mixture is observed (Cloisite 20A), only partially exfoliated and fully exfoliated clay platelets are observed. There are no large agglomerates observed and, therefore, the enhanced dispersion of the clay platelets, when Cloisite 20A is used as the reinforcing filler, is indicative of the higher tensile toughness that is observed relative to that of the nanocomposites generated with the other organoclays. It is interesting to note that the tensile modulus of the nanocomposites generated with Cloisite 20A is approximately 15% lower than that of the nanocomposites prepared with Cloisite 30B even though there is a higher degree of exfoliated clay platelets as observed in the TEM images. These results suggest that hydrogen bonding may play a larger role on the enhancement of the modulus for nanocomposites than previously thought.

The location of the clay platelets is also affected by the structure of the organic amine compound that is used to form the organoclay (see Fig. 6.8). When the clay platelets are surface modified with a polar amine compound (Cloisite 30B), the organoclay has an affinity for the PBT phase (see Fig. 6.8(d)) while the organoclay has an affinity for the PC phase (see Fig. 6.8(c)) when the clay platelets are surface modified

with a non-polar amine compound (Cloisite 20A). However, the clay platelets do not have an affinity for either the PC or PBT phase when the organoclay Cloisite 15A is used to reinforce the PC/PBT blends (see Fig. 6.8(a)). These results support the hypothesis that the organoclay structure in some way promotes transesterification at the interface between the PC and PBT phase, and that the extent of reaction is affected by the chemical structure of the organoclay.

6.3.6 Effect of Organoclay Loading and Structure on the Rheology of PC/PBT/nano-clay Composites

Although particulate fillers are added to polymer melts to increase the stiffness or rigidity and/or reduce the cost of the blend, they also can have a significant affect on the rheological properties and, hence, the ability to process the composites. Rheological properties are also sensitive to small changes in the morphological state and to the molecular weight of the materials. Therefore, the effect of organoclay loading and structure on the rheological properties of the nanocomposites is investigated in this section.

In order to determine effects of organoclay loading on the viscoelastic flow behavior of the nanocomposites, G' and $|\eta^*|$ of the nanocomposites prepared by using Cloisite 30B as well as the PC/PBT matrix are illustrated in Fig. 6.9 and Fig. 6.10 at 260°C (i.e., the melt processing temperature of the materials). G' and $|\eta^*|$ of the nanocomposites generated with the nano-talc are also shown for comparative purposes. The magnitude of G' in the low frequency region (long relaxation times) increases with an increase in nanoparticle loading. However, the increase in the magnitude of G' in the low frequency region is more pronounced when the organoclay is used to reinforce the PC/PBT blends as opposed to the nano-talc. For example, G' at a frequency of 0.1 rad/s increases by approximately 90% when the organoclay loading of the nanocomposites is increased from 3 wt% to 6 wt% while G' is only increased by 20% when the nano-talc loading of the nanocomposites is increased from 3 wt% to 6 wt% at the same frequency. The rheological behavior of G' at low frequencies is in good agreement with the observed flexural modulus of the composites. An increase in G' at low frequencies is indicative of

an increase in the long relaxation times of the material and, therefore, inhibits stress relaxation of the polymer chains. This allows for a higher degree of orientation to be locked into an injection molded part, and hence, higher modulus. For example, the flexural modulus of the composites generated with the organoclay significantly increases with an increase in particle loading while G' at low frequencies also increases significantly with an increase in clay loading. Furthermore, the flexural modulus of the nanocomposites generated with nano-talc only slightly increases with an increase in talc loading, which is in good agreement with the small increase in G' at low frequencies that is observed when the talc loading is increased.

In the high frequency region, the magnitude of G' at high frequencies is below that of the unfilled PC/PBT matrix, and it decreases with an increase in nanofiller concentration. This is unusual behavior for particulate filled systems. Typically, G' in the high frequency region for particulate filled systems converges to that of the matrix. However, Yoon et al. [5] have observed similar results for PC nanocomposites. They attributed the reduction in G' at high frequencies to a reduction in the molecular weight of the PC matrix. In our case, the reduction in G' at high frequencies with an increase in particle loading is more pronounced when nano-talc is used to reinforce the PC/PBT matrix as opposed to the organoclay. The reduction in G' at high frequencies is most likely due to loss in molecular weight, but in the case of the organoclays, it is possible that the reduction in G' at high frequencies may be due to enhanced compatibility (better adhesion) between the filler and the matrix or lowering of the interfacial tension between the PC and PBT phase.

The complex viscosity, $|\eta^*|$, of the nanocomposites decreases with an increase in filler concentration, but the magnitude of the decrease is more pronounced when the nano-talc particles are used relative to that of the organoclays. The viscosity at a frequency of 1 rad/s is reduced by 50% and 76% at organocaly loadings of 3 and 6 wt% relative to that of the PC/PBT matrix, while it is reduced by 70% and 90% at nano-talc loadings of 3 and 6 wt% relative to that of the PC/PBT matrix. The reduction in the viscosity that is observed when nanofillers are used is most likely due to a decrease in molecular weight of the matrix. Even though there is a significant reduction in viscosity and most likely in molecular weight with an increase in particle loading, the flexural and

tensile modulus of the filled nanocomposites still increase with an increase in particle loading as shown earlier.

Besides from particle loading, the organoclay structure is also expected to have a significant effect on the rheological properties of the nanocomposites. The effect of organoclay structure on G' and $|\eta^*|$ as a function of frequency for the nanocomposites are illustrated in Fig. 6.11 and Fig. 6.12 at an organoclay loading of 2 wt%. The magnitude in G' of the PC/PBT matrix is also shown for comparative purposes. The magnitude of G' at low frequencies increases with the addition of organoclay, but the structure of the organic amine group used to form the organoclay has little influence on the magnitude of G' in the low frequency region. However, the organoclay structure does affect G' in the high frequency region. In the high frequency region, the magnitude in G' is lower than that of the PC/PBT matrix, regardless of the organoclay structure. The reduction in G' at high frequencies with organoclay structure correlates with the observed increase in compatability (see Fig. 6.2 and Table 6.1). The largest reduction in the magnitude of G' at high frequencies is observed for the nanocomposites prepared by using Cloisite 20A. The addition of Coisite 20A to the PC/PBT matrix enhanced the compatibility of the PC and PBT phase to a greater degree than the other organoclays. The smallest reduction in the magnitude of G' at high frequencies is observed for nanocomposites generated with Cloisite 25A, which had the lowest compatibility with the PC and PBT phase relative to the other organoclays. The reduction in the magnitude of G' with organoclay structure can be attributed to enhanced compatibility (better adhesion) between the filler and the matrix or lowering of the interfacial tension between the PC and PBT phase.

The complex viscosity, $|\eta^*|$, of the nanocomposites decreases with the addition of organoclay and the magnitude of the decrease is affected by the organoclay structure. With the exception of the nancomposites generated with Cloisite 30B, the reduction in viscosity is enhanced with an increase in the compatibility between the organoclay and the PC/PBT matrix. The greatest reduction in viscosity (70% at a frequency of 1 rad/s) relative to that of the matrix is observed for the nanocomposites prepared by using Cloisite 30B, even though the best enhancement in flexural and tensile properties are observed for these nanocomposites. The significant reduction in the viscosity for the nanocomposites generated with Cloisite 30B is most likely due to a loss of molecular

weight of the PC/PBT matrix. At the elevated temperatures employed during the compounding and molding steps, the hydroxyl groups from the organic amine compound may have catalyzed the degradation of the PC phase.

6.4 Conclusions

The effect of organoclay loading and structure on the dimensional stability, structure-property relationships, and rheological behavior of PC/PBT/nano-clay composites was investigated. It was found that by using the organoclay (Cloisite 30B) as opposed to nano-talc, the flexural strength and tensile toughness of the nanocomposites increased by 12% and 27%, respectively, at a particle loading of 1 wt% while maintaining a flexural modulus of 2.5 GPa. The flexural and tensile modulus of the nanocomposites increased with an increase in particle loading even though the viscosity was significantly reduced due to a loss of molecular weight of the PC/PBT matrix and/or an increase in the compability of the interface between the PC and PBT phase, which varied with organoclay structure. The largest enhancement in flexural and tensile modulus was observed for nanocomposites prepared by using Cloisite 30B due to hydrogen bonding between the carbonyl group of the PC phase with that of the hydroxyl end groups located on the surface of the chemically modified clay platelets while the highest tensile toughness was observed for the nanocomposites generated with Cloisite 20A. The high tensile toughness for the nanocomposites generated with Cloisite 20A was attributed to the formation of a single-phase mixture and the lack of agglomerates on the size scale of 2-3 um in diameter.

6.5 Acknowledgements

The authors would like to gratefully acknowledge the support from the DaimlerChrysler Challenge Fund. We would also like to thank Southern Clay Products for donating the organoclays, Nanova for donating the nano-talc particles and Steve McCartney at the Materials Research Institute in Blacksburg, VA for photographing and developing the images obtained by means of transmission electron microscopy (TEM).

6.6 References

1. W.S. DePolo and D.G. Baird, *Polymer Composites*, Submitted September (2005).

2. D. Wu, X. Wang, Y. Song, and R. Jin, *J. Appl. Polym. Sci.*, **92**, 2714 (2004).

3. M. Alexandre, P. Dubois, T. Sun, M. Garces, and R. Jerome, *Polymer*, **43**, 2123 (2002).

4. K.M. Lee and C.D. Han, *Polymer*, **44**, 4573 (2003).

5. P.J. Yoon, D.L. Hunter, and D.R. Paul, *Polymer*, 44, 5341 (2003).

6. Physical Properties Bulletin from Southern Clay Products, Inc.

7. D.C., Wahrmund, D.R. Paul, and J.W. Barlow, *J. Appl. Polym. Sci.*, **22**, 215 (1978).

8. A.N. Wilkinson, and S.B. Tattum, *Polymer*, **38**, 1923 (1997).

9. S.B. Tattum, D. Cole, and A.N. Wilkinson, *J. Macromol.Sci.-Phys. B.*, **39** (4), 459 (2000).

10. S.Y. Hobbs, V.L. Groshans, M.E.J. Dekkers, and A.R. Shultz, *Polymer Bulletin*, **17**, 335 (1987).

11. B.D. Hanrahan, S.R. Angeli, and J. Runt, *Polymer Bulletin*, **14**, 399 (1985).

12. G. Pompe, and L. Haubler, *J. of Polym. Sci.: Part B: Polym. Phys.*, 35, 2161 (1997).

13. P. Sanchez, P.M. Remiro, and J. Nazabal, *J. Appl. Polym. Sci.*, **50**, 995 (1993).

14. D. Delimoy, C. Bailly, J. Devaux, and R. Legras, *Polym. Sci. Eng.*, 28, 104 (1988).

15. S.Y. Hobbs, M.E.J. Dekkers, and V.H. Watkins, *Polymer Bulletin*, 17, 341 (1987).

16. D.G. Baird, W. Huang, and J. Huang, *J. of Injection Molding Technology*, 5(4), 233 (2001).

17. K. Mitsuishi, *Die Angewandte Makromolekulare Chemie*, **248**, 73 (1997).

18. Z. Li and K.A. Narh, *Composites: Part B*, **32**, 103 (2003).

19. D.A. Brune and J. Bicerano, *Polymer*, **43**, 369 (2002).

Table 6.1: Glass transition temperatures determined by dynamic mechanical thermal analysis for PC, PC/PBT matrix and PC/PBT/organoclay composites.

Material	Tan δ peaks, °C
PC	160
PC/PBT	132
Cloisite 15A	107
Cloisite 20A	102
Cloisite 25A	126
Cloisite 30B	120

Table 6.2: Mechanical Properties of the PC/PBT matrix and PC/PBT/organoclay composites as a function of organoclay structure at a concentration of 2 wt%.

Material	*Flexural Modulus (GPa)*	*Flexural Strength (MPa)*	*Tensile Modulus (GPa)*	*Tensile Strength (MPa)*	Tensile Toughness *(MPa)*
PC/PBT	2.1 ($\pm$ 0.02)	65 ($\pm$ 1.0)	2.2 ($\pm$ 0.02)	40 ($\pm$ 1.0)	107 ($\pm$ 3.0)
15A	2.48 ($\pm$ 0.01)	79 ($\pm$ 2.0)	2.3 ($\pm$ 0.04)	51 ($\pm$ 1.0)	35 ($\pm$ 2.5)
20A	2.54 ($\pm$ 0.01)	79 ($\pm$ 1.3)	2.4 ($\pm$ 0.06)	55 ($\pm$ 1.1)	91 ($\pm$ 2.6)
25A	2.56 ($\pm$ 0.02)	81 ($\pm$ 0.7)	2.3 ($\pm$ 0.08)	48 ($\pm$ 1.4)	41 ($\pm$ 2.4)
30B	2.65 ($\pm$ 0.02)	86 ($\pm$ 1.0)	2.8 ($\pm$ 0.05)	51 ($\pm$ 1.3)	32 ($\pm$ 1.8)

Closite 15A and Cloisite 20A

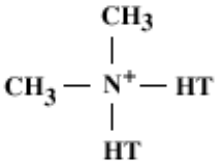

2M2HT

Cloisite 25A

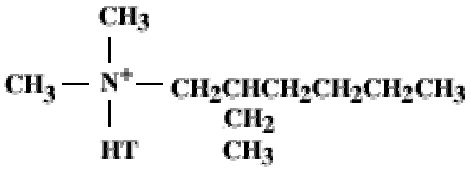

2MHTL8

Cloisite 30B

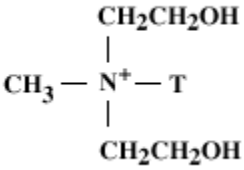

MT2EtOT

Figure 6.1: Molecular structure and nomenclature of organic amine salts used to chemically modify the surface of the nano-clay platelets. The substituents on the nitrogen are designated as: M = methyl, HT = Hydrogenated Tallow, L8 = 2-ethylhexyl, and 2EtOT = 2-hydroxy-ethyl [6]. The surface modifier concentration is 125, 95, 95, and 90 meq/100 g clay for Cloisite 15A, 20A, 25A, and 30B, respectively.

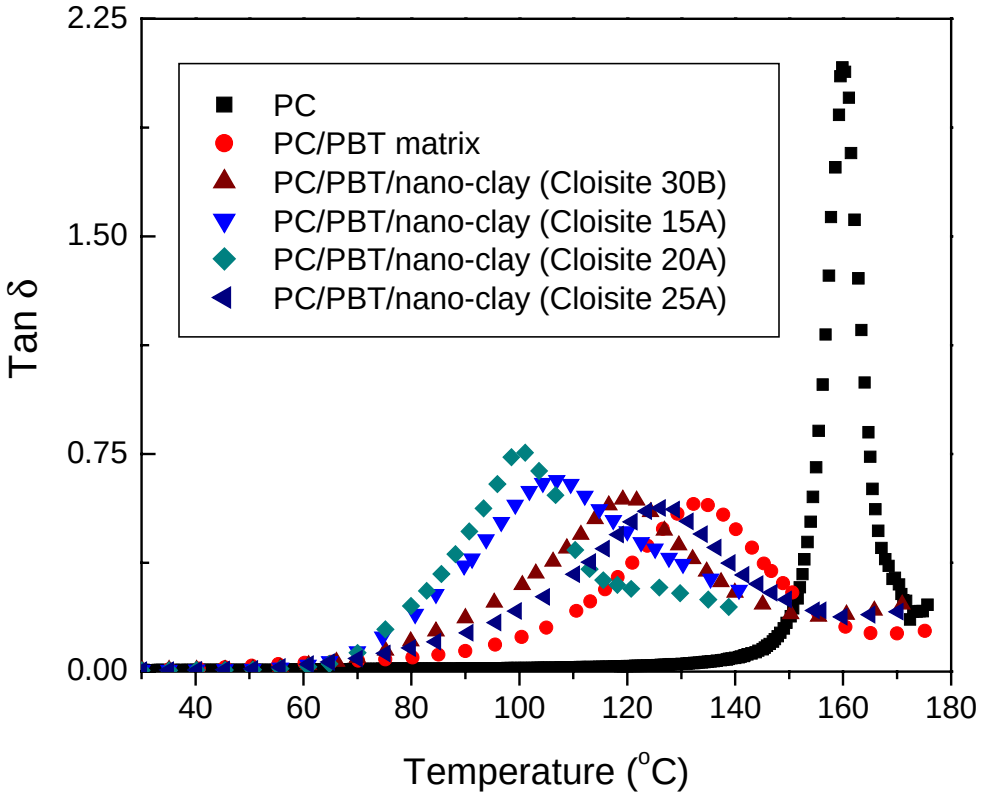

Figure 6.2: Tan δ as a function of organoclay structure for PC/PBT/nano-clay composites. The tan δ of PC and the unfilled PC/PBT matrix are included for comparitive purposes. The PC/PBT blend ratio is 60/40 by weight and the concentration of the organoclays is 2 wt%. A temperature ramp of 5°C/min was applied.

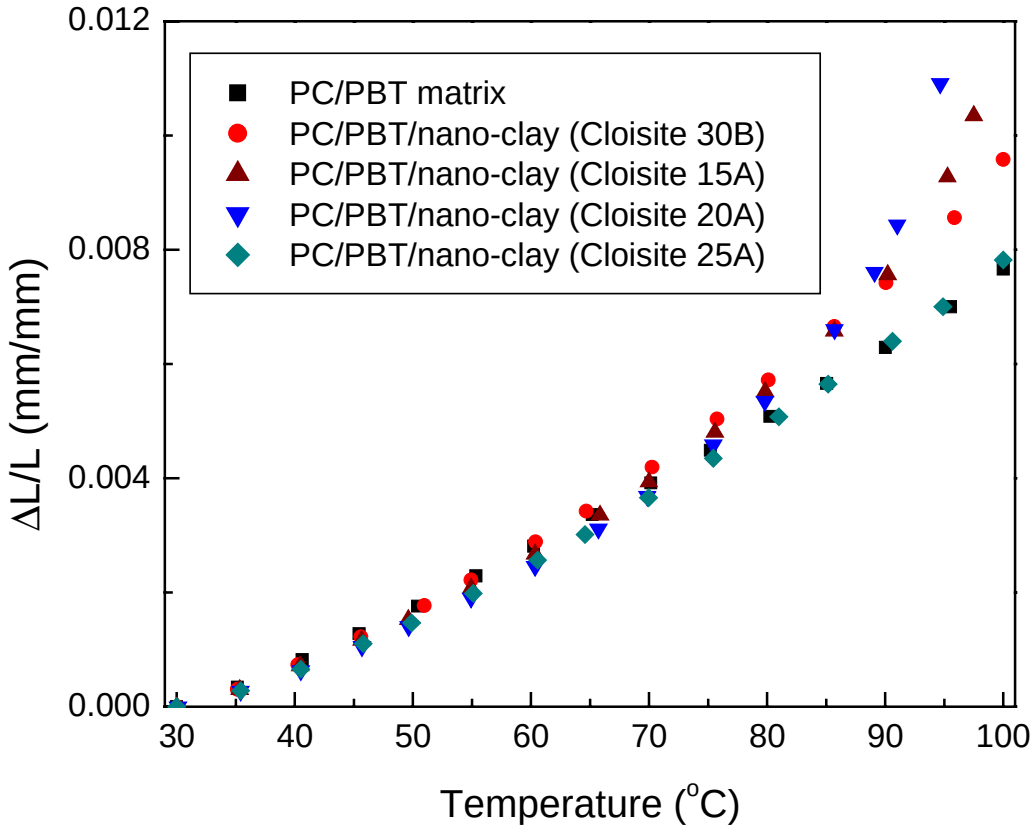

Figure 6.3: Thermal strain (mm/mm) of PC/PBT/nano-clay composites as a function of organoclay structure. The PC/PBT blend ratio is 60/40 by weight and the concentration of the organoclays is 2 wt%. A temperature ramp of 5°C/min was applied.

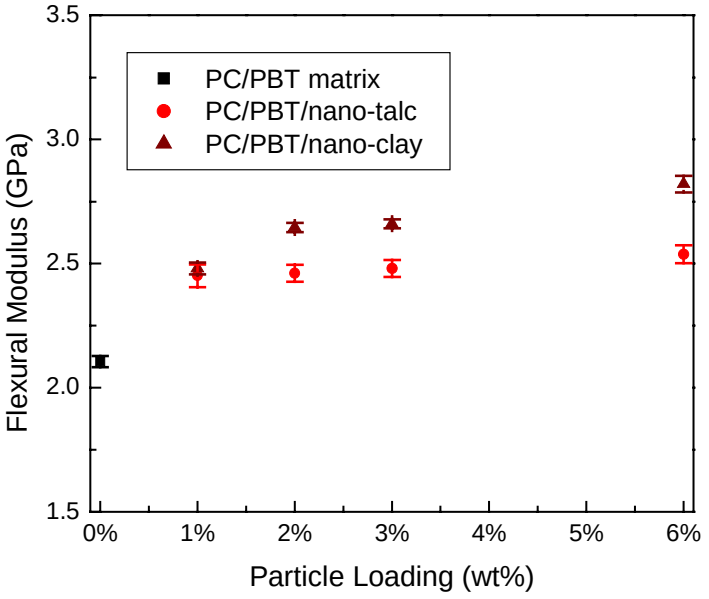

(a)

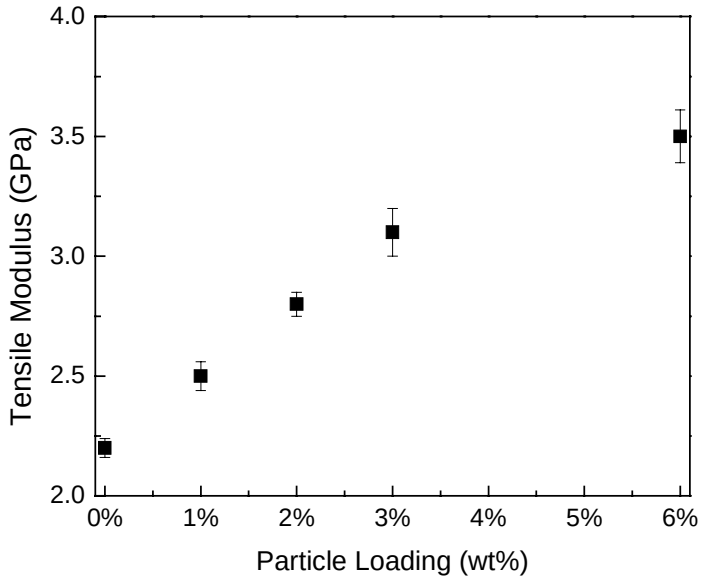

(b)

Figure 6.4: Comparison of (a) flexural modulus and (b) tensile modulus as a function of particle loading for PC/PBT/Cloisite 30B nanocomposites. The PC/PBT blend ratio is 60/40 by weight. A nano-clay loading of 0% by weight refers to the PC/PBT matrix. The effect of nano-talc loading on the flexural modulus of PC/PBT/nano-talc composites is also included for comparative purposes.

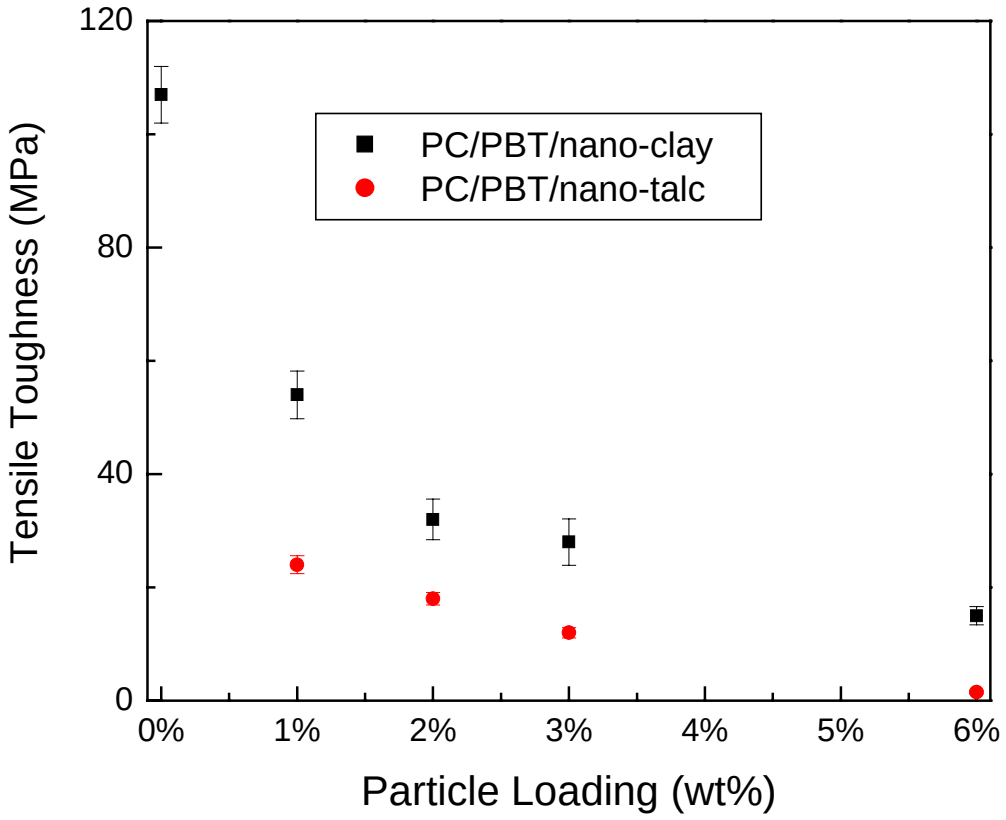

Figure 6.5: Comparison of tensile toughness as a function of particle loading for PC/PBT/Cloisite 30B nanocomposites. The PC/PBT blend ratio is 60/40 by weight. A nano-clay loading of 0% by weight refers to the PC/PBT matrix. The effect of nano-talc loading on the flexural modulus of PC/PBT/nano-talc composites is also included for comparative purposes.

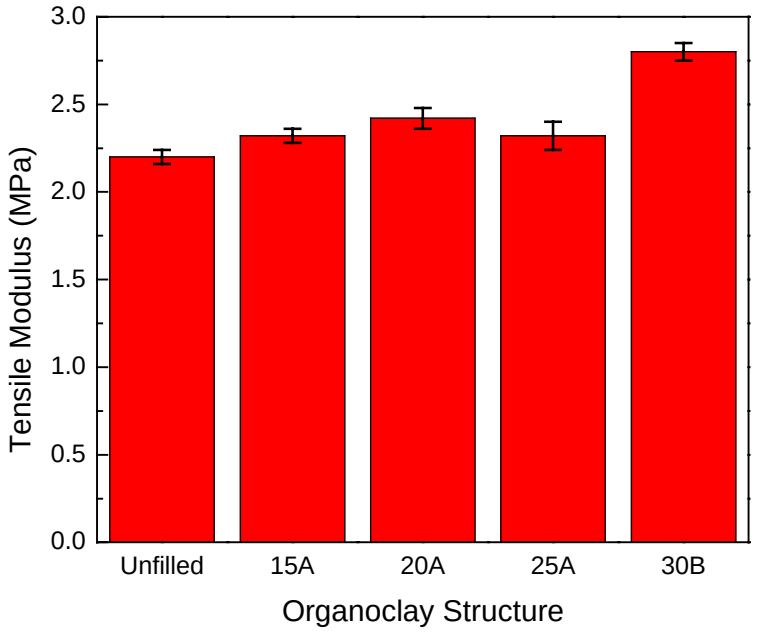

(a)

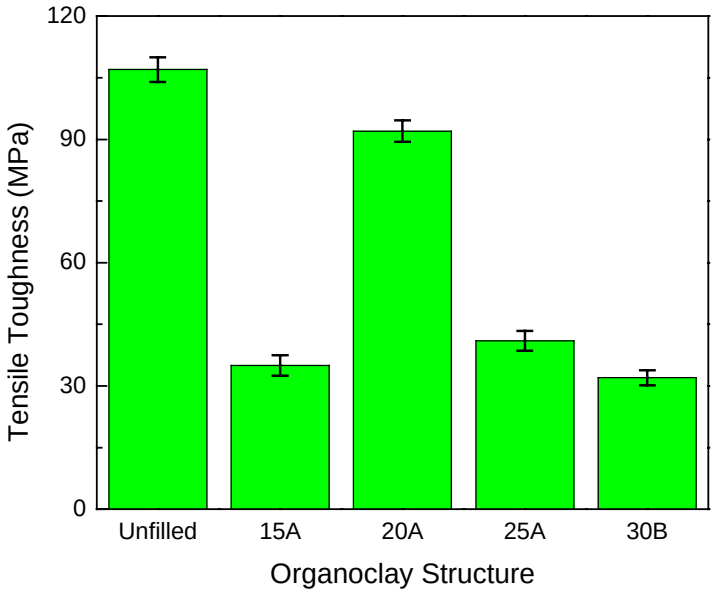

(b)

Figure 6.6: Comparison of (a) tensile modulus and (b) tensile toughness as a function of organoclay structure for PC/PBT/nano-clay composites. The PC/PBT blend ratio is 60/40 by weight and the nano-clay concentration is 2 wt%.

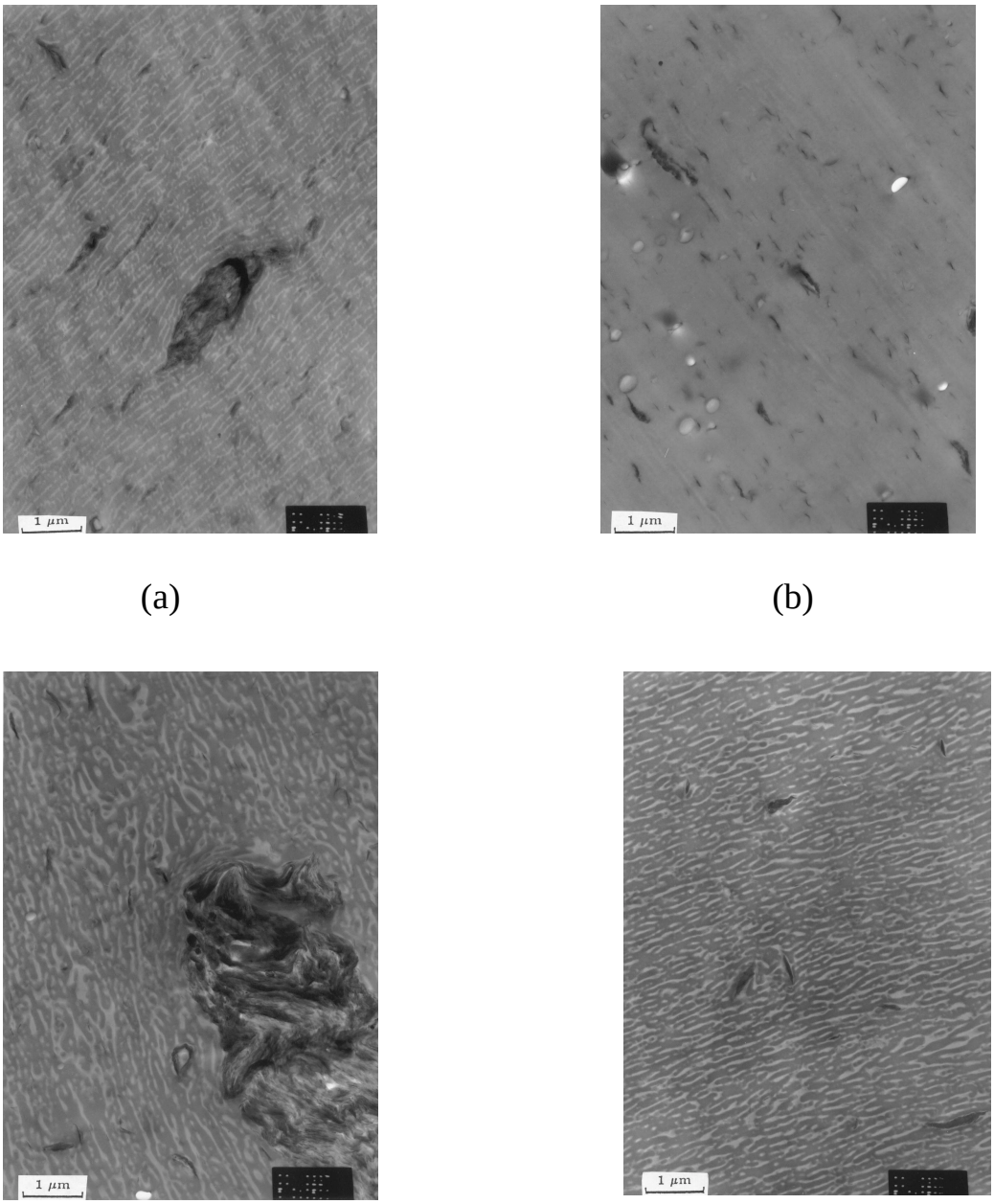

Figure 6.7: Transmission electron photomicrographs of PC/PBT/nano-clay composites as a function of organoclay structure: (a) Cloisite 15A; (b) Cloisite 20A; (c) Cloisite 25A; (d) Cloisite 30B. The PC/PBT blend ratio is 60/40 by weight and the nano-clay concentration is 2 wt%. The dark gray phase is PC, the white or light gray phase is PBT, and the black platelets are the talc particles.

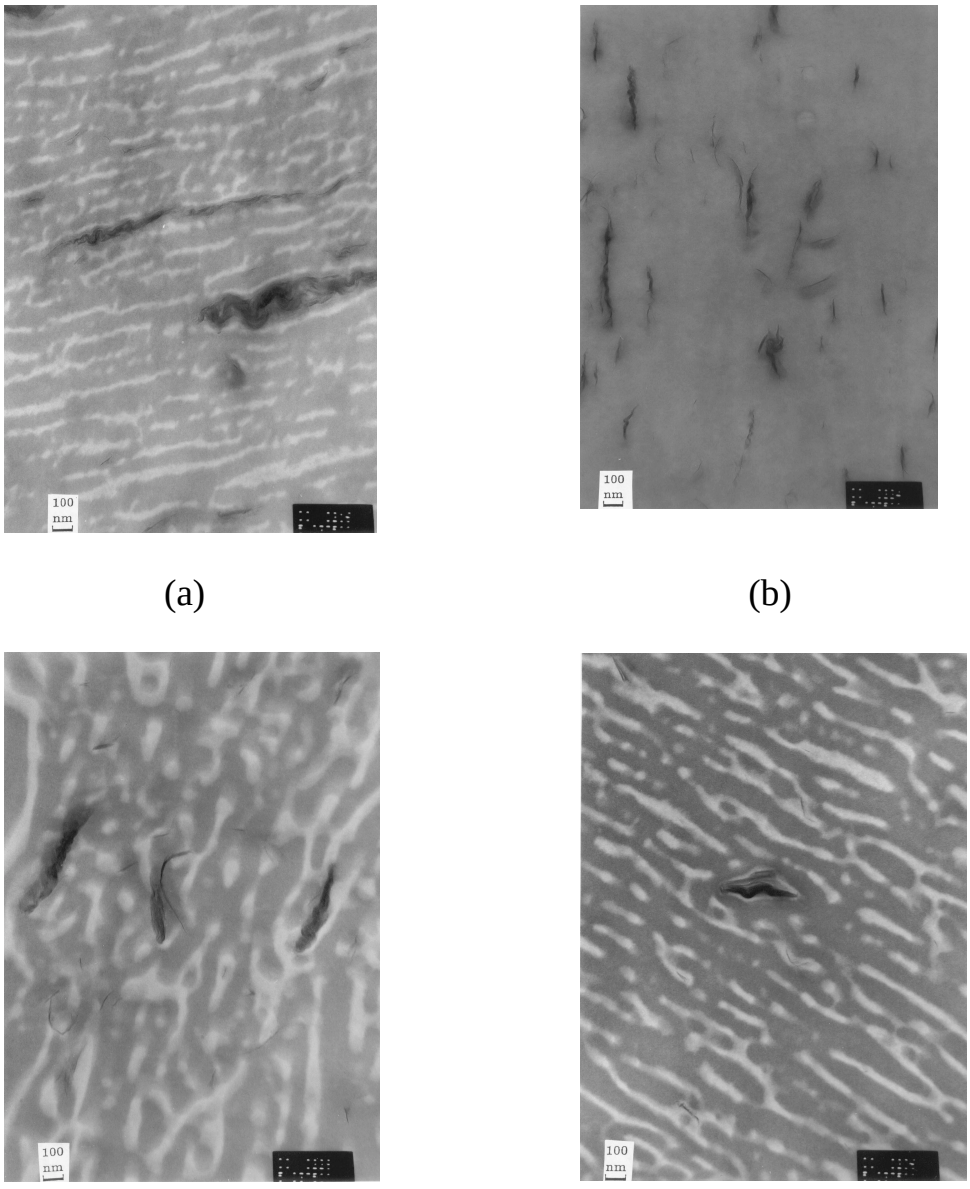

Figure 6.8: Transmission electron photomicrographs of PC/PBT/nano-clay composites as a function of organoclay structure (at a higher magnification): (a) Cloisite 15A; (b) Cloisite 20A; (c) Cloisite 25A; (d) Cloisite 30B. The PC/PBT blend ratio is 60/40 by weight and the nano-clay concentration is 2 wt%. The dark gray phase is PC, the white or light gray phase is PBT, and the black platelets are the talc particles.

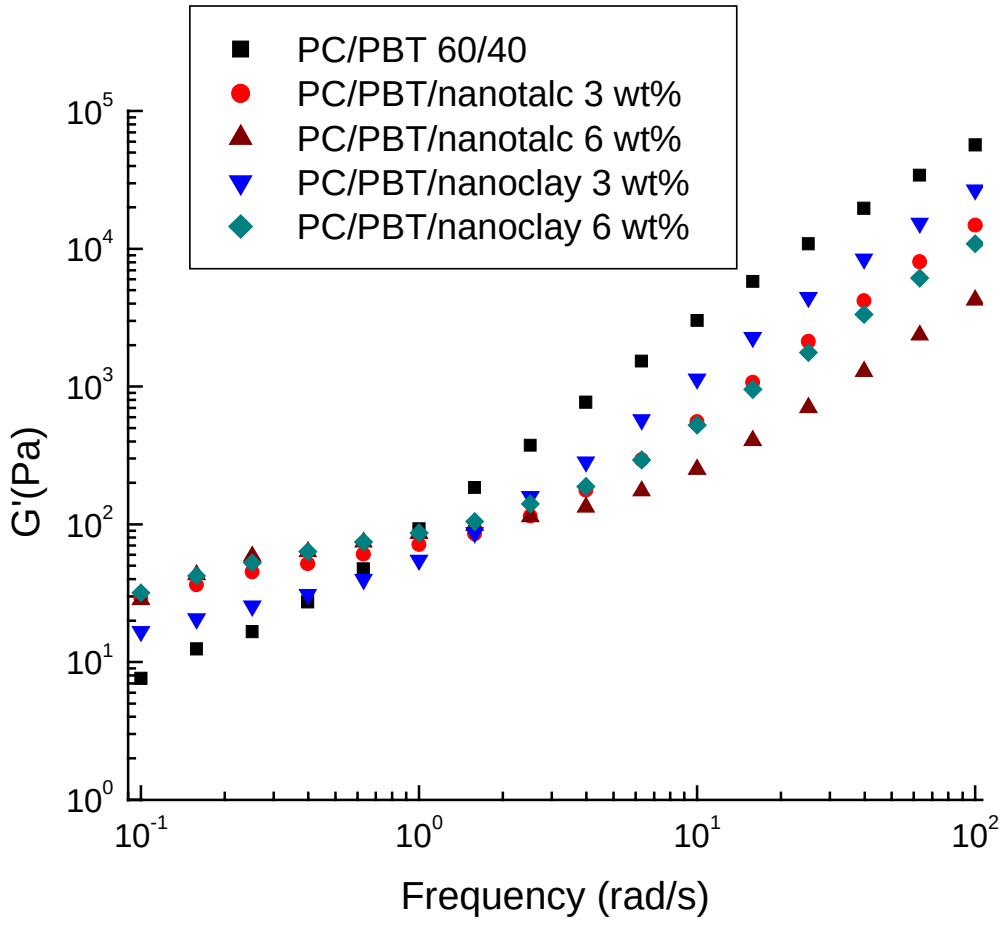

Figure 6.9: Comparison of storage modulus, G', as a function of organoclay loading for PC/PBT/nano-clay composites at a temperature of 260°C and a strain of 5% under nitrogen. The PC/PBT blend ratio is 60/40 by weight. The effect of nano-talc loading on the flexural modulus of PC/PBT/nano-talc composites are also added for comparative purposes.

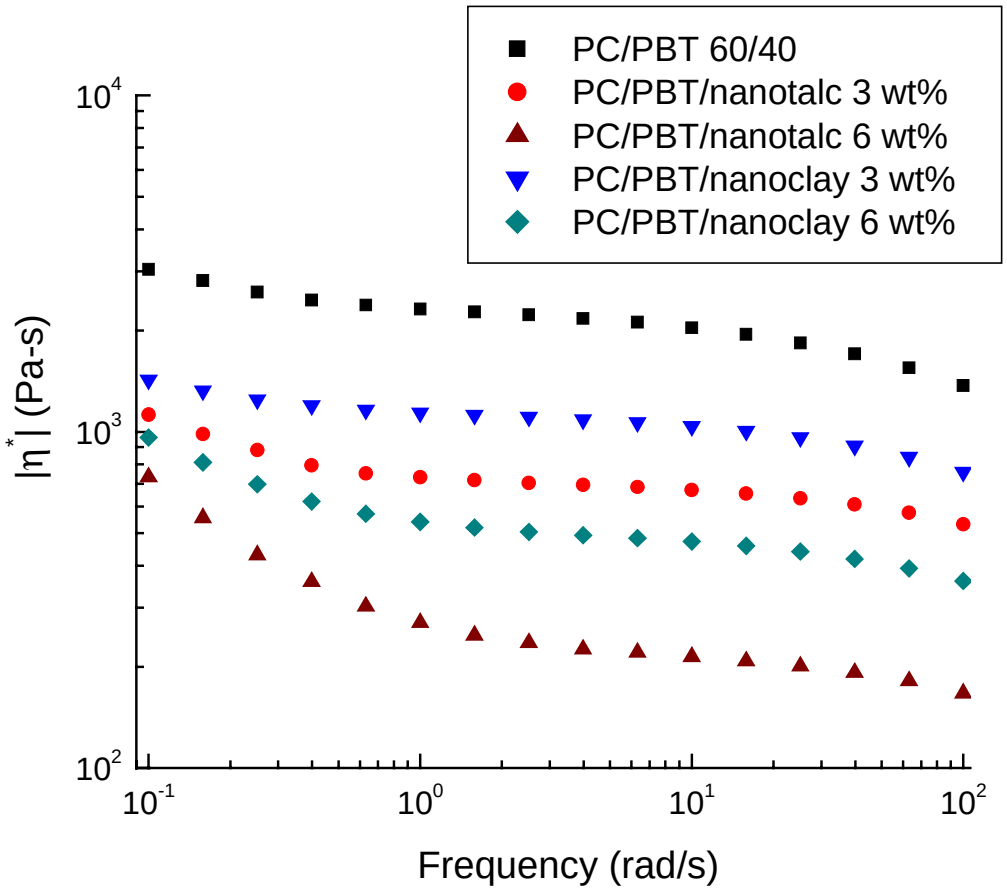

Figure 6.10: Comparison of complex viscosity, $|\eta^*|$, as a function of organoclay loading for PC/PBT/nano-clay composites at a temperature of 260°C and a strain of 5% under nitrogen. The PC/PBT blend ratio is 60/40 by weight. The effect of nano-talc loading on the flexural modulus of PC/PBT/nano-talc composites are also added for comparative purposes.

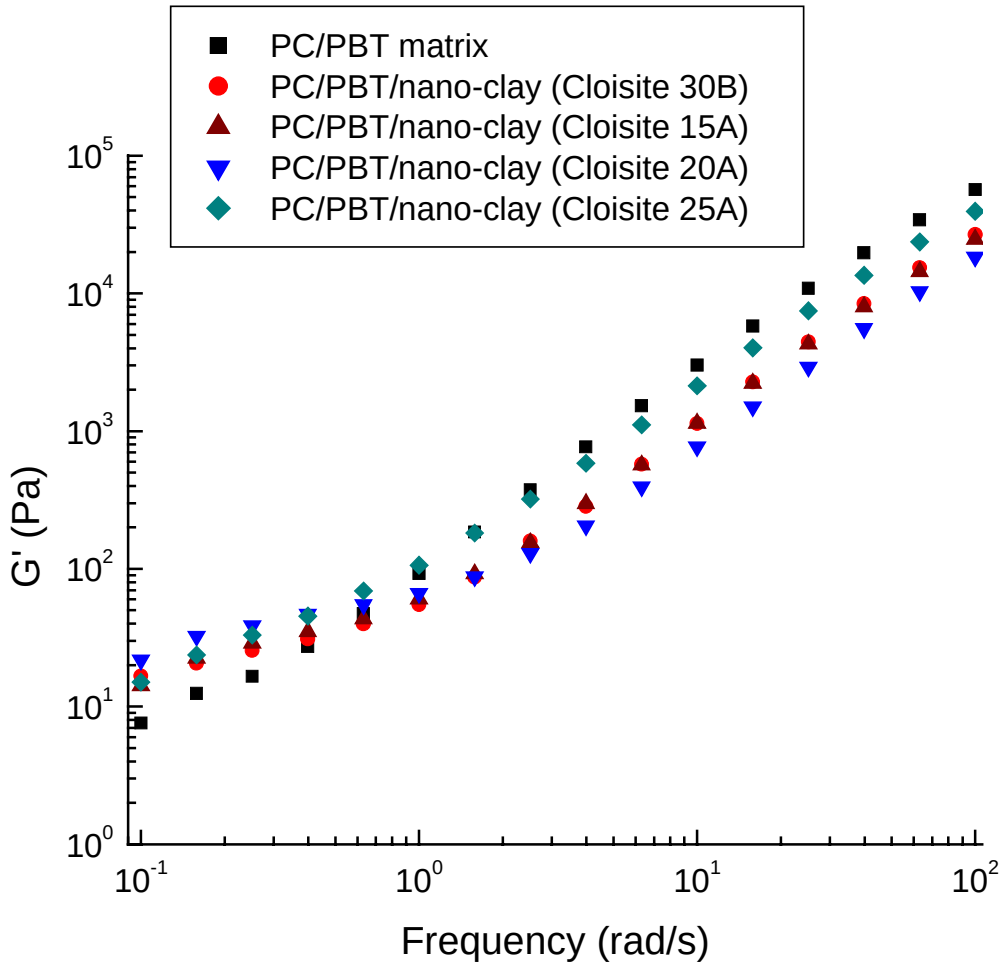

Figure 6.11: Comparison of storage modulus, G', as a function of organoclay structure for PC/PBT/nano-clay composites at a temperature of 260°C and a strain of 5% under nitrogen. The PC/PBT blend ratio is 60/40 by weight and the organoclay concentration is 2 wt%.

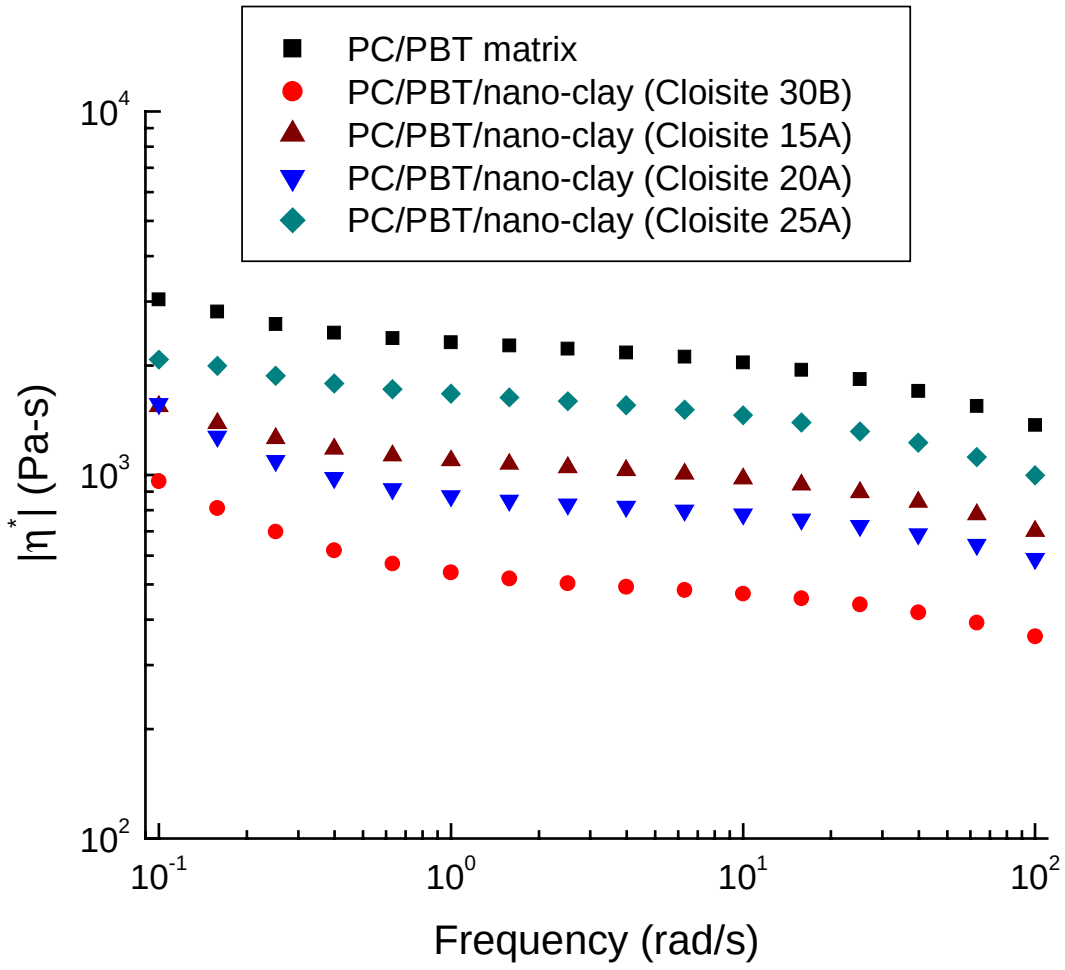

Figure 6.12: Comparison of complex viscosity, $|\eta^*|$, as a function of organoclay structure for PC/PBT/nano-clay composites at a temperature of 260°C and a strain of 5% under nitrogen. The PC/PBT blend ratio is 60/40 by weight and the organoclay concentration is 2 wt%.

7.0 Recommendations for Future Work

This study has been concerned with the dimensional stability and the structure-property relationships of thermoplastics reinforced with particulate and fiber fillers. In the first part of this study, a better understanding on the origins of warpage for polypropylene composites reinforced with thermotropic liquid crystalline polymers (TLCP) was developed. In the second part of this work, minimizing the particle loading of reinforced PC/PBT composites being produced for the manufacture of car door panels without sacrificing the dimensional stability, i.e. the coefficient of thermal expansion (CLTE) and shrinkage of injection molded flat panels, or modulus was accomplished by using nanoparticles as opposed to micron-sized particles. However, in doing so, this study has uncovered new questions regarding the effects that particulates and/or fiber fillers have on the dimensional stability and structure-property relationships of reinforced thermoplastics. Some of the future work to answer these questions is as follows:

- A model that accurately predicts the stress growth and stress relaxation of flow induced stresses generated during mold filling and subsequent cooling after cessation of flow for fiber reinforced thermoplastics must be developed.

- There needs to be more extensive studies on the surface chemistry, i.e. the interactions that occur between that of the filler and the matrix, for PC/PBT blends reinforced with the organoclay particles.

- Develop a method to enhance the dispersion of the nanoparticles in order to maximize the modulus enhancement of the PC/PBT/nanofiller composites by use of supercritical CO_2 as a dispersing agent.

A detailed explanation of the recommendations for future work of this project is described in the paragraphs that follow.

The warpage of fiber reinforced thermoplastics is caused by an imbalance in the residual stresses that remain in an injection molded part after it has been ejected from the mold and cooled down to ambient temperatures. The most common belief is that warpage is primarily due to thermally induced stresses due to shrinkage (density changes) and an imbalance in CLTE between the flow and transverse direction of injection molded parts. Therefore, frozen-in flow-induced stresses that are due to an increase in the primary normal stress difference and, hence, orientation of the macromolecules as well as

inhibition of stress relaxation with the addition of fibers is often neglected. In this study, it was shown that the role frozen-in flow reduced stresses plays a much more significant role in the warpage of fiber reinforced thermoplastics than otherwise thought. However, in this study, the role of the frozen-flow induced stresses relative to that of the thermally induced stresses was determined in a qualitative manner. Therefore, in the future, the effect of flow induced stresses on the warpage of fiber reinforced thermoplastics must be taken into account by modeling the mold filling and cooling of reinforced thermoplastics during the injection molding process. In order to do so, a rheological constitutive equation that can describe the flow behavior of filled thermoplastics must be chosen. Based on the vast literature on the subject it has been found that, typically, the orientation of the fibers and the flow behavior and the orientation of the thermoplastic during mold filling and cooling are decoupled. Furthermore, with the exception of the empirical Leonov model, most theoretical models are modified Newtonian models that do not account for shear-thinning behavior, which is typically observed for filled polymer systems. Also for most theoretical models, stress relaxation after cessation of flow instantaneously relaxes to zero. Therefore, these models are not useful for accurately predicting the orientation or residual stresses that develop during the filling or cooling stage in injection molding. Therefore, these models cannot accurately predict the dimensional stability of molded parts. On the other hand, Doi's molecular theory, which was extended by Doraiswamy and Metzner to fiber-filled systems, does predict stress growth behavior of filled systems and accurately predicts fiber orientation in the flow direction. Furthermore, the model should be able to account for stress relaxation of filled systems. Therefore, Doi's molecular model modified by Doraiswamy and Metzner may be able to accurately predict the orientation and residual stresses that develop during the cooling stage of injection molding, and therefore, the dimensional of injection molded parts. Once the model is developed, it can be compared to the experimental results reported in this study.

In the second part of this study, the overall goal was to minimize the particle loading of reinforced PC/PBT blends while maintaining a required level of stiffness, i.e. modulus, without sacrificing the dimensional stability. By doing so, the tensile toughness can be increased and the overall weight of the part can be reduced, which is advantageous

for automotive purposes. It was found that by using nano-talc as opposed to fine talc particles, the level of talc reinforcement could be reduced from 6 to 1 wt% without sacrificing the dimensional stability, i.e. CLTE and shrinkage of injection molded plaques, or flexural modulus of the PC/PBT/talc composites at a PC to PBT blend ratio of 60/40 by weight or greater. Further benefits included a 14% increase in flexural strength, 50% increase in the tensile toughness and 3% reduction in the density of the PC/PBT/talc composites. Furthermore, the use of organoclays to reinforce the PC/PBT blends lead to improved mechanical properties as opposed to using nano-talc at an equivalent level of reinforcement. This was attributed to the higher aspect ratio and better dispersion of the organoclay particles. However, images of the PC/PBT nanocomposites obtained by means of TEM showed that the nanoparticles were at most partially exfoliated with the nanoparticles and in many cases agglomeration of the nanoparticles were present regardless of the surface modification applied to the surface the nanoparticles. Furthermore, it was shown that when the PC/PBT blend was miscible due to the presence of the organoclay Cloisite 20A, the organoclay was well dispersed within the PC/PBT matrix and there were no signs of large agglomerates, which lead to the greatest enhancement of tensile toughness. However, the PC/PBT blends that were reinforced with Cloisite 30B still had a much greater modulus relative to that of the blends reinforced with Coisite 20A even though agglomeration of the organoclay particles was observed. This was most likely due to hydrogen bonding of the hydroxyl groups at the surface of Coisite 30B with that of the carbonyl group in the PC phase. Based on the above findings, in the future, there needs to be more extensive studies on the interactions that occur between that of the filler and the matrix in order to get a better understanding of these results. In particular, the surface chemistry between the polymer phases and organoclays must be studied in greater detail. Furthmore, dispersion of the nanoparticles must be enhanced in order to maximize the modulus enhancement for these systems. It may be possible to improve the dispersion of the nanoparticles by using supercritical CO_2 as a dispersing agent. The two advantages in using CO_2 is: 1) it will reduce the processing temperature that is required to melt process the nanoparticle reinforced PC/PBT blends and, therefore, reduce degradation of the surface treatment due to the high processing temperatures that are usually employed in melt blending PC/PBT blends,

and 2) the polar nature of the dispersing agent may help to break up the galleries into separate platelets by reducing the polymer/filler interactions and/or lowering the surface tension between the PC and PBT phase.